

Material Fingerprinting

Understanding how differences in geology impact metallurgical plant performance

van Duijvenbode, J.R.

DOI

[10.4233/uuid:013727ea-91b4-47cb-959c-b83a1f2cbbdd](https://doi.org/10.4233/uuid:013727ea-91b4-47cb-959c-b83a1f2cbbdd)

Publication date

2023

Document Version

Final published version

Citation (APA)

van Duijvenbode, J. R. (2023). *Material Fingerprinting: Understanding how differences in geology impact metallurgical plant performance*. [Dissertation (TU Delft), Delft University of Technology]. <https://doi.org/10.4233/uuid:013727ea-91b4-47cb-959c-b83a1f2cbbdd>

Important note

To cite this publication, please use the final published version (if applicable). Please check the document version above.

Copyright

Other than for strictly personal use, it is not permitted to download, forward or distribute the text or part of it, without the consent of the author(s) and/or copyright holder(s), unless the work is under an open content license such as Creative Commons.

Takedown policy

Please contact us and provide details if you believe this document breaches copyrights. We will remove access to the work immediately and investigate your claim.

JEROEN R. VAN DUIJVENBODE



MATERIAL FINGERPRINTING

**UNDERSTANDING HOW DIFFERENCES IN GEOLOGY
IMPACT METALLURGICAL PLANT PERFORMANCE**

Material Fingerprinting

Understanding how differences in geology impact
metallurgical plant performance

Material Fingerprinting

Understanding how differences in geology impact
metallurgical plant performance

Dissertation

for the purpose of obtaining the degree of doctor
at Delft University of Technology
by the authority of the Rector Magnificus Prof. dr. ir. T.H.J.J. van der Hagen,
Chair of the Board for Doctorates
to be defended publicly on
Thursday 23 March 2023 at 15:00 o'clock

by

Jeroen Robert VAN DUIJVENBODE

Master of Science in Applied Earth Sciences,
Delft University of Technology, the Netherlands,
born in Hellevoetsluis, the Netherlands

This dissertation has been approved by the promotor.

Composition of the doctoral committee:

Rector Magnificus,	chairperson
Dr. M.W.N. Buxton	Delft University of Technology, promotor
Prof. dr. ir. J.D. Jansen	Delft University of Technology, promotor
Dr. M. Soleymani Shishvan	Delft University of Technology, copromotor

Independent members:

Prof. dr. ir. E.C. Slob	Delft University of Technology
Prof. dr. G.T. Nwaila	University of the Witwatersrand, South Africa
Prof. dr. ir. H.J. Glass	University of Exeter, Camborne School of Mines, UK
Dr. ir. D.L. Schott	Delft University of Technology
Prof. dr. ir. T.J. Heimovaara	Delft University of Technology, reserve member

The research described in this thesis was performed in the Resource Engineering group at Delft University of Technology, Department of Geoscience and Engineering, Faculty of Civil Engineering and Geosciences. The research data has been shared by AngloGold Ashanti.

Keywords: Material fingerprinting, geometallurgy, material tracking, metallurgical plant performance

Printed by: Proefschriftspecialist

Front & Back: Cover design by Dyon van den Berg @Thesignstudio and Jeroen R. van Duijvenbode

Copyright © 2022 by Jeroen R. van Duijvenbode All rights reserved.

ISBN 978-94-6384-430-7

An electronic version of this dissertation is available at
<http://repository.tudelft.nl/>

Contents

Summary	ix
Samenvatting	xi
List of abbreviations	xv

Chapter 1

Introduction

1.1 Context	2
1.2 Research scope and approach	4
1.3 Dissertation outline	5

Chapter 2

Literature review

2.1 Material classification	8
2.2 The impact of material hardness	10
2.3 Summary	12

Chapter 3

Material fingerprinting – Part I: concept

3.1 Definition	14
3.2 Concept	14
3.3 Differentiation from traditional geometallurgy	17
3.4 Challenges	18



Chapter 4

Data acquisition techniques

4.1 Introduction	22
4.2 Geochemical properties	22
4.3 Mineralogical properties	26
4.4 Mechanical rock properties	27
4.5 Datasets of this dissertation	30

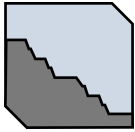


Chapter 5

Multivariate analysis techniques and clustering

5.1 Introduction	34
5.2 Feature engineering	34
5.3 Cluster analysis	43





Chapter 6

Tropicana Gold Mine

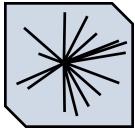
6.1 Introduction	48
6.2 Geology	52

Chapter 7

Material fingerprinting – Part II: framework

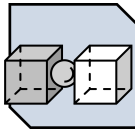
7.1 Introduction	60
7.2 Conceptual framework	61
7.3 Fingerprint confidence	67
7.4 Case study	69
7.5 Discussion	73
7.6 Conclusions	74

Chapter 8

Multi-element geochemical data clustering

8.1 Introduction	76
8.2 Methods	77
8.3 Quality assurance and quality control	80
8.4 Results	84
8.5 Discussion	99
8.6 Conclusions	101

Chapter 9

Between and within material type variability

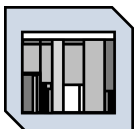
9.1 Introduction	104
9.2 Methods	104
9.3 Results	110
9.4 Discussion	124
9.5 Conclusions	127

Chapter 10

Material tracking simulation

10.1 Introduction	130
10.2 Methods	131
10.3 Results	137
10.4 Discussion	150
10.5 Conclusions	151

Chapter 11

Processing performance

11.1 Introduction	154
11.2 Methods	155
11.3 Processing response data	157
11.4 Results	162
11.5 Discussion	172
11.6 Conclusions	173

Chapter 12

Discussion

12.1 Synthesis of research objectives	176
12.2 Interpretation and implications of the main results	177
12.3 Perspectives and limitations	180

Chapter 13

Conclusions and recommendations

13.1 Conclusions	186
13.2 Recommendations	187

References	191
-------------------------	-----

Appendix	207
-----------------------	-----

Acknowledgements	211
-------------------------------	-----

Curriculum Vitae	213
-------------------------------	-----

Publications	215
---------------------------	-----

Summary

To extract raw materials responsibly and sustainably, the minerals industry has to continuously optimise the mine-to-metal process and requires an entirely different valuation model. Currently, most operational decisions (e.g., ore-waste boundaries, short-term scheduling, blending policies, dispatch decisions) are evaluated using a revenue-based model. Such a model derives the value of the material from its estimated metal content (grade \times tonnage). However, metallurgical attributes which largely define the processing costs (revenue losses) are left out of the equation since they are either missing or unreliable. In a future optimisation step, it should be possible to offset the anticipated revenue against an aggregated metallurgical cost based on, for example, energy consumption, throughput, recovery and reagent consumption. This drives the need for an improved method to describe the to-be-processed material, which determines the influence of geological behaviour (the material type) on the processing performance (associated with the costs).

This dissertation presents a high-level data fusion method that uses sensor data to characterise and classify material and create diagnostic fingerprints. First, in **Chapter 2** material classification and the importance of hardness are reviewed highlighting some of the current research limitations and indicating the contributions of this dissertation. Then, the material fingerprinting concept is presented in **Chapter 3** and further elaborated on in **Chapter 7**. The chapters in between these two provide all the required background information related to the data acquisition techniques for geochemical, mineralogical and physical rock properties (**Chapter 4**) and multivariate analysis techniques and clustering (**Chapter 5**). Using these fingerprints, the aim is to describe and understand how geology impacts metallurgical plant performance.

For doing this, four extensive studies using data from the Tropicana Gold Mine, Australia (**Chapter 6**), have been selected in which the input dataset size and quality vary. The motivation is that it should be possible to fingerprint material using high-quality and more expensive data but also with lower-quality, cheap, and rapidly acquired data. The fingerprinting methodology makes an important contribution to the synthesis and description of geological attributes by providing a new data layer that groups samples which underwent similar geological processes together in an objective manner.

The first study, in **Chapter 8** fingerprints were created using a multi-element dataset from exploration drill hole samples clustered using an agglomerative hierarchical clustering method. This showcased that 1) the high-quality geochemical data can function as a litho-geochemical classifier, 2) distinct spatial contextual relationships with geochemical variability at a deposit scale, and 3) domain-related material class proportions assist in interpreting different processing proxies such as the Equotip hardness, Bond Work index, impact breakage (A_{xb}), and processing recovery and reagent consumption.

The second study in **Chapter 9** proceeds by investigating the within- and between material type differences (dispersion variance) based upon clustering results from a geochemical and mineralogical dataset. This dataset was derived from the rapidly and routinely acquired grade control samples. In this study, each material type was a proxy for the constitutive material hardness properties and provided a more comprehensive understanding of comminution behaviour. Assessment of the spatial-contextual relationships of material types showed, for example, how a phengitic-epidote K-feldspar rich domain (schistosity and softer) separated from a harder, shorter wavelength phengitic plagioclase-rich feldspar dominated domain. This further proved that the fingerprints were indeed a proxy for the geochemical and mineralogical characteristics of mineralised material, but also for the material hardness experienced during milling.

The third study in **Chapter 10** replicated the dispatch movements of fingerprints from the pit to the stockpiles and the crusher. This further established relationships between the crusher input feed (using fingerprints from the second study) and the mill and leach circuit processing responses. This was done using a forward simulator model, which spatially and temporally modelled stockpiles and accounted for blending effects. Assessment of the spatial-temporal modelling showed realistic geological variability similar to that seen in the pit and spatial cohesion, which enables temporal reconciliation of the crusher input feed composition (as time series).

In the final study in **Chapter 11**, these crusher feed attributes were linked to the actual plant performance to identify which and in which manner specific geological features affect the comminution and leach behaviour. A novel continuous wavelet tessellation and data mosaic method were applied to assess these relationships. This method applies a multiscale and multivariate analysis that transforms time series signals into continuous temporal domains consisting of samples of similar fingerprints. These domains showed material variability at different scales and were used to analyse the corresponding metallurgical plant performance (comminution and leaching). The geological variability observed at strategical levels matched the distinct modes of processing, whereas, at the tactical resolution, this related to the minor scale variability in the processed blend composition.

In conclusion, material fingerprints are used to understand how geology impacts metallurgical plant performance. With comprehensive literature reviews, clustering techniques and mathematical simulations the research results matched the expectations and were geologically substantiated, thus increasing confidence in the method and interpretation applied in this study. Ultimately, implementing these results in operation would impact the tactical and strategical decision-making and facilitate optimising operational decisions.

Samenvatting

Om grondstoffen op verantwoorde en duurzame wijze te winnen, moet de delfstofindustrie het grondstof-tot-metaalproces voortdurend optimaliseren en is een volledig ander waarderingsmodel vereist. Momenteel worden de meeste operationele beslissingen (b.v. erts-afval onderscheiding, korte termijnplanning, mengbeleid, materiaal locatie bepalingen) geëvalueerd aan de hand van een op inkomsten gebaseerd model. Een dergelijk model leidt de waarde van het materiaal af van het geschatte metaalgehalte (concentratie \times tonnage). Metallurgische kenmerken die in grote mate de verwerkingskosten bepalen (inkomstenverliezen) worden echter buiten beschouwing gelaten omdat zij ontbreken of onbetrouwbaar zijn. In een toekomstige optimaliseringsstap moet het mogelijk zijn om de verwachte inkomsten te verrekenen met een totale metallurgische kostprijs op basis van bijvoorbeeld energieverbruik, productiecapaciteit, hergebruik en consumptie van chemicaliën. Dit drijft de behoefte aan voor een verbeterde methode om het te verwerken materiaal te beschrijven, die daarbij de invloed van de geologie (de materiaalsoort) op de verwerkingsprestaties (geassocieerd aan de kosten) bepaalt.

Dit proefschrift presenteert een data-samenvoegingmethode die sensorgegevens gebruikt om materiaal te karakteriseren en classificeren en om diagnostische vingerafdrukken te maken. Als eerste, in **Hoofdstuk 2** wordt materiaal classificatie en het belang van hardheid besproken, waarbij enkele van de huidige onderzoeksbeperkingen worden benadrukt en de bijdragen van dit proefschrift worden aangegeven. Vervolgens wordt het concept van *material fingerprinting* gepresenteerd in **Hoofdstuk 3** en verder uitgewerkt in **Hoofdstuk 7**. De tussenliggende hoofdstukken beschrijven alle benodigde achtergrondinformatie met betrekking tot de data-acquisitietechnieken voor geochemische, mineralogische en fysische eigenschappen van gesteenten (**Hoofdstuk 4**) en multivariate analysemethoden en dataclustering (**Hoofdstuk 5**) om de vingerafdruk te maken. Aan de hand van deze vingerafdrukken wordt getracht te beschrijven en te begrijpen hoe geologie de prestaties van metallurgische productieprocessen beïnvloedt.

Om dit te doen, zijn vier uitgebreide onderzoeken uitgevoerd met behulp van gegevens uit de Tropicana Gold Mine te Australië (**Hoofdstuk 6**). Deze onderzoeken gebruiken datasets van verschillende grootte en datakwaliteit omdat men van het materiaal een vingerafdruk kan maken met behulp van hoogwaardige en duurdere gegevens, maar ook met laagwaardige, goedkopere en snel te verkrijgen gegevens. Dit laat zien dat de vingerafdruk methode een belangrijke bijdrage aan de synthese en beschrijving van geologische attributen kan leveren doordat het een nieuwe dimensie van data biedt waarbij monsters zijn gegroepeerd, op een objectieve manier, die vergelijkbare geologische processen hebben ondergaan.

Als eerste, zijn in **Hoofdstuk 8** vingerafdrukken gemaakt met behulp van een multi-element dataset van monsters afkomstig van exploratie boringen die werden

gegroepeerd met behulp van een agglomeratieve hiërarchische clustermethode. Dit toonde aan 1) dat de hoogwaardige geochemische gegevens kunnen functioneren als een litho-geochemische classificatie, 2) dat er verschillende ruimtelijke contextuele relaties bestaan met geochemische variabiliteit op een ertslichaam schaal, en 3) dat domein-gerelateerde materiaalklasse-verhoudingen helpen bij het interpreteren van verschillende vermalingseigenschappen zoals de Equotip-hardheid (Leeb), Bond Work-index (BWi), impact breekbaarheid (Axb), hergebruik of chemicaliën verbruik.

De tweede studie in **Hoofdstuk 9** gaat verder met het onderzoek van de variabiliteit binnen en tussen materiaaltypes (spreiding variatie) te onderzoeken op basis van clusteringsresultaten van een geochemische en mineralogische dataset. Deze dataset is afkomstig van kwaliteitscontrole monsters die snel en routinematig verkregen zijn. In deze studie was elk materiaaltype een indicatie voor de bijdragende materiaalhardheidseigenschappen en gaf het een uitgebreider begrip van de brekings-eigenschappen. Een verdere beoordeling van de ruimtelijk-contextuele relaties van materiaaltypen toonde bijvoorbeeld aan hoe een fengiet-epidoot kaliveldspaat-rijk domein (hoge schistositeit en zachter) zich scheidde van een harder, met kortere golflengte fengiet plagioklaas-rijk veldspaat gedomineerd domein. Dit bewees verder dat de vingerafdrukken inderdaad een indicatie waren voor de geochemische en mineralogische kenmerken van gemineraliseerd materiaal, maar ook voor de hardheid van het materiaal tijdens het malen.

De derde studie in **Hoofdstuk 10** reproduceerde de transportbewegingen van vingerafdrukken van de open-pit naar de opslagfaciliteiten en de breker. Dit vergemakkelijkte verdere vaststelling van relaties tussen het toevoermateriaal van de breker (met behulp van vingerafdrukken uit de tweede studie) en de verwerkingsreacties van het maal- en uitloogcircuit. Dit werd gedaan met behulp van een voorwaarts-simulator model, waarin de voorraden ruimtelijk en in de tijd werden gemodelleerd en waarbij rekening werd gehouden met mengeffecten. Uit de beoordeling van de ruimtelijk-temporele modellering bleek dat er sprake was van realistische geologische variabiliteit, vergelijkbaar met die in het ertslichaam. Dit zorgde ervoor dat de samenstelling van de toevoer van de breker in de tijd (als tijdreeksen) met de verwerkingsreacties kon worden vergeleken.

In de laatste studie in **Hoofdstuk 11** werden deze eigenschappen van de brekervoeding gekoppeld aan de werkelijke prestatie van de breker om vast te stellen welke specifieke geologische kenmerken het vermalings- en uitlooggedrag beïnvloeden en op welke wijze. Hiervoor werd er een nieuwe continue golf-vlakvullings- en datamozaïekmethode toegepast om deze verbanden te beoordelen. Deze methode past een multischaal- en multivariate analyse toe die tijdreeksignalen omzet in continue tijdsdomeinen bestaande uit selecties met vergelijkbare vingerafdrukken. Deze domeinen vertonen materiaalvariabiliteit op verschillende tijdsschalen en worden gebruikt om de bijbehorende prestaties van de metallurgische fabriek (vermaling en uitloging) te analyseren. De geologische variabiliteit die op strategisch niveau werd waargenomen, stemde overeen met de verschillende verwerkingswijzen, terwijl dit op tactische niveau verband hield met de variabiliteit op kleine schaal in de samenstelling van het verwerkte mengsel.

Samenvattend heeft deze dissertatie laten zien hoe materiële vingerafdrukken werden gebruikt om te begrijpen hoe geologie de prestaties van metallurgische processen beïnvloedt. Met uitgebreide literatuuroverzichten, clustertechnieken en wiskundige

simulaties kwamen de onderzoeksresultaten overeen met de verwachtingen en waren geologisch onderbouwd, waardoor het vertrouwen in de methode en interpretatie die in deze studie zijn toegepast toenam. Uiteindelijk zou het implementeren van deze resultaten in de operatie de tactische en strategische besluitvorming beïnvloeden en operationele beslissingen verder optimaliseren.

List of abbreviations

AAS	Atomic Absorption Spectroscopy
Axb	Impact breakage
AC	Air Core
AFO	Albany-Fraser Orogen
AGA	AngloGold Ashanti
BV	Best Value
BS	Boston Shaker
BWi	Bond Ball Mill Work index
clr	centred log-ratio
CRM	Certified Reference Materials
CWT	Continuous Wavelet Tessellation
DDH	Diamond Drill Hole
DL	Detection Limit
F_{80}	80% passing size feed
FW	Footwall
GC	Grade Control
HA	Havana
HorRat	Horwitz Ratio
HPGR	High Pressure Grinding Rolls
HS	Havana South
HW	Hanging Wall
ICP	Inductively Coupled Plasma
ICP-MS	Mass Spectrometry
ICP-OES	Optical Emission Spectroscopy
LDL	Lower Detection Limit
ME	Multi-Element
ML	Machine Learning
MWD	Measurement-While-Drilling
PC	Principal Component
PCA	Principal Component Analysis
PRSD	Predicted Relative Standard Deviation
XRD	X-Ray Diffraction
pXRF	portable X-Ray Fluorescence
QAQC	Quality Assurance and Quality Control
RC	Reverse Circulation
RFID	Radio-Frequency IDentification
ROM	Run-Of-Mine
RSD	Relative Standard Deviation

SD	Standard Deviation
SWIR	Short Wave Infrared
SZ	Shear Zone
TGM	Tropicana Gold Mine
TP	Tropicana
TS	TerraSpec
VNIR	Visible Near Infrared
w_i	work index

1

Introduction

This first chapter places the topic of this dissertation into context and addresses how representative samples can be generated which form the base of all analyses performed in this dissertation. It also presents the research scope and approach. Finally, the last part of the chapter gives a general overview of the structure and the content of the subsequent chapters.

Parts of this chapter were created based upon discussions with L. M. Cloete and his overview of basic understanding and concepts related to geometallurgy. Other parts of this chapter have been published in: **van Duijvenbode, J. R.** and M. W. N. Buxton (2019). Use of time series event classification to control ball mill performance in the comminution circuit - A conceptual framework. In *Real Time Mining - 2nd International Raw Material Extraction Innovation Conference*, Freiberg, Germany, pp. 114-123, and **van Duijvenbode, J. R.**, M. W. N. Buxton, and M. Soleymani Shishvan (2020). Performance improvements during mineral processing using material fingerprints derived from machine learning - A conceptual framework. *Minerals* 10(4), 366. doi:10.3390/min10040366.

1.1 Context

Optimisation of the mining extraction process is an important area for sustainable value creation and cost reduction across many mining operations (e.g., Hoal and Frenzel (2022); Mining Modular (2017)). To achieve this, mine sites require improvements in the ability to spatially characterise material as it moves through the reconciliation chain. This will enable them to moving from drill bit to metal (e.g., gold bar) process control in which geochemical, mineralogical, comminution, recovery and reagent consumption attributes are considered. However, the approach to unlocking such a full value using these geometallurgical considerations is complex and extensive, and no comprehensive method exists yet to link separate geometallurgical components and datasets. Such a data integration method is developed in this dissertation and is called material fingerprinting. This will be used to understand how differences in geology impact metallurgical plant performance.

The main problem to be solved is the lack in understanding of the root cause causing variations in the metallurgical processing plant performance. Typically, this root cause is caused by the insufficient understanding of the chemical composition, mineralogy, texture and fracturing of plant feed resulting in non-optimal blends. These primary rock attributes define the secondary material attributes (including processing behaviour), are spatially abundant and can be cheaply measured in vast quantities from available sensor data (see Chapter 4). Therefore, finding an approach to describe the to-be-processed material using these datasets provide the means to link geometallurgical variation with machine behaviour caused by geological changes. Afterwards, if the variable geological behaviour is understood, modelled and can be identified at various stages in the mining process then machine performance can also be understood, controlled and optimised.

One important driver for implementing such an approach is the electrical energy consumption of the comminution circuit. The crushing and grinding units are among the most energy-demanding machines resulting in high operational expenditures, and account for up to 4% of global electrical energy consumption (de Bakker, 2013; Bortnowski et al., 2021; Jeswiet and Szekeres, 2016). Especially, with respect to the current circumstance of extortionary rises in energy and gas prices that also affect the mining operating costs (Mining Technology, 2022) this is an very important concern. Therefore, an essential aspect of optimisation is modelling the metallurgical behaviour of the plant feed on, for instance, the ball mill performance. Optimisation can increase the throughput, improve the recovery and reduce the energy utilisation as well as the chemical usage per ton of processed material (lower the environmental footprint). Consequently, overall operational expenditures will drop, making lower grade ore economical to mine. However, this might be challenging due to the lack of knowledge of how different materials react to different operational settings (Suriadi et al., 2018). Therefore, to obtain optimised mining decisions, it is necessary to consider geological and metallurgical (or geometallurgical) attributes which affect the comminution circuit.

Typically, this sustainable value creation from rock samples starts from the moment of data acquisition which could, for example, be during the first contact of a drill bit with the rocks. At this point in time, measurement-while-drilling sensors gather lots of data about the rock characteristics and show deviations likely caused by

geological variability. This is already a first indication of potentially distinct material characteristics and should inform any further decision making regarding the mining, hauling and processing of these rocks. Similarly, integration of geological logging data, sample analyses and spatial modelling will make material knowledge more complete and stipulate the data insights to group samples in geometallurgical classes (fingerprints) which behave similar in terms of actual processing behaviour (also see the analogy in Explanation 1). Then for new samples or plant feed blends it is possible to predict how they will behave in the processing plant. Comparison of these expected blend fingerprints with the actual plant performance will eventually give insights into the actual root cause of changing plant performance.

This quest for the impact of geology on metallurgical plant performance is fundamental to this dissertation and will be researched using data from a gold mine. The main scientific contributions are related to the detailed description and examples of the fingerprinting concept and framework. Material fingerprinting makes an important contribution to the synthesis and description of geological attributes by providing a new data layer that groups samples which underwent similar geological processes in an objective manner. Furthermore, the relevance of this study for the mining industry is that these methods and interpretations could inform about the expected processing conditions of to-be-processed material and thus give insights into the energy consumption and optimal processing conditions.

Explanation 1.1: The fingerprinting approach allows to predict for a new material blend the processing behaviour and choose the optimal processing conditions. The important benefit of fingerprinting is that this can be achieved without a large amount of expensive metallurgical tests. Instead, fingerprinting characterises material classes based upon adequate and representative proxy data (including some historical metallurgical tests).

Translated into an analogy of cakes: The fingerprinting approach allows to predict the taste and texture of an unsliced cake (Figure 1.1a), and eventually to propose the best consumption method. This can be achieved without slicing and tasting the cake before the party. Instead, fingerprinting pre-defines various recipes to form different tastes and textures (Figure 1.1b-e) based upon the available ingredients resulting in different cake types. Without an exposure to the baking process but with the knowledge of the known ingredients and having an unsliced cake, the best consumption method can be identified (fork or spoon) (Figure 1.1f).



FIGURE 1.1: Analogy showing the fingerprinting of a cake (orebody) to find out what its optimal processing conditions are (see Explanation 1.1). It also shows a sampling dilemma by a variety of cake layers. Green stars denote possible sampling locations. Source: Own illustration based upon Google Images.

1.2 Research scope and approach

The expected link between the geology and metallurgical plant performance and the need for optimisation of the plant performance are translated in the following hypothesis which will be tested in this dissertation:

Hypothesis: A material fingerprinting based process control framework that considers metallurgical properties is the way forward to make optimal mining decisions. In addition, these fingerprints may help to understand bottlenecks in the comminution circuit and over-consumption of chemicals in the processing plant.

This hypothesis will be tested by introducing an innovative framework related to fingerprinting constitutive material attributes with the following aim:

Aim: Demonstrate the use of a material fingerprinting framework that enables mapping of material classes, which are representative of comminution and recovery behaviour.

These classes further help finding relationships of how differences in geology impact metallurgical plant performance and aid in understanding these root causes. To achieve the aim of the research, the following specific objectives and the related research questions were formulated:

- **Objective 1:** Design and implement a material fingerprinting framework that uses constitutive material attributes as input to identify specific processing optimisation opportunities:
 - Q Is it possible to separate geological material characteristics resulting in distinct classes in a data-driven approach that may be relevant to process optimisation choices?
- **Objective 2:** Once the framework is designed and implemented, study the relationships of fingerprints with the processing behaviour, specifically at the ball mill.
 - Q Would it be possible to use pre-characterisation methods to distinguish between material classes that will behave differently in the processing plant?
 - Q Based upon our understanding of the geology and mineralogy, what is the root cause of the detected performance losses/gains?
- **Objective 3:** Development of a data-driven approach to geometallurgy with the aim to make optimal operational decisions, e.g., advancements in tactical geometallurgy:
 - Q What are the decisions required to optimise the plant feed and/or operational decisions to reduce performance losses and improve the future behaviour of the processing plant?
- **Objective 4:** Validation of data relations with a pilot study:
 - Q To what extent are variations in actual performance caused by differences in the feed material properties?

The presented dissertation on fingerprinting of material attributes is based on data from the Tropicana Gold Mine (TGM), Western Australia. Over 20+ years, the mine carefully collected, documented and stored every sample measurement in a database. A portion of this data is considered, analysed and presented in this dissertation.

1.3 Dissertation outline

To achieve the aim and investigate the objectives of this research, this dissertation is divided into 13 chapters. Figure 1.2 provides an overview of how the chapters link with each other. The dissertation is structured as follows:

- Chapter 1 provides a general introduction.
- Chapter 2 provides a literature review of the main literature used in this dissertation.
- Chapter 3 introduces and gives an overview of the material fingerprinting concept.

- Chapter 4 presents a review of data acquisition techniques that were used to capture the data integrated in the dissertation.
- Chapter 5 evaluates various multivariate analysis techniques and explains a few fundamentals about data clustering.
- Chapter 6 introduces the Tropicana Gold Mine, which is the case study mine of this dissertation. This includes the regional and local geology and forms a reference for the remainder of this dissertation.
- Chapter 7 continues based upon Chapter 3 and provides details of the framework related to material fingerprinting. It also includes a discussion on the acquired confidence in material attribute measurements.
- Chapter 8 presents the findings of the multi-element analysis case study. This is a dataset of high-quality used to characterise the geochemical signature of large orebody domains. Furthermore, the chapter gives a first validation of the material fingerprinting concept.
- Chapter 9 presents results of between and within material type variability seen across different orebody domains. These insights were generated from geochemical and mineralogical data captured for daily grade control.
- Chapter 10 develops a (simulation) framework for material tracking using stockpile models.
- Chapter 11 presents how the processing actuals are linked to the input material fingerprints.
- Chapter 12 discusses the objectives, methods and results of this dissertation.
- Chapter 13 summarises the conclusions of the research.

Material Fingerprinting:

Understanding how differences in geology impact metallurgical plant performance

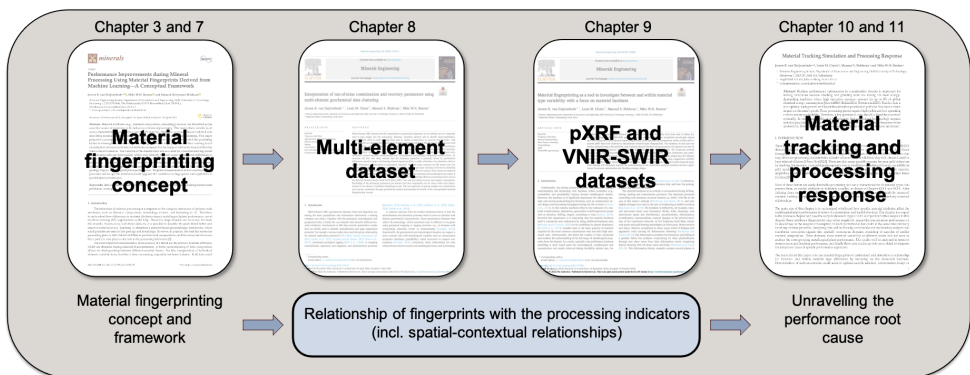


FIGURE 1.2: Dissertation overview.

2

Literature review

This chapter presents a literature review highlighting the need for material fingerprinting. Several aspects of the fingerprinting approach are reviewed, which only have been partly explored in literature but not exploited and applied on a large scale. The chapter further addresses how geochemical and mineralogical data help to develop a link between the geology and metallurgical plant performance with examples from previously published literature. Furthermore, it is indicated how these studies vary compared to the current study and what the current study additionally addresses.

Parts of this chapter have been published in:

van Duijvenbode, J. R. and M. W. N. Buxton (2019). Use of time series event classification to control ball mill performance in the comminution circuit - A conceptual framework. In *Real Time Mining - 2nd International Raw Material Extraction Innovation Conference*, Freiberg, Germany, pp. 114-123, and

van Duijvenbode, J. R., M. W. N. Buxton, and M. Soleymani Shishvan (2020). Performance improvements during mineral processing using material fingerprints derived from machine learning - A conceptual framework. *Minerals* 10(4), 366. doi:10.3390/min10040366, and

van Duijvenbode, J. R., L. M. Cloete, M. Soleymani Shishvan, and M. W. N. Buxton (2021). Material fingerprinting as a potential tool to domain orebody hardness and enhancing the prediction of work index. In *Application of Computers and Operations Research in the Mineral Industry (APCOM 2021)*, Online, pp. 181-192, and

van Duijvenbode, J. R., L. M. Cloete, M. Soleymani Shishvan, and M. W. N. Buxton (2022). Interpreting run-of-mine comminution and recovery parameters using multi-element geochemical data clustering. *Minerals Engineering* 184, 107612. doi:10.1016/j.mineng.2022.107612.

2.1 Material classification

An expected outcome from geochemical studies is that the mineralisation and alteration processes result in zones or domains with distinct geochemical characteristics (CSA Global, 2018; Brauhart, 2019; Escolme et al., 2019; Faraj and Ortiz, 2021; Gaillard et al., 2018; Gazley et al., 2015; Grunsky and de Caritat, 2019; Halley, 2020; Motoki et al., 2015; Zhou et al., 2017). These geochemical domains then reflect the mineralogy, which sometimes may be difficult to recognise using geological mapping or logging practises, e.g., in domains with overprinting alteration events or metasomatism (Caciagli, 2016). Sequentially, the geochemical and mineralogical domains can support a more concrete link with metallurgical variables such as comminution properties (hardness, grindability), metal recoveries or reagent consumption (Caciagli, 2016). However, these relationships are commonly only inferred from extensive small-scale metallurgical tests, such as breakage, liberation, and abrasiveness, as described by Wikedzi et al. (2018) and Lynch (2015) or de Azevedo Barbosa et al. (2021), modelled using simulation (Madenova and Madani, 2021), or focus only on the Bond Work Index (Bhuiyan et al., 2019). The purpose of this dissertation is to address this gap, because published studies that consider the relationships of geochemical and mineralogical material classes with both comminution (processing) characteristics and recovery potential are lacking.

There are two problems in using existing datasets from mining companies in order to examine these relationships and address this gap. Firstly, geochemical datasets are typically challenging to interpret because they are collected across multiple years and using different laboratories, analytical tools with various levels of confidence and methods. Therefore, careful analysis needs to be done to interpret the multi-dimensional data effectively and create confidence in the results (Grunsky and de Caritat, 2019). Secondly, historical data collection (and especially metallurgical test data) typically does not conform to an ideal tiered geometallurgical data structure as was defined by Dominy et al. (2018); Keeney (2010) (further explained in Chapter 7). These two limitations indicate that significant efforts still need to be done to fuse multi-element (ME) proxy data (or other geological data) with the comminution and recovery characteristics at a large scale.

So far, only a limited number of published geometallurgical case study examples were successful in stitching the geology and processing data together. For example, Bhuiyan et al. (2022) demonstrate that a portable X-Ray Fluorescence (pXRF) to Bond Work Index (BWi) relationship is favoured in order to acquire a relationship. Wambeke et al. (2018) show the use of a similar relationship for the application of real-time reconciliation of BWi values, whereas, in Johnson et al. (2019), the mine favours a Visible Near Infrared - Short Wave Infrared (VNIR-SWIR) hyperspectral imaging application to predict recovery and throughput. Other studies show material characterisation of solely VNIR-SWIR mineralogy along drill holes (Abweny et al., 2016; Arne et al., 2016; Kazimoto, 2020) or mineralised outcrops (Booyesen et al., 2022). Only the study from Wambeke et al. (2018) discussed that a previously characterised material classification or fingerprint (in the Resource block model) also exists as a fingerprint at a later stage in the processing plant. This ability and characteristic should form part of the foundation of these data-driven fingerprints to better characterise material.

Recent machine learning techniques have also been applied to in the literature on understanding, for instance, the feed material composition. Some examples include, but are not limited to: image analysis of ore composition on conveyor belts (Tessier et al., 2007) and analysing of drill-core textures (Tiu, 2017; Donskoi et al., 2015); hyperspectral face scanning for mineralogical compositions (Austin et al., 2019; Koerting, 2021); mineralogy and textural relationships with grindability (Tøgersen et al., 2018; Bulled et al., 2009); or real-time reconciliation of a geometallurgical model based on actual plant performance (Wambeke et al., 2018). These examples indicate that measured and correlated variables should be jointly considered to improve the understanding of how geology impacts metallurgical plant performance. Neglecting these correlations will result in a loss of information. The geological attributes of plant feed data are key for the mill performance, so if it is possible to have data fusion of various sensors responses that could resemble all the material (like a fingerprint), then it could give insight into the plant behaviour.

Generally, after the geology team carefully characterised the material to be mined, there is a handover of the material information to the mine planning and scheduling team. They will ensure that the material is mined promptly and allocated to the correct destination, i.e., unmineralised material to the waste dump, higher-grade or material that meets the specified or desired cut-off grade material to the stockpile, or the crusher. Thus, the only constant factor between these teams, and also the plant operating team, is the material they are dealing with. This implies that it is of utmost importance that the material is similarly classified or treated from the beginning to the end. The material only appears in different forms; initially, the material is studied in the context of resource modelling and then used in a Reserve block model for mine planning and grade control. Next, the material or fingerprint is within a truck and stockpile, and finally, it is on conveyor belts or in pipes in the processing plant. Having a uniform classification throughout all these processes and having the ability to track the fingerprint composition at any time gives an opportunity for optimisation and eventually reduces cost and increases revenue.

Tracking and modelling the ore flow between the mine and the mill has been subject to various studies. Some studies used an average ore transportation time (Varannai et al., 2022) or detailed mass balance systems (Both and Dimitrakopoulos, 2021; Meech and Baiden, 1987; Wambeke et al., 2018). Other studies focused on the mass flow within the stockpiles themselves and used painted rocks (Parker, 2009) and radio-frequency identification (RFID) tracers (Jansen et al., 2009) or based the tracking upon silver mineralogy and texture in a multi-stage flotation process (Tiu et al., 2021). Servin et al. (2021) created a digital twin of a mine flow using pseudo-particles representing material and simulated the particle flow from mine to mill. A common practice in most of these applications is to characterise the stockpile or mass flow using a single arithmetic weighted average of grade and tonnage values (Morley and Arvidson, 2017). However, this results in a lack of temporal knowledge about the material variability and spatial variability within the stockpiles or material flow themselves. Therefore, proper stockpile management is of utmost importance in order to keep track of the material quality (Zhao et al., 2015).

Young and Rogers (2021) indicated the importance of modelling large (lower-grade) long-term stockpiles as these are often underrated and tend to have limited precision

(high variability) in terms of the quantification of their material characteristics. Stockpiles can be created with different objectives (Assimi et al., 2021; Young and Rogers, 2021), such as run-of-mine (ROM) stockpiles, which usually blend material characteristics and provide opportunities for tactical blending. Pre-crusher stockpiling is often used for its operational simplicity. However, this lowers confidence in the ore grade and reduces feed quality certainty (Jupp et al., 2013). A general review of stockpiles, their classifications (Assimi et al., 2021; Young and Rogers, 2021), and reconciliation practices (Morley and Arvidson, 2017) will not be further discussed for brevity.

So far, two prior studies, related to material tracking, have been conducted at the case study mine of this dissertation. Firstly, Wambeke et al. (2018) presented a real-time resource reconciliation pilot study based on 120 hours of mill performance data with relatively simplistic build/reclaim cycles for the ROM stockpiles using a month's truck cycle data. Secondly, Both and Dimitrakopoulos (2021) implemented a similar material tracking system but used a daily interval resolution for a half year of data. The main shortcoming of both studies is that they did not consider material attributes that adequately characterise the mineralogical and geochemical attributes of the feed. The current research is applied at the same mine, however, the tracking implementation needs to be changed, expanded and advanced. This should comprise stockpile modelling for short-term and long-term stockpiles and being able to follow material over at least longer than one year.

Thus, to interpret varying comminution or recovery characteristics fingerprinting and tracking material from different geological domains are essential, which reflect changes in mineralogy, rock texture and rock competency. One could consider clustering elemental concentrations as a first step to constructing these fingerprints. Clustering is a method to partition samples with similar characteristics (Romary et al., 2015). In the case of multi-element data clustering, this results in a geochemical signature and may correlate to a specific suite of minerals, but also with physical and mechanical properties such as grain size, texture, hardness, or brittleness of the related material. For example, Hunt and Berry (2017) show the correlation between Point load index and Equotip across different deposit styles. Although the current study focuses primarily on using geochemical and mineralogical data, material fingerprints should ideally be constructed using a multivariate combination of geophysical and geomechanical data as these constitutive attributes can easily be added to the fingerprints during clustering. In general, this process can be considered an addition, refinement or validation of the clustering classes or fingerprints.

2.2 The impact of material hardness

Hardness refers to the resistance of a material to indentation, penetration or deformation by means such as abrasion, drilling, impact, scratching or wear (Lynch, 2015). The material hardness is a record of the meso- and microscale shear zone kinematics (i.e., faults, folds, shearing), rock formation processes, rock massiveness (grain size distribution), unconformities and deformations (Bonnici, 2012). Commonly, this is mineralogically expressed as differences in crystallisation, metamorphism, textural changes or the mechanical hardness of the constituent minerals (Tiu, 2017). For example, the dominant rock formation processes yielding the original rock hardness

at the orebody of the Tropicana Gold Mine occurred between ca. 2640-1140 Ma (Blenkinsop and Doyle, 2014). Since then, it only slightly changed over time due to weathering effects at shallow surfaces (Ogunsola et al., 2017). During operations, the material hardness is encountered during drilling, blasting, loading and comminution processes.

Understanding the resistance, mechanical attributes and rock formation processes is material specific and determines the crushability and grindability of orebody domains. Since the crushing and grinding units are among the most energy-demanding machines (Jeswiet and Szekeres, 2016), it is important to take material hardness into account to determine optimal energy usage. Consequently, material hardness informs strategic and tactical geometallurgical decisions, such as comminution circuit design and forecasting throughput during the life of mine (Dominy et al., 2018). Traditionally, the mining industry focuses primarily on testing hardness during dedicated metallurgical studies before mining (e.g., King and Macdonald, 2016; Michaux and O'Connor, 2020). The mineralogical, metallurgical and comminution test results retrieved during such feasibility studies are used for preliminary hardness modelling (see, for example, de Azevedo Barbosa et al., 2021; Montoya et al., 2011). However, in such metallurgical studies only limited efforts are made to determine why and how the mineralogy and rock texture impacts the material hardness.

An analysis of the deformation history from an ore deposit may help to understand the combined causes describing the material hardness. For instance, at the Tropicana Gold Mine, biotite with pyrite and gold assemblages (at other parts, biotite-sericite and minor chlorite) crystallised in shear zones in K-feldspar pegmatitic rocks (during D3 deformation following Blenkinsop and Doyle, 2014). This deformation postdates the formation and folding of a gneissic fabric but predates overprinting by other phyllosilicates through new shear zones from later deformation events comprising dextral shearing (D4, D5 shear zones and folds following Blenkinsop and Doyle, 2014). This deformation history contains several phases in which mineralogy and texture of the rock has changed, which affected the original rock hardness. Other factors that may affect ore processing characteristics include volumes that are silicified, clay rich, sheared, and/or have internal dilution (Hoal and Frenzel, 2022). Therefore, fingerprinting can potentially describe hardness variability due to its link to distinct domains of hydrothermal mineral phases (Molnár et al., 2017; Roache, 2019), fluid pathways in shear zones (Hood et al., 2019), or deformation events (Blenkinsop and Doyle, 2014).

Besides the direct impact of hardness on crushability and grindability there are also several indirect impacts caused by variability in and/or insufficient understanding of material hardness. For instance, Both and Dimitrakopoulos (2021) showed evidence for the Tropicana Gold Mine that typically harder material corresponds to lower throughput and softer material with a higher throughput. Furthermore, insufficient grinding efficiency causes a poor gold grain exposure resulting in a poor gold extraction by leaching. There is also variability in gold speciation, gangue mineralogy with cyanide and oxygen consumers (i.e., arsenic, sulphides) or other deleterious minerals (clay) or coarse gold (Coetzee et al., 2011), which may require longer retention times if the material is not milled sufficiently. Most of these factors are easily detectable pre-mining and can be used to characterise different material types, as shown in Chapter 8 and 9.

2.3 Summary

The literature review revealed among others the following key gaps:

- Metallurgical relationships are commonly only inferred from extensive small-scale metallurgical tests and there is a lack of finding associated relationships with geochemical and mineralogical characteristics.
- Insufficient understanding on the cleaning and data preparation practices for large industry datasets. In addition, there are only a limited number of published geometallurgical case studies stitching geology and processing data together.
- Documentation of an application that can track and model the ore flow between the mine and the mill is limited or only subject to implementation by commercial software packages. In addition, the main shortcoming is that these applications lack the tracking and characterisation of mineralogical and geochemical attributes.
- There is no methodology that facilitates linking processing plant feed attributes with the production actuals. These two large multivariate datasets contain data at regular intervals, but require a more objective, multi-scale and open to classification method to domain periods with similar processing conditions.

The highlighted research shortcomings from the previous paragraph are addressed in this dissertation, and therefore, the contributions to literature are:

- Insights into the confidence of different datasets that can be used to adequately characterise material (Chapter 7).
- Clustering of geochemical and mineralogical data to characterise material signatures. These results will be analysed in relation to observed hardness and recovery proxies from similar samples (Chapter 8 and Chapter 9).
- Material fingerprints will be considered in a spatial context to characterise domains where specific fingerprints may be more abundant than other (Chapter 8 and Chapter 9).
- Characterisation of the material needs to be consistent (and tracked) from the mine through all unit processes to the processing plant in order to link processing response to the material (Chapter 10).
- The material characteristics will be analysed in terms of consequences on mineral processing to define true geological root causes defining this behaviour (Chapter 11).

Chapter 3 to 6 will further facilitate the understanding of the main research described in Chapter 7 to 11. In particular, these chapters will define, introduce and explain the material fingerprinting concept (Chapter 3), the different data acquisition techniques (Chapter 4), multivariate analysis techniques and clustering (Chapter 5) and background information on the Tropicana Gold Mine (Chapter 6).

3

Material fingerprinting – Part I: concept



This chapter presents a brief overview and general workflow of the material fingerprinting concept. It explains the general concept, which aims to better adhere to the complex and inherent material heterogeneity. It puts a new perspective in contrast with the more traditional geometallurgical modelling approach. Chapter 7 is closely related to this chapter and will provide more details about the material fingerprinting framework. It focuses on the executed methodology as applied in this dissertation.

This chapter is based upon a concept research proposal originally drafted by M. W. N. Buxton and T. Wambeke. The initial proposal forms the basis of the work outlined in this chapter and has evolved since then and is adapted for this dissertation chapter. Parts of this chapter were published in: **van Duijvenbode, J. R.**, M. W. N. Buxton, and M. Soleymani Shishvan (2020). Performance improvements during mineral processing using material fingerprints derived from machine learning - A conceptual framework. *Minerals* 10(4), 366. doi:10.3390/min10040366, and **van Duijvenbode, J. R.**, L. M. Cloete, M. Soleymani Shishvan, and M. W. N. Buxton (2022). Interpreting run-of-mine comminution and recovery parameters using multi-element geochemical data clustering. *Minerals Engineering* 184, 107612. doi:10.1016/j.mineng.2022.107612.

3.1 Definition

The rationale behind material fingerprinting is to create a data-driven link between ore and the comminution behaviour by means of material “fingerprints”. A fingerprint contains attributes or a combination of attributes based on data from material measurements at a given time and location which serve as unique identifiers. Ultimately, it is an indication of a material class that can inform or influence the processing behaviour.

Definition: A material fingerprint is a machine learning-based classification of measured material attributes compared to the range of attributes found within an exploration area or defined using available mineral resources or reserves (van Duijvenbode et al., 2020).

Figure 3.1 shows several general locations or moments where ore fingerprints can be defined and indicates how the fingerprint is present from the exploration or mining phase until the grinding and eventually leaching phase. Realistically, the fingerprint composition changes in each phase (dilution, blending, etc.), and at several phases, there are knowledge gaps because the composition can only be simulated using material tracking at a certain resolution. Measurements of fingerprint attributes at the crushing and grinding stage (e.g., belt geochemistry or mineralogy analysers) could validate the fingerprint composition at those stages and help relate fingerprints to the material origin and increase confidence in the material understanding. In addition, the identified locations of gaps in Figure 3.1 could indicate new strategic locations for geological attribute measurements.

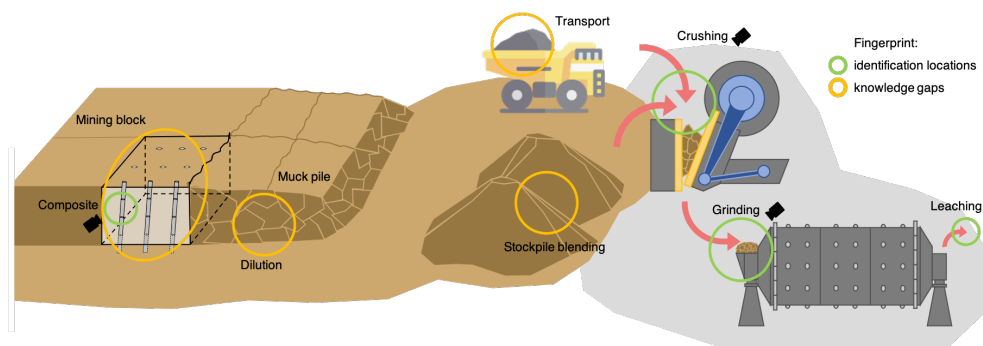


FIGURE 3.1: Fingerprint identification (green circles) and fingerprint composition knowledge gaps (orange circles) from the exploration/mining until the grinding stage.

3.2 Concept

The newly proposed geometallurgical or material fingerprinting approach consists of three fundamental components which are schematically summarised in Figure 3.2.

The concept aims to forward predict the metallurgical response of an available blending option or fingerprint. In an ideal scenario, if the predictions indicate that the blend results in an undesirable response (e.g., lower throughput, increased reagent consumption), the blend could be adjusted accordingly. The following three components form the basic foundation of the material fingerprinting concept:

1. **Material characterisation** (also see Chapters 8 and 9): Mineralogical and geochemical composition, rock texture and fracturing are mostly linked with the root cause of geometallurgical variation. The presence of primary rock attributes (compositional properties, e.g., mineral and elemental) defines the secondary material attributes (physical properties, e.g., density, texture and mechanical properties, e.g., hardness). It is inferred from proxy measurements of available sensor technology (see Chapter 4). The combination and interactions of the primary attributes can be used to define “fingerprints” for material characterisation and classification. Additionally, fingerprints will be constructed such that fingerprint blending can be performed, similar to material blending. The understanding of plant performance is then primarily based on these primary fingerprints and may eliminate the need for testing secondary rock attributes. If the root cause is understood and similar geometallurgical conditions are observed elsewhere in the deposit, then it is possible to extrapolate plant behaviour predictions with reasonable accuracy.
2. **Material tracking** (also see Chapter 10): Success depends on constructing a relatively accurate material tracking model from mine to mill. The main task of the model is to track or follow the fingerprints of each truckload from the moment of excavation through stockpiles to the plant, including direct crusher tips and stockpile blending. The tracking model is vital in constructing an extensive database linking the processing responses with material fingerprints.
3. **Model development** (also see Chapter 11): Machine learning (ML) techniques are applied to the linked data from Step 2. These data will be used to train, test and validate models and build confidence in the reliability and utilisation of the knowledge. This results in a direct data-driven transition from primary fingerprints to predicted behaviour (informed by actual plant response). In contrast, the conventional process consists of translating secondary rock attributes to predicted behaviour based on an empirical incomplete validated relationship.

From a holistic viewpoint, the aim of the material fingerprinting concept is to avoid putting attributes or samples in “boxes”, which are typically associated with a quantitative or categorical pre-defined description (e.g., specific lithological or mineralogical groups, low vs. high classifications). Instead, the fingerprinting approach will still group attributes or samples, but what this group entails is merely defined and constrained by all the samples and constitutive attributes belonging to the group, and this is not a priori defined.

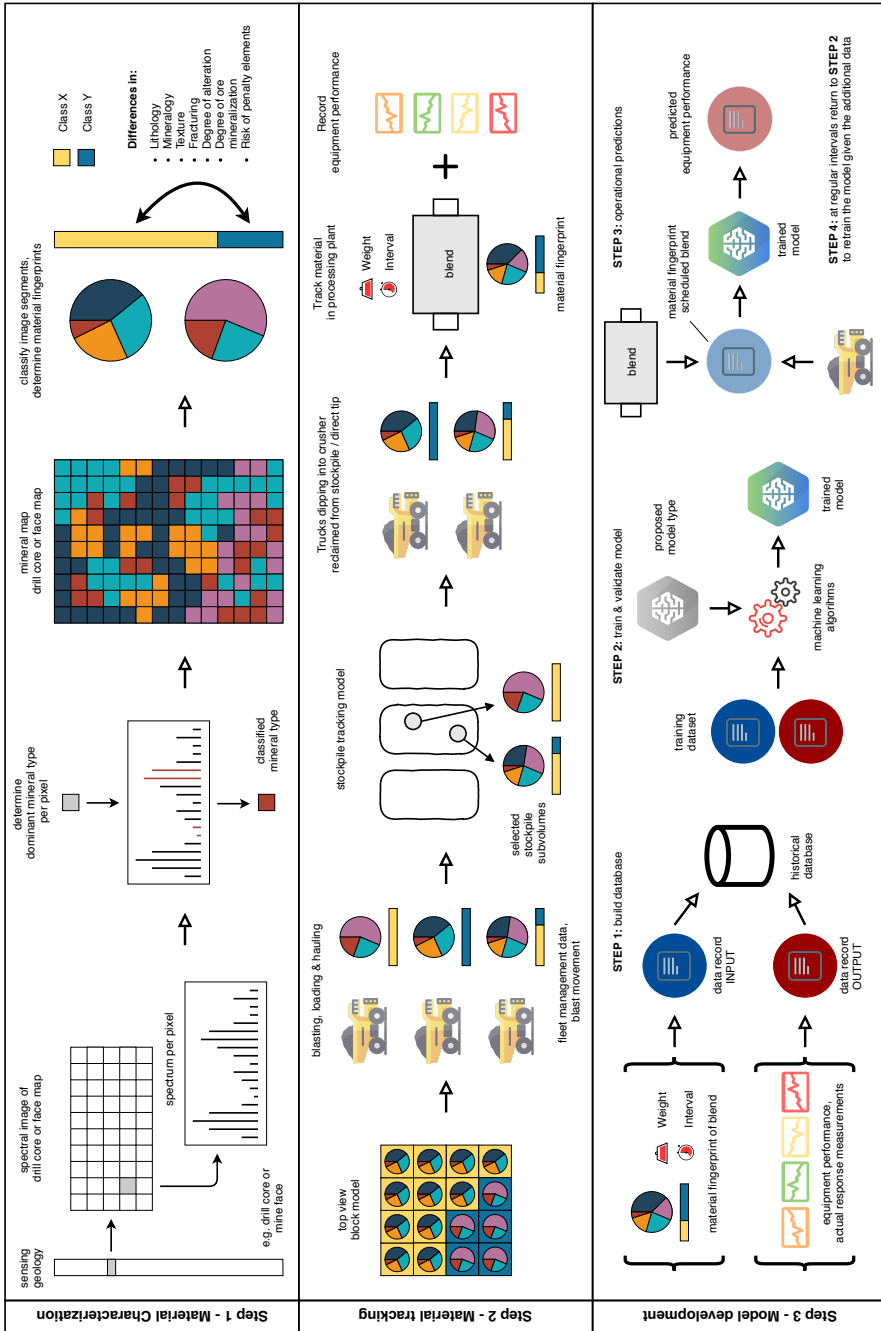


FIGURE 3.2: Material fingerprinting concept overview, after M. W. N. Buxton and T. Wambeke. See Chapter 7 for more details about each step.

3.3 Differentiation from traditional geometallurgy

The fingerprinting concept includes various enhancements to the more traditional geometallurgical approach. For instance, fingerprinting puts more emphasis on using proxy data to find relationships with harder-to-obtain datasets. Traditional geometallurgy uses mainly results from time-consuming metallurgical laboratory testing of secondary rock attributes (e.g., strength, hardness) which are relatively expensive compared to assay testing. This results in a low number of available data points from which plant performance is modelled and designed. Furthermore, these metallurgical test data are generally not indicative of the root cause affecting the specific plant performance (e.g., presence/absence of certain material types).

The sparse data availability affects the fidelity of spatial estimates in traditional geometallurgical models. It sometimes causes spatial modelling to be impossible, generates low confidence results or is indicative for only a distinct (small and local) area. Consequently, plant performance predictions are often only accurate on a large scale and can't capture local variability, limiting their application during operational decision-making. Occasionally higher-order mathematical relationships are developed using proxy data to approach characteristics of the processing response (e.g., Keeney et al., 2011; Lopera, 2014). However, most of the times mining operations do not fully grasp the value of a structured data collection effort resulting in an insufficient amount of data to rely on.

In addition, historical data collection typically does not conform to an ideal tiered geometallurgical data structure, as presented in Figure 3.3 (Dominy et al., 2018; Keeney, 2010). An introduction to the data acquisition techniques shown in Figure 3.3 and used in this study, will be presented in Chapter 4. In practice, for adhering to the fingerprinting concept, samples should be selected to collect data for each level using various techniques because at each level, the samples have varying support, confidence and spatial coverage. At increasing levels, the relationships to the processing signatures and thus confidence increases. However, testing samples becomes more expensive, which results in fewer samples being measured. For example, there are only limited moments that a mine performs detailed metallurgical laboratory tests from Level 3 or Level 4. Often this is only linked with pre-feasibility or feasibility studies of new areas or extensions of domains.

The problem is that geometallurgical proxy data (Level 1), typically does not provide a direct measure of metallurgical response. However, it can still be used to infer metallurgical characteristics via correlations as part of the fingerprinting concept (e.g., similar to Johnson et al., 2019; Bhuiyan et al., 2022). In contrast, historical Level 3 and 4 data (representing most metallurgical tests) are commonly not co-located to lower-order data types, and insufficient effort is made to establish direct correlations to Level 1 or Level 2 data types. Conversely, most samples collected during daily operations of the mine are from Levels 1 and 2. If good correlations are established between Level 1 to 4 since the inception of a project, it is possible to use more densely spaced proxy or support data at a later stage. The establishment of such correlations is desirable because more densely spaced proxy or support data provides a more representative view of ore variability across and within domains. This in turn drives inherent metallurgical characteristics that may ultimately manifest as process response variability.

The adherence to such a tiered geometallurgical data structure should be implemented as a standard procedure on mine sites as part of the fingerprinting concept to establish relationships between the geology and metallurgical plant performance. Another benefit of employing the ideal tiered geometallurgical data structure is that it allows one to proactively domain the deposit of interest and align subsequent metallurgical sampling to the resulting domains. This ensure a more effective coverage, which is especially important when dealing with the allocation of sparse higher-order tests.

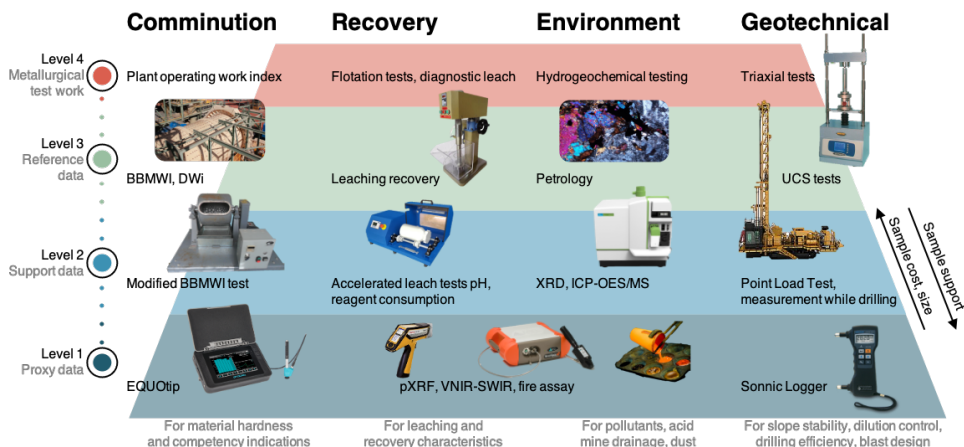


FIGURE 3.3: Tiered geometallurgical data types, after Dominy et al. (2018); Keeney (2010), and L. M. Cloete, personal communication. The exemplary tests or techniques may move between levels depending on their application. Image sources: manufacturer brochures or websites, AngloGold Ashanti, T. Roache. For abbreviations see List of abbreviations.

3.4 Challenges

For each of the indicated concept components (Section 3.2) are some data limitations or key challenges identified that need to be considered while using the material fingerprinting concept.

Material characterisation:

- Key geological attributes include chemical composition, mineralogy, alteration and texture. Two rocks with identical chemical composition may, for example, not exhibit consistent comminution behaviour on account of mineralogical and/or textural differences.
- Typical material attribute measurements tend to be fairly noisy (data variance) and relate to material heterogeneity. Data must be effectively filtered and calibrated to resemble the true material attributes. It also needs to be normalised over the different years and conditions of testing devices.

- Continuously cross-calibration and validation are needed for the material proxy datasets, allowing to switch between datasets based on availability effectively. Any existing overlap in datasets will be of great interest. Collection of colocated data is of key importance.
- The ability to discriminate the root cause may be limited by the ability to find material classes, maximise the across class variability, minimise the within-class variability and connect classes with the root causes. In addition, differences in processing behaviour may be due to different processing conditions and not only material attributes.

Material tracking:

- Non-linear relationships of material blending do not necessarily complicate the tracking model. However, they will make it more challenging to make models capable of blending the fingerprints and accurately relating them with plant performance.
- Material recirculation in the comminution circuit should be defined. Recirculation will force the need for defining new blend fingerprints originating from fingerprints at that moment in the circuit.
- The actual representative scale of material packages changes throughout the tracking process. Initially, fingerprints defined within the grade control block model are split across various trucks transporting the rocks to their destination. This would be a fingerprint encompassing the truckload material. A truck fingerprint is typically split into smaller particles in the processing plant and spread across a longer time frame due to material flow (i.e., the original fingerprint disperses).

Model development:

- This work relies on the availability of large datasets representing the material variability present at the mine. So far, about nine years of production data are available. Considerations should be made whether that are enough data points (event labels) to train large models. A potential solution is the creation of synthetical data or an artificial environment to produce data.
- Performance decisions (e.g., keeping a constant gold grade or certain oxide blend) could be made in favour of the crushing, grinding or leaching stage and could also be achieved by proper material blending. However, once material enters the comminution circuit, it is difficult to rehandle the material, and any pre-classification should be done through stockpiling before the crusher.
- Comminution should consistently be evaluated from both a breakage (blasting/crushing, etc.) and grinding (milling) perspective. Brittle minerals may, for example, be relatively easy to crush but may be difficult to mill.

- At this stage, out of scope, but ultimately both the strategic and tactical models will benefit from real-time updates based on actual performance data streamed from plant sensors. This will back-inform calibration assumptions and should, over time, give insight on complex blending effects, which are likely non-linear.

4

Data acquisition techniques



This chapter presents a review of data acquisition techniques that were used to capture the data integrated in this dissertation. This chapter forms a comprehensive summary describing the capabilities and limitations of the techniques. The reader is referred to cited references for a more detailed description. Each technique's output can potentially contribute to the generation or enhancement of material fingerprints.

News articles: “The willingness within the mining industry to adopt new technologies is growing over the past years. Some recent news articles capture how mining companies are often frontiers in adopting or testing new techniques. For instance, companies are already testing the use of hydrogen-powered mining trucks and blast hole drill rigs^a; adoption of autonomous drill fleets^b; companies invest in satellites with up to 5-meter resolution hyperspectral imaging cameras^c, use of drones for metal and critical minerals exploration^d. But also, ore transportation using a mineral transport vessel propelled partially by sails.^e”; All articles were accessed at 14 January 2022.

^a<https://im-mining.com/2021/08/30/fortescue-future-industries-begins-testing-hydrogen-powered-mining-truck-blasthole-drill-rig/>;
<https://www.bbc.com/news/business-59576867>

^b<https://www.macmahon.com.au/en-au/latest-news/item/39-trop-auto-drill>

^c<https://www.mining.com/rio-tinto-satellite-startup-launch-early-partnership/>

^d<https://www.australianmining.com.au/news/bhp-aligns-with-kobold-for-billionaire-backed-exploration-tech/>

^e<https://www.mining.com/web/vale-set-to-receive-first-ever-wind-powered-ore-carrier/>

4.1 Introduction

If geological attributes were to be identified as the source of changing plant behaviour, then they can act as key characteristics to resemble material. The occurring differences can then be found, for instance, in lithology, mineralogy, texture, fracturing, degree of alteration or the degree of ore mineralisation. These profound differences can be identified due to recent developments in sensor technology which have shown the potential to collect information on metallurgical properties directly or by measurement of proxies.

Selecting the type of sensor data to characterise material depends on discoverable events in the sensor response data with respect to the material attributes measured. Figure 4.1 shows a typical data collection (sampling) overview using a range of techniques implemented at mine sites, including the distribution of samples and tests across the different geometallurgical levels. Note that the corresponding level related to these data acquisition techniques can change depending on the focus of the study. The datasets used and described in this dissertation are highlighted and briefly explained. Finally, Section 4.5 presents an overview of the different combinations of techniques used in each chapter.

4.2 Geochemical properties

Geochemical analyses (or assays) provide qualitative and quantitative information on the geochemical composition in a sample media. Some elements are present with depleted, background/normal level or enriched concentrations and are suitable to use as high data-quality exploration datasets. These datasets are typically used

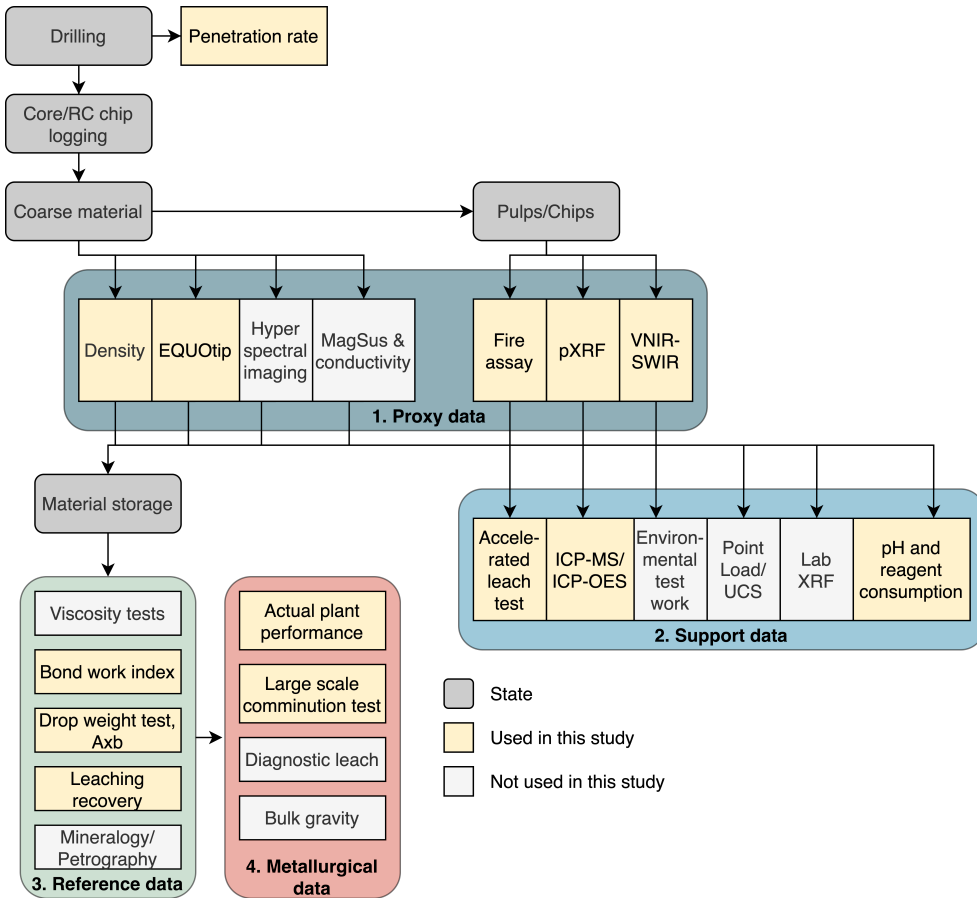


FIGURE 4.1: Overview of a typical geometallurgical data collection workflow and techniques used on mine sites. The techniques used in this study are highlighted in yellow.

throughout the entire life cycle of the mine. The four analytical techniques (four-acid digest, X-Ray Fluorescence, fire assay, leach recovery) explained in the following sections are well suited to capture most of the decomposition for geological materials.

Geochemical surveys intend is to provide a spatial geochemical description of the general geology or dominant geochemical processes as expressed in the rocks being sampled (Grunsky and de Caritat, 2019). The assay results are especially useful as they can create plots of the major elements that show stoichiometry of the expected alteration minerals (Brauhart, 2019). This can be used to classify rock composition or alteration mineralogy. For example, a K/Al vs Na/Al molar ratio plot maps the sericite alteration; an Al-K-Mg ternary plot maps relative proportions of sericite vs chlorite; a Ca-K-Na ternary maps feldspar compositions and shows if Ca is lost or retained as feldspars are altered; a Ca-Fe-S ternary plot maps pyrite and anhydrite (Halley, 2020).

4.2.1 Four-acid digest

A four-acid multi-element analysis is an effective laboratory technique that first prepares a sample by digestion and then analyses the elemental composition using a spectrometer. The technique involves mixing the sample, usually in the form of a powder, with a combination of nitric, perchloric, hydrofluoric and hydrochloric acid to break down most silicate and oxide minerals allowing for a “near-complete” analyses of most minerals and analytes. During the dissolution, care should be taken to minimise the loss of volatile elements such as As, Se, Sb, Te, and Tl, while minimising retention of Al and Ti (Halley, 2020; Hu and Qi, 2014).

After digestion, the sample is sent to an analytical instrument that measures the elemental concentration. These instrumentations typically provide 48 elements in their standard elemental suite, but it is possible to analyse up to 60 elements. Inductively Coupled Plasma (ICP) techniques are the most common and can have various finishes, such as Optical Emission Spectroscopy (ICP-OES) and Mass Spectrometry (ICP-MS). The acid digest is converted at high temperature to a plasma in these techniques. Subsequently, an optical emission spectrum (ICP-OES) is produced where each element has a unique emission spectrum. Alternatively, ICP-MS can be used to separate the elements or molecules based on their unique mass signature (Grunsky and de Caritat, 2019). These inherent differences make each technique more suitable for a particular suite of elements. See Chapter 8 for an example of the combinations between elements and the preferred instrumentation retrieved from laboratory data.

These techniques have a few limitations regarding the use of acids because they dissolve silicate minerals and are thus sample destructive. For example, if the four-acid digest was not taken to incipient dryness before adding the hydrochloric acid, then Al, Ti and other trace elements tend to remain in the test tube as an insoluble fluoride complex. Zircon is also a difficult mineral to dissolve and may relate to significantly underreported Zr, Hf, Y and heavy rare earth elements. Chromium is also frequently underreported (Yamasaki et al., 2016).

4.2.2 X-ray fluorescence

Portable X-ray fluorescence (pXRF) has become a routine analytical tool for geochemical analysis. It is useful for screening large numbers of intermediate to ore grade elements quickly and cost-effectively. Within the mining industry, measurements are typically taken on grade control drill samples (drill chips) such that the results can assist daily in geometallurgical characterisation and lithological differentiation. Within this dissertation, the pXRF measurement results also come from grade control assays and form one of the largest datasets. This results in a spatially dense understanding of the material attributes and can, for instance, be used to classify material before sending it to its appropriate destination rapidly.

The XRF device has an X-ray source that illuminates the sample, which results in the ionisation of its constitutive elements. This ionisation causes movements of electrons between the electron shells and, in doing so, emits fluorescence (electromagnetic radiation) with wavelengths (0.01 to 10 nm) unique to each element. Detecting these energies and intensities will relate to a sample’s atomic makeup and determine the elemental concentrations (Gazley and Fisher, 2014).

A few limitations related to the use of pXRF will be discussed next. Firstly, it has relatively higher detection limits than laboratory-based assay methods because it is less sensitive and has a more comprehensive element suite. Secondly, a pXRF instrument can be optimised and calibrated for a certain rock type or matrix. However, measuring a different rock type may give erroneous measurements (Gazley and Fisher, 2014). Thirdly, the focal point of a pXRF measurement is about 10 mm in diameter. Thus, a sample needs to be homogenised appropriately to be representative. Fourthly, moisture in samples weakens X-rays and results in lower concentrations measured (Parsons et al., 2013). The previous two issues can be minimised by pulverising and drying the samples before analysing them. Moreover, each device needs to be calibrated, and appropriate quality assurance and quality control checks must be in place. See Gazley and Fisher (2014) for a more detailed overview regarding the appropriate use of pXRF.

Example 4.1: This example shows a typical trade-off that needs to be made prior to selecting the analysis method. Many rock types are composed of silicon dioxide (SiO_2), of which the abundance is an indicator of the rock composition. Unfortunately, four-acid digestion methods are unable to measure Si as one of the key elements. It forms a volatile SiF_4 complex during the reaction with hydrofluoric acid in the digestion process (Hu and Qi, 2014). Therefore, the preferred analysis method of Si is using a lithium borate fusion, but this requires the preparation of a fused bead prior to digestion, which increases interference effects during analysis (Halley, 2020). Silicon can also be added to the suite of elements using a pXRF measurement, but this may again give lower measurement precisions.

4.2.3 Fire assay

Fire assay is similar to four-acid digestion, a preparation method performed before analysing the samples using ICP-OES or ICP-MS. This method is vital in determining the precious metal content of samples (Au, Ag, Pt, Pd) as the unique chemical properties of these elements pose challenges in normal geochemical analysis. They often occur heterogeneously (nugget effect) and in small quantities in geological material. This makes it difficult to measure the concentration from only a small sample amount (IPMI, 2015). Additionally, acid digestion can lose gold due to preg robbing (adsorption) if specific sulphides or carbonaceous matter is present (Miller et al., 2016; Mustapha et al., 2014).

After sample preparation, the samples and activator chemicals are placed in crucibles and heated to more than 1000°C with lead oxide. The heat will melt the sample into a metal-lead mixture and a slag containing the base materials and other contaminants. These two parts are then split by cupellation. After heating the gold-bearing part again, there will remain a small amount of precious metal which can be analysed (Hu and Qi, 2014; IPMI, 2015).

4.2.4 Leach recovery

Leach recovery tests using ore material define how much cyanide extractable gold is in a sample and how long it takes to extract this. This amount indicates the potential bulk recoveries while processing similar material in metallurgical processes and circuits. The technique is typically based on pulverising a sample for a fixed time to produce an average of 80% passing 75 μm (similar product size obtained after the ball mill). The sample is then combined with a leach solution including sodium cyanide (NaCN), sodium hydroxide (NaOH) and typically also with LeachWELL™, which is a cyanide leach accelerating agent (MPC, 2018). After mixing, the resulting solution can be sampled and analysed at various time intervals using ICP-MS for Au (Intertek Genalysis, 2019; SGS, 2020).

The total Au concentrations measured in the slurry, solution and solids at different stages of the process is typically defined as the head grade. Then, the ratio of the total gold removed from the solution and head grade will determine the total gold extraction percentage or recovery. The tail or remaining solids are typically analysed for gold using fire assay (because it should have much less Au) and define the tail grade. This is typically the residue that will be stored in the tailings storage facility, so it should be as little as possible. It is also important to consider the reagent consumption (e.g., NaCN and NaOH) for each test because these materials may form a significant cost. Trade-offs should be made between a higher recovery or an increased reagent consumption.

4.3 Mineralogical properties

Mineralogical properties of rocks are commonly collected using reflectance spectroscopy on the visible and near-infrared (VNIR) and short-wave infrared (SWIR) spectral range. This range from the electromagnetic spectrum is useful since it will detect diagnostic features produced by specific minerals. These features are diagnostic for the constituent minerals and other components and properties such as abundance, chemical bonds and crystalline structure (Laukamp et al., 2021). However, the downside is that most major rock-forming minerals have an abundance of potential vibrational modes. Thus, a thorough understanding of potential factors (spectral mixing) contributes to the resulting reflectance spectra (Laukamp et al., 2021). This also reflects that only a particular group of minerals (e.g., iron oxides, sulphates, micas, amphiboles) can be identified on the VNIR and SWIR spectral ranges (Clark and Rencz, 1999; Terracore, 2022), see Laukamp et al. (2021) for one of the more recent updates and reviews on characteristics of the mineral structure and groups. Note that minerals not active in these ranges may, however, show signatures at longer wavelengths >2500 nm. Analysing infrared reflectance spectra is typically done by spectral geologists and can add significant value to the mineralogical understanding (fingerprinting) of an orebody.

4.3.1 VNIR-SWIR spectroscopy

Mineral characterisation using VNIR-SWIR spectroscopy works similarly to pXRF. However, VNIR-SWIR mineral spectroscopy uses wavelengths in the range of 500 to

2500 nm, whereas pXRF uses X-ray (0.01 to 10 nm). The VNIR is typically from 350 to 1000 nm and is based upon the electronic absorption features, SWIR is from 1000 to 2500 nm and reflects vibrational absorption features in minerals (based on Clark and Rencz (1999) and Gupta (2017)).

Interpretation of mineralogical properties from VNIR-SWIR is commonly done using the position and intensity (troughs and peaks) of the absorption features since they state something about the mineral or the element causing the absorption or vibration. Figure 4.2 shows a summary of absorption feature locations as seen in many, but not all, minerals due to crystal field absorptions. This can be used for the identification and semi-quantification of minerals. This exercise is almost always related to correlating multiple features observed at different wavelengths (Pontual et al., 2008).

In the VNIR region, there are elements depicted or elements associated with the absorption feature, which are element transitions, where energy from the light source causes energy changes in the material, which results in the transition of ions in the atom, causing the absorption feature (mainly metal ions). Whereas the SWIR region depicts molecular bonds and changes introduced to these molecular bonds caused by incoming energy and resulting in vibrations. However, the relative position and intensity of absorption features are influenced by, for instance, particle size, mineral mixtures, view geometry, surface roughness, surface coating or water content (Gupta, 2017; Kurz, 2011; Laukamp et al., 2021).

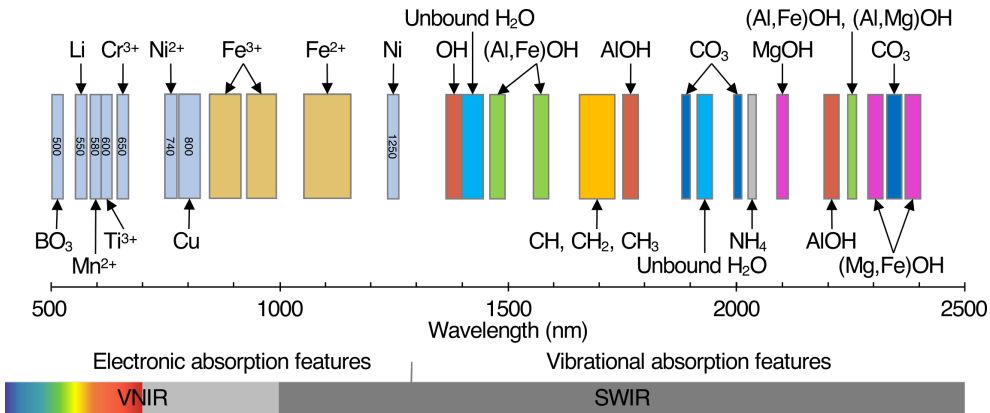


FIGURE 4.2: Typical electronic and vibrational absorption features in the VNIR and SWIR spectral range, after Corescan (2021); Hunt (1977).

4.4 Mechanical rock properties

One key mechanical rock property of interest for the mining industry is the material hardness. The hardness may define whether a sample is easy or hard to crush or grind but can also indicate whether elements of interest may easily liberate from the sample matrix. Commonly, hardness is considered as the resistance of the material against the penetration, deformation or indentation of a specific and typically harder

indenter (Frank et al., 2019; Lynch, 2015). There are different ways to assess or express the hardness unit. For example, it may be expressed by the rebound characteristics, from the amount of energy required (by the machine) to grind the sample to a specific grind size or by the time it takes to drill through a one-meter solid and competent rock sample.

Typically, the hardness relates to the ease of liberation and breaking of a large particle into smaller particles (at different scales from m to μm). The rate or ease of this depends on the type of minerals present in the rock and the size, shape and spatial arrangement of the mineral grains (i.e., the ore texture) (Lynch, 2015). Within a mine, the liberation of rock particles or minerals starts by blasting the rock. However, the second and main step occurs within the comminution circuit through crushing and grinding. During the comminution process, harder samples typically show a higher resistance against impact, abrasion, shear, attrition or compression, see Figure 4.3 (Napier-Munn et al., 1996). However, a hard signature can also relate to increased brittleness meaning that it can easily break, crack, or snap into smaller particles without any deformation. A more ductile hard material will first deform before breaking apart as it shows plastic deformation (ores with higher clay content).

This dissertation uses results from four data acquisition techniques to assess the material hardness. These techniques and their interpretations will be explained in the subsequent Sections.

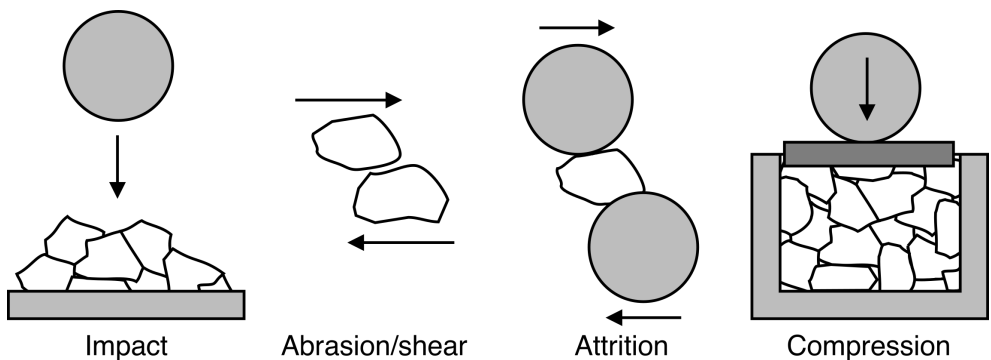


FIGURE 4.3: Typical breakage mechanisms occurring during comminution processes, adapted from Lynch (2015).

4.4.1 Bond work index

The Bond ball mill work index (w_i or BWi in kWh/t) can be determined using results from the Bond Ball Mill Grindability Test and principles from Bond's law of comminution (Bond, 1952, 1961). This index provides a measure of the specific energy or ball mill power draw (P in kW) required to grind a ton of ore in the ball mill from a known feed particle size (F_{80} in μm) to a certain product particle size (P_{80} in μm) using a specific throughput (T in t/h):

$$\frac{P}{T} = w_i \times \left(\frac{10}{\sqrt{P_{80}}} - \frac{10}{\sqrt{F_{80}}} \right) \quad (4.1)$$

The BWi is a material property determined by the blend composition and is an indicator of the resistance of the material in terms of abrasion and impact to ball milling. Therefore, this indicator is typically used to describe the material hardness, where a higher BWi value indicates harder material. This is a relatively expensive test to conduct, but on the other hand, it will give direct results that link with the processing parameters since the comminution plant energy consumption is typically expressed in kWh/t of ore. Matching the test results with actual plant behaviour may give a direct relationship between the test and potential behaviour while processing similar material.

4.4.2 Drop weight test, Axb

The drop weight test is a laboratory test, commonly referred to as the JK Drop Weight Test (JKTech Laboratory Services, 2015). This test measures the ore resistance to breakage parameters typically expressed by three parameters: A and b, hence Axb, and t_a . The test consists of two main parts measuring the impact and abrasion parameters and a detailed description can be found in JKTech Laboratory Services (2015) and Napier-Munn et al. (1996). The first part of the test measures the impact breakage (high energy) by dropping a steel drop-head onto a sample. Prior to the measurement, the sample (~100 kg) is split in five size fractions. Each size fraction is then broken using the weight which is dropped from three heights (energy levels). The broken particles are collected and sized and the size distribution is analysed and represented in a single value t_{10} . This value is defined as the per cent passing one tenth of the original particle size. A set of t_{10} values and specific energies for the 15 energy/size combinations are then used to define the parameters A and b using the following equation:

$$t_{10} = A \left(1 - e^{-b \times \text{applied specific energy}} \right) \quad (4.2)$$

The resulting A and b parameters are ore-specific dimensionless parameters determined by fitting a model to the experimental data generated from the drop weight test (Mwanga et al., 2015). The parameters A and b have no physical meaning but were found to be a useful index of ore hardness with respect to the ball mill. Higher values of Axb indicate a softer ore.

The second part of the test involves grinding (abrasion, low energy) the samples using a tumbling test with a single size fraction to define the abrasion parameter t_a . For the purpose of this dissertation, the main focus has been on the Axb parameter as opposed to t_a .

4.4.3 Equotip rebound hardness

Rebound hardness testing is done using an EQUOtip device, of which the result is typically called Equotip rebound hardness. The Equotip rebound hardness test is a rebound velocity hardness tester that is non-destructive, quick and easy to perform. It can be applied directly to whole or cut core surfaces. The device has a tungsten carbide tip spring mounted in an impact body and, after initiation, impacts under spring force with known impact energy on the sample and then rebounds. It measures

the speed before (V_i) and after impact (rebound, V_R) with a magnet passing through a coil. This movement generates induction voltage which is proportional to the speed of impact, and this gives the hardness value called the Leeb. Leeb values are between 0 and 1000, where a higher value indicates harder material. The Leeb value is calculated by:

$$Leeb (Ls) = 1000 \left(\frac{V_r}{V_i} \right) \quad (4.3)$$

The resulting hardness value typically depends on a combination of factors, including the grain size and immediate grain support, surface roughness, localised micro-scale volume integration and the mineral hardness at the point of impact (Frank et al., 2019; Hunt and Berry, 2017).

4.4.4 Drilling penetration rate

The penetration rate (m/hr) is directly derived from measurement-while-drilling (MWD) parameters and defines the time required to drill through a one-meter rock mass using a typical blast hole drill rig. When machine operating conditions are kept constant, then the penetration rate data can indicate the strength and hardness of intact rock (Rai et al., 2015). The penetration dataset is spatially dense, mainly consisting of blast hole information at every 0.1 m (vertical), where blast holes are horizontally spaced 5 – 10 m. This parameter is a very abundant material hardness indicator since it is collected continuously along every hole drilled. However, one of the limitations of the penetration rate as a proxy for hardness is that it is likely to be affected by other factors like discontinuities, cracks, voids or fractures in the rock mass. A lower penetration rate indicates that it is more difficult to drill through the rock mass (competent rock) thus that a harder rock type is faced. In contrast, a higher value may also indicate a more fractured zone.

4.5 Datasets of this dissertation

The techniques described in the previous sections and datasets are commonly acquired, collected and stored by mining operations and provide a lot of data to research (as done in this dissertation). All samples and data shown in this dissertation have been acquired through the Tropicana Gold Mine operation, and there are no tests or experiments specifically conducted for this dissertation. It also means that a thorough understanding of each acquisition technique is necessary before the data can be used and interpreted appropriately.

Table 4.1 presents an overview of the different combinations of techniques and datasets used in each chapter. A filled circle indicates that the dataset was directly used as input, a hashed circle indicates that the dataset was only used for analysis and understanding, and an empty circle indicates that the dataset was not used in that case study. The confidence associated with these typical datasets will be discussed in Chapter 7.

TABLE 4.1: Overview of the datasets used or discussed in each major dissertation chapter. Filled circle (●): directly used as input, hashed circle (⊗): only for analysis, empty circle (○): not used at all.

Dataset used	Chapter 8		Chapter 9	Chapter 10	Chapter 11
	ME Case Study I 30,687 samples	ME Case Study II 8,627 samples	Block feature clustering >200,000 samples	Material tracking >886,000 truck movements	Processing actuals >3 year of processing data
Logged geology (lithology, alteration)	●	●	●	○	○
Four-acid digest (ICP-OES, ICP-MS)	●	●	○	○	○
pXRF	○	○	●	○	○
Fire assay	●	●	●	●	●
Leach recovery	○	●	○	●	●
VNIR-SWIR	○	○	●	⊗	⊗
Bond work index	○	●	●	●	●
Drop weight test results (Axb)	○	●	●	●	○
Equotip hardness	○	●	●	●	○
Penetration rate	○	○	●	●	●
Material fingerprints	⊗	⊗	⊗	●	●
Material tracking	○	○	○	●	●
Actual processing response	○	○	○	○	●

5

Multivariate analysis techniques and clustering



This chapter describes the general workflow for implementing a clustering framework. It elaborates on the data preparation, feature engineering and clustering of geochemical datasets. Additionally, several examples illustrate the practical implementation of each step.

5.1 Introduction

Clustering is a multivariate analysis technique that aims to cluster a sample of subjects based on similar signatures with little or no prior knowledge. A multivariate approach is especially useful because the traditional view of measuring and (subjectively) interpreting individual material attributes to classify material is not sufficient anymore (van Duijvenbode and Buxton, 2019). In that respect, clustering is a relatively quick and simple method to investigate the relationships between many different variables. This study uses clustering to find a relationship between the input features (geochemical and mineralogical data) and processing response which indicate the mechanical material attributes (e.g., hardness, ease of gold liberation, etc.).

Constructing a clustering framework (Figure 5.1) typically starts with case-specific data preparation and selection (e.g., collecting, cleaning, feature engineering). The result is a dataset with as many features as available for its constitutive samples and without missing data. Additional samples with missing data can be included, but appropriate missing data imputation techniques should be selected (e.g., Martín-Fernández, 2003). This dataset functions as input for a clustering algorithm, whose output is a label for each input sample (van Duijvenbode and Buxton, 2019) and indicates the group or cluster to which the sample is assigned. This will typically be the result of the clustering framework. Commonly the quality of the data separation will be assessed using a performance evaluation or clustering metrics.

This chapter covers several fundamentals of data preparation for clustering and provides background information for the performed clustering in the following chapters. In addition, it is a reference for performing an applied clustering framework focused on data originating from the mining industry.

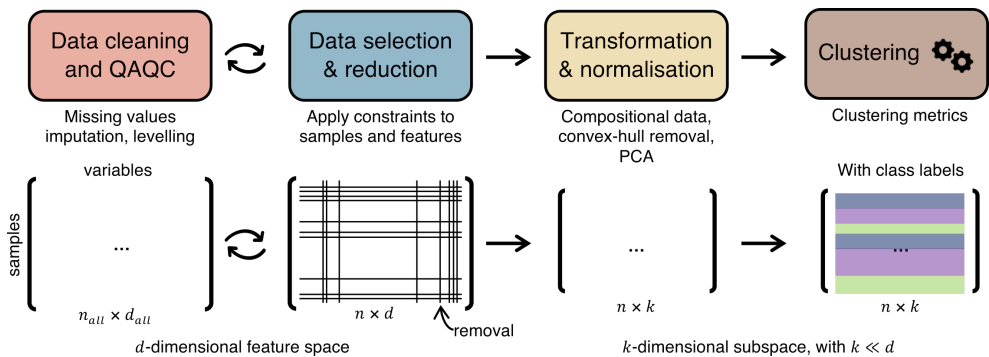


FIGURE 5.1: Schematic overview of a clustering framework.

5.2 Feature engineering

The purpose of feature engineering is to enable the execution of statistical measures to reveal (linear) relationships, which may represent the stoichiometry and relationships of the elements that make up minerals, rock-forming minerals and subsequent processes that modify mineral structures, including hydrothermal alteration, weathering

and water-rock interaction (Grunsky and de Caritat, 2019). The feature engineering section is split into three steps, of which the first two are iterative:

- 1a. (Section 5.2.1) Data cleaning using quality assurance and quality control (QAQC)
- 1b. (Section 5.2.2) Data selection and reduction
2. (Section 5.2.3) Transformation and normalisation

The first step of the feature engineering in preparation for clustering and subsequent analysis is an iteration of the data QAQC (cleaning) and data selection/reduction steps. Iteration is recommended because below detection limit (censored) or missing data may be imputed while cleaning based upon samples not selected during the data selection phase. Conversely, selecting data samples may only be possible if one understands which data is appropriate to use and clean. The subsequent sections will primarily focus on the preparation of a geochemical dataset for clustering, but also examples of VNIR-SWIR data and Equotip Rebound hardness data are given.

5.2.1 Data cleaning and QAQC

The two main datasets used in this study are geochemical and mineralogical datasets. The geochemical dataset contains results of analysing the elemental concentration of pulverised rocks, and the mineralogical dataset contains mineralogical feature interpretations. Typical problems associated with these datasets include compositional data closure, missing values, censoring, merging and levelling different datasets (Grunsky and de Caritat, 2019). The main reason is that statistical analysis is not suitable when zeros are present in a dataset. The following paragraphs list various QAQC steps necessary to be executed or checked in order to get a clean data matrix suitable as clustering input.

- **Dealing with missing (no data) or censored values (below detection limit):** there are various methods for finding replacement values for censored data. These may include substitution or imputation using additive replacement, simple replacement (half the detection limit) or multiplicative replacement strategies (Martín-Fernández, 2003; Palarea-Albaladejo et al., 2014). The easiest solution is to remove samples from the dataset that miss one or more of the to be considered variables (features). Another frequently used approach is to use half the DL as a replacement value.
- **Bias and precision:** quality of geochemical datasets can be evaluated using blank, repeat or standard measurements. Part of the standards measurements includes comparing the analytical results of Certified Reference Materials (CRMs) with their documented reference values (Figure 5.2). Checking the precision and accuracy (bias) of these measurements then gives an indication of the quality of the other samples corresponding with samples of the same batch. Not all elements (for example, Ag, Figure 5.2) can be checked with a single CRM, and therefore, there are frequently multiple CRMs added to batches. Chapter 8 gives a detailed overview of checking the ME dataset its quality using bias and precision indicators.

The bias and precision of a VNIR-SWIR spectrometer are usually omitted by calibration using a white reference and black reference sample. In addition, some mines create their own mineralised standards, which are useful to calibrate the spectral results.

- **Levelling:** batches of geochemical or mineralogical data are typically collected across multiple years and using different laboratories, analytical tools and methods (Figure 5.2). In addition, the detection limits or resolution of common analytical techniques has improved over time. If significant deviations are found across time, it may be necessary to level (normalise) parts of the datasets. For instance, the wear of an Equotip impact body (the probe) degrades over time due to the impact of measurements (Frank et al., 2019). There are significant differences in calibrated hardness results on a test block using a new or old tip. Calibrating the Equotip measurements may be a solution to compare measurements regardless of the probe lifetime.

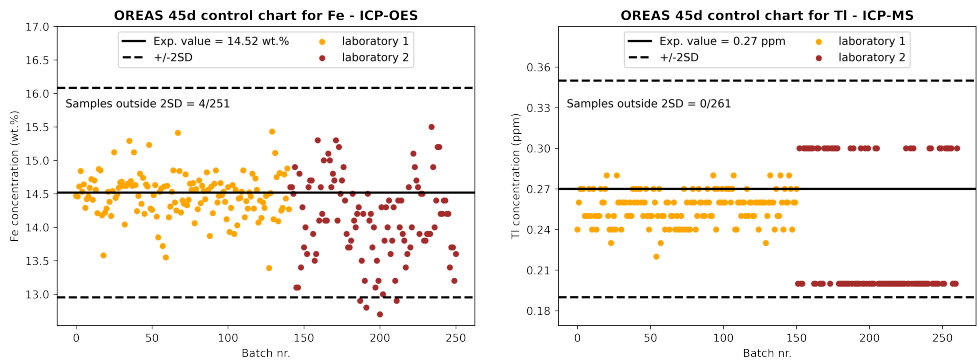


FIGURE 5.2: Control chart for Fe and Tl measured as part of analysing the OREAS 45d certified reference material (CRM) samples. Two different laboratories and two different measurement techniques (ICP-OES and ICP-MS).

Example 5.1: Figure 5.2a indicates that the measurement precision of Fe for laboratory 1 is more consistent and has a small bias below the expected value. The Fe results from laboratory 2 have a larger spread with some outliers. If these were gold assays, then a mine would insist that all assays in a batch were repeated if the reported value was $>2SD$ away from the expected value. Figure 5.2b shows that for Tl (thallium), laboratory 1 and 2 have a different detection limit of 0.02 ppm and 0.1 ppm, respectively. Therefore, the measurement precision/bias of batches sent to laboratory 2 should be checked with a different CRM with a higher expected value for Tl.

5.2.2 Data selection and reduction

Defining the dataset and features that will function as input for the clustering is considered as data selection and may be as simple as collecting the geochemical or mineralogical dataset. However, the probably more essential step, data reduction, involves the removal of samples or features from the dataset that are not necessary or may be considered as outliers in the clustering process.

Sample-based constraints focus on selecting the appropriate samples from the dataset. There were two main constraints applied to the geochemical and mineralogical datasets used in this study:

1. **Spatial constraints:** an assay dataset typically contains samples from the main target area (mine) but also from exploration regions, see Figure 5.3. Spatially constraining is key to capture the underlying variability in the samples from the target area and not being influenced by other processes dominant outside the main area of interest.

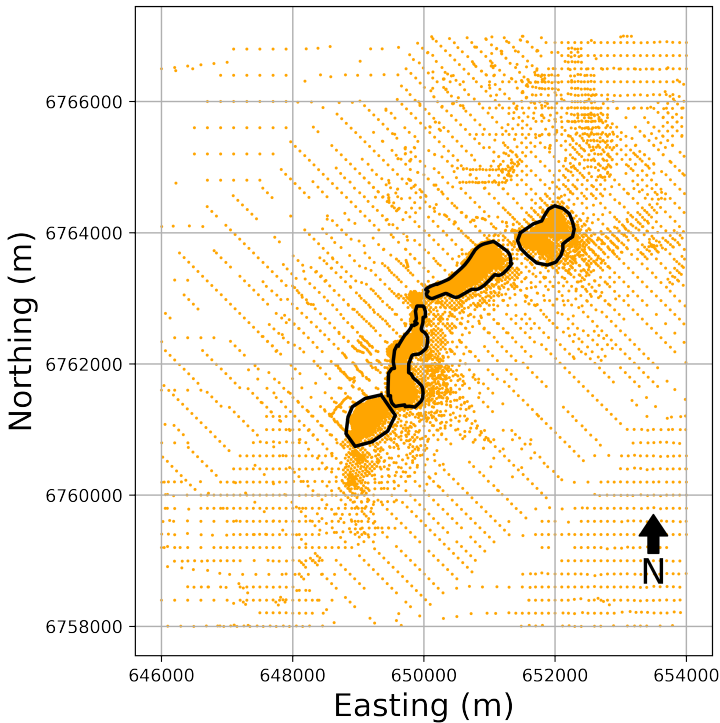


FIGURE 5.3: Data reduction example - Spatially constraining samples to only select those from within the open pit extents (black outlines).

2. **Geological constraints:** when analysis results are available, it is typically easier to discriminate the mineralised material from the pure waste material spatially further away from the mineralised zone than to discriminate different ore

types within the mineralised material. For example, separating unmineralised metachert or garnet-bearing amphibolitic gneiss from mineralised feldspathic gneiss is easier than separating quartzo-feldspathic gneiss from a feldspar-rich gneiss which could both be mineralised (see Figure 5.4 and Chapter 8.4.1, Case Study I results). If the latter is desired, it could be worthwhile to remove those samples logged as any of the lithologies related to the unmineralised material. This will ensure that during clustering, the focus is placed on unravelling the inherent (mineralogical, geochemical) differences of the mineralised material (Chapter 8.4.2, Case Study II results).

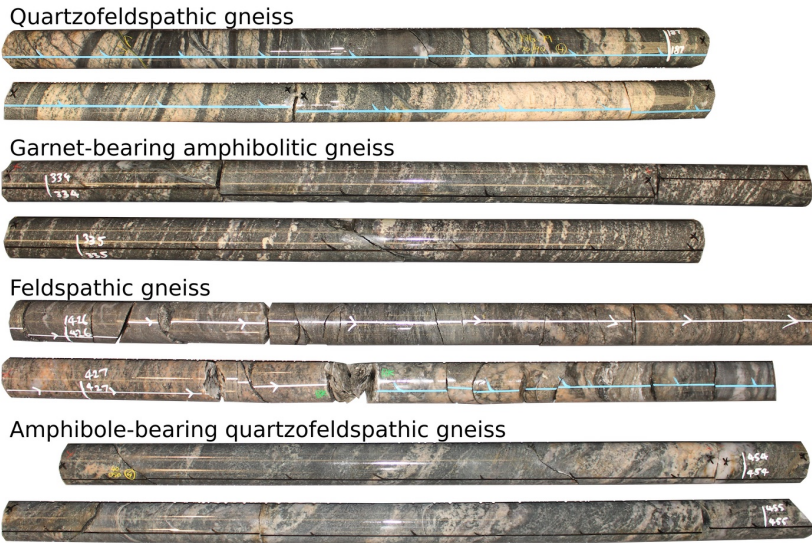


FIGURE 5.4: Data reduction example - Separating samples based upon the logged lithology.

Feature-based constraints focus on selecting those features present in the dataset suitable for clustering. For example, Chapter 9 shows how regions from raw spectral data are considered as features instead of the more commonly used feature extraction approach based upon wavelength position and absorption depth. One additional feature-based constraint applied to the geochemical dataset in this study is worth elaborating.

An important criterion to cluster samples is to decide upon which features this will be done. With assay data, this will most likely be the set of elements. Laboratory multi-element analysis results may typically provide 48 elements in their standard elemental suite. However, across many years and different measurement campaigns, the mining companies' dataset may contain up to 60 different elements, if not more. Considering the useability and suitability of each element may help to select the elemental suite for further consideration and make a trade-off to select an element or not (see Figure 5.5).

The useability of an element is the percentage of samples of the entire dataset that have a certain element measured. For example, there are probably fewer samples across a dataset measured for rare earth elements than the common rock-forming elements, which are part of almost any elemental analysis suite. Similarly, a typical pXRF dataset doesn't contain Pd and Au, but it may be measured using fused disc XRF analysis. Suitability considers the presence of the assay result. It indicates whether the elemental concentration is less than the lower limit of detection (DL), within or above the detection limit. A too high percentage of samples with censored data (below or above DL) can affect the derivation of associations in the clustering (Grunsky and de Caritat, 2019). As mentioned above in the data cleaning step, data imputation methods can be used to replace missing values. However, this may add bias to the results but has the advantage that more samples can be selected.

Example 5.2: Figure 5.5 shows an overview of the usability and suitability of the XRF dataset ($n=162,398$) used in Chapter 9. Elements are sorted based on their contribution to cumulative useability. Selection using the useability and suitability constraints identifies Al, Ca, Cr, Fe, K, Mn, Nb, Pb, Rb, S, Si, Sr, Ti, Zn and Zr as suitable elements for further analysis.

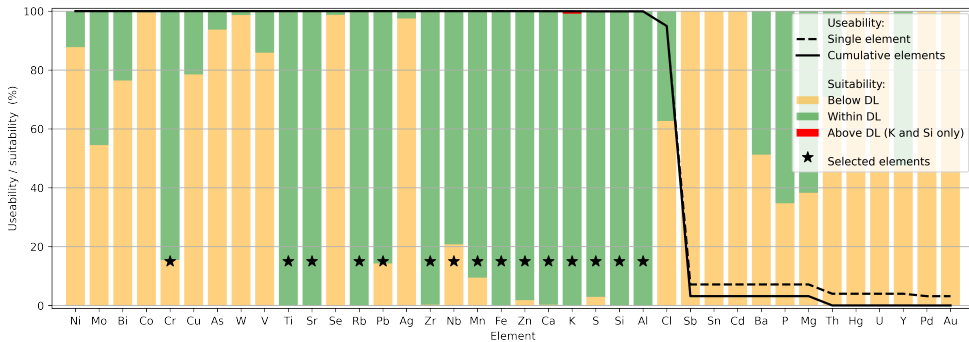


FIGURE 5.5: Constraints of useability and suitability of assay results define the elements for further analysis.

5.2.3 Data transformation and normalisation

Before clustering, the last step is to appropriately transform and normalise the feature values in a form suitable for the clustering algorithm. If data are not scaled appropriately, then the clustering may be affected by the scale of the input values (Zheng and Casari, 2018). For example, Au may be measured in ppb, while Fe is commonly reported in %. Scaling both concentrations to ppm puts the feature values in the same unit, but Au is still closer to 0 ppm, whereas Fe may be above 80,000 ppm. Common normalisation operations, each resulting in a different distribution of feature values, include min-max scaling, where $x \in [0, 1]$, variance scaling (standardisation) or l^2 normalisation (Wierzchoń and Kłopotek, 2018; Zheng and Casari, 2018). Standardisation entails replacing the original value x_i of the Au and Fe variables by the quotient

$(x_i - \text{mean}(x)) / (\sqrt{\text{var}(x)})$. This centres the value distributions around the mean 0 with a variance of 1 for each variable, making it a suitable input for clustering.

The shape of individual VNIR-SWIR spectral features is influenced by the overall shape of a spectrum (background continuum). Currently, the convex hull method is the most used approach to remove the background spectrum and is one of the underlying methods for single feature extraction (Hecker et al., 2019; Rodger et al., 2021). The result of this normalisation is that absorption features are always between zero and one and can readily be interpreted. An example of a continuum-removed spectrum, or hull quotient, may be found in Chapter 9. The continuum removal technique is a common normalisation method for spectral data and is applied in various studies (e.g., Dalm, 2018; Koerting, 2021).

The remainder of this section focuses on the required transformation and normalisation steps of geochemical data before clustering. These data need to be treated appropriately in order to respect the relative scale and multivariate nature of geochemical compositions. A subsequent dimension reduction of the features using principal component analysis is commonly performed to reveal hidden structures in the dataset. These structures will aid in identifying associations among variables that explain geological and geochemical processes (e.g., Davies and Whitehead, 2006; Grunsky, 2010; Ordóñez-Calderón et al., 2017; van den Boogaart and Tolosana-Delgado, 2018).

5.2.3.1 Compositional data

Compositional data are multivariate data where the variables or components represent some part of a whole (Aitchison and Egozcue, 2005; Pawlowsky-Glahn et al., 2011). These variables are measured on the same scale and unit system and are constrained by a constant sum property.

Example 5.3: A rock sample is pulverised and analysed by ICP-OES and ICP-MS for its elemental concentrations. The total ppm measured for a subset of 41 elements is 279,401 ppm. In compositional data analysis, this sum depends on the number of elements measured and unit (ppm), and in this case, it indicates that only 279,401 (27.9%) of the million parts were measured. The remaining composition of the ~70.1% is thus unknown (non-measured elements, for example, oxygen and silicon). Inappropriately accounting for this compositional nature gives problems in statistically analysing these data. Source: TGM sample ID 30185563.

The above example shows two issues for statistical analysis: 1) the total sum (if all elements were measured) has a maximum of 1,000,000 ppm, thus not free in the entire real number space ($-\infty$ to $+\infty$), and 2) the constant sum constraint must force at least one covariance or correlation to be negative; when one elemental concentration gets larger, the others must necessarily decrease (Rossi and Deutsch, 2014).

These problems are attributed to the closure of a dataset (Aitchison, 1999). Before samples can be compared, the sample composition requires a transformation to log-ratio coordinates with respect to the identified elements. Such a transformation transforms the data coordinates from the simplex, d-dimensional composition with

the positive real number space to the Euclidean real space, which is more suitable for statistical analysis (van Duijvenbode et al., 2022a). The three common transformations are the additive log-ratio (alr), centred log-ratio (clr) and the isometric log-ratio (ilr) (Aitchison, 1999). A simple choice of a transformation well fitted to geochemical datasets is clr and is used in this study and recommended for the mining industry-related geochemical datasets. See also Bhuiyan et al. (2019); Escolme et al. (2019); Grunsky et al. (2014); Grunsky and de Caritat (2019) for other studies using clr on a geochemical dataset. The other transformations are also used. For example, Ordóñez-Calderón et al. (2017) used ilr-transformed variables and a subsequent K-means clustering. The main reason to use the clr transformation is that it transforms the data in orthogonal axes, and this results in vectors with a zero-sum giving a dataset centred around the geometric mean. See Figure 5.6 for an example of how the relationship between Sc and Ba of a ME dataset changes by plotting the raw data and clr-transformed data on a bivariate plot.

The centred log-ratio is given by dividing each variable (x_i) by the geometric mean $g(x) = \sqrt[D]{x_1 \dots x_D}$ of the composition (D) of the individual samples and then taking the logarithm, mathematically expressed as Rossi and Deutsch (2014):

$$clr(x) = \log \frac{x_i}{g(x_D)} \quad (i = 1, \dots, D) \quad (5.1)$$

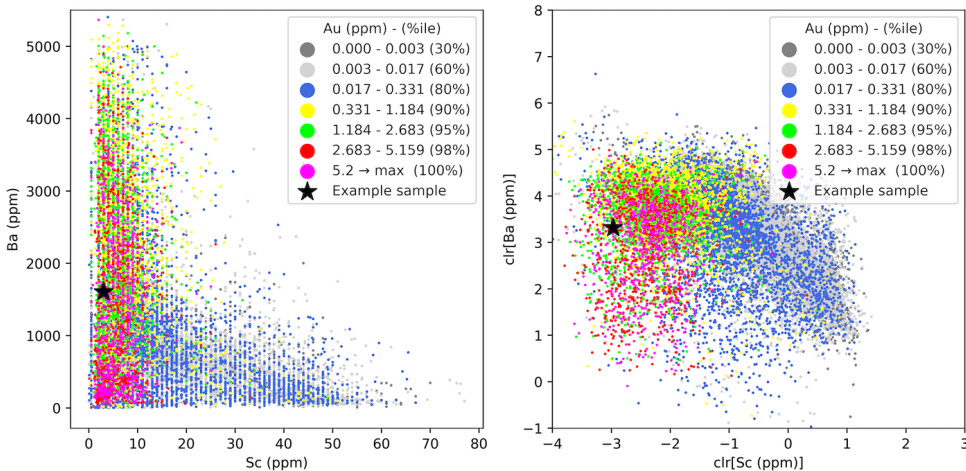


FIGURE 5.6: Bivariate plots of Sc-Ba and $clr(Sc)$ - $clr(Ba)$. The \star indicates the sample discussed in Example 5.4.

Example 5.4: The sample from Example 5.3 contains 3 ppm Sc and 1,604 ppm Ba and is highlighted by the \star in Figure 5.6a. The elemental geometric mean of the sample is 58.27, thus $clr[Sc] = \log(3/58.27) = -2.97$ and $clr[Ba] = \log(1,604/58.27) = 3.32$ are the new clr transformed values of the elements. These values are also highlighted in Figure 5.6b. Source: TGM sample ID 30185563.

5.2.3.2 Principal Component Analysis

Principal component analysis (PCA) is a statistical method used for dimension reduction of a multivariate dataset. If applied, it will transform a correlated multivariate distribution into orthogonal linear combinations of the original variables. This new projection approaches the direction of maximum variance in the original k -dimensional data and projects it onto a new subspace, d -dimensional, with equal or fewer dimensions than the original one (typically $k \gg d$). The first principal components (PC), part of the new set of variables, interpret the directions that describe the largest amount of variance in the k -dimensional space of the original data. Each subsequent PC represents the direction of the largest remaining variance that is orthogonal to those of the previous PCs (Jolliffe, 2002).

The following section explains that a measure of dissimilarity is used to either separate or group samples together in cluster analysis. One possibility is to use the Euclidean distance between a pair of samples in the k -dimensional space. When the d PCs account for most variation in all samples, an alternative dissimilarity measure is the Euclidean distance between a pair of samples in the d -dimensional subspace (Jolliffe, 2002). Interesting is that the Euclidean distances in both spaces are identical, if enough variance is captured in the PCs, then the only advantage is that fewer calculations need to be done (Jolliffe, 2002). Therefore, the main reasons to use PCA prior to clustering are 1) to capture the same data variance in a smaller subset of variables and 2) to reduce computation time.

Example 5.5: Chapter 8 shows clustering of a dataset ($n = 30,687$) with 41 clr transformed elemental concentrations (41-dimensional). After PCA, 95% of the dataset variation was captured in 24 PCs (24-dimensional). In contrast, Chapter 9 shows the clustering of 128,584 spectral samples with 800 features. In this case, PCA reduced 800 features to nineteen features (accounting for 95% data variance). Especially in the second example, computational efficiency plays a key role and performing PCA is worthwhile.

The mathematical process of PCA involves calculating the covariance matrix of all features (Jolliffe, 2002). Decomposing this matrix into its eigenvectors (PCs) and eigenvalues and selecting the top k eigenvectors based on the corresponding eigenvalues gives the lower-dimensional dataset (after transforming with the original data). In the example above, the cumulative explained variance of the first 24 and 19 eigenvalues accounted for approximately 95% of the variance. Analysing the eigenvalue and eigenvectors, in terms of loadings and scores of the features contributing to the PCs, is used to investigate sample-feature relationships and the grouping structure (intra-sample relationships). For example, The PCs of geochemical data can reflect linear processes associated with stoichiometric constraints and offers a significant advantage for subsequent process validation (Grunsky and de Caritat, 2019). Visualisation is frequently done on a biplot with principal components on the axis and the variables and samples represented as vectors (loadings) and coordinates (scores), respectively. There are various alternatives to PCA, for instance, Bruce et al.

(2002) proposes a dimension reduction of hyperspectral data using a discrete wavelet transform feature extraction.

5.3 Cluster analysis

Clustering is an unsupervised classification problem where the goal is to determine a structure among the data, with no labelled or response variables to lead the process. The function of clustering techniques is to partition the samples into subsets (called clusters) so that observations in the same cluster are similar in some sense (Romary et al., 2015). In a geostatistical or mining context, one can expect to obtain a classification of the data that then also presents some spatial continuity. For example, clustering the geochemical and mineralogical attributes from weathered and Fresh material will most likely delineate homogeneous areas in the deposit with the weathered samples spatially located above the Fresh material. Various clustering techniques exist, which also include the actual spatial location (xyz) of samples (Fouedjio et al., 2017; Romary et al., 2015), but these are not further discussed or used in this dissertation. The use of such algorithms may improve results.

One of the inputs of any clustering algorithm is a distance or metric measuring the dissimilarity, similarity or proximity between two samples and may depend on the variable types (e.g., categorical or continuous). For example, the distances for each cluster pair with numerical variables can be stored in a Euclidean distance matrix (Everitt et al., 2011) calculated by:

$$d_{Eucl}(p, q) = \sqrt{\sum_{k=1}^n (x_{pk} - x_{qk})^2} \quad (5.2)$$

where x_{pk} and x_{qk} are, respectively, the k th variable value of the n -dimensional observations for samples p and q . Differences in clustering techniques (e.g., K-means clustering, agglomerative hierarchical clustering, density-based spatial clustering of applications with noise; DBSCAN) are often found in small modifications of this distance metric and may, for example, include different weights for various points. The second input is closer related to the algorithm chosen and concerns how to measure the proximity between groups of samples (inter-group proximities). This will be explained only for the clustering algorithm used in this dissertation, namely hierarchical agglomerative clustering.

5.3.1 Agglomerative hierarchical clustering

There are a number of different methods that can be used to carry out a cluster analysis, including hierarchical clustering techniques. Others include optimisation-based (K-means), model-based, density-based (DBSCAN) or fuzzy clustering techniques. Hierarchical clustering techniques may be subdivided into agglomerative and divisive methods. Their difference is that agglomerative methods successively fuse samples into clusters until there is only one cluster remaining, whereas divisive methods separate the cluster into finer clusters (Everitt et al., 2011). The agglomerative hierarchical clustering method is used in this dissertation.

The agglomerative hierarchical clustering method is iterative and starts with each sample as a singleton cluster. Then, the algorithm calculates the distance for each cluster pair (Euclidean distance matrix) and finds the closest pair. The metric to calculate the inter-group proximities can differ, and the present study uses Ward's method (Ward, 1963). This method minimises the sum of squares of distances between samples and the cluster centres to which the samples belong. Next, the two selected clusters closest to each other are merged into a new cluster. Afterwards, the distance matrix is updated by calculating the new distance from the new cluster to all other clusters. These merge and update steps are repeated until only one cluster is formed (Wierchoń and Kłopotek, 2018).

5.3.2 Clustering metrics

Deciding upon the final number of clusters or classes is a difficult task, and various graphical or numerical metrics can be used to aid in this decision making. This dissertation jointly draws on one graphical metric and three numerical metrics, which are internal clustering validation measures (Aggarwal and Reddy, 2014). None of the metrics requires that the ground truth of the class labels are known and are therefore useful for geochemical and mineralogical datasets. Ideally, one would like to find a solution where between-cluster variation is high and the within-cluster variation is low. The final number agreed upon across the metrics is used for the final clustering exercise. Each metric will be explained briefly:

- **Dendrogram:** Figure 5.7 shows a dendrogram of a hierarchical structure obtained after hierarchical clustering. A dendrogram illustrates the fusions or divisions made at each stage of the analysis and shows relationships between samples. It may also show which class will split (or join) next or was split prior to the selected number of classes. A dendrogram can also show which two or more clusters may be formed or observed within an individual cluster. Dendrograms can also be used as an exploratory data analysis tool to make data-driven decisions on grouping variables together to reduce feature dimensions (Ordóñez-Calderón et al., 2017). This metric is more of a visual aid for selecting the final number of clusters.
- **Silhouette index:** The silhouette coefficient score relies on the pairwise difference in between-cluster distances and within-cluster distances. This score displays how close each sample in one cluster is to samples in the neighbouring clusters. The score is between $[-1,1]$, with low values for incorrect clustering and high values for highly dense clustering. Scores around zero indicate overlapping clusters because the samples are on or very close to the decision boundary between two neighbouring clusters (Rousseeuw, 1986).
- **Caliński-Harabasz index:** The Caliński-Harabasz criterion combines the within and between distance matrices to evaluate the quality of partition. The maximum indicates that the underlying number of clusters has the best partition quality and is a good indication of the number of clusters to select. If the values for an increasing number of clusters appear to form a horizontal, ascending or descending line, then there is no reason to prefer one solution to the others (Caliński and Harabasz, 1974).

- **Davies-Boulding index:** This index is based on a ratio of within-cluster and between-cluster distances and signifies the average similarity between clusters. The similarity metric takes the distance between clusters and the size of the clusters themselves into account. Values closer to zero indicate a better partition (Davies and Bouldin, 1979).

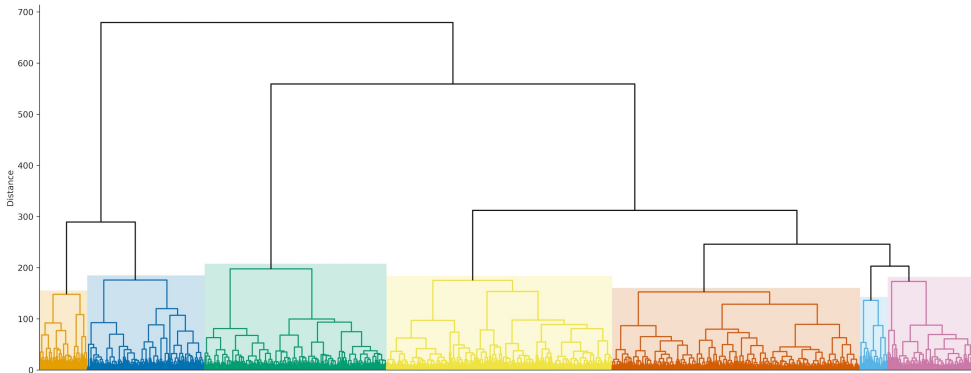
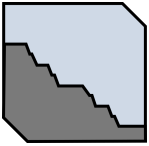


FIGURE 5.7: Dendrogram showing the agglomerative clustering hierarchy of 30,687 samples from the Chapter 8 Case Study I sample set. Setting a threshold at seven classes will group samples together, indicated by the different colours.

6

Tropicana Gold Mine



This chapter gives a brief introduction to the Tropicana Gold Mine, Western Australia. First, it describes the mine locations and brief history. Then, the regional and local geology are discussed. The background information given in this chapter is important for understanding the geochemical, mineralogical and hardness variations discussed in the remaining chapters.

6.1 Introduction

The Tropicana Gold Mine (TGM) project is located 330 km east-northeast of Kalgoorlie-Boulder on the western edge of Western Australia's Great Victorian Desert (Figure 6.1). The project is currently owned 70% by AngloGold Ashanti Australia Ltd and 30% by Regis Resources Ltd. As of 2022, more than 3 Moz Au is produced and a further 126.2 Mt grading 1.7 ppm Au for 6.95 Moz of gold remaining in Resources and 43.1 Mt grading 1.7 ppm Au for 2.38 Moz in Reserves (Regis Resources Limited, 2022).

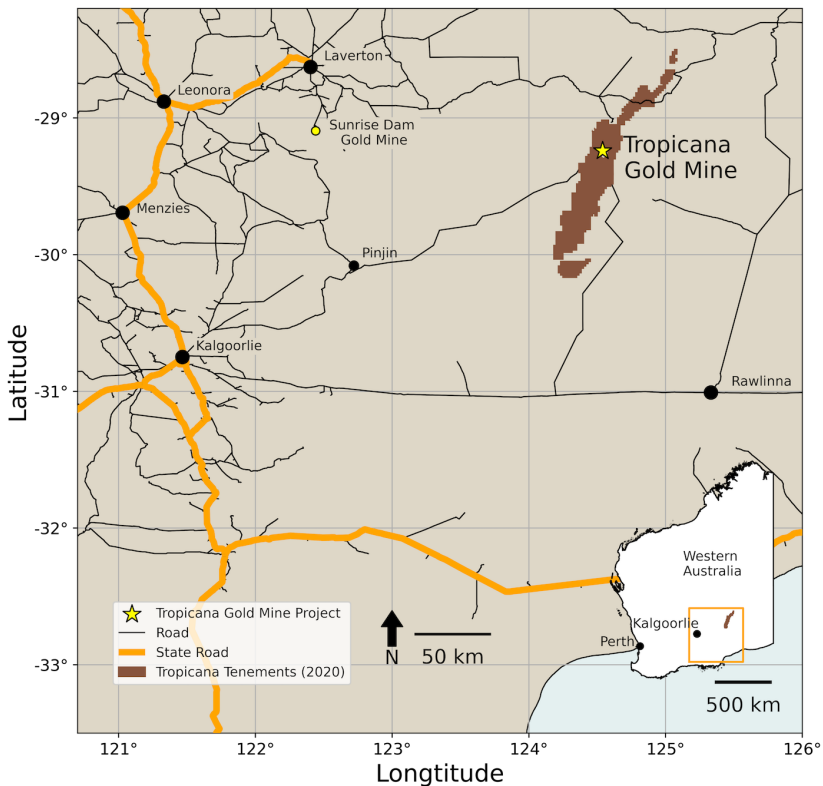


FIGURE 6.1: Regional map of Western Australia and the Tropicana Gold Mine area.

The Tropicana gold deposit was discovered in 2005 through the interest in a single historic 31 ppb gold-in-soil anomaly evident in historical Western Mining Company data reported in open-file reports. Since then, vast amounts of air core (AC), reverse circulation (RC) and diamond drill hole (DDH) drilling were conducted, resulting in the discovery of the Tropicana and Havana zone in 2005-2006. Ongoing drilling identified the Havana South and Boston Shaker zones resulting in a total strike length of mineralisation of >5 km (Figure 6.2). Mineralisation dips shallowly ($\sim 30^\circ$) to the SE and extends at least ~ 1.5 km down dip but remains open at depth. TGM started as an open pit mining operation with conventional drill and blast and load and hauling techniques in 2012, with the first gold produced in 2013. The mine transitioned partially into underground mining at the Boston Shaker zone in 2020 and is currently

further exploring underground mining below the other zones. Underground mining takes place using an open stoping method. Within the processing plant, rocks containing gold are reduced to $\sim 75 \mu\text{m}$ in a primary and secondary crushing circuit with a High Pressure Grinding Rolls (HPGR) and a ball mill. The final slurry is thickened, and the gold is extracted using a carbon-in-leach recovery circuit with a capacity of between 8-9 Mtpa (AngloGold Ashanti and Independence Group NL, 2010; Kent et al., 2014).

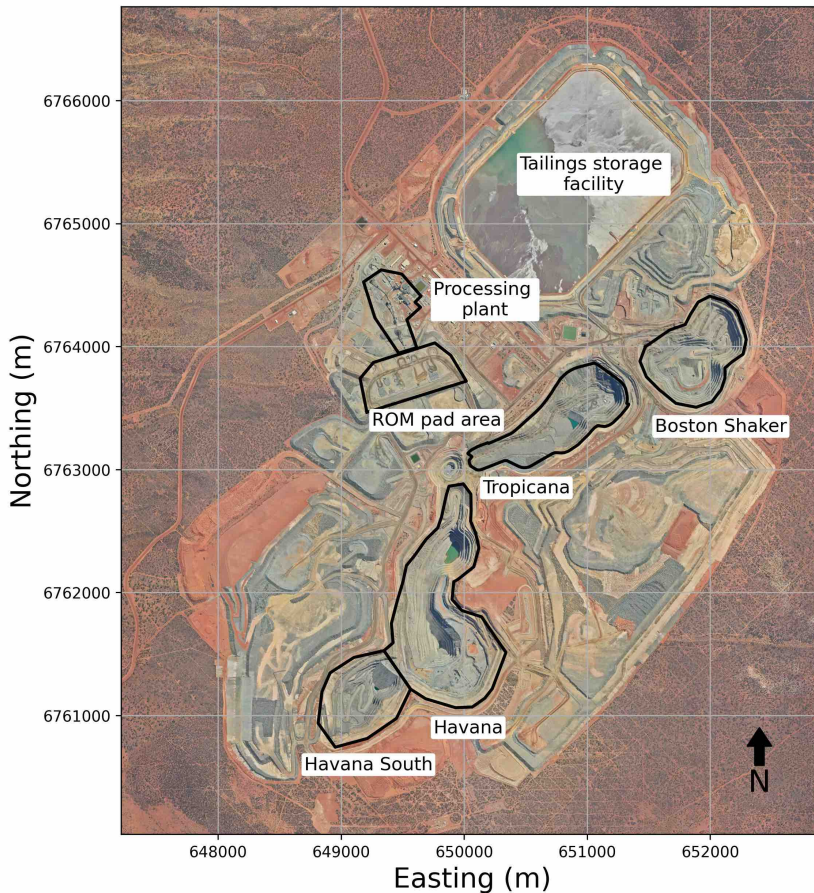


FIGURE 6.2: Tropicana Gold Mine aerial overview as of January 2022. GDA94 / MGA zone 51 grid.

Figure 6.3 contains a more detailed overview of highlights in the Tropicana Gold Mine project history. The shaded regions are representative of the total meters drilled using AC, RC and DDH drilling (smoothed). As of 2022, ongoing projects include the trade-off from a cutback in Havana vs underground mining below Havana to reach material below the open pit; development of the underground drift to Tropicana; extensional drilling around the known deposits to increase resource and reserves, and other exploration work in the Tropicana surrounding.

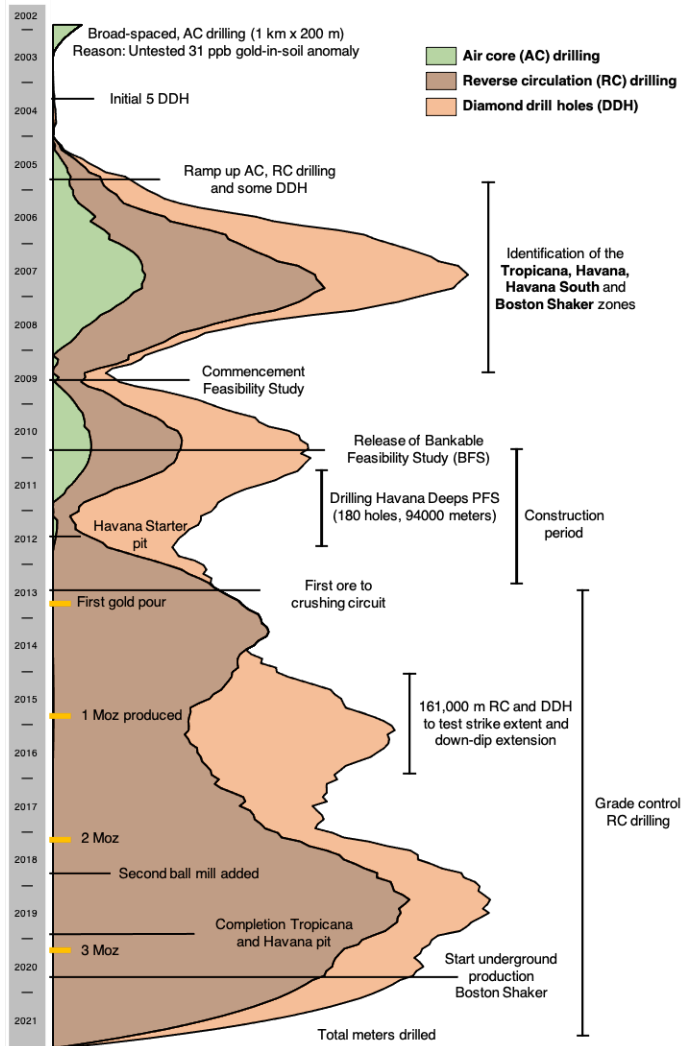


FIGURE 6.3: Timeline of key events in the Tropicana Gold Mine history. The shaded regions indicate the total meters drilled (cumulative and smoothed) for AC, RC and DDH holes in the mine area.

The Tropicana Gold mine, including the regional and local geology and style of mineralisation, have been subject to a number of studies in the past, and an overview is collected in Table 6.1. These studies include research on geology, ore genesis, structural architecture and litho-geochemistry. More recently, a few studies were published about material attribute updates through reconciliation, throughput prediction using drilling penetration data, and as part of this dissertation, material fingerprinting (Table 6.1). Finally, it must be mentioned that understanding of the Tropicana deposit has substantially been enhanced by numerous in-house reports by TGM geologists and consultants (S. Brown, personal communication).

TABLE 6.1: Literature studies related with the Tropicana Gold Mine.

Year	Geology	Structure	Geochemistry	other	Description	Reference
2006	X				Preliminary mineralogical study based only on a few drill holes. Initial description of the P-T conditions at the TGM deposit.	Saunders (2006)
2007	X				Basic description of regional setting and geology based upon early work done.	Doyle et al. (2007)
2011	X				Geology of the Albany-Fraser Orogen.	Spaggiari et al. (2011)
2014	X	X			Seismic and magnetotelluric characteristics of the Albany-Fraser orogen. Collection of work by several authors.	Spaggiari and Tyler (2014)
2014	X	X			Framework for the geological architecture and structural evolution for TGM.	Blenkinsop and Doyle (2014)
2014			X		Mineral Resource Estimation practices at TGM.	Kent et al. (2014)
2015			X		Comprehensive geochronological study including U/Pb dating of zircon and monazite, Pb/Pb dating of rutile, Pb/Pb and Os/Re dating pyrite and Ar/Ar dating of biotite. This analysis is used to describe the post-peak metamorphic timing for gold mineralisation.	Doyle et al. (2009, 2013, 2014)
2015	X	X			Regional affinity and geological evolution of the Tropicana Domain. Includes U/Pb dating of zircon and Re-Os dating of pyrite.	Kirkland et al. (2015)
2015			X		Insights into High Pressure Grinding Rolls (HPGR) operational controls.	Gardula et al. (2015); Kock et al. (2015)
2016			X		Lithochemical insights into the Archean host package and their pre-peak metamorphic tectonic setting implications and nature of the hydrothermal alteration.	Crawford and Doyle (2016)
2017	X	X			Description of the tectonic evolution at the regional scale and the resulting structural setting of the Tropicana Domain.	Occhipinti et al. (2018)
2017	X	X			Summary paper about Tropicana describing the where, what, how and why, but with a focus on the structural and tectonic settings.	Occhipinti et al. (2017)
2018			X		Case study showing the updating of spatial work index estimates based on actual ball mill performance data from TGM. The study includes a material tracking application.	Wambeke et al. (2018)
2019			X		Mining face grade determination using hyperspectral imaging techniques.	Austin et al. (2019)
2020			X		Attempt to constrain the timing between the high-grade metamorphic further and overprinting alteration mineral assemblages by applying Rb-Sr dating on biotite grains from different mineral assemblages.	Olerook et al. (2020)
2021	X	X	X		Further analysis of the mineralogy, geochemistry, geochronology, and structural geology of TGM deposits within the framework of mineralised textures. Proposes a revised paragenetic sequence.	Hardwick (2021)
2021			X		Geometallurgical throughput prediction using drilling penetration data and various basic geological attributes.	Both and Dimitrakopoulos (2021)
2022			X	X	Material fingerprinting at TGM using multi-element assay data to interpret comminution and recovery parameters in mineral processing.	van Duijvenboode et al. (2022a)
2022			X	X	Material fingerprinting at TGM using pXRF and VNIR-SWIR data to help interpret material hardness proxies. It spatially considers data in 12 × 12 × 3m blocks representing local geochemistry and mineralogy.	van Duijvenboode et al. (2021, 2022b)
2023			X		Application of material tracking and comminution and leach performance analysis.	Chapter 10, Chapter 11

6.2 Geology

6.2.1 Regional geology

The TGM is situated in the Tropicana Domain or Plumridge Terrane (both used in literature), a zone that separates the in situ eastern margins of the Archaean Yilgarn craton from the Albany-Fraser orogen (AFO), Western Australia (Figure 6.4) (Crawford and Doyle, 2016). The AFO is a NE trending arcuate Neoproterozoic – Mesoproterozoic orogenic belt and defines the SE extends of the West Australian Craton (Occhipinti et al., 2018). The AFO belt is divided into several fault-bound zones (Figure 6.4), characterised by distinct lithologies and tectonic history. The

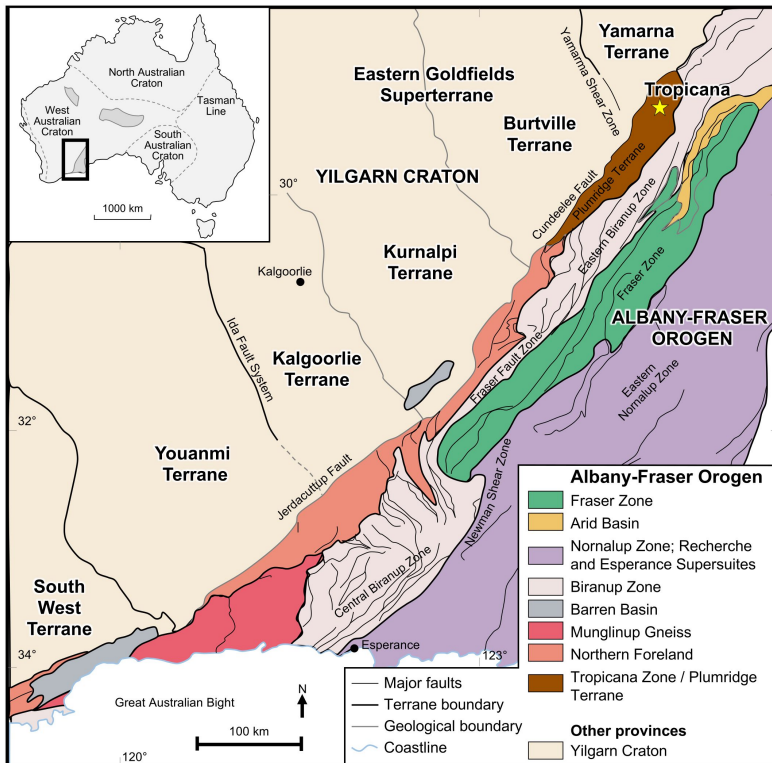


FIGURE 6.4: Geological map of the Albany-Fraser Orogen (right) with respect to the eastern margin of the Yilgarn Craton (left), Western Australia showing the location of the Tropicana gold deposit. Lat/Long; WGS 84; modified after Spaggiari et al. (2011).

Tropicana Zone or Tropicana Domain lithologies dominantly comprise Archaean crust (2.7 Ga) and is strongly modified by amphibolite- to granulite-facies grade metamorphism with reworked Archaean or Proterozoic affinities and later granitic intrusions metamorphosed to greenschist facies (Doyle et al., 2015). Outcrops in the region are sparse and thus are most domain scale geological interpretations mainly based on regional geophysical datasets (magnetics, gravity and seismic). These

interpretations are, where applicable, supported by local outcrops, mine geology and drilling campaigns (Spaggiari et al., 2011).

6.2.2 Local geology

The Tropicana Domain comprises Archaean variably deformed gneissic lithologies, which comprise a sequence of Neoproterozoic low-granulite to upper-amphibolite felsic gneisses and amphibolites. Closer to the mine, the granulite facies quartzofeldspathic gneisses are highly deformed and truncated by moderately east to southeast dipping shear zones (Figure 6.5). The TGM area itself has widespread Cenozoic cover overlying sporadic non-metamorphosed sediments. The known mineralisation extends over about 7 km as a planar stratiform body dipping $\sim 30^\circ$ to the SE. These mineralised zones occur as one or two laterally extensive planar lenses with a moderate dip. The favourable host to mineralisation is a preferentially deformed feldspathic gneiss facies (Crawford and Doyle, 2016; Hardwick, 2021). Post mineralisation faulting resulted in four distinct structural domains, from north to south: Boston Shaker, Tropicana,

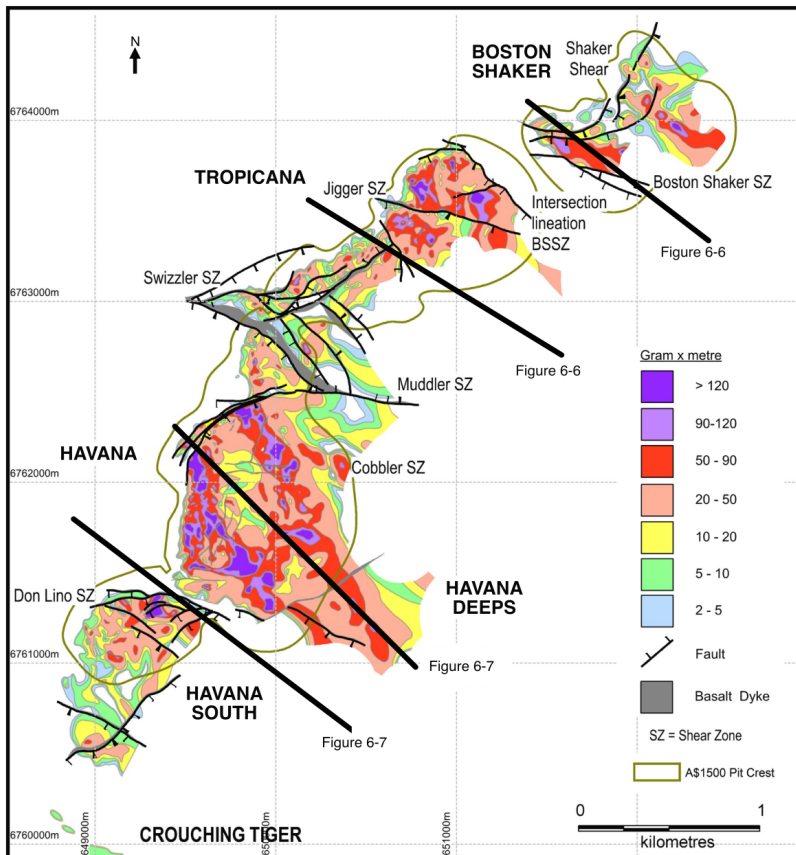


FIGURE 6.5: Structural domains and shear zones superimposed on a grade (g/t) \times thickness (m) plot (2014). GDA94 / MGA zone 51 grid.

Havana (including Havana Deepes) and Havana South (Figure 6.5). Most economic gold mineralisation occurs within high gold grade shoots, including the southeast plunging mineralised zones at Boston Shaker, Tropicana NE, Havana and Havana South.

Geological units: The favourable host to mineralisation is a preferentially deformed feldspathic gneiss facies (Crawford and Doyle, 2016). The more recent mineralised textures study by Hardwick (2021) focused on differentiating between the different feldspathic gneiss facies based on the framework silicate modal mineralogy. Higher-grade mineralisation relates with a more perthitic K-feldspar lithology, whereas the more common plagioclase rich feldspathic gneisses relate with lower gold grades. The hanging wall is a predominantly thick and continuous garnet-bearing amphibolite unit with subordinate meta-ferruginous chert (also see next paragraph and Figure 6.6 and Figure 6.7). Post-mineralisation tholeiitic dolerite dykes typically cross-cut and stope out the mineralisation (causing ore body dilution). Additionally, some pre- to syn-mineralisation mafic alkaline intrusions were in contact with mineralised horizons within Havana-Havana South (Roache, 2020), possibly also in the other domains, but not specifically identified. Both the gneissic lithologies and dykes have been overprinted by pervasive alteration and deformation mainly related to biotite-pyrite rich shear zones, which occur sub-parallel to the regional gneissosity. The regional gneissic banding is typically observed in the core and associates with the alignment of framework minerals (Blenkinsop and Doyle, 2014).

There have been eight major rock units (see Figure 6.6 and Figure 6.7) recognised at the deposit scale based on visually determined modal proportions of the major rock-forming minerals: quartz, feldspar, plagioclase, amphibole, pyroxene, and garnet (Hardwick, 2021; Saunders, 2006). These lithologies include: meta-ferruginous chert, garnet-bearing amphibolite, garnet-absent amphibolite, garnet-bearing quartzofeldspathic gneiss, amphibole-bearing quartzofeldspathic gneiss, plagioclase-bearing quartzofeldspathic gneiss, quartzofeldspathic gneiss and feldspathic gneiss (Table 6.2). Minor lithologies include coarser-grained feldspathic pegmatites, “Archaean dolerite”, and later Proterozoic dykes. Each lithology is variably modified by the overprinting alteration and deformation, particularly the feldspathic gneiss unit, which forms the preferred host to gold mineralisation (Hardwick, 2021). Hardwick (2021) provided a detailed description of these major and some minor lithologies, including modal mineralogy and average major elemental concentrations and will thus not be repeated here. However, Chapter 8 Figure 8.1 shows the results after clustering elemental concentrations from the TGM ME analysis dataset representing these lithologies. Several clusters are strongly associated with specific lithologies and show similar geochemical averages, as documented by Hardwick (2021).

Geological architecture and structural evolution: There have been five major deformation phases (D1-D5) been recognised at Tropicana, forming the main geometric controls on mineralisation (Blenkinsop and Doyle, 2014). However, examination of the relative timing of the gold deposition has been subject to various studies (Blenkinsop and Doyle, 2014; Hardwick, 2021; Kirkland et al., 2015; Olierook et al., 2020; Occhipinti et al., 2017). The recent study by Hardwick (2021) found that rare microscale gold

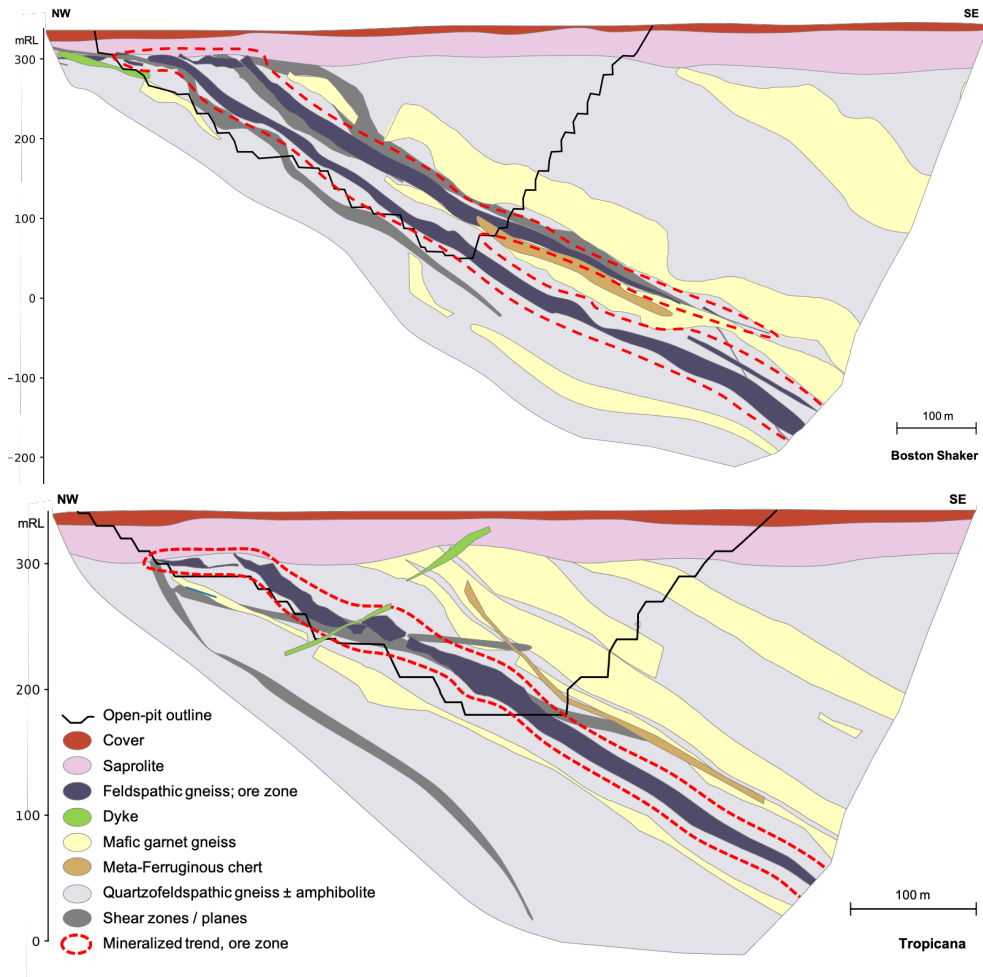


FIGURE 6.6: Schematic NW-SE cross-sections of the TGM deposits (100 m thick). Top: Boston Shaker, at 651930 mE, 6763690 mN, azimuth 37°. Bottom: Tropicana, at 650822 mE, 6763187 mN, azimuth 31.7°, similar to the cross-section from Olierook et al. (2020). Also, see Figure 6.5 for the location. GDA94 / MGA zone 51 grid.

already occurred as inclusion within minerals considered to have formed during prograde and/or pre-peak high-grade metamorphic conditions (approximately 2,650 Ma). This period is prior to the commonly believed peak high-grade metamorphism with subsequent mobilisation during partial melting (at 2,629 Ma). Nonetheless, the overprinting alteration and deformation (D3, c. 2520 Ma) are thought to play a significant role in liberating, remobilising and potentially upgrading earlier formed gold mineralisation (Doyle et al., 2015). During this phase, the prior high-grade metamorphic gneissosity assemblage is overprinted by subparallel localised zones of shearing and brecciation (S3) infilled with white mica biotite and pyrite formed during NE-SW directed shortening (D3). The S3 shears are, in turn, overprinted

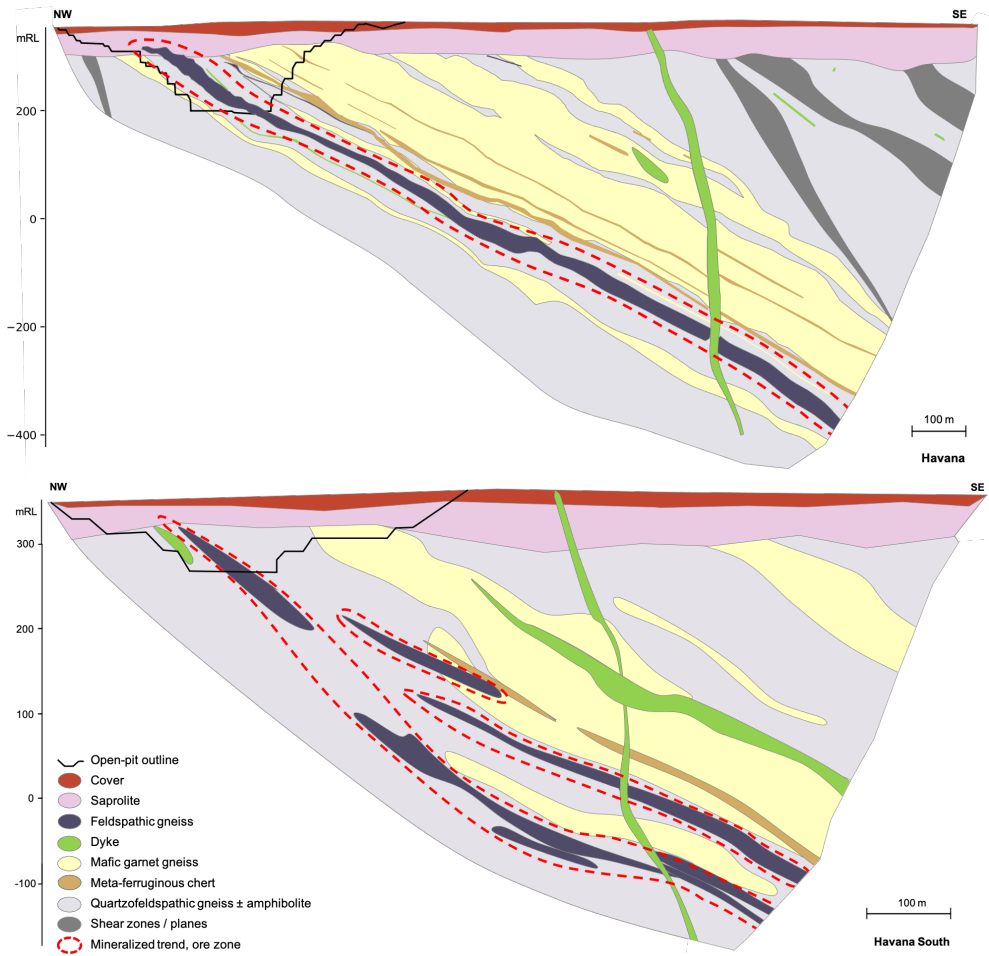


FIGURE 6.7: Schematic NW-SE cross-sections of the TGM deposits (100 m thick). Top: Havana, at 650148 mE, 6761622 mN, azimuth 45°, similar to the cross-section from Crawford and Doyle (2016). Bottom: Havana South, at 649753 mE, 6761137 mN, azimuth 37°. GDA94 / MGA zone 51 grid.

by unmineralised chlorite-white mica alteration and shearing (S4) (Blenkinsop and Doyle, 2014).

Mineralisation: The mineralised zone is characterised by biotite-sericite-pyrite alteration which is seen at the highest gold grade domains with primarily phengite ± biotite and at lower gold grade domains by increasing chlorite-rich muscovite (Doyle et al., 2015; Roache, 2016). In addition, several epidote-phengite rich domains are observed (Roache, 2016), also see Chapter 8 of this dissertation. Figure 6.8 shows an example of a feldspathic gneiss unit showing intervals of sericite-biotite, biotite-pyrite and sericite-biotite-chlorite alteration. Perthitic K-feldspar rich end-members have a higher K/Al (molar) ratio than the plagioclase-rich end-members. Hardwick (2021)

discriminated that these higher K/Al molar ratios of the feldspathic gneiss units are more controlled by higher modal proportions of perthitic K-feldspar with partial melting textures rather than by enrichment in biotite (since higher K/Al (molar) trends towards the K-feldspar node on an Al-K-Mg molar ternary plot). The mineralised rock exhibits significant enrichment in S and the ore elements (Mo, Te, Tl, Ag, Au, W) and K-group elements (K, Rb, Hf, Zr, U) (Crawford and Doyle, 2016).

TABLE 6.2: Overview of the major lithologies at the Tropicana Gold Mine (Doyle et al., 2007; Hardwick, 2021).

Lithofacies	Mineral assemblage ¹	Description	Characteristic elemental concentrations
Meta-ferruginous chert	Higher modal proportions of pyrrhotite	Intercalated with hanging wall amphibolite.	Highest Fe ₂ O ₃ (16.4%)
Garnet-bearing amphibolite	Amp – Px – Bt – Grt	Mafic, part of hanging wall and footwall. Main difference in presence/absence of almandine garnet.	High Fe ₂ O ₃ (10.8%), CaO (7.3%) and MgO (5.5%)
Garnet-absent amphibolite	Amp – Px – Bt		Similar Fe ₂ O ₃ (8.8%), CaO (5.4%) and MgO (5.6%)
Garnet-bearing quartzofeldspathic gneiss	Fsp – Pl – Qz – Bt – Grt	Minor variations in the modal mineralogy of garnet, amphibole or plagioclase.	Relatively similar, main difference in K ₂ O, Na ₂ O and P ₂ O ₅
Amphibole-bearing quartzofeldspathic gneiss	Fsp – Pl – Qz – Bt – Amp		
Plagioclase-bearing quartzofeldspathic gneiss	Pl – Qz – Bt ± Fsp		
Quartzofeldspathic gneiss	Fsp – Pl – Qz – Bt	Perthitic K-feldspar and plagioclase.	Low S (0.18%) and Fe ₂ O ₃ (3.3%)
Feldspathic gneiss	Fsp – Bt ± Qz – Amp	Preferred host to gold mineralisation. Higher modal proportions of pyrite and perthitic K-feldspar, decrease in plagioclase content.	Moderate Fe ₂ O ₃ (4.9%), near-equal CaO, NaO and K ₂ O (~3.4%)
			Moderate Fe ₂ O ₃ (5.4%) and K ₂ O (5.4%), lower CaO and NaO (~2.9%).

¹ Amp: amphibole, Bt: biotite, Fsp: feldspar, Grt: garnet, Pl: plagioclase, Px: pyroxene, Qz: quartz.



FIGURE 6.8: Core tray photographs of plagioclase (lower molar K/Al) and perthitic K-feldspar rich (higher molar K/Al) feldspathic gneiss domains with distinct zones of alteration. SR: sericite, BI: biotite, PY: pyrite, CHL: chlorite, CC: calcite, EP: epidote. Drill hole TPD234.

7

Material fingerprinting – Part II: framework



This chapter presents the material fingerprinting conceptual framework in more detail, as briefly outlined in Part I - Chapter 3. It elaborates on the applied methodology and gives insights into the confidence change of material understanding through this framework. Furthermore, it discusses a small applied case study to get a first impression of material fingerprinting.

Parts of this chapter have been published in:

van Duijvenbode, J. R., M. W. N. Buxton, and M. Soleymani Shishvan (2020). Performance improvements during mineral processing using material fingerprints derived from machine learning - A conceptual framework. *Minerals* 10(4), 366. doi:10.3390/min10040366.

7.1 Introduction

The behaviour of mineral processing is a response to the complex interaction of primary rock attributes, such as chemical composition, mineralogy, texture, and fracturing (Dominy et al., 2018; Guntoro, 2019; van Duijvenbode and Buxton, 2019). Therefore, to understand how differences in material attributes impact metallurgical plant performance, novel machine learning (ML) applications could help. However, large datasets are necessary for these ML models. Successively, with these datasets, it is possible to describe the plant blend better and improve metal recovery. Lamberg (2011) described a particle-based geometallurgy framework, where small particles are used to link geology and metallurgy. However, in practice, the feed that enters the processing plant is still a blend of different particles and compositions. The interaction between these particles also plays a vital role in the processing behaviour (Mwanga et al., 2015).

The most important characteristics (data sources) of a blend are the primary material attributes obtained during material characterisation. A better understanding of their composition allows for distinguishing between different material classes. For this, interpretation of individual datasets could be made, but this is time-consuming, especially for fused datasets. If all data could be combined, this assembles all the specific characteristics. It reveals the lines between the chemical and mineralogical systems by partially selecting the important features of each dataset. Several case studies demonstrated the value of mineralogical and textural information through data fusion to optimise process performances such as comminution (Little et al., 2017; Tessier et al., 2007; Tøgersen et al., 2018). Based on this success, new ML techniques could reveal the links between the data.

Abundant data gathering: The remaining open questions for the mining industry are which material data are relevant, where to acquire them, how can they be understood, and what is the confidence in them.

Therefore, to maximise the data utility for decision-making, the data have to be of high confidence. Lund et al. (2015) could, for example, extract mineral texture for process prediction, and Dalm et al. (2018) were able to separate waste particles from gold ore particles and distinguish between different ore types without measuring the gold concentration. The data do not inherently resemble the potential extractable knowledge and, thus, confidence should be gained in understanding and interpreting it. After appropriate (useful) data selection, much value can be gained from feature selection/engineering (data transformations) (Zheng and Casari, 2018), whereas these new features better express the specific characteristics of a class of material. Even though this class could be indicative of the material, it lacks direct interpretation due to the transformations. Therefore, it is important to have domain knowledge to assess the classification value. Domain knowledge can direct the appropriate problems to be solved, identify the appropriate ML techniques, assess the classification outputs, and evaluate metrics of correlation between data variables (von Stosch et al., 2014). Thus, the maximisation of data utility in mining requires an extensive assessment and

generation of data confidence and the ability to recognise the degree of confidence at different stages of mining.

This chapter attempts to resolve these issues by answering the questions on which types of material attribute data are relevant and what the moment of acquisition informs about confidence in material understanding. It also attempts to address how the data can be used for improved behavioural predictions during mineral processing. The aim is to provide a new framework for material characterisation and to quantify the degree of confidence of whatever the data resembles. Firstly, the concepts are explained for each component of the material fingerprinting framework. Secondly, the degree of confidence of different datasets (or acquisition techniques) and the unit processes in the mining cycle are explained. This may help to identify measurement localities and the required techniques, which could upgrade the degree of confidence. Finally, additional commodity-related examples are used to illustrate the potential for practical implementation of a material fingerprinting framework.

7.2 Conceptual framework

Data from different types of material and equipment are collected in a mining operation at regular intervals. The data from the material would directly resemble the effect of equipment on handling this material. Therefore, considering this data flow, the initial data would be generated during the material characterisation. Afterwards, the data (or material attribute classes, fingerprints) can be followed throughout the unit operations until the corresponding material is processed. These concepts, related to geometallurgy, mine to mill tracking, and reconciliation, are not new. Geometallurgy relies predominantly on mineralogy, intergrowths analysis, associations and grain sizes from small datasets (Dominy et al., 2018; Jansen et al., 2009; van den Boogaart and Tolosana-Delgado, 2018). The novelty of the proposed concept is that routinely acquired material attributes are taken without making a (direct) interpretation. For example, mineralogical data will not be interpreted in terms of spectral endmembers. Instead, they will be analysed based on features, including noise and reflectance, by a machine learning model. Eventually, this concept could eliminate the necessity for offline analysis and bulk metallurgical test work.

An overview of the concept can be seen in Figure 7.1. The physical state of material (intact, mixed, blended, responsive) changes at different unit steps of the mining cycle. However, when the material attribute classes (fingerprints) at each unit step are fully known, then the initially generated data gives confidence about understanding the root cause(s) of changing performance in mineral processing. The concept methodology gives insight into upgrading the confidence degree, as well as the understanding of the material composition at various stages during the mining cycle. Implementation would allow for controlling the performance variability over time and continuous validation of the identified and measured material classes.

The concept can be developed through the use of a self-learning system, which could learn to forecast the performance of mineral processing based on so-called material “fingerprints”. This system is self-learning because it uses a learning feedback loop in which forecasts are assessed against the actual performance and used to upgrade fingerprint confidence. Regular revision can be automated and involves

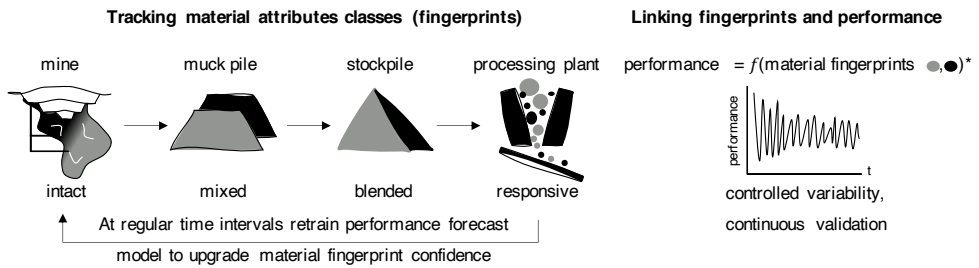


FIGURE 7.1: Concept of material fingerprints. Material attribute classes (fingerprints) can be tracked through the unit operations of a mining cycle and indicate the performance of processing them. Regular revision of the material fingerprint confidence over time (feedback loop) allows for controlling the performance variability and continuous validation. *Neglecting the changing process unit operating conditions.

retraining the performance forecast model given the additional data. A revision could be triggered at different moments in time and may be based on the throughput of the processing plant and the (in)homogeneity of an orebody. The revision frequency is, therefore, operation-specific. Historical data will be kept, and, depending on the spatial variability in the ore body, selective data batches can be used to converge the model to reality and forecast the processing performance.

The three requisites that help to better link material fingerprints with the processing performance are as follows (equivalent to the three components mentioned in Chapter 3):

- **Material characterisation (Section 7.2.1):** development of ML tools that fuse data originating from various sensor responses together to form initial material fingerprints. The initial fingerprints are obtained by means of an unsupervised ML framework (i.e., clustering of the fused data), and the results are assessed for usefulness. Iteratively upgrading the initial fingerprints classification with new data gives improved confidence and higher fidelity in characterising new material fingerprints. Revision may be done with supervised ML techniques (i.e., neural networks).
- **Material tracking (Section 7.2.2):** following the fingerprints throughout the unit processes of mining and identifying the change in the confidence of the fingerprint. This insight provides the means to identify and tackle material knowledge gaps.
- **Model development (Section 7.2.3):** construction of a second ML model which maps selected fingerprints to the performance of mineral processing. The selected input fingerprints for this model are fingerprints of blends and are, for example, composed of many smaller fingerprints identified during grade control mapping. If these blend fingerprints (input) match the sampling frequency of the performance of mineral processing, i.e., the - output - (e.g., specified by the particular operation), then they can function as input and output of a training data set of the ML model. Semi/Near-real-time mapping allows

upgrading the blending or compositing strategy for the classes to maximise mineral processing performance.

The following sections provide details on exploiting these requisites and serve as a foundation for understanding how differences in geology impact metallurgical plant performance.

7.2.1 Material fingerprints

Rock constituents: Most geological rock differences can be explained by the chemical bonding or individual elements that the material is composed of. Depending on the structure, how those elements are arranged and bonded together gives different minerals. The combination of these particular minerals gives rocks, and various combinations of rocks or lithologies define ore or waste (Grunsky and de Caritat, 2019).

Currently, many material attributes are measured to characterise the material and classify ore or waste types. The composition of one sample by its material attributes is represented by the pathways (lines) in Figure 7.2 and shows how n samples are separated into three different material types (1, 2, 3). The white circles represent the presence of a measured elemental concentration of the samples (e.g., Al, Na, Au, Mg), found minerals (e.g., biotite, chalcopyrite), rock classification (e.g., granite, dolerite), or mechanical and physical properties (e.g., texture, hardness, grain size). Pathways of the same colour represent how one material type has different constitutive attributes which could characterise this material type and distinguish it from others. Therefore, different material types can be characterised by combinations of attributes, and all available attributes are not necessarily needed to identify a material type. For

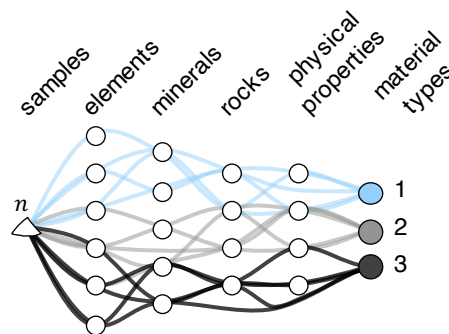


FIGURE 7.2: Conceptual diagram of material characterisation. Samples are composed of chemical elements and form into specific minerals, which form rocks or lithologies and have unique physical properties. The absence, presence or combination of these attributes helps to differentiate material types. Colours are used for the discrimination of possible pathways to characterise material types.

instance, the absence of a considerable Au concentration helps classify waste material. Therefore, such a sample does not necessarily need further analysis of the rock and its physical properties.

The traditional view of measuring and (subjectively) interpreting individual material attributes to classify material is not sufficient anymore. Alternatively, the geochemical, mineralogical, lithological, physical, or mechanical signatures of samples can be found through unsupervised learning techniques (i.e., clustering). A clustering algorithm may cluster similar signatures together and could therefore be used to form initial material fingerprints. A (material) fingerprint is defined as a classification of the measured and constitutive material attributes compared to the range of material attributes found within an exploration area or defined using available mineral resources or reserves.

An ML framework to obtain fingerprints through unsupervised learning is shown in Figure 7.3a. The framework starts with case-specific data preparation and selection (e.g., collecting, cleaning, feature engineering). For more information on this step, the reader is referred to Chapter 5 (Zheng and Casari, 2018; Aggarwal, 2015). The result is a dataset with as many features as available for its constitutive samples and with no missing data. This dataset functions as input for an unsupervised learning model, which its output is a label for each input sample. In the case of a clustering algorithm, this will be the cluster label to which the sample is assigned and could provide multiple output cluster labels. In this case, five clusters are identified (labelled A-E). Extracting meaningful clusters useful for a specific application is not trivial and requires cluster verification through human decision-making (Aggarwal, 2015; Everitt et al., 2011). Eventually, different proportions of clusters or classes (Figure 7.3b) will be equivalent to the various ore and waste types. This proportionality is useful for the design of blending rules and is possible because proportions (or classes) are additive, whereas individual attributes are not.

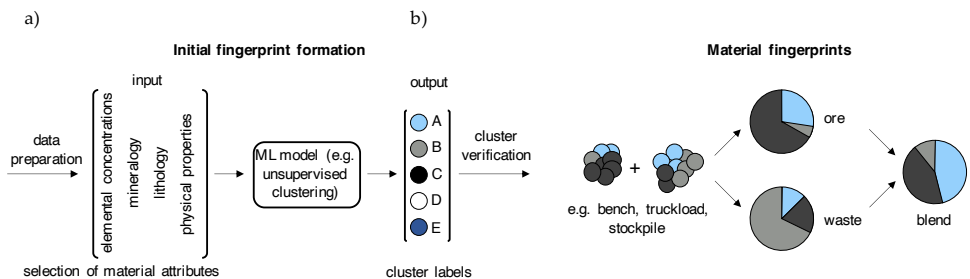


FIGURE 7.3: a) An example where initial fingerprint formation is done through unsupervised clustering. Clustering generates potential cluster or class labels and may act as training data input for another machine learning (ML) model, which can characterise new fingerprints from measured material attributes; b) An example where three (A, B, C) class outputs are used to explain proportionality of classes. The proportionality of classes allows the formation of fingerprints that characterise ore, wastes or blend types.

In the unsupervised clustering model, related processing information of the samples is not included because that information will only be included after the fingerprint classes are defined (see also Section 7.2.3). Furthermore, material properties

directly related to the processing behaviour, such as work index or reagent consumption, are not collected in large quantities. On the one hand, ML models require very large and human-labelled data sets, which unfortunately are not always available. On the other hand, many mining companies have a lot of exploration or grade control data available, which can be employed.

7.2.2 Tracking of fingerprints

During mineral exploration programmes, degrees of confidence are given to classify resources and reserves. The goal is to increase confidence and to understand the type of material before mining commences, whereas, during mining, this exploration paradigm is inverted because relocating material causes the material knowledge to be lost, which decreases the confidence. During each process of the mining cycle, the fingerprint confidence can be determined, as elaborated on in Section 7.3. The loss of confidence can be solved by material tracking as it provides the means to follow the material fingerprints and confidence loss during mining.

A proposed material tracking system would benefit from a particle breakage model, such as that described by Lamberg (2011); Servin et al. (2021), to describe inheriting features from big to smaller rocks (particles). This model should be combined with fleet management systems (Caterpillar, 2020; Mining Modular, 2017) to enable the following of fingerprints throughout the unit operations of a mining cycle. With such models in place, it is possible to identify locations where there is a gap in the understanding of the fingerprint composition. Such a gap is present, for example, at tracking material through stockpiles and at understanding the blending of fingerprints. The way that ore is added to stockpiles does not correspond to the way that ore is reclaimed from the stockpile. A build/reclamation model of a stockpile, which tracks the material through the stockpile, could give a better overview of the material flow, see Chapter 10. In addition, at locations with a gap (e.g., a blasted bench, truck, stockpiles), it is possible to do new measurements with appropriate sensors (e.g., hyperspectral imaging or RFID tags (radio frequency identification) (Jansen et al., 2009; Boubanga-Tombet et al., 2018) and consequently increase the fingerprint confidence, which ultimately improves the forecast of the processing behaviour.

Considering the development of a reserve or grade control block model, the origin of a fingerprint is within the smallest mining unit (SMU). At this stage, a fingerprint is a collection of the estimated block parameters related to the spatial position. As soon as drilling commences within this block, new material attributes are obtained. Therefore, it should be possible to modify the fingerprint with new parameters and ask for a hybrid character. Implementation of the hybrid character can be seen in Figure 7.4. During reallocation of the material, this hybrid character also allows the fingerprint to break down into smaller pieces, which then form fingerprints again. For each of the fingerprints, it is possible to classify and predict the processing behaviour (Section 7.2.3), thereby allowing for better decision-making regarding the material allocation, blending strategies, or processing settings. If there is a subsequent unit process, then this can be used to update the fingerprint data attributes again.

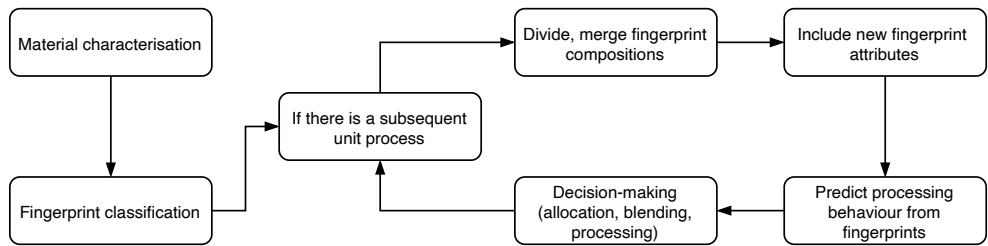


FIGURE 7.4: Flowsheet on how the hybrid fingerprint character allows for changes in the fingerprint composition during the unit processes of a mine and allows for better decision-making.

7.2.3 Model development

A second ML model can make predictions of equipment performance parameters from the fingerprint of a scheduled blend. Therefore, a fingerprint obtains its full potential when it does not represent one class of material but rather a blend of classes. Here, the proportionality of classes plays an essential role (Figure 7.3). The input of the model consists of different fingerprint class proportions, and the construction of the ML model training dataset is done in two steps. Step one is finding the performance indicators for different (pure) classes and simple class proportions. Step two may find the relationships with varying proportions considering all classes from historical data.

To further illustrate the primary purpose of the ML model, the example described below uses the throughput of the ball mill and shows the construction of the training dataset from step one. The effect of changing process unit operating conditions, such as the effect of mill liner wear on the processing performance, is not considered at this stage:

Example 7.1: Appropriate breakage tests could provide initial class throughput predictions of the different fingerprint classes and simple fingerprint class proportions (e.g., 50% class A and 50% class B). These properties can, for example, be derived from Bond ball mill grindability tests, drop weight tests or test equivalents (see Section 4.4) from representative diamond drill core samples (Mwanga et al., 2015; Alruiz et al., 2009).

These fingerprint labels then represent the throughput, or more generally, the comminution properties, such as the grinding power required for a given throughput of material under ball mill grinding conditions. As a result, the ML model can predict the throughput (output) from the (simple) input fingerprints. These input fingerprints may be single-class fingerprints or combinations of fingerprints in different proportions. This output directly reflects how the ball mill would perform by processing this material.

However, it is impossible to do breakage tests for all possible class proportionalities, and, therefore, additional proportional relationships between blend fingerprints and

the actual ball mill response can be found from either historical or actual performance data. Then (step two), these data can be added as additional training data to improve the previous model. Adding the historical data is possible if the fingerprints of the plant feed material (with proportions of classes) can be reconstructed and if the associated measured performance data are available. In cases where such data are not available, then the fingerprint classes of the to-be-processed plant feed and actual performance data could be used. These two data sources should reveal similar links between the fingerprint and associated processing behaviour, from which a model should be able to make operational predictions. This can be done when the material fingerprint of a scheduled blend function as an input of a trained model, which outputs the predicted equipment performance. These prediction forecasts will improve if, at regular intervals, the model is retrained (feedback loop) with new fingerprints and actual performance labels.

The secondary purpose of the ML model is to allow for a retrospective and iterative confidence upgrade. The upgrade goes from the inferred to the measured and back again to the proven fingerprints (explained in Section 7.3). This can be done with the last feedback loop by comparing the predicted versus the actual performance. This can be achieved as described in the framework of van Duijvenbode and Buxton (2019). Moreover, upgrading the blending or compositing strategy for classes is key to maximising mill performance and minimising environmental footprint.

7.3 Fingerprint confidence

Due to the ease of collecting vast quantities of data in different types and formats, care should be taken in the selection of the data for fingerprint classification. Furthermore, the kind of sensor data choice depends on valuable discoverable features in the sensor response data. Examples of usages and caveats of data are as follows:

- Subjective geological interpretations.
- Hyperspectral images have specific properties like colour, edges, and shapes that can be used for determining textures and mineralogy, but this approach is data-intensive and sometimes complex to interpret.
- The detection limits of elemental concentrations measured using specific geochemical analytical techniques.
- Down-hole geophysics is used primarily for interpretations of homogeneity and bulk properties but not for forward prediction of material attributes.

Due to differences in the nature of each technique and resulting dataset, the degree of confidence of the data is also different. Therefore, a new approach to quantify the confidence of mining-related data used for ML could help. This approach arises when the confidence is linked with the mineral reserve and mineral resource category terms from, for example, the JORC code or NI43-101 (Administrators, 2011; JORC Code, 2012). This way, five different terms are available to describe a proxy of the confidence in data used for ML. The inferred, indicated, measured, probable, and proven terms will quantify the quality of different datasets and the understanding of material

representations (fingerprints). The terminology is used because such terminology is commonly used and accepted by resource/reserve practitioners and will assist in visualising and appreciation of data quality. The goal is to increase confidence and to understand the type of material before mining commences by understanding the material. Explanations of the degree of confidence (in increasing order) in the context of this chapter can be expressed as found in Table 7.1.

TABLE 7.1: Terminology on the degree of confidence of mining industry data.

Confidence degree	Description	
low	Inferred	Inferring of properties through proxies is needed.
	Indicated	Good indication of what the data or material encompass(es).
	Measured	Provision of an exact measured result, but without much representation, i.e., not that useful yet.
	Probable	Reliable indication or representation (measured), and more information can be derived from the data.
high	Proven	Exact measured results which directly provide additional information.

Care should be taken to not directly link the degrees of confidence to formal resources or reserves classifications (Administrators, 2011; JORC Code, 2012). In general, this proposed concept would apply to a mining operation and, therefore, all material would be classified as a reserve. Based on this concept, Figure 7.5 shows the degree of confidence for selected datasets. The datasets are grouped in mineralogical, geochemical, (geo)physical, or combinatorial identification datasets. The confidence consists of a box and its representative colour.

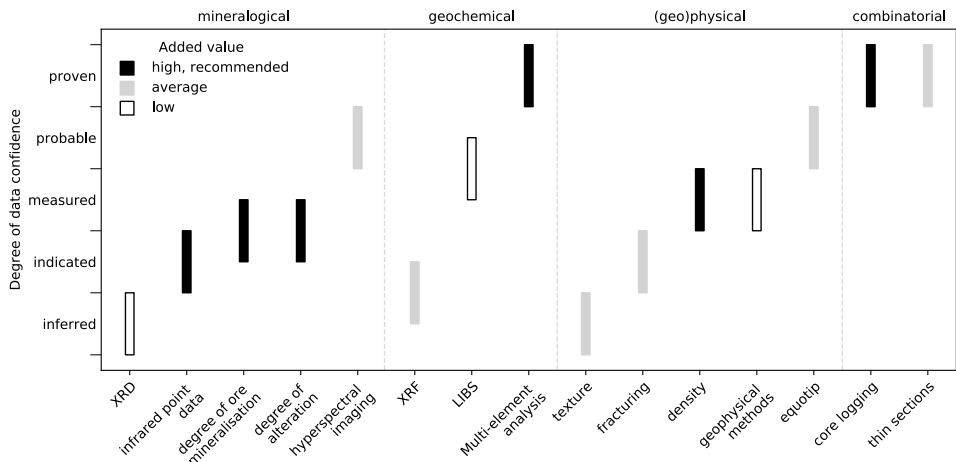


FIGURE 7.5: Indicative ranges of dataset-specific confidence in the quality, quantitative nature, robustness, and representativity. The box colour is based on added value to the fingerprint classification.

The ranges in Figure 7.5 are based on confidence in the quality, quantitative nature, robustness and representativity of the data. The box colour is based on two things: 1)

the added value of this data to an already existing fingerprint classification and 2) the type of information that is useful for predicting the behaviour of mineral processing. The added value of a dataset may be high and recommended, average, or low. For example, XRD (x-ray diffraction) measurements are done on a relatively small sample with time-consuming sample preparation. Afterwards, it is possible to infer properties (quantitative mineralogical interpretations) for particular minerals via Rietveld analysis (Zhou et al., 2018). Therefore, XRD datasets resemble an inferred degree of confidence. On the other hand, a single infrared (VNIR-SWIR) or pXRF dataset will only give inferred or indicated material properties. Although the samples are measured with high precision, their representative spot size is small. Moreover, further interpretation of spectral data is necessary to make use of the result. Laser-induced breakdown spectroscopy (LIBS) has a lower confidence than multi-element analysis because it requires extensive calibration efforts, but provides higher confidence data than XRF due to its low detection limit and capability to detect more elements. Nevertheless, adding an infrared or pXRF dataset to a fingerprint built based upon a multi-element and core logging dataset (of proven confidence) adds value. This could, for example, show the lines between geochemistry and mineralogy because the given elemental concentrations from multi-element analysis relate to the minerals found within the XRF results (the minerals are composed of these elements).

In theory, all types of data can be used for a fingerprint, but different aspects such as the precision, accuracy, resolution, and sensitivity of the data should be considered. For the fingerprint classification, it is not necessary to always interpret the individual data sources for the goal of understanding and, therefore, data fusion should cover two aspects. Firstly, it should increase the confidence in the data representing the material attributes; additionally, it should converge this confidence to a reality. This way, it increases the indirect confidence of an inferred analytical technique, as well as the degree of fingerprint confidence. Secondly, doing sequential measurements with an inferred analytical device should provide the same confidence and enhance the inferred data source to a measured data source (feedback loop in Figure 7.1). Once a successful fingerprint classifier is in place, it is possible to measure a fingerprint with one sensor and know the related behaviour of mineral processing. For example, suppose that multi-element data are used to classify the fingerprint classes (unsupervised clustering), and an ML model is trained with mineralogical data (infrared) and the multi-element class labels. If the fingerprint classes are explored for processing behaviour, then, from a new infrared measurement, it is possible to get a proxy for the processing behaviour.

Please note that the suggested confidence classifications in Figure 7.5 (and the subsequent Figure 7.6) are only based on the author's experience with the selected datasets and mining operations.

7.4 Case study

After the formation of fingerprints, they can be used for the prediction of processing behaviour as they incorporate all available chemical, mineralogical, physical and mechanical attributes. As discussed in Section 7.3, the confidence of fingerprints obtained after the ML approaches is determined by the confidence of the datasets used

to generate them. Adding more attributes would generally increase the fingerprint confidence. Additional effects which affect the fingerprint confidence are related to whether they were obtained through direct measurements or through proxies and whether the input dataset were single-variate or multivariate. This section describes a case study to further illustrate the usefulness of fingerprints in mining. The case study shows the application of using fingerprints and its associated confidence degree in an open-pit mining operation.

The emphasis is on describing the type of available data in each unit process of a mining cycle, as well as on the impact of different processes on fingerprint confidence. The goal is to show how the degree of confidence of fingerprints plays a key role during a mining operation. Figure 7.6 shows, for each unit process, indicative estimations of the expected degree of the fingerprint confidence and the cumulative number of data points, which describe the fingerprint attributes. A confidence region (coloured shaded area) indicates the degree of confidence, and it increases or contracts in height based on the confidence at each unit process and optimality scenario. A suboptimal and an optimal scenario are shown in Figure 7.6. The difference in these scenarios results from the capability of incorporating sensing techniques. Here, optimal refers to a scenario where the mine minimises energy consumption and maximises recovery by understanding the material fingerprints. On the other hand, a suboptimal scenario relates to limited use or acquisition of sensor data to understand material attributes. The confidence degrees of the suboptimal and optimal scenarios may overlap with each other.

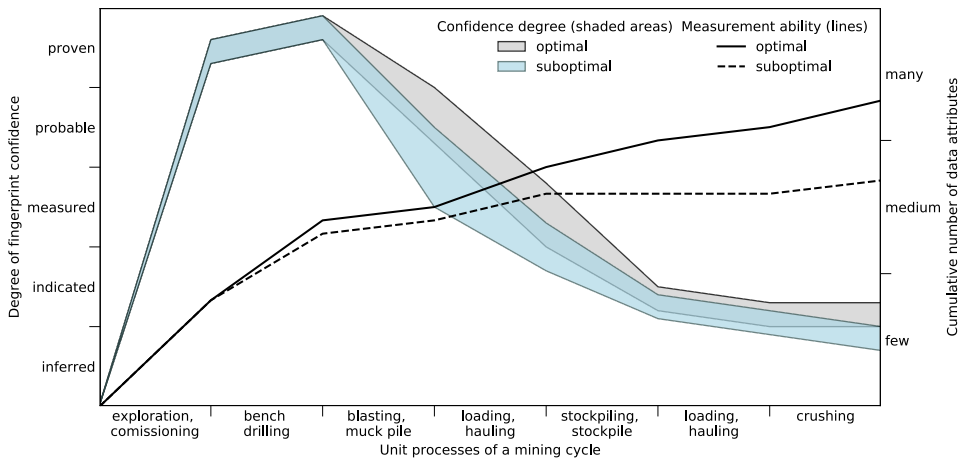


FIGURE 7.6: Indicative estimation of the degree of confidence in the fingerprint and the cumulative number of available data attributes throughout the mining cycle for two scenarios. The difference can be found in the degree of optimality and relates to the capability of incorporating sensing techniques.

For each of the unit processes from Figure 7.6, the paragraphs below describe how the indicative estimation of the degree of confidence in the fingerprint and the cumulative number of available data attributes are derived.

Exploration, commissioning: The goal during exploration and commissioning of a mine is to define proven fingerprints. This is done by collecting as many material attributes as possible to classify the material as proven reserves, which will be mined out. Therefore, the fingerprint confidence at this stage increases from no confidence to a proven degree of fingerprint confidence. This is also the starting point of the mining operation, and the first time the fingerprint is defined based upon the available data. Most of the black highlighted datasets from Figure 7.5 were collected before mining commences, and they give a basic amount of material attributes.

Bench drilling: Grade control drilling allows for indirect measurement of the defined, proven fingerprints and, therefore, increases the confidence and number of attributes. Rock chips are usually analysed using VNIR-SWIR, which gives new inferred mineralogical data and increases the fingerprint confidence. For example, a dense 6×6 m drilling pattern gives one infrared measurement for each 5 m composite per hole. A $120 \times 60 \times 10$ m bench then provides 400 additional infrared spectra. Depending on the analytical methods in place, the mineralogy can easily be added as an attribute to the fingerprints.

Blasting, muck pile: Blasting decreases the fingerprint confidence towards the probable and measured degree of confidence. The reason is that the material is fragmented, mixed and diluted across grade boundaries. However, the confidence loss can be limited by optimised blast processes for different rock types. Additional muck pile modelling could account for the blast movements and tell the approximate material location. It should be mentioned that if the blast design or analysis is incorrect, the confidence will steepen more rapidly. Since the muck pile is the direct result of blasting, it will show the effectiveness of the blast and always give additional data.

Loading, hauling between muck pile and stockpile: Loading and hauling is an essential process in determining the fingerprint confidence for two reasons. Firstly, a loader or excavator picks up individual measured small fingerprints, where unavoidable mixing of fingerprints takes place. Therefore, it is essential to rely on a good classification of the material. Secondly, proper allocation of the material increases the likelihood of having uniform stockpile compositions with one blend of material (with one known blend fingerprint composition). Depending on the allocation and the ability to track the material, the degree of fingerprint confidence decreases towards a measured confidence as the material is still known. However, there is more significant uncertainty in the exact location. The ability to decide on the dispatch location of the material increases the number of data attributes.

Stockpiling, stockpile: Typically, stockpiles are built up from different types of material, and mixing of material takes place during stockpiling. Therefore, the fingerprint confidence decreases and only a good indication of where a fingerprint is situated is possible. However, from the fingerprints of stockpiles, it is known that the material is mainly ore and, therefore, the confidence spread decreases. Stockpile sampling gives new fingerprint attributes and, for example, additional XRF analysis or hyperspectral imaging could quickly endorse the fingerprint compositions.

Loading, hauling between stockpile and primary crusher: Fingerprints resemble blends of material at the stockpile and, therefore, reclaiming this material does not decrease the confidence much. The cumulative number of attributes increases because the reclamation source and time, the time of delivery to the crusher, and the blend composition that determines the processing behaviour are known. Therefore, keeping track of the material fingerprints related to feeding of the primary crusher is an important step and allows for linking the processing behaviour with the last known fingerprint.

Crushing: In the primary crusher, the material is diluted if it originates from different stockpiles or combined with direct tips. Hence, the fingerprint confidence decreases. If the feed is from one stockpile, the confidence will remain the same. Summing up all the previous unit process steps shows that the confidence of the composition of the material that goes into the grinding circuit is at the inferred degree. However, if the expected fingerprint is linked with the processing behaviour data, then the knowledge about a fingerprint increases significantly.

Commodity-specific examples

Mines exploiting different commodities utilise similar unit processes, but the complexity of these unit processes changes due to different geological conditions. Three examples of various commodities with their related differences in the confidence of fingerprints are as follows:

- High-quality **iron ore** may be possible to distinguish from waste material based on colour, and using this as an attribute could increase the confidence in the selection of material for the stockpiles. Usually, the key factor in mining iron ore is strongly related to the quality (penalty elements) rather than the grade. Furthermore, iron ore characterisation can rely on the hyperspectral features and magnetic susceptibility of iron-bearing minerals (Ramanaidou and Wells, 2011). This might provide valuable attributes not further relevant to other commodities. Magnetic susceptibility measurements at the muck pile, loaders, trucks, or stockpiles would provide valuable extra fingerprint attributes.
- Porphyry **copper ore**, similar to iron ore, is mined in large-scale mining operations. However, the copper grade is usually very low, and, thus, lots of gangue material must be mined. If more confidence is obtained in characterising fingerprints that represent the higher-grade material, more efficient operations can be made. For example, the alteration minerals associated with porphyry copper deposits have characteristic infrared spectral features (Dalm et al., 2017) and could be used to link the behaviour of copper processing with fingerprints.
- Open-pit **gold** mining operations usually entail mining abundant gangue material for a relatively small amount of gold. However, most of the processed material will contain some gold and can be extracted. High-grade material can be identified when the typical alteration associated minerals related to, for example, gold veins are found. Then, these alteration minerals can be detected

with different techniques and be an indicator of the material (Dalm et al., 2018). Thus, better characterisation of ore fingerprints reduces the amount of waste processing and, additionally, minimises the environmental footprint.

7.5 Discussion

There is a large potential value for material fingerprinting in modern mining operations with vast quantities of accessible and clean managed data. The data fusion should be preferentially using high-confidence data so that proven fingerprints can be obtained. The creation of fingerprints could, for example, rely on high-dimensional clustering of apparently unrelated features. Afterwards, these fingerprints can be linked with the processing behaviour through neural networks. However, it remains to be seen how effectively the concept of fingerprints can be applied retrospectively to existing or old mines. In particular, when there are already large stockpiles or waste dumps, or the data are inaccessible, in the wrong format, or lacking in quantity/representativity, then this approach might not be beneficial.

The applicability of fingerprints could also substitute and reinforce expensive metallurgical tests. For example, if core samples with representative fingerprints are tested, then these results may better resemble the behaviour of processing compared to a limited number of metallurgical bulk samples (not considering changing process unit operating conditions). In addition, a mill needs to be designed to handle the hardest material from the ore reserves, although that is only a small portion of the ore. Therefore, instead of changing the physics of the mill to process this material better, the fingerprints can be relied on, which better represent all material. An understanding of the fingerprints could permit an optimal blending and feeding strategy. For this blend, the potential recovery is known and, therefore, the required feed rate for achieving it.

There is a significant drop in the fingerprint confidence between the moment of mining and processing. Tracking of fingerprints and having the ability to measure them allows for lowering this drop as the confidence can be upgraded through the feedback loop. The implementation of the feedback loop also allows for real-time reconciliation of material grades against fingerprint estimates and a recalibration of the fingerprint classifiers.

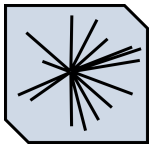
Fingerprints allow an operation to identify material through the process, regardless of resembling a block model's block, truckload, stockpile, or mill feed. Therefore, their use can also be extended towards flotation and (pyro)metallurgy. In particular, in confined and controlled conditions, like flotation, their use enables understanding the occurring physical and chemical mechanics and the produced type of waste or tailings. Moreover, the capacity to decide the composite of the blend gives the ability to produce customised (or zero) waste.

7.6 Conclusions

This chapter introduced the conceptual framework where fingerprints derived from machine learning are used as a tool for linking material attributes and blend compositions with the expected and obtained behaviour of processing. Defining fingerprints from high-confidence-based data and having the ability to measure and then track them throughout the unit operations of a mine gives confidence in the use and ability of fingerprints. Eventually, having an increase in confidence allows for optimising the behaviour of mineral processing. Fingerprints are built up using the fusion of vast quantities of data acquired during material characterisation, and they may be found through unsupervised clustering. Therefore, insight was given into the usefulness of these different datasets and into how well fingerprints characterise the material at each step of the unit processes of mining. The descriptive case study showed that the confidence degree of the composition of the material that enters into the primary crusher is inferred. In practice, this means that it is not understood what the material composition (or blend) is. By means of material tracking and a feedback loop for upgrading the degree of fingerprint confidence, this confidence can be increased towards a measured and, eventually, a proven fingerprint. A proven fingerprint can directly reflect the expected processing behaviour, improve the recovery, and reduce the amount of waste. Successful implementation gives retrospective value to all the collected data and could be useful in many operations.

8

Multi-element geochemical data clustering



This chapter shows how material fingerprints were created from multi-element geochemical data clustering. This includes showing of how a large raw industrial size dataset is cleaned and clustered. The resulting clustering classes show that each class has distinct mineralogical, geochemical and physical material properties and have spatial-contextual associations with the distribution of comminution and recovery parameters.

Parts of this chapter have been published in:

van Duijvenbode, J. R., L. M. Cloete, M. Soleymani Shishvan, and M. W. N. Buxton (2022). Interpreting run-of-mine comminution and recovery parameters using multi-element geochemical data clustering. *Minerals Engineering* 184, 107612. doi:10.1016/j.mineng.2022.107612.

8.1 Introduction

The previous chapter introduced the material fingerprinting framework and indicated the importance of creating strong relationships with high-quality data to get confidence in the use and ability of fingerprints. This chapter will demonstrate the construction of fingerprints based upon multi-element data which was classified as a dataset with a proven degree of confidence being able to give exact measured results and direct relationships to other datasets.

ME geochemical datasets (four-acid digestion) are among the most quantitative and informative information a mining company can collect. Together with the geological, mineralogical, and geophysical data, it forms the core datasets that describe different material attributes. Geochemical or ME data provide quantitative results that are chiefly used to identify mineralisation and gage exploration potential. For example, various studies have used this proxy relationship for mineral exploration potential (CSA, 2018; Gazley et al., 2015; Grunsky and de Caritat, 2019; Zhou et al., 2017), automated geological logging (Hill et al., 2020), or mapping mineralisation signatures and magmatic and hydrothermal processes (Brauhart, 2019; Escolme et al., 2019; Gaillard et al., 2018; Halley, 2020; Motoki et al., 2015). However, in view of this dissertations context, there has been a lack of published studies that consider the relationships of ME-based material classes with both comminution (processing) characteristics and recovery potential. The purpose of this Chapter is to address this gap. The following paragraphs discuss practices in merging mining related datasets to prepare the ME and metallurgical datasets for analysis.

Geochemical datasets are typically challenging to interpret because they are collected across multiple years and using different laboratories, analytical tools and methods. Therefore, careful analysis needs to be done to interpret the multi-dimensional data effectively (Grunsky and de Caritat, 2019). The current chapter shows the efforts undertaken to ensure a reliable dataset could be used for further analysis. Such efforts include adequate levelling of multiple datasets and detection of missing values. Furthermore, ME data are compositional and require transformation to log-ratio coordinates to account for closure (Aitchison, 1999; Grunsky and de Caritat, 2019; Pereira et al., 2016).

The cleaned datasets will then be used to retrospectively stitch ME proxy data and metallurgical test data together using geochemical data clustering, mineralogical interpretations, and considerations of spatial domains, addressing the existing lack of colocated datasets. Colocation is typically limited due to the infrequency of metallurgical test campaigns relative to gold assays and ME analysis, which is typically collected on every meter of drill core or chips. In metallurgical testing, the entire core length spanning the zone is typically used as a single composite, which effectively smooths the result and may underrepresent the overall variability of the response. Typically, the issue of non-colocation can still be overcome by ME analysis of sample splits from the larger metallurgical sample. These can then be used, in conjunction, to interpret processing properties from different geological domains that reflect changes in mineralogy, rock texture and rock competency. The remainder of this section discusses the structure of the chapter.

This chapter presents an unsupervised clustering approach of ME data and investigates the relationship between the resulting classes and comminution and recovery

parameters. Clustering is done for two case studies from the Tropicana Gold Mine, Western Australia, which show one clustering exercise each. Case Study I is focused on finding geochemical signatures related to (predominantly) gold mineralisation. In comparison, Case Study II focuses on unravelling the root cause of observed processing behaviour for the different mineralisation styles. This is done based upon re-clustering the Au-mineralised classes defined in Case Study I. This relationship between mineralisation and comminution behaviour is explained by exploring each class's geochemical signature and then linking them with legacy metallurgical test results across the different classes and spatial domains. The contribution is to provide tools to extract value from industrial-scale geochemical datasets and quantify material classes in terms of processing parameters. First, the data pre-processing steps are explained. This may help other researchers to extract similar values out of raw datasets. Second, we show the dimension reduction and clustering approach. Third, the geochemical signatures of the clustering classes are explored and illustrated how these relate to typical comminution and recovery parameters.

8.2 Methods

8.2.1 Data acquisition and pre-processing

This study focuses on 30,687 ME samples from the Tropicana Gold Mine area collected until June 2019. These samples have been routinely collected during exploration and were predominantly taken over one-meter intervals from NQ2 diamond core (core approx. 75.7 mm in diameter) across the orebody and adjacent unmineralised envelope (up to 18 m) in the hanging wall and footwall of the deposit. The samples were analysed in four different laboratories by four-acid digestion, which is a technique that effectively decomposes almost all rock-forming minerals (Grunsky and de Caritat, 2019). The resulting acid solution was then analysed by inductively coupled plasma optical emission spectrometry (ICP-OES) or inductively coupled plasma mass spectrometry (ICP-MS). The final results contain elemental concentrations for 48 elements. In addition, the samples were also assayed for gold (Au) concentration using (primarily) a 50 g charge fire-assay analysed by solvent extraction Atomic Absorption Spectroscopy (AAS) or MS. This dataset with samples and elemental concentrations was further filtered and prepared by the following three steps:

1. Element availability: The objective was to indicate for all samples whether the measured element must be considered for further clustering or not. Only elements that were measured in >95% of the samples were considered. This mostly represents the suite of common elements analysed in commercial four acid digest packages. Any additional element (Re, Ge, Eu) added would reduce the potential number of samples by at least 15%. The analysed (44) elements are Ag, Al, As, Ba, Be, Bi, Ca, Cd, Co, Cr, Cs, Cu, Fe, Ga, Hf, In, K, Li, Mg, Mn, Mo, Na, Nb, Ni, P, Pb, Rb, S, Sb, Sc, Se, Sn, Sr, Ta, Te, Th, Ti, Tl, U, V, W, Y, Zn and Zr. The Au concentration is also known for most samples but not further considered during clustering. Excluding Au from clustering guarantees that the resulting class signatures focus on major and other trace elements, describing the geochemical environment where Au may be found.

If, for a specific element, the proportion of values less than the analytical detection limit is too high, then an element value becomes a boolean indicator addressing whether an element is present or absent in a sample. There are two issues with these elemental concentrations in preparing them for clr representation. Firstly, if they are considered for closure, they will most likely distort the actual values of other elements since the real elemental concentration is unknown. Secondly, if this element is ignored in its entirety, we also neglect the important information that the element is present in some samples.

Various imputation techniques for below detection or missing data exist, including a simple substitution, lognormal replacement or multivariate expectation maximisation algorithms (Palarea-Albaladejo et al., 2014). In the dataset, As, Bi, Sb and Te were censored in about 60% of the samples and Se was censored in 93.5% of the samples. Martín-Fernández et al. (2012) recommend excluding elements with >30% of values below detection limit, which was done for Se, but not for As, Bi, Sb, and Te. After testing with the inclusion or removal of these elements, it was found that limited differences were found in the clustering results. Therefore, it was preferred to keep these elements, as especially As and Te are important trace elements in an orogenic Au deposit. Note that during Case Study II, this percentage of values below detection limit dropped below 30%. All elemental values below detection limit were simply substituted with values half of the detection limit (Carranza, 2011; Grunsky and Smee, 1999).

2. Data quality: The data are acquired across multiple years (2003–2019), four different laboratories, and with different analysis methods. Therefore, the quality of the geochemical data was checked and confirmed using 1,053 certified reference material (CRM) measurements representing the two largest laboratories. The other two laboratories are used infrequently and, due to the small sample representation (accountable for 1% of the samples), assumed to have no major influence on the precision or bias of the dataset. In 95% of the batches, at least one of the following seven CRMs were used consistently: AMIS0167, OREAS 24b, OREAS 25a, OREAS 45d, OREAS 45e, OREAS 502b or OREAS 520. The expected concentration of each element and its variation range (at two standard deviations) are known for these standards. Based on these known values, the interlaboratory (reproducibility) and intralaboratory (repeatability) data quality is checked. If all conditions are satisfied, then the data are considered high enough quality, and no additional data filtering is required. When differences in the precision of samples or elements are noticed, individual batch samples or elements can be discarded.

The three quality metrics used are precision, bias and Horwitz Ratio (HorRat). The precision indicates the deviation from the best value (BV) expressed as the percent relative standard deviation (RSD%) of the CRM values. The accuracy is reported as bias which is calculated as the percent difference between the average CRM value obtained from the laboratory measurements and the best value (BV) recommended by the CRM certificate (Ordóñez-Calderón et al., 2017). The HorRat is a metric that quantifies the measurement performance with respect to precision (Horwitz and Albert, 2006) and is calculated (for single-laboratory validation) as follows:

$$\text{HorRat}_r = \frac{\text{observed relative SD}}{\text{predicated relative SD}} = \frac{\text{RSD}_r}{\text{PRSD}_R} \quad (8.1)$$

where PRSD_R the predicted reproducibility obtained from the Horwitz equation and calculated as $\text{PRSD}_R = 2 \cdot (\text{certified value}_{\text{CRM}} \times 10^{-6} (\text{ppm to concentration}))^{-0.15}$, and subscript r and R indicating the repeatability (intralaboratory) and reproducibility (interlaboratory) conditions, respectively. This equation transforms the RSD% found to a fraction of the RSD% expected and equals to 1 for exact correspondence. The precision is better than expected if the HorRat is <1 , and poorer if >1 . Under reproducibility conditions, the empirically acceptable range is from 0.5 to 2.0 and under repeatability conditions between 0.3 and 1.3 (Horwitz and Albert, 2006; Rivera et al., 2011).

3. Transformation and normalisation: The ME data used are compositional in nature and have associated problems of closure (Aitchison, 1999). Before samples can be compared, the sample composition will require transformation to log-ratio coordinates with respect to the identified elements. This study uses a centred log-ratio (clr) transformation, which transforms the data coordinates from the simplex, an n -dimensional composition within the positive real number space, to the Euclidean real space, which is more suitable for statistical analysis (Aitchison, 1986; Bhuiyan et al., 2019).

8.2.2 Clustering

This study used agglomerative hierarchical clustering to partition the samples into clusters (Wierzchoń and Kłopotek, 2018). The clustering method is iterative and starts with each sample in its own cluster. Then, the algorithm calculates the distance for each cluster pair (Euclidean distance matrix) and finds the closest pair. The metric to calculate the distance can differ, and the present study uses Ward's method. This minimises the sum of squares of distances between samples and the cluster centres to which the samples belong. The two selected clusters are merged into a new cluster. Afterwards, the distance matrix is updated by calculating the new distance from the new cluster to all other clusters. These merge and update steps are repeated until only one single cluster is formed (Wierzchoń and Kłopotek, 2018). The final number of clusters is selected based upon the silhouette score, Calinski-Harabasz index and Davies-Bouldin index. All these metrics are internal clustering validation measures and are used to determine the optimal number of clusters (Aggarwal and Reddy, 2014). The final number agreed upon across the methods is used for the final clustering exercise. The number of clusters is dependent on the set of input samples.

8.3 Quality assurance and quality control

8.3.1 Precision, bias and HorRat

Table 8.1 summarises the analytical results for OREAS 45d and a few selected elements described in this study. The results for all other CRMs and elements are provided in Supplementary Materials Table A.1 from van Duijvenbode et al. (2022a). The CRM analysis indicates precision better than 10% for most major and trace elements, and 10 to 15% for Ag, In and Zn. The bias is better than $\pm 10\%$ for most elements in both laboratories. Laboratory 2 has a bias of 35% for Ag and -11.7% for Cr. The same precision and bias conclusions are generally valid for all other CRMs and elements (Supplementary Materials Table A.1 from van Duijvenbode et al. (2022a)). The intralaboratory $HorRat_r$ ratios obtained for most elements were within the acceptable range of 0.3 – 1.3 under repeatability conditions (Table 8.1). However, laboratory 2 has suspect $HorRat_r$ values for various oxide bearing elements (e.g., Al, Ca, Fe) measured with OES, while the precision and bias are within 10%. Several possible causes emerge from the analysis of HorRat values displayed in Figure 8.1.

TABLE 8.1: Analytical data for intralaboratory measurements of OREAS 45d for laboratories 1 and 2. Precision is expressed as percent relative standard deviation (RSD%). Bias is calculated as the percent difference between the average and the best value (BV) of the OREAS 45d certificate. The lower detection limits (LDL) are reported for the analytes and analysis method used by the laboratory. The entire table, including the remaining elements and CRMs, can be found in Supplementary Material Table A.1 from van Duijvenbode et al. (2022a).

Elem.	Analysis method	Unit	BV	Laboratory 1						Laboratory 2						
				LDL	Avg.	SD	RSD(%)	Bias(%)	$HorRat_r$	LDL	Avg.	SD	RSD(%)	Bias(%)	$HorRat_r$	
Ag	MS	ppm	0.2	0.1	BV is too close to the LDL value						0.05	0.27	0.04	14.8	35	0.7
As	MS	ppm	13.8	2	13.9	0.52	3.7	0.5	0.3	1	13.4	1.17	8.7	-2.7	0.8	
Bi	MS	ppm	0.31	0.05	0.32	0.02	6.2	3.2	0.3	0.1	0.3	0.02	6.7	-3.2	0.4	
In	MS	ppm	0.1	0.05	0.09	0.01	11.1	-10	0.5	0.02	0.09	0.01	11.1	-10	0.5	
Mo	MS	ppm	2.5	0.1	2.49	0.1	4	-0.4	0.3	0.1	2.65	0.15	5.7	6	0.4	
Rb	MS	ppm	42.1	0.1	42.3	1.32	3.1	0.5	0.3	0.05	43.7	2.22	5.1	3.8	0.6	
Sr	MS	ppm	31.3	0.5	32.1	1.39	4.3	2.6	0.5	0.1	32.7	1.83	5.6	4.2	0.6	
Th	MS	ppm	14.5	0.05	14.4	0.34	2.4	-0.6	0.2	0.05	14.8	0.96	6.5	2.1	0.6	
U	MS	ppm	2.63	0.05	2.62	0.11	4.2	-0.4	0.3	0.05	2.67	0.18	6.7	1.5	0.5	
Al	OES	%	8.15	0.005	8.09	0.19	2.3	-0.7	0.8	0.01	7.91	0.6	7.9	-3	2.7	
Ca	OES	ppm	1854	50	1918	110	5.8	3.5	1.1	50	1924	136	7.0	3.8	1.4	
Cr	OES	ppm	549	1	549	29.3	5.3	0.1	0.9	10	484	26.6	5.5	-11.7	0.9	
Fe	OES	%	14.51	0.01	14.5	0.32	2.2	-0.3	0.8	0.01	14.12	0.61	4.3	-2.7	1.6	
K	OES	ppm	4123	20	4227	129	3.1	2.5	0.7	100	4072	184	4.5	-1.2	1.0	
Mg	OES	ppm	2447	20	2404	83.9	3.5	-1.7	0.7	20	2378	110	4.6	-2.8	0.9	
Na	OES	ppm	1006	20	1003	46.5	4.6	-0.3	0.8	50	980	48.4	4.9	-2.6	0.9	
S	OES	ppm	486	50	486	20.7	4.3	-0.1	0.7	20	482	31.4	6.5	-0.8	1	
Zn	OES	ppm	45.7	1	44.1	4.13	9.4	-3.6	1	5	45.8	4.93	10.8	0.2	1.2	

Figure 8.1a and Figure 8.1b contain the intralaboratory $HorRat_r$ values for laboratories 1 and 2, respectively. A darker red square indicates higher HorRat values (>1.3) than expected and can be explained by three causes. First, a few outliers cause the RSD% to increase too much (outliers above BV: Ca, Mn, Na, Pb, Zn, Zr; outliers below BV: Cr, Fe, K, S, Ti). Removing these outliers would decrease the HorRat value within the acceptable ranges. Second, there is a relatively larger bias in the measurements either below (As) or above (Sb) the BV. This is often in conjunction with the BV being

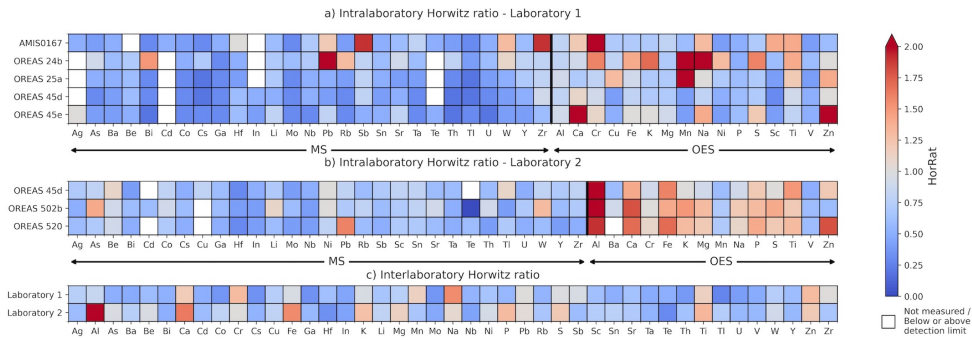


FIGURE 8.1: Intralaboratory (a and b) and interlaboratory (c) Horwitz ratio overview of certified reference material (CRM) – element pairs measured in two laboratories. The empirical accepted intralaboratory Horwitz ratio range is between 0.3 and 1.3, and the interlaboratory Horwitz ratio range is between 0.5 and 2.0.

close to the LDL (Pb, Sc), resulting in less precise measurements. However, this is not indicated as a problem because other CRMs are better to assure the precision and bias of these elements in the dataset. Third, a large group of the elements (Al, Ca, Fe, P, S, Ti, Zn) measured with ICP-OES in laboratory 2 have precision and bias better than $\pm 10\%$ (Supplementary Material Table 1 from van Duijvenbode et al. (2022a)), but $HorRat_r$ close to or above 1.3. For most of these elements, the SD is smaller than expected from this CRM, indicating that the laboratory measurements are better than anticipated. A dark blue square indicates lower $HorRat$ values (<0.3) than expected and links to the following cause. There is a large group of elemental concentrations (Bi, Cs, Th, Tl, U) within ± 1 SD. This means that there is a higher RSD% as anticipated from the CRM. Finally, a white square indicates that no proper data were available because the measurement technique cannot measure the specific element or the CRMs elemental concentration is in $>50\%$ of the measurements below the detection limit. This, for example, is the case with Cd and Te of OREAS 45d.

The interlaboratory $HorRat_R$ values are represented in Figure 8.1c and indicate how laboratories 1 and 2 perform compared. The shown $HorRat_R$ values are the mean of the $HorRat_r$ values presented in Figure 8.1a and Figure 8.1b. In laboratory 1, there are a few elements (Co, Cs, Ga, Mo, Tl) with $HorRat_R$ values much lower than the acceptable lower limit of 0.5. Laboratory 2 has slightly higher $HorRat$ values for most oxide elements. As indicated above, the precision and bias for these elements are still good.

Additionally, there are a few large outlier measurements that were not removed prior to analysis, for example, Al. Also, note that an elevated Al concentration can indicate that the digestion was not taken to incipient dryness and causes the Al to remain in the test tube as an insoluble fluoride complex. Outliers were not removed because the large dataset and applied transformations would reduce their effect. Overall, the Al (and the other oxides) $HorRat$ values for laboratory 2 are inappropriate, but its precision (7.2%) and bias (2.3%) are good. Since the $HorRat_R$ values of most of the elements are within the acceptable ranges (0.5–2.0), it can be concluded that the four-acid digestion measurements of the different laboratories can be compared.

8.3.2 Summary of data reduction constraints

In summary, it is observed that there is a difference in precision for certain elements. For most oxide bearing elements, such as Al, Ca, K, Mn, Na, S and Ti, there is a small overestimation of the concentration (average RSD% is 5.5%, bias is +2.3%). The majority of the other elements are of good quality and may experience underestimation rather than overestimation. As a result, this reduces the tendency for over-optimistic conclusions. Most of the values can be improved by simply removing a single outlier. This means that the batch measurements are reliable and that the different instrumentation methods can be compared. The results from blanks indicate no significant contamination with elements of interest in this study. In addition, the mine's standard quality assurance and quality control procedure for every batch would have highlighted measurement deviations, and the corresponding batches would be re-assayed prior to uploading them to the database. Accordingly, the ME geochemical dataset is deemed of good quality.

Indium, Cd and Se were removed from the original list of elements resulting in 41 elements being considered for clr transformation: Ag, Al, As, Ba, Be, Bi, Ca, Co, Cr, Cs, Cu, Fe, Ga, Hf, K, Li, Mg, Mn, Mo, Na, Nb, Ni, P, Pb, Rb, S, Sb, Sc, Sn, Sr, Te, Ta, Th, Ti, Tl, U, V, W, Y, Zn and Zr. The values of these elements underwent clr transformation and, afterwards, were normalised by a z-score normalisation. The feature dimension of this dataset was reduced using Principal Component Analysis. The number of principal components (PCs) was automatically set to the amount that can describe 95% of the data variance. The lower-dimensional dataset, i.e., the output of the PCA, functioned as the input for clustering.

Several data reduction measures are considered before clustering based upon the precision, bias and HorRat values. These constraints are primarily taken to produce discrete clustering classes not affected by any of the observed elemental concentration deviations. Any following conclusions may consider the excluded elements again, but while taking their flaws into account. The following data constraints are taken:

- Although not obvious from the quality metrics, indium was measured outside the 2 SD range in 31% (average RSD% of 9%) of the CRM measurements and was also in 65% of the samples below the detection limit. Therefore, indium will not be considered during clustering.
- Determining the precision and accuracy of Cd was difficult as it was only possible with two CRMs. The corresponding HorRat was sufficient (~ 0.6); however, its precision (11.3%) and bias (60%) were considered to be too high and, therefore, Cd will be ignored.
- Most HorRat and z-score acceptable range breaches could be linked to one CRM element outlier. This does not mean that the entire batch was wrong. There was one batch with significant outliers (>4 SD) in 31 elements. The samples corresponding to this batch were not further considered.
- The effect of outliers, in general, is also reduced by the performed clr transformation (this is especially useful for the oxide bearing elements).

8.3.3 Comminution and recovery proxies

A few material hardness proxies were collected at TGM and were selected for review in this study based on availability. These include: the Bond Ball Mill Work index (BWi in kWh/t), the JK rock breakage parameters and expressed as comminution index Axb and Equotip rebound hardness measurements. The BWi determines the relative energy requirements to deliver a specified target particle size (typically either 106 μm or 75 μm) given a certain feed particle size, and are rock-specific dimensionless parameters determined by fitting a model to the experimental data generated from a drop weight test (Lynch, 2015). Higher values of Axb indicate softer rocks, whereas higher values of BWi indicate harder rocks. The BWi and Axb values are infrequently collected during metallurgical testing campaigns. However, they are direct proxies for processing attributes such as throughput and resulting grind size (Lynch, 2015). Equotip measurements are taken on diamond drill core, aligned to the standard Au assay intervals of one meter. Generally, ten measurements were taken per sample, and for this study, simply the median value was chosen to give one data point per meter. The measurements are frequently colocated with samples used for ME analysis but also include larger portions of the immediate hanging and footwall. The Equotip hardness-testing tool yields Leeb (Ls) values, where a higher Leeb corresponds with a harder sample.

Figures 8.2a-c show summary statistics of Equotip, BWi and Axb measurements taken on primarily mineralised material across all deposits. The Leeb values (Figure 8.2a) are at the high end of the value range (between 0 and 1000 Leeb), indicating relatively hard rock properties. The mineralised material itself has an expected Leeb value between 750 and 850. Higher values probably relate to increased proportions of quartz, amphibolite and garnet content in the samples. Figure 8.2b displays the BWi histogram with a bimodal distribution where one mode is around 16 kWh/t,

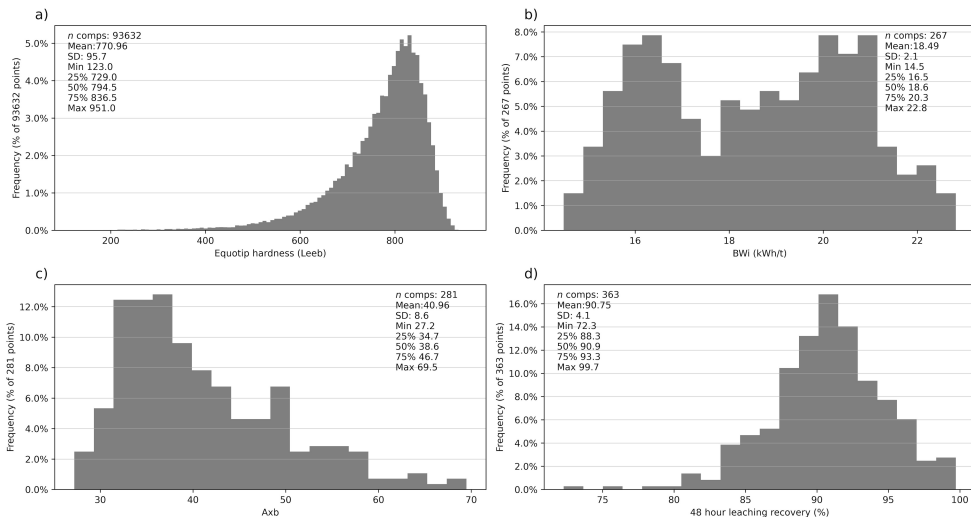


FIGURE 8.2: Summary statistics. Histograms of the Equotip rebound hardness, BWi, Axb and 48-hour leach recovery taken across all geological domains.

and the other one is closer to 20 kWh/t. In contrast, the Axb (Figure 8.2c) shows a right-skewed distribution with the mode around 38.6. The lower BWi typically resembles samples closer to the surface and is related to either the lower saprolite or Transitional ore. The absence of a bimodal signature in the Axb most likely resembles the different test responses on these rock types.

The recovery proxies used in this study are the 48-hour leach recovery (in %), lime consumption (kg/t) and cyanide consumption (kg/t). Figure 8.2d shows summary statistics of the recovery values. Among these composites, there is an average recovery of 90.75%. The recovery typically decreases with the depth of the mined material and due to increasing S and Te content (Baker, 2020).

8.4 Results

8.4.1 Case Study I: Geochemical mineralised and unmineralised rock separation

8.4.1.1 Elemental patterns derived from PCA

The 30,687 samples with 41 input features (clr-transformed element values) were reduced to 24 PCs accounting for 95% data variability. Element eigenvectors are plotted in PC1-PC2 and PC2-PC3 space in Figure 8.3. A few generalised features are evident from these biplots, which account for 59% of the data variability. Five groups of elements are defined by similar vector orientation and magnitude: 1) with positive PC1 loadings, there are elements generally indicating mafic/ultramafic units, e.g., Ca, Co, Cr, Fe, Mg, Mn, Ni, and Zn; 2) a negative PC1 and positive PC2 relates to elements which are commonly associated with gold mineralisation at TGM (Crawford and Doyle, 2016), e.g., Ag, As, Bi, Mo, S, Te, U, and W; 3) the negative loadings of PC2 identifies elements related to sodic alteration (Be, Na, Sr), and 4) in combination with negative PC3 loading also with elements related to potassic alteration: K, Rb, Ba, Tl, and Cs; 5) elements with a positive PC3 loading relate to the

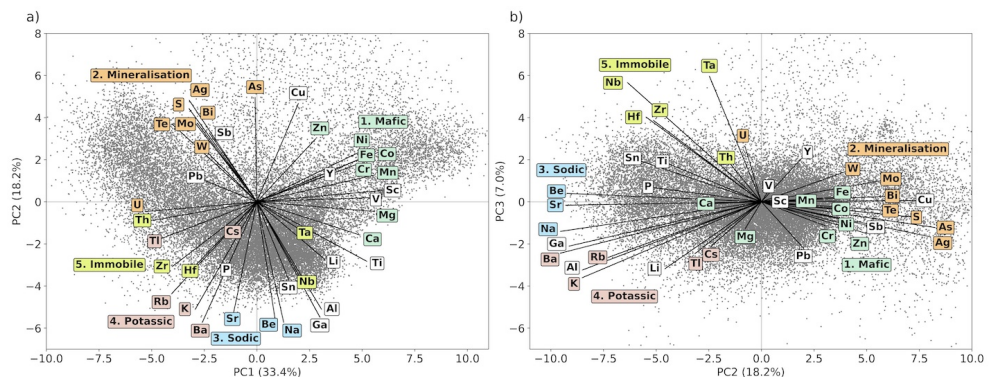


FIGURE 8.3: Principal component biplot of clr-transformed elements plotted on a) PC1-PC2 space and b) PC2-PC3 space.

8.4.1.2 Geochemical discrimination

The easiest way to discriminate mineralised vs unmineralised classes (based on Au grade) is to look at the Au content of each sample within the classes. The Au data was attributed according to the clustering classes and viewed as statistical boxplots in Figure 8.5. Three classes (W1, W2, W3) only contained samples with Au <0.3 ppm and were denoted barren/unmineralised, and two classes (W4, W5) had >85% of the samples below 0.1 ppm Au (and only 2–5% was above the mine's cut-off grade of 0.3 ppm Au). The remaining two classes (MIN1, MIN2) relate more to the mineralisation signatures and will be clustered again in Section 8.4.2. The clustering

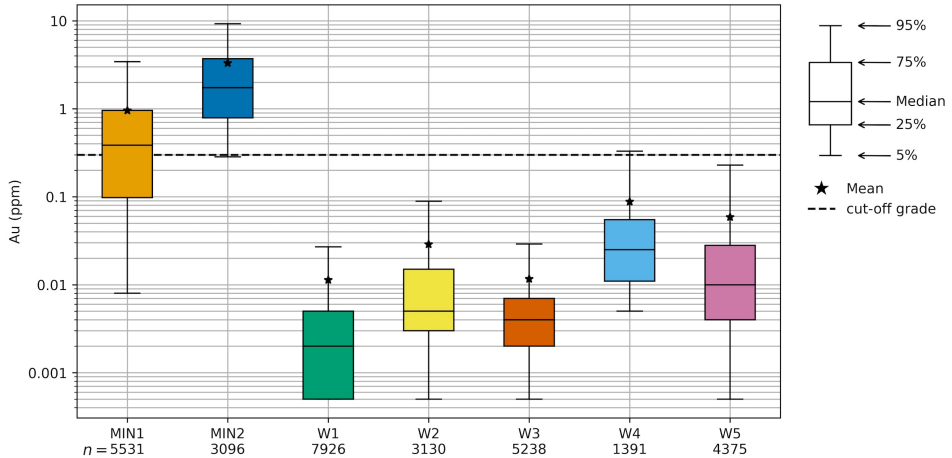


FIGURE 8.5: Box and whisker plot of Au grade (ppm) for the clustering classes of Case Study I.

itself did not consider the Au concentration as a variable, which means that the geochemical signatures of the resulting classes are distinct enough for mineralised and unmineralised signature separation, as will be discussed in Sections 8.4.1.3 and 8.4.1.4. Figure 8.6 shows how the clustering classes spatially align with different geological units in a 100 m width Havana South cross-section. This demonstrates great spatial contiguity and validates that the obtained classes are also coherent with the geological interpretation.

To further assess the variability of the framework silicate mineralogy in the classes, the bulk rock ME data are plotted in an alkali-alumina molar ratio diagram (Figure 8.7). This diagram shows the variations in bulk rock chemistry related to changes in mineral modal proportions per class (Davies and Whitehead, 2006). This diagram plots proportions of the mobile alkalis (Na and K) divided by the relatively immobile Al against each other. Various ideal mineralogical compositions of typical rock-forming minerals are also indicated, including the position of the least altered feldspathic gneiss and mafic garnet gneiss based upon logging. The position of samples plotting above the albite-K-feldspar tie line likely reflects analytical measurement issues since one would not expect a natural sample to fall beyond this line.

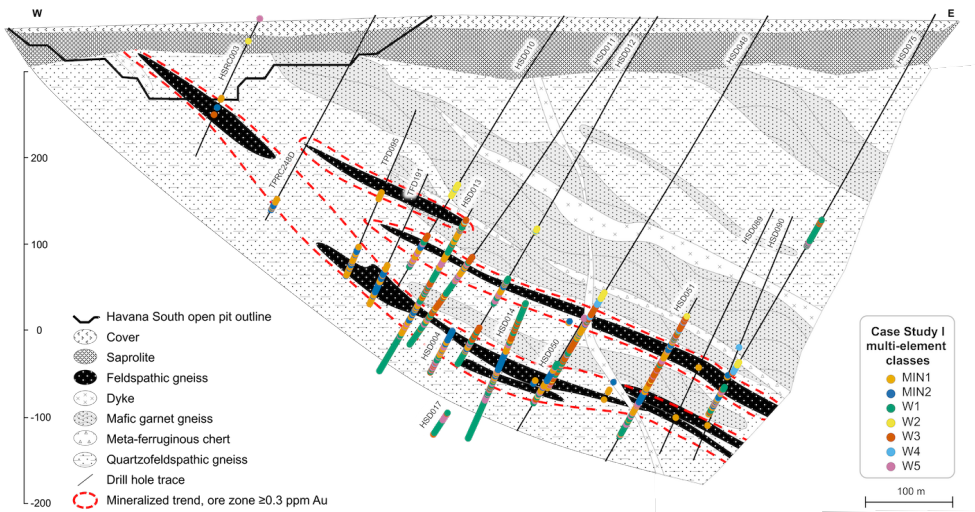


FIGURE 8.6: Schematic EW cross-section of the Havana South domain showing the deposit geology (100 m thick at 649753 mE, 6761137 mN, azimuth 37° , GDA94 / MGA zone 51 grid). The ME class labels from Case Study I are superimposed on the drill holes.

The identified classes show a typical igneous and meta-igneous rock classification. The most felsic classes (MIN1/MIN2) are mineralised, showing a relative K enrichment and trend towards the K-feldspar \pm biotite node in Figure 8.7. The relatively unaltered feldspathic gneisses (class W5) are between $0.18 \leq K/Al \leq 0.3$ and $0.3 \leq Na/Al \leq 0.4$. Still felsic, but the more quartzofeldspathic gneisses (class W1), which are less sodic and a little more potassic, follow the albite-muscovite tie line indicating more sericite alteration. The more felsic/intermediate (class W3) and mafic (class

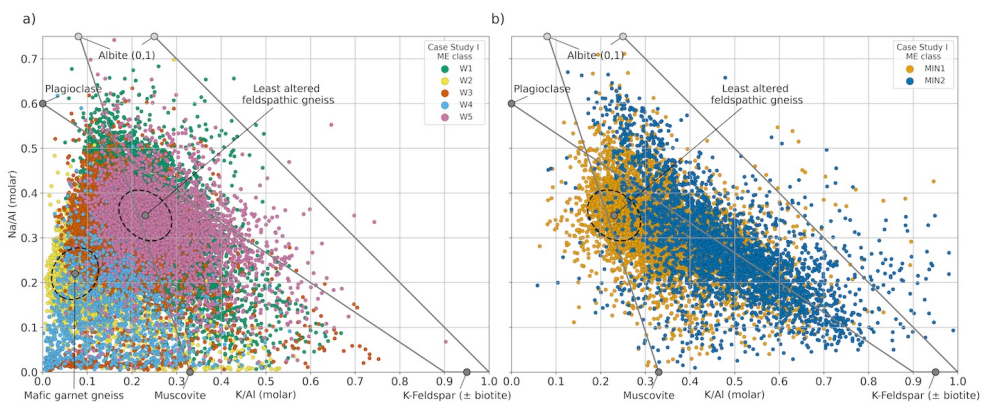


FIGURE 8.7: Multi-element samples from Case Study I plotted on the alkali-alumina ratio plot to assess alteration phases, after Davies and Whitehead (2006), thematically attributed by clustering classes.

W2) classes trend towards the origin. The highest point density of the garnet-bearing gneisses logged samples (mafic rocks) is between $0.02 \leq K/Al \leq 0.13$ and $0.15 \leq Na/Al \leq 0.27$. Finally, class W4 is closely related to a meta-ferruginous chert.

The following sections discuss the geochemical signature of each class and association with the alkali-alumina molar ratio diagram in more detail. The lithological descriptions of the classes are supported by the logged geology corresponding to the sample intervals (Figure 8.4) and the observed plotting location in Figure 8.7. Box and whisker plots of the elemental concentrations of samples found within each class for Case Study I can be found in Supplementary Material Figure A.2 from van Duijvenbode et al. (2022a).

8.4.1.3 Unmineralised material related classes (W1, W2, W3, W4 and W5)

Relative to the mineralised classes, the unmineralised classes show lower elemental concentrations of the mineralisation indicating elements, e.g., Au, S, Te, Tl, W, Mo, Bi, and Sb (see Supplementary Material Figure A.2 from van Duijvenbode et al. (2022a)). Therefore, the geochemical signature of W1, W2 and W3 represent non-gold bearing materials.

- Waste class 1 (W1, $n = 7,908$) is dominated by an unmineralised quartzofeldspathic gneiss signature (Figure 8.4a) and relates to metamorphosed felsic volcanics or intrusive units. The PC2 component is very low, indicating the feldspar association. Figure 8.7 shows moderate Na/Al (molar) ratio values (0.2 to $0.5Na/Al$) trending towards increasing modal proportions of plagioclase and albite, indicating a more sodic feldspar. Minor amounts of quartz-feldspar-bearing pegmatites also characterise this class. Geochemically, this class is characterised by a relative Na and K concentration almost equal to MIN1 and MIN2 but lacking the trace elements associated with mineralisation (Ag, As, Bi, Sb, Te).
- Waste class 2 (W2, $n = 3,123$) has a geochemical signature related to (mafic) garnet-bearing amphibolitic gneiss. It is the most mafic rock type demonstrated by a positive loading of PC1. This lithology is unmineralised (typically <0.01 ppm Au) and does generally have chlorite +/- calcite alteration. This class also captured chlorite dominated schists and a few unshered basalts and Proterozoic dolerites. The mafic rock signature is observed in the relatively higher concentrations of most major elements (Ca, Fe, Mn, Mg) and lower concentrations of K. This can also be seen in Figure 8.7 since most W2 samples are trending towards the origin and are located near the mafic garnet gneiss node.
- Waste class 3 (W3, $n = 5,214$) has a geochemical signature that is a mixture of class W1 and W2. All samples fall between the mafic garnet gneiss and the least feldspathic gneiss node in Figure 8.7. It mostly represents garnet-bearing amphibolitic and quartzofeldspathic gneiss rock types but also captures some biotite/chlorite dominated schists and saprolitic clays close to the surface (visibly distinct at Na/Al (molar) ≈ 0). Generally, these samples are less mafic, indicated by less chlorite alteration.

The geochemical signature of class W4 and W5 primarily represents unmineralised material with some trace Au mineralisation (2–5% of the class samples are above 0.3 ppm Au).

- Waste class 4 (W4, $n = 1,391$) samples all fall below the albite to muscovite tie line. This class has relatively higher Ag, As, Bi, Mo, Pb, Sb and Zn concentrations (high PC2) compared to the other unmineralised classes. Almost 54% of this material is logged as a meta-ferruginous chert (relatively high Fe and low Al), reflecting high modal proportions of pyrrhotite and (lesser) pyrite and magnetite (Hardwick, 2021).
- Waste class 5 (W5, $n = 4,375$) has a high point density directly at the least altered feldspathic gneiss node, similar to W1 (Figure 8.7), representing samples with the least altered alkali signature. Compared to W1, this class has less quartz and is less sodic and more potassic, hence the trace mineralisation. Relative to MIN1/MIN2 and the mineralisation-related elements, this class lacks the higher Zr, Hf, Th, indicating a more distal spatial correlation with the gold system. Spatial contiguity indicates that these samples form part of the immediate hanging wall (Figure 8.6).

8.4.1.4 Mineralisation associated classes (MIN1 and MIN2)

Mineralised class 1 (MIN1, $n = 5,531$) and class 2 (MIN2, $n = 3,096$) both have an Au-mineralised related geochemical signature, where MIN2 represents the high Au grade material (Figure 8.5). The geochemical signature of both classes relates to a feldspathic gneiss, where MIN1 has a more distinct quartz character (typically found in logging). These classes have similar Fe and K concentrations as the quartzofeldspathic gneiss classes (W1 and W5) but lower concentrations of Ca and Na. This higher relative proportion of Fe and K is accounted for by higher modal proportions of pyrite and K-feldspar (less biotite) and lower plagioclase proportions (Hardwick, 2021). Both classes are characterised by an enriched K/Al (molar) ratio, where MIN1 is generally a bit lower. Figure 8.7 shows that the samples predominantly fall along the tie line between the ideal mineral composition of Ca-Na plagioclase and K-feldspar/biotite. This suggests that these classes reflect increasing potassic alteration from a relatively unaltered with primary Ca-Na feldspar to a highly altered and mineralised K-feldspar rich rock. The same is true for the increasing Au grade towards the K-feldspar node. The low-grade samples are more linked to lower K/Al (molar) ratios and are relatively plagioclase rich.

8.4.1.5 Summary of Case Study I

Geochemical data clustering from 30,687 samples revealed that two classes ($n = 8,627$) were predominantly related to the gold mineralisation signature found at TGM. The clustering did not take Au concentration into account as a variable, demonstrating that geochemical data is distinct enough for mineralised and unmineralised material to be discriminated. Furthermore, the approach is data-driven and automated hence repeatable classification can be done. Another approach to split mineralised and unmineralised material would be to use the logged lithology and Au grades. However,

this may be complicated by the subjectivity of geological logging and the nuggety nature of Au assay data. Despite these limitations, the results showed that significant overlap was found between the defined classes and logged lithology, hence the classes can be used as a first pass litho-geochemical classification of mineralised and unmineralised material. In the next section, the two mineralised material classes are re-clustered to find geochemical signatures typically associated with comminution and recovery characteristics of mineralised material at TGM.

8.4.2 Case Study II: Interpretation of comminution and recovery parameters

The first case study showed the effectiveness of clustering geochemical data and how it could discriminate mineralised material from unmineralised material (waste). The second case study is a sequel to the previous case study and has the aim to find geochemical signatures typically associated with comminution and recovery characteristics of mineralised material at TGM. This part continues only with the indicated mineralised related material classes (MIN1 and MIN2) only since these are expected to dominate the processing stream. The samples ($n = 8,627$) corresponding with these classes are selected and the original sample elemental concentrations are again clr-transformed and normalised.

8.4.2.1 Elemental patterns derived from PCA

PCA reduced the 41 element features to 26 PC features, and a new clustering was performed. Two more PCs are required to describe the 95% data variation compared to Case Study I. This is as expected because the samples are geochemically more similar and, therefore, more components are needed to explain the data variation. A visualisation of the scaled and ordered eigenvalues of PC1 and PC2 for all elements can be seen in Figure 8.8. Note that a biplot similar to Figure 8.4 would not have shown a separation based upon lithology since 82% of the samples were logged either as feldspathic gneiss ($n = 5,726$) or quartzofeldspathic gneiss ($n = 1,344$). See Supplementary Material Figure A.3 from van Duijvenbode et al. (2022a) for biplots of PC1-PC2 and PC1-PC3.

Figure 8.8 shows that a positive PC1 is mostly related to elements that are indicative of mineralisation and dominated by positive loadings on U, Bi, Te, Sb, W, Mo, As, and S. The oxide bearing elements found (Ca, Ti, Mg, Al) are found at a lower PC1. A positive PC2 loading has a larger association with the mafic indicating elements (Ni, Cr, Co, Cu, Fe, Ag). However, this would in the felsic gneiss logged samples be more considered as metal associations. At a low PC2 are the relative immobile high field strength element (HFSE) pairs Hf and Zr, Nb and Ta, and low field strength elements Sr and Rb.

It is observed that this PC analysis is more focused on grouping samples with similar degrees of positive and negative relationships with given element eigenvectors together rather than separating major rock units from each other, as was found in Case Study I. This is the desired effect because most of the samples are mineralised and, therefore, clustering partitions will indicate geochemical differences due to the alteration and mineralisation. Ultimately resulting in different metallurgical responses.

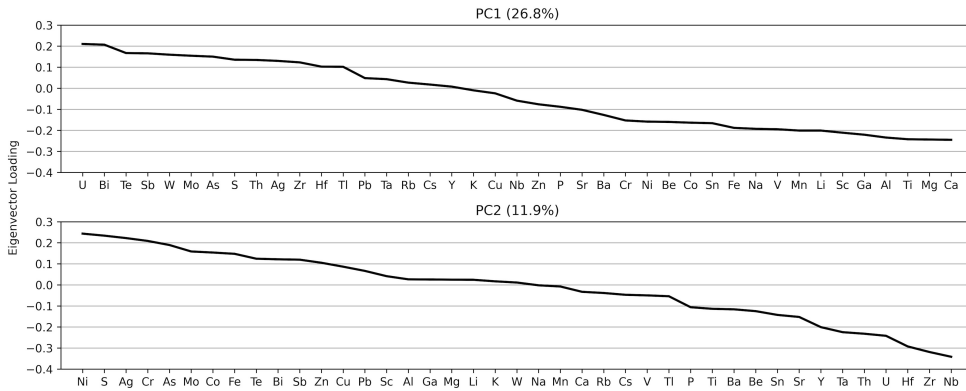


FIGURE 8.8: Case Study II related scaled and ordered eigenvalues of PC1 and PC2 for all elements.

It is found that the mineralised material can best be partitioned in five clusters indicated by the peak and trough in the Silhouette score and Davies-Bouldin index score, respectively (see Supplementary Material Figure A.1 from van Duijvenbode et al. (2022a)).

8.4.2.2 Geochemical signatures

To discuss the geochemical signatures of the classes, it is useful to first look at the gold grade of the classes to find out which material classes have the highest likelihood of being processed. Analysing the classes for their gold content indicates that all classes have an average Au grade above the 0.3 ppm cut-off grade and have a high likelihood to be considered as run-of-mine material. Figure 8.9 shows boxplots of the Au grade per class. The median Au grade of the mineralised waste or low grade (LG) class is 0.15 ppm; the marginal grade (MG) class is 0.54 ppm; high grade 1 (HG3) is 0.86 ppm; high grade 2 (HG2) is 1.33 ppm, and high grade 3 (HG1) is 2.63 ppm. Note that the average Au grade per class is higher than the median.

Medium and Lower-Grade mineralisation classes (MG, LG): Due to a large number of samples ($n = 30,687$) and the constraint of having only seven classes in Case Study I, there are still unmineralised samples not separated yet from the mineralised material since they have fairly similar geochemical characteristics as the mineralised feldspathic gneiss. These classes have notably minor or absent K-feldspar compared to the high-grade classes. Their composition is more plagioclase-bearing \pm quartz with amphibole-biotite. These samples are commonly found in the immediate (unmineralised) hanging wall and footwall lithologies.

Figure 8.10a shows that the MG ($n = 1,882$) and LG ($n = 2,464$) samples plot the closest to the least altered feldspathic gneiss node, are mostly below the plagioclase-K-feldspar tie line, and slightly disperse towards the muscovite (LG) or K-feldspar (MG) node. These class signatures are more associated with increasing sericite-biotite-chlorite alteration. Figure 8.11 shows that relative to the high-grade classes, MG

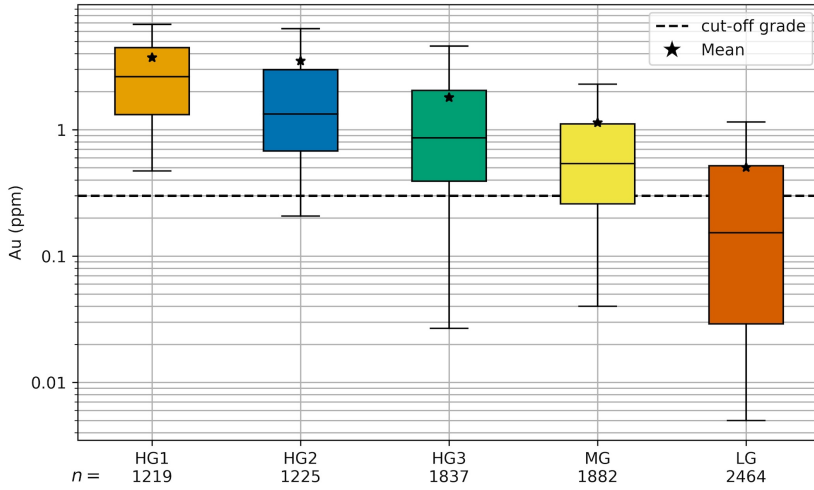


FIGURE 8.9: Box and whisker plot of Au grade (ppm) for the clustering classes of Case Study II. HG: high grade, MG: marginal grade, LG: low grade.

and LG typically have lower concentrations in the ore elements associated with the sulphide and telluride minerals. Within the K-group elements (K, Ba, Rb, Cs, including Al) and oxide minerals (P, Th, U, Zr, Hf), it is evident that MG is more similar to HG2, whereas LG is similar to HG3.

High-grade classes (HG1, HG2, HG3): The three high-grade Au-mineralised classes all fall along the plagioclase–K-feldspar trend line (Figure 8.10b), and these samples are predominantly logged as feldspathic gneiss or feldspathic pegmatites. HG3 ($n = 1,837$) has the lowest K/Al and highest Na/Al molar ratios and is partially

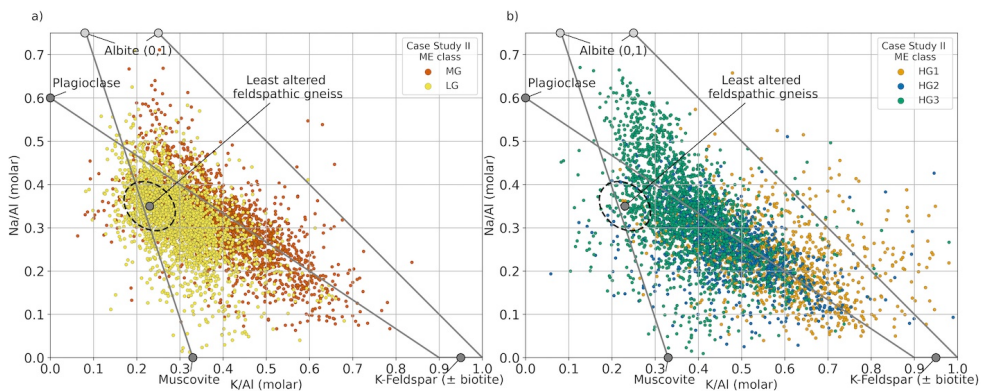


FIGURE 8.10: Multi-element samples from Case Study II plotted to the alkali-alumina ratio plot, after Davies and Whitehead (2006), thematically attributed by clustering classes.

still characterised by some sericite-chlorite alteration. HG2 ($n = 1,225$) and HG1 ($n = 1,219$) have increasing K/Al and decreasing Na/Al molar ratios and have a more abundant biotite-sericite or biotite-pyrite alteration. Hardwick (2021) discriminated that these higher K/Al molar ratios of the feldspathic gneiss units are more controlled by higher modal proportions of perthitic K-feldspar rather than by enrichment in biotite (since higher K/Al (molar) trends towards the K-feldspar node on an Al-K-Mg molar ternary plot). The mineral classification also ranges from phengite \pm biotite with the highest gold grade (HG1) to increasingly chlorite-rich, muscovite-bearing domains associated with the lowest gold grade (HG3, but also still in MG and LG).

HG1 is the richest in K and S of the three classes. The main difference between these classes is their relative degree of enrichment in ore metals (Bi, Te, Tl, Ag, Sb, Mo, Th, U, W), where HG3 has the lowest relative proportions (Figure 8.11). In terms of geochemistry, HG1 and HG3 are more alike. They both have higher concentrations in the transition metals (Co, Cr, Cu, Ni), whereas HG2 (and MG) has higher concentrations in the high field strength elements (Zr, Hf, Nb and Ta). Interestingly, 77% of HG1 samples are spatially located within the Boston Shaker domain. This class demonstrates the known high-grade ore shoot characteristics (including biotite/pyrite alteration).

8.4.2.3 Spatial domains

The composites analysed for Equotip, BWi, Axb or recovery are typically gold grade and geologically-constrained metallurgical samples and thus incompletely reflect in-situ geochemical (and mineralogical) variability. In addition, not all available composites have complementary ME data. This makes it challenging to match the ME classes directly with the hardness proxies and explore their potential relationships. To increase colocated samples, all ME and hardness samples have been grouped according to their spatial location, i.e., per orebody and constructed domains. It is assumed that the geochemical class signatures would be fairly similar within such a domain, and there should be a relationship with the metallurgical test results. Traditionally, these domains came from Au grade resource modelling (≥ 0.3 ppm Au), but some have been split by the modelled faults to represent coherent geochemical domains better. Figure 8.12 shows the spatially and geochemically constrained orebody estimation domains for the Tropicana Gold Mine. For example, between domain TP_3 and TP_4, there is a shear zone obliquely intersecting the line of mineralisation in E to SE direction (Blenkinsop and Doyle, 2014). This shear zone is associated with an alteration event and increased schistosity which affects the material hardness.

The proportion of each ME class within the domains is defined and shown in Figure 8.13. This shows a spatial zonation of the ME class signatures, but also that the hanging wall and footwall of the different domains are geochemically distinct. In general, the clustering is effectively separating various geochemical and mineralogical associations from each other, characterising the different alteration and deformation events taking place with varying intensities, mineralogy and timings (Blenkinsop and Doyle, 2014). For example, at Boston Shaker, there is high Au grade material clustered in HG1, and then only lower grade samples in HG3 and relatively unmineralised material in LG. This indicates that the classes identify unique geochemical

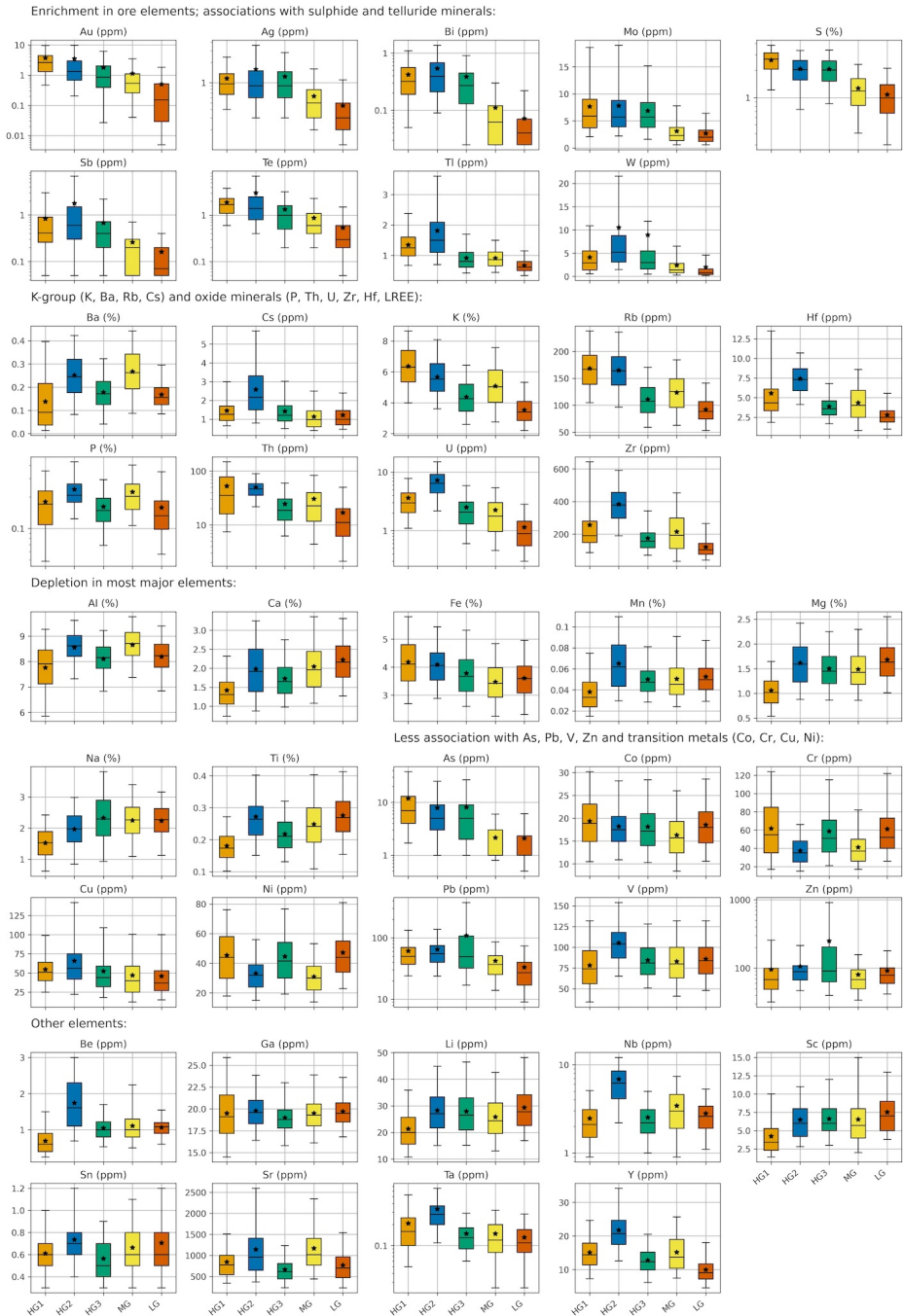


FIGURE 8.11: Box and whisker plots of elemental concentrations of Case Study II samples. See Figure 8.5 for an explanation of the box and whisker parameters and Figure 8.9 for the number of samples per class.

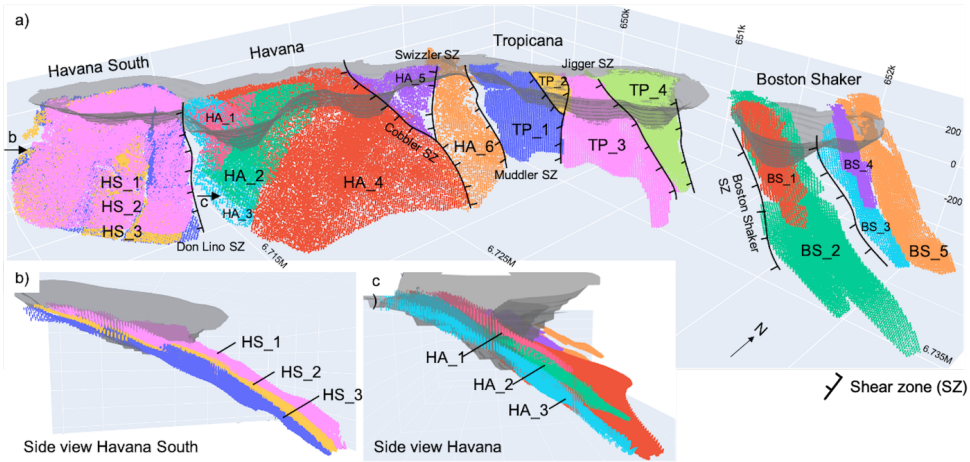


FIGURE 8.12: a) Overview of the selected orebody domains (≥ 0.3 ppm Au) for the Tropicana Gold Mine (mineralisation over 5 km strike length), b) side view of Havana South, and c) side view of Havana domains. GDA94 / MGA zone 51 grid.

signatures associated with various mineralised fluid source compositions, alteration and resulting mineralogy.

Figure 8.13 shows that the HG1 geochemical signature accounts for 36–58% of the Boston Shaker domains (green shaded), whereas HG1 is almost absent in the other domains. This characterises the biotite and pyrite dominated assemblages with an increased abundance of white mica in the K-feldspar (higher grade). Another large group of domains (HS_2, HS_3, HA_3, HA_4, TP_1-3, orange shaded) have on average 5% HG1, 22% HG2, 17% HG3, 31% MG and 25% LG. However, there is a switch in the proportion of MG and LG between the Havana and Havana South, and Tropicana domains. This fairly similar geochemical signature typically observed in the footwall lodes demonstrates the more plagioclase rich domains (typically lower grade and with chlorite being dominant over muscovite) with intermediate composition phengitic rock.

The hanging wall mineralisation lodes at Havana and Havana South (HS_1, HA_1 and HA_2, blue shaded) all have high HG3 (26–56%) with variable MG and LG, but absence of HG1 and HG2, indicating a high degree of geochemical similarities. These lodes are more phengite dominant with biotite \pm quartz but also indicate more muscovite + chlorite in the alteration (larger proportion of MG and LG). These three domains are the shallowest mineralisation lenses (see Figure 8.6, top feldspathic gneiss ore zone, Figures 8.12b-c) found in the Havana and Havana South regions. Note that the number of samples ($n = 7,746$) in Figure 8.13 is not equal to the Case Study II samples ($n = 8,627$) as the remaining samples were found outside the considered domains and ME samples or metallurgical test results were not sufficiently available for all domains.

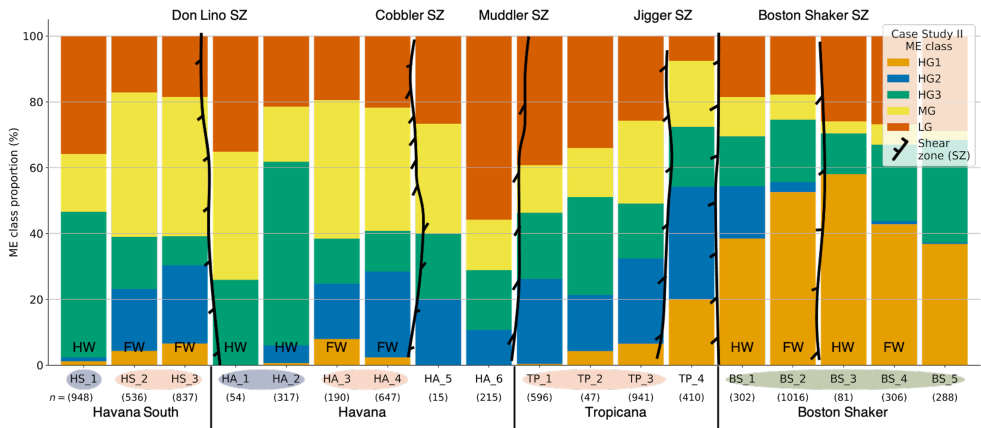


FIGURE 8.13: ME class proportions (Case Study II) typically found in selected Tropicana Gold Mine orebody domains (x-axis). The shaded domains have roughly similar geochemical signatures. Also, see Figure 8.12 for the spatial configuration, SZ = shear zone, HW = hanging wall, FW = footwall.

8.4.2.4 Hardness and recovery attributes

During (pre-)feasibility studies, these domains have been adequately sampled to determine the hardness and recovery parameters. Figure 8.14 shows the average ± 1 SD BWi (kWh/t), Axb, Equotip hardness (Leeb), and 48-hour leach recovery composite data for the considered domains. This analysis indicates that domains with similar geochemical signatures also frequently have similar material hardness and 48-hour leach recovery behaviour. In addition, it is now possible to propose an explanation for the variations (if any) in the metallurgical proxies.

The following results are derived from the combined domain-based ME class proportion and Equotip hardness, BWi and Axb metallurgical test results split per domain (Figure 8.14):

- HS_1, HA_1 and HA_2 (blue shaded) have similar geochemical signatures (high HG3 + variable MG/LG). The BWi (18.4 kWh/t) and Axb (41.7) of HS_1 is lower and higher, respectively, compared to HA_1 (BWi: 20.1 kWh/t, Axb: 30.5) and HA_2 (BWi: 20.3 kWh/t, Axb: 33.1). These domains are rich in the transition metals (Cr, Ni) and poor in Hf, Zr, Nb and Ta, concentrations demonstrating the expected geochemical signature of HG2 (and LG). These domain samples have a low K/Al and a high Na/Al ratio, indicating less clay and thus harder characteristics (trending more towards the albite node instead of K-feldspar). HS_1 may have a lower hardness due to the shear zone separating Havana South and Havana having changed the feldspathic gneiss textures. This domain also has an increasing proportion of white mica with chlorite alteration.
- Domain HS_2, HS_3, HA_3, HA_4 and TP_1-3 (orange shaded) are generally quite hard due to larger proportions of plagioclase rather than K-feldspars. This, in conjunction with the presence of quartz (and minor garnets), make these relatively hard domains. The HS_2 and HS_3 composite samples are

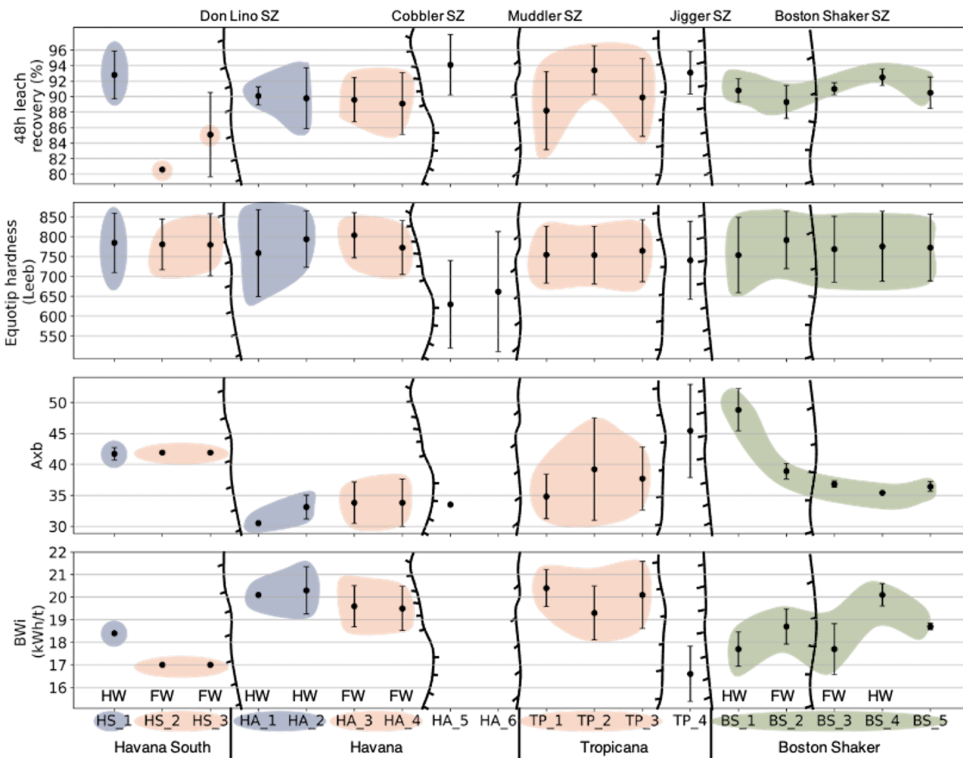


FIGURE 8.14: Average BWi, Axb, Equotip and 48-hour leach recovery composite data for the considered spatial domains. The shaded regions indicate domains with shared geochemical signatures (Figure 8.13). Vertical lines indicate displacements of the orebodies by minor or major faults (also see Figure 8.12). SZ = shear zone, HW = hanging wall, FW = footwall.

closer to the surface and affected by weathering resulting in softer material (<18 kWh/t). The other domain composites have a fairly consistent BWi of 19.8 ± 1.2 kWh/t. A gradational trend of slightly increasing (reduced hardness) Axb from 34 to 39 and decreasing (reduced hardness) Leeb from 800 to 760 is observed as one transition towards domain TP_3, where it abruptly changes due large “Jigger” shear zone (right-hand side of Figure 8.12a) separating zone TP_3 and TP_4. TP_4 returns a much lower BWi (16.6 kWh/t), higher Axb (45.5) and lower Leeb values (742), indicating much softer rock. This domain (TP_4) is associated with a strongly (sheared) phengitic white mica-affiliated rock type, exhibiting significantly softer hardness and elevated recovery. There is also a change of class proportion for this domain, where an increased HG1 (20%, high molar K/Al) and slightly higher HG2 (34.1%) proportion present relative to its neighbouring domain TP_3.

- The Boston Shaker domains (green shaded) have an elevated (HG1) proportion related to a more perthitic K-feldspar rich (increased K/Al) rock. The increased

proportion of white mica and biotite tend to soften (BWi: 18.5 ± 1.0 kWh/t) these domains compared to plagioclase feldspar dominated domains (more HG3). Within Boston Shaker, the most notable difference is in the hanging wall domain BS_1, which has increased HG2 (16%) and decreased LG (18.5%) class proportions. This is a more sheared and phengitic white mica-affiliated domain exhibiting similar characteristics as TP_4 (high Axb).

The following results are derived from the combined domain-based ME class proportion and 48-hour leach recovery metallurgical test results split per domain (Figure 8.12):

- The 48-hour leach recovery results from domains HA_3, HA_4 and TP_1-4 (orange shaded) are quite variable. TP_2 and TP_4 have a relatively high recovery, around 93%, whereas the recovery of the others is between 88.2 and 89.9%. A possible explanation for the lower recovery in these domains is the evidence of preg-robbing eluded to by Baker (2020). The cause is unknown as there is usually very little organic carbon in the ore to explain the effects by adsorption into carbonaceous material. The effects may be caused by the reduction of gold onto arsenopyrite or possible chalcopyrite surfaces, but this is unlikely due to the low As concentration (~ 3.5 ppm) (Baker, 2020).
- Unfortunately, the increased 48-hour leach recovery for HS_1 (93%), HA_5 (94%), TP_2 (93.4%) and TP_4 (93.1%) cannot be explained by similarity of the geochemical class proportions (Figure 8.13). HS_1 has a larger HG3 proportion, and these samples are trending towards the albite node on the alkali-alumina plot and have lower S and Fe. Whereas TP_4 has significantly higher K/Al (molar) ratios (and HG1), higher S and Fe, and these samples are more trending towards the perthite K-feldspar node. Especially HS_1, HA_5 and TP_2 have in common that they are quite shallow and that the tested material types are predominantly lower saprolite and Transitional saprolite rock compared to the Fresh rock parts of, for example, the Boston Shaker domains (green shaded).
- The recovery data associated with higher proportions of HG1 domains (Boston Shaker) reflect observations seen at the mine site; elevated As, Te and S material (HG1, Figure 8.11) leaches poorly (89.3–92.5%) under standard conditions and will most likely increase the cyanide consumption. These elevated elemental concentrations would suggest increasing amounts of gold associated with tellurides and arsenopyrite, affecting the recovery. The increased sulphur (a known cyanocide) may cause higher cyanide demand. This is typically combated by increased oxygen and lead nitrate demand. The NaCN consumption for the Boston Shaker domains (high HG1 and sulphur) is almost double (0.48 ± 0.15 kg/t) compared to the other domains (0.25 ± 0.23 kg/t). The lime consumption is much lower (0.67 ± 0.19 kg/t) than the other domains (2.53 ± 1.10 kg/t).

8.4.2.5 Summary of Case Study II

This case study showed that clustering of mineralised material is possible and generated classes with distinct geochemical, mineralogical and physical attributes. Including the spatial context of the ME data proved to give valuable insight into the coexistence of various classes and resulting metallurgical properties. For instance, similar geochemical class signatures were found across multiple orebodies. Additionally, there are various effects of known structural control events (with alteration stages) observed within the domain signature, such as changes in the geology, alteration assemblage and mineralisation. The resulting material hardness can typically be explained by the class compositions found within domains, whereas the recovery tends to be explanatory with elevated or depleted elemental concentrations.

8.5 Discussion

The shear zone-controlled alteration of the protolith towards the mineralised assemblages was previously described by Crawford and Doyle (2016). Geochemically, these processes relate quite well with the observed HG1/HG3 and HG2/MG class properties. Crawford and Doyle (2016) described a decrease in SiO_2 , major elements (Fe, Mg, Ca, and Ti) and transition metals (V, Ni, Cr, Co, and Zn) accompanied by a strong increase in K-group elements in the shear zone assemblages. This character is more prevalent in HG2/MG than in HG1/HG3 (Figure 8.11). Mineralogically, this increase in K-group elements is reflected by the stabilisation of abundant K-feldspar, biotite and white mica. Then, the decrease in abundance of the major elements and transition metals is reflected by the destruction of hornblende, augite, and Fe-Ti oxides in the protolith gneisses as the new alteration assemblage quartz-K-feldspar-biotite-pyrite stabilised in the shear zones (Crawford and Doyle, 2016). The formation of the alteration assemblage was also accompanied by the breakdown of mafic minerals in the protolith gneisses. Some of the Fe, Mg, and Ti released were trapped in the pyrite and lower-Ti biotite, however, the mass balance of Ti is not fully resolved and not completely reported by Crawford and Doyle (2016).

The shear zone assemblage of the TGM deposit also has implications for the physical properties of the rocks. For example, there is an abrupt change in hardness of TP_4 (BWi: 16.6 ± 1.2 kWh/t, Axb: 45.4 ± 7.5) compared to TP_3 (BWi: 20.1 ± 1.5 kWh/t, Axb: 37.7 ± 5.1) caused by the "Jigger" shear zone crosscutting the deposit (as shown in Figure 8.14). At TP_4, the decrease in hardness is accompanied by an increase in HG1 and HG2, reflected mineralogically by a strongly (sheared, schist-like) phengitic white mica-affiliated rock type. This suggests that the proximal distance from a shear zone has additional influence on the material hardness and probably the particle size and recovery. This hypothesis is tested by analysing the dilatancy around the shear zones, which commonly reflect the degree to which fluid-dominated or rock-buffered processes acted (Hodkiewicz et al., 2008). The dilatancy implies that during the feldspar-to-mica reactions occurring in these fault zones, the released silica may have precipitated in these dilatant sites. This increased the fault rock strength by cement hardening and reduced its permeability (Wibberley, 1999).

This process has a significant impact on the material hardness and is observed across various domains. For example, a related and noticeable geochemical difference

can be found within Tropicana. TP_4 has a higher average molar K/Al (0.47 ± 0.14) ratio and thus implies a more perthitic K-feldspar feldspathic gneiss than the more plagioclase rich feldspathic gneiss at TP_3 (K/Al ratio: 0.37 ± 0.12). Another shear zone that can be considered to test this hypothesis is the Boston Shaker shear zone. BS_1 has a similar high molar K/Al ratio and equally soft rock characteristics (BW_i: 17.7 ± 0.8 kWh/t, Axb: 48.8 ± 3.4) as TP_4. In this domain, the perthite-rich feldspathic gneiss progressed from a clast supported breccia to matrix-supported breccia (Hardwick, 2021). It is evident that similar strength-controlling mechanisms occurred at other high-intensity strain domains and that each had specific implications on the resulting geochemistry and mineralogy, hence variations in the class proportions of the domains.

Given the geochemical differences between the classes, it is expected that the resulting rock hardness is a combination of various rock properties. It must be mentioned that the authors are aware of the non-additive properties of material hardness. The individual or cumulative effect of the following three proposed hardness relationships is unknown.

- The HG2 and MG classes are characterised by elevated HFSE concentrations (Zr, Hf, Nb, Ta). These elements are usually found in accessory minerals of high density (apatite, zircon) and can indicate fractional crystallisation of felsic alkaline magmas (Motoki et al., 2015). Therefore, these elevated proportions are expected to contribute to the hardness observed in, for example, HS_2, HA_3, HA_4 and TP_1-3.
- There is a large difference between the BW_i and Axb of the blue shaded domains (HA_1, HA_2 and HS_1) and green shaded domains (Boston Shaker). This transition from dominance in HG3 (blue domains) to HG1 (green domains) is related to an increase in the modal proportion of perthitic K-feldspar (higher K/Al molar ratio). As a result, there is less energy required to grind the rocks at Boston Shaker. However, the Leeb hardness indicates almost similar rock characteristics. The contradiction of soft/hard indications of the BW_i, Axb and Equotip rebound hardness (Leeb) tests may represent the nature of the tests and their relation to hard or brittle material. For example, BW_i and Axb are destructive tests, whereas Equotip is a non-destructive test. Equotip hardness generally reflects the mineralogical rebound hardness based on the observed matrix crystal structure, whereas the BW_i reflects the combined resistance to abrasion and impact, and Axb the compression resistance. Typically, the Leeb value becomes lower as the rocks are more sheared (such as in TP_4 or HA_5) because of the development of a more dominant fabric and the conversion of feldspar to sericite (mica). Hence, the likelihood of hitting a hard mineral grain (feldspar, quartz, garnet) diminishes and hitting a fine, softer matrix material increases. Thus, the class composition of Boston Shaker results in an easier to grind rock type, however, within the crystal matrix, there are equally hard grains observed with Equotip hardness testing as in the blue shaded domains.

- At Tropicana, coarse-grained feldspathic pegmatite is similar to the feldspathic gneiss in terms of major elemental concentration and is therefore not discriminated in this study. However, the main differences between the two lithologies are in the grain size (>4 mm) of framework silicates rather than changes in modal mineralogy (Hardwick, 2021). Pegmatites tend to be composed of relatively hard minerals, so contributing to the observed and measured hardness of the composites. Pegmatites are more frequently logged in MG ($n = 249$) and LG ($n = 125$) samples compared to HG1 ($n = 107$), HG2 ($n = 37$), and HG3 ($n = 56$) and therefore expected to contribute more to the hardness observed in the high MG and LG domains.

Understanding the deleterious characteristics of the ore, such as oxygen or cyanide consumers, preg-robbbers/borrowers, or passivation due to tellurides is a complex undertaking and requires extensive testing (Coetzee et al., 2011). The following examples are observed at the mine and could be linked with the ME class or domain characteristics. For instance, there is an inverse relationship between cyanide and lime especially observed in the blue and green shaded domains. The blue shaded domains (HA_1, HA_2 and HS_1) have a high HG3 with variable MG and LG, but absence of HG1 and HG2, characterising a high lime consumption (>2.2 kg/t) and low cyanide need (<0.31 kg/t). The following two observations may explain this high lime need. Firstly, these classes have proportionally more Mg and clays in the representing material, which tend to decrease the pH resulting in an increased lime consumption (du Plessis et al., 2021). Secondly, HG3 typically has higher concentrations in metal grades (Ni, Zn, Pb, Cu) and lower or equal concentrations of ore elements (Ag, Bi, Mo, Sb) than HG1. These metal-bearing minerals tend to reduce leach kinetics and lower the pH and must be combated by adding lime but less NaCN.

8.6 Conclusions

This chapter presented an agglomerative hierarchical clustering approach using multi-element geochemical data from the Tropicana Gold Mine, Australia. This approach was very effective in classifying the logged lithology, alteration or mineralisation and could, for example, discriminate unmineralised, marginal-grade and high-grade gold classes. The work involved exploring classes for their unique geochemical signature, relating classes with their typical comminution and recovery parameters, and explaining the observed processing attributes and their cause.

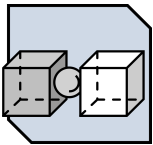
The chapter started with an extensive data quality assurance and successfully demonstrated how an industry scale four-acid digestion dataset could be cleaned to ensure no significant bias between interlaboratory and intralaboratory measurements. Case Study I presented the separation of 30,687 ME samples in seven classes through clustering. The clustering was primarily driven by the dominant mafic, felsic, garnet-bearing, garnet-absent, chert or quartz containing geochemical signatures of the gneissic rock found in each class. This demonstrated that the classes picked up different original host rocks and alteration assemblages seen across domains. The two gold-bearing classes were easily separated from the others (not based upon Au). Case Study II ($n = 8,627$ samples) continued with the two mineralised classes and demonstrated further partitioning in five classes: three high-grade classes, one

marginal-grade class and one low-grade class. This clustering placed a greater emphasis on grouping assemblages with relative increased or decreased elemental concentrations rather than separating major rock units.

The geochemical data were spatially combined with metallurgical test results by considering all results within a constrained ≥ 0.3 ppm Au grade resource domain. This bridged the gap between these two different datasets. The geochemical signatures of the classes and domains were then used to explain the differences in observed breakage properties (Leeb, BWi, Axb) and recoveries. This new approach of interpreting comminution and recovery related parameters demonstrated the benefits of material fingerprinting and suggests including mineralogical data in future to enhance results. Additionally, it would be beneficial if an adequate metallurgical test for each combination of geochemical composition and spatial (sub)domain was undertaken to improve understanding of the hardness and recovery characteristics. Future research will focus on increasing the sample representativity and include additional spatial context.

9

Between and within material type variability



This chapter demonstrates the clustering of pXRF and VNIR-SWIR data to create material type representations which help to interpret material hardness proxies. This work uses larger regions from the spectral data to characterise mineralogical signatures and resulted in discovering a new epidote-related feature, which, together with the white mica, is of significant importance in spatially domaining material hardness.

Parts of this chapter have been published in:

van Duijvenbode, J. R., L. M. Cloete, M. Soleymani Shishvan, and M. W. N. Buxton (2022). Material fingerprinting as a tool to investigate between and within material type variability with a focus on material hardness. *Minerals Engineering* 189, 107885. doi:10.1016/j.mineng.2022.107885.

9.1 Introduction

The previous Chapter addressed how fingerprints were constructed using high-quality ME data. One of the limitations from the results was that the input datasets had a relatively coarse spatial resolution because the samples originated from exploration drill holes sampling. The main aim of this Chapter is to construct new material fingerprints to further understand between- and within material type differences by focusing on hardness and spatially closer spaced samples from grade control point data sources. This could also be referred to as the dispersion variance within the classes of domains and between domains.

This will be done by firstly demonstrating the construction of material fingerprints of mining blocks using grade control (GC) point data sources (pXRF and VNIR-SWIR measurements), secondly explaining the rock attributes for each material type, and thirdly demonstrating spatial contextual relationships of the material types with hardness and alteration mineral assemblages. This will be tested/validated by linking each fingerprint with the typical BWi, Axb, Equotip and penetration proxy parameters characterising the comminution behaviour of this material. Finally, it is shown how the learnt fingerprint (material type) to work index relationships can be improved by exploring the within material type variability.

9.2 Methods

Data were obtained from several Tropicana Gold Mine (TGM) sources. Most of the mineralogical (VNIR-SWIR, $n = 128,584$) and geochemical data (pXRF, $n = 162,398$) were collected from collocated GC drilling samples, others originated from exploration drill hole samples. These samples represent the geochemical and mineralogical variability within the ≥ 0.3 ppm Au grade resource modelling domains. Most of these measurements were taken on drill chips and pulps from GC drilling and, therefore, had a dense spatial resolution (typically 6×6 m or 9×9 m). The resulting 1 m samples were sent to an on-site laboratory for analysis. The hardness data will be discussed in Section 9.2.3.

The preparation workflow of this study is schematically summarized in Figure 9.1 and consists of two parts. The first part prepares a block model ($12 \times 12 \times 3$ m) containing geochemical (Section 9.2.1) and mineralogical data (Section 9.2.2) attributes. However, two problems had to be overcome. Firstly, geospatial modelling of VNIR-SWIR features is not as common as modelling geochemical data (e.g., using kriging). Therefore, an additional preparation step of the mineralogical data is proposed to create a categorical variable indicating the type of mineralisation of a sample. This consists of agglomerative hierarchical clustering of the spectral responses as outlined in Section 9.2.2 and gives the spectral or mineralogical class indicator which can be assigned to the sample. Secondly, the modelling itself is a problem as the variety and scale of data obtained from different sample measurements (including the to-be-considered hardness data) complicates merging datasets. To overcome this challenge, all samples were assigned to the nearest block from the ≥ 0.3 ppm Au grade resource modelling block model from the mine based on their spatial location. These samples within a constrained block volume should, given their spatial proximity, relate to

each other (material blend). Subsequently, only blocks with sufficient samples were considered for further analysis (block feature clustering), and no spatial modelling of attributes was required. Finally, a spatially dense block model was still obtained due to the vast number of samples and spatially dense GC drilling grid.

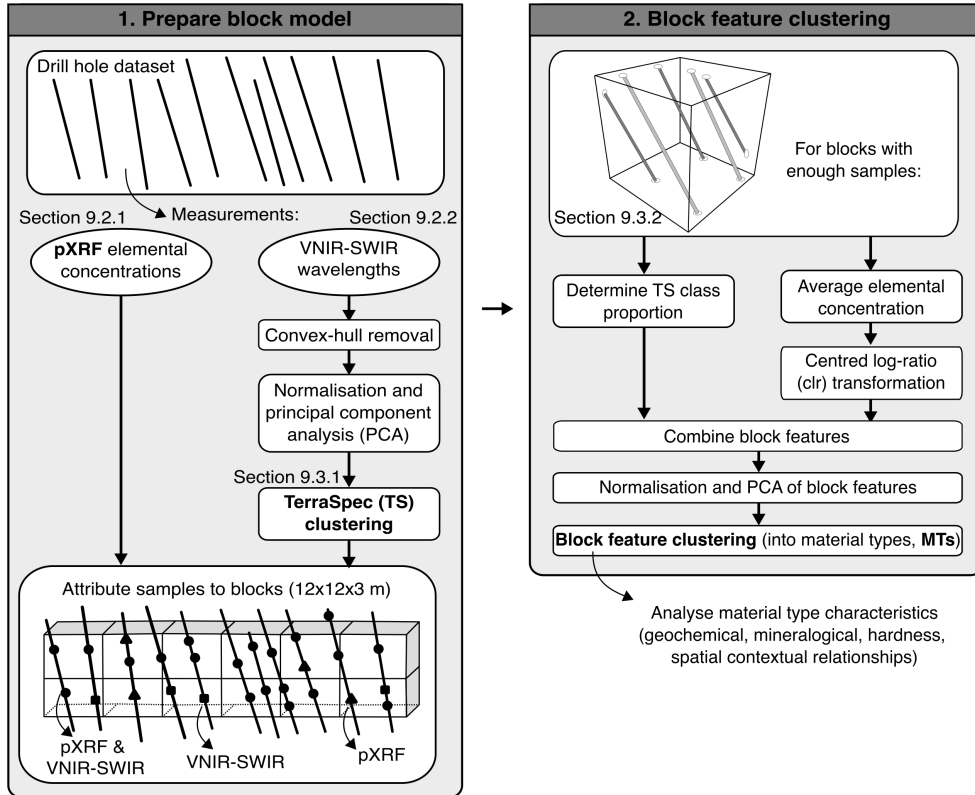


FIGURE 9.1: Schematic workflow of the block model preparation and block feature clustering approach.

The second part involves clustering block features into material types and analysis with hardness proxies. As a result of the first part, most samples had a set of elemental concentrations and an assigned spectral class obtained through the clustering. Note that some samples only had VNIR-SWIR measurements, and others only pXRF measurements. The block feature clustering approach aims to increase the spatial resolution and context of the sample results. This will result in a block model where each block with sufficient data (no simulation done) in the mine plan is valued not only on Au grade but on a combination of the 15 elements and VNIR-SWIR data (the block features). The resulting material attribute classification will then become a proxy for the comminution indices. This allows for scale-up from sample to block; all individual samples within a block were merged and further prepared for block feature clustering by the following steps:

1. Average the elemental concentrations to get a unique geochemical signature

per block. Since pXRF data are compositional in nature, they require a further transformation to log-ratio coordinates to account for closure (Aitchison, 1999). Therefore, the concentrations are transformed using a centred log-ratio (clr). This transforms the data coordinates from the simplex, an n -dimensional composition within the positive real number space, to the Euclidean real space more suitable for statistical analysis (Aitchison, 1986). Note that the clr transformation is done using all block geochemical signatures and not per block.

2. Determine the proportion of each spectral class (Section 9.2.2) based upon all classes found within a block. These class proportions are useful as they provide a quantitative description of the mineralogical blend characteristics.
3. Combine the spectral class proportions and pXRF features and normalise by a z-score transformation to obtain values in a similar range.
4. Reduce the feature dimension of these block features (spectral class proportions and pXRF clr-transformed concentrations) using PCA. The number of PCs is automatically set to the amount that can describe 95% of the data variance.
5. Cluster the block features PC dataset using agglomerative hierarchical clustering to partition the blocks into clusters (Wierzchoń and Kłopotek, 2018). The algorithm starts with each block as an individual cluster. Next, pairs of clusters are successively merged based upon similarity until all clusters have been merged into one big cluster containing all blocks. These clusters represent so-called “*material types*” with similar mineralogical and geochemical attributes. Note that the mineralogical data (Section 9.2.2) is clustered using the same clustering technique.

The final block material type (fingerprint) is a combination of pXRF elemental concentrations (Section 9.2.1) and a separate VNIR-SWIR data clustering approach (Section 9.2.2). The initial assumption is that geochemistry and mineralogy then largely explain the legacy material hardness parameters and constrain distinct hardness domains.

9.2.1 Geochemical data

The geochemical dataset ($n = 162,398$ samples) used in this study originates from portable XRF (pXRF) measurements taken on samples from within the ≥ 0.3 ppm Au grade resource modelling domains. The bulk concentrations of the following (15) elements were considered: Al, Ca, Cr, Fe, K, Mn, Nb, Pb, Rb, S, Si, Sr, Ti, Zn and Zr. Other elements including Ag, As, Bi, Cl, Co, Cu, Mo, Mg, Ni, Se, V and W were not considered because more than 50% of their values reported under the detection limit. In addition, the samples were assayed for gold using a 50 g charge fire-assay and subsequently analysed by solvent extraction Atomic Absorption Spectroscopy (AAS). The Au concentration was not used in the clustering as this ensures that emphasis is placed on major and other trace elements for classification (van Duijvenbode et al., 2022a). The gold concentration is only used in this study to help interpret the different material types and constrain the domains. Figure 9.2 shows an example of the geochemical data and indicates how the Au, Zr, K and S concentrations can

be used to characterise the hanging (HW) and footwall (FW) ore zones, dominantly hosted in felsic gneiss of the Havana deposit, and how the geochemistry changes with depth. It also shows, that the non-Au elements will be deterministic in identifying zones of various geochemical composition related to Au mineralisation.

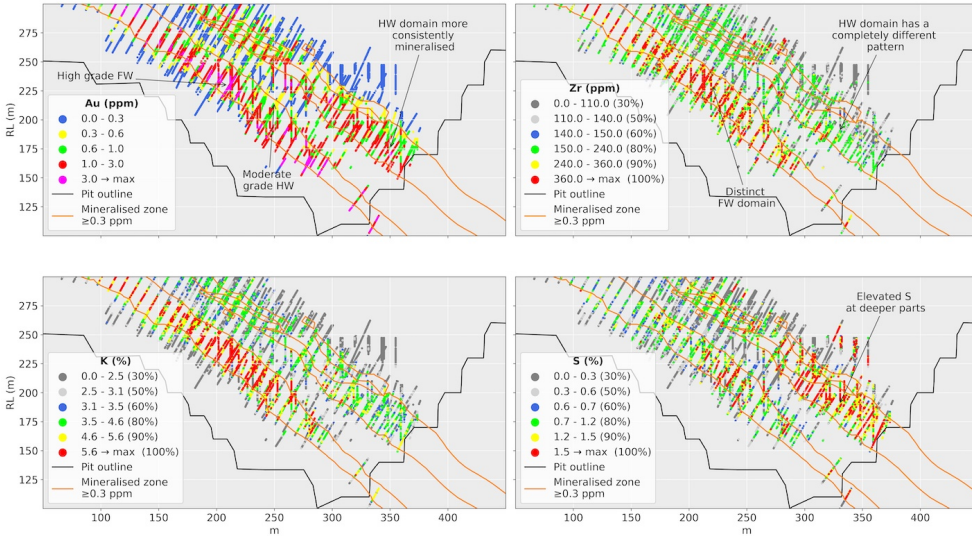


FIGURE 9.2: pXRF concentrations of Au, Zr, K and S in relation with the hanging (HW) and footwall (FW) lodges at Havana (50 m thick cross-section). The block feature clustering approach only considers samples within the modelled mineralised zone.

Since inception of the Tropicana Gold Mine operation, samples have been analysed in an on-site laboratory using an automated sample preparation circuit where both pXRF and VNIR-SWIR data are routinely captured. The laboratory adheres to routine data checks, which renders further quality control before conducting this research redundant. These controls include routine certified reference material (three per hundred samples), blank (first sample in each laboratory job and into the sequence of samples before each zone of mineralisation), repeat and duplicate measurements. QA/QC results are reviewed on a batch-by-batch and monthly basis. Any deviations from acceptable precision or bias indicators are acted on with repeat and check assays (AngloGold Ashanti, 2016). In addition, the number of samples ($n = 162,398$) used in this study likely reduces statistical errors and renders the database resilient for errors.

9.2.2 Mineralogical data

The mineralogical dataset consists of 128,584 spectral measurements on samples from within the ≥ 0.3 ppm Au grade resource modelling domains. The measurements were taken using an ASD TerraSpec mineral spectrometer (hereafter referred to as TS data), and each spectral response covers the reflectance of the electromagnetic spectrum at the VNIR and SWIR regions (350–2500 nm). Processing and interpretation of the results were undertaken using two processes. The first process uses unprocessed

spectral responses, whereas the second process uses a standard suite of absorption features typical for gold systems.

The first process aims to use unsupervised learning (clustering) to generate classes of mineralogically similar samples. The clustering uses “raw” or unprocessed spectral responses as input and, therefore, omits the need for mineralogical identification and absorption feature creation (Pontual et al., 2008; Rodger et al., 2021). Additionally, using uninterpreted spectra may reveal hitherto unknown textural or hardness signatures not recognised or identified before. Each spectral response was prepared by subdividing the wavelength range into four sub-regions: 500 to 750 nm, 1300 to 1450 nm, 1850 to 2000 nm and 2150 to 2400 nm. Figure 9.3a shows a typical TS spectrum with the four regions of interest highlighted. These regions were selected because they contain the most spectral variability. The selected regions and corresponding typical spectral response (Pontual et al., 2008) are described in Table 9.1. In terms of identifying and characterising the white mica composition, the 2150–2400 nm region is of particular interest for two reasons. Firstly, the wavelength of a diagnostic Al-OH absorption feature between 2180 nm and 2228 nm (w_{AlOH}) defines the white mica composition and is thus useful for spatial mapping of mineralised domains. For example, a muscovite white mica corresponds with the lower wavelengths (<2216 nm) and phengitic white mica to higher wavelengths (>2216 nm). Phengite at TGM is especially closely spatially associated with gold and shear zones controlling lode geometry (Roache, 2019). This can, for example, differentiate K-feldspar-dominated domains (higher work index, harder) from mica-dominated domains (lower work index, softer). Secondly, the abundance (depth at 2205 ± 25 nm, d_{AlOH}) can then be used to differentiate the feldspar vs sericite composition.

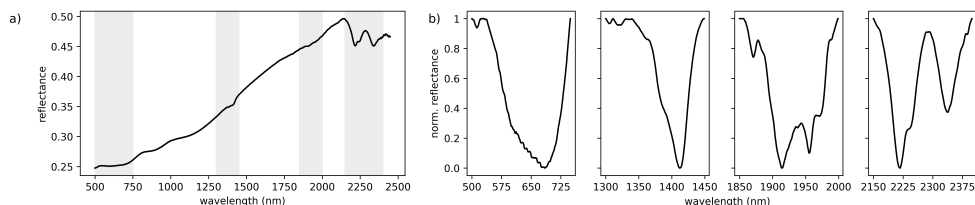


FIGURE 9.3: Convex-hull removal of TerraSpec spectrum; a) an example TerraSpec spectrum with the four selected regions used for clustering; b) normalised hull-quotient spectrum for each region.

The spectral response in each region was smoothed and normalised by a convex-hull removal (CHR) to remove dependence upon reflectance. This ensures that the spectra can be compared because the absorption features are purely a function of depth and width (Pontual et al., 2008). The benefit of this approach can be seen in the 500–750 nm region, as will be discussed in Section 9.3.5. Usually, these predominantly iron-related features are depressed because the convex hull removal over the entire spectrum. However, doing this across a smaller region preserves features and may magnify their expression (Figure 9.3b).

The data from each region were combined, and each wavelength feature ($n = 800$) was normalised by removing the mean and scaling to unit variance. Then, the feature dimension was reduced by principal component analysis (PCA). The number of

TABLE 9.1: Spectral regions and characteristic absorption features used in this study.

Spectral feature	Defining characteristics of the feature extraction origin (Pontual et al., 2008), description and classification if applicable (Roache pers. comm).	Reg. (nm):			
		500-750	1300-1450	1850-2000	2150-2400
Fe-features	Fe-features, visible part of the spectra.	X			
w1400	Stretching vibrations of hydroxyl groups (OH). Within sheet silicates (kaolin group, white mica, smectite, chlorite), this is mostly located between 1390 and 1445 nm (Laukamp et al., 2021)		X		
w1900	Water features. The shape and intensity vary based on the mineral.			X	
wAlOH	Wavelength position of the Al-OH absorption feature (2205 ± 25 nm). Proxy for white mica composition. With longer wavelengths, substitution of Mg and Fe for Al into a more phengitic white mica.			X	
wFeOH	Wavelength position of the Fe-OH absorption feature (2253 ± 15 nm). Proxy for chlorite composition. Mg-rich chlorite <2252 nm, Fe-rich chlorite >2252 nm.			X	
wMgOH	Wavelength position of the Mg-OH absorption feature (2335 ± 25 nm). CO ₃ and Mg-OH bearing minerals or secondary features of Al-OH.			X	
Weathered/ fresh	Ratio of the depth of Mg-OH and 1400 nm OH features. Used as a filter for weathered- and fresh material classification.	X	X		
Sericite SWIR crystallinity	Ratio of the depth of Al-OH and 1900 nm H ₂ O feature. Increasing values represent increasing SWIR crystallinity of sericite, illite or kaolinite. The sericite crystallinity is useful to detect shear zones. The feldspars in high crystalline sericite are (almost) completely converted to white mica/sericite, whereas with lower crystalline values, significant remnants of the feldspars are still present (Pontual et al., 2008; Dalm et al., 2014).		X	X	
dAlOH/dMgOH	Ratio of depth Al-OH and Mg-OH features. It can be used for different purposes depending on conditions: <ul style="list-style-type: none"> • Rock type discrimination. Higher values indicate relatively felsic rocks (>1.2), intermediate (0.8–1.2), lower values mafic (<0.8). • White mica vs chlorite/carbonate (or biotite). Lower values indicate white mica + chlorite (biotite); at higher values, chlorite is negligible. 			X	
dMgOH/dFeOH	Ratio of depth Mg-OH and Fe-OH features. Measure of relative abundance of amphibole to chlorite (biotite). Amphibole >3 , biotite 2–3, chlorite <2 (flexible).			X	

principal components (PCs) was automatically set to the amount which describes 95% of the data variance. Finally, the lower-dimensional dataset functions as input for a clustering algorithm. This study used an agglomerative hierarchical clustering approach (Wierzchoń and Kłopotek, 2018) but, in addition other algorithms were tested (K-means, density based methods). After clustering, each sample is assigned a class label related to a specific suite of mineralogical signatures occurring within the four wavelength regions.

The second process uses The Spectral Geologist (TSG; Version 8.0.7.4, CSIRO, Perth, WA, Australia) software to provide quick and reliable interpretations of predefined mineralogical features (Laukamp et al., 2021). These spectral interpretations were assumed to be valid since they are generally used in-house, having been refined over many years. The main proxies considered are described in Table 9.1. This process is primarily used to provide mineralogical interpretation to the classes from the first clustering process. In addition, these results may capture signatures from the regions not considered above.

9.2.3 Material hardness proxy data

After analysing the geochemical and mineralogical results of the material types, the focus shifted to the hardness characteristics of each identified material type. These characteristics were identified using the following four legacy hardness proxy datasets jointly:

- Equotip rebound hardness measurements (unit is Leeb, Ls) were primarily taken on diamond drill core with intervals of one metre. Generally, ten measurements were taken per sample, and for this study, simply the median value was chosen to give one data point per meter. This hardness value is calculated from the impact and rebound speed ratio and typically reflects the mineralogical rebound hardness based on the observed matrix crystal structure. A higher Leeb corresponds with a harder sample.
- The Bond Ball Mill Work Index (BWi in kWh/t) and the JK rock breakage parameters (Lynch, 2015) expressed as comminution index A_{xb} , were infrequently collected on diamond drill cores during metallurgical testing campaigns. The BWi reflects the combined resistance to abrasion and impact, whereas A_{xb} reflects the compression resistance. Higher values of BWi indicate harder ore, whereas higher values of A_{xb} indicate a decreased hardness.
- The penetration rate (m/hr) was directly derived from the time required to drill through a one-meter rock mass. When machine operating conditions are kept constant, this represents a material hardness indicator since the parameter is collected continuously along every hole drilled. This study considered only penetration rates from GC drilling of ~ 10 – 12 m long blast holes. Lower values indicate harder rock mass since the material takes longer to penetrate, and therefore delivers less drilled meters per hour.

9.3 Results

9.3.1 VNIR-SWIR clustering

PCA reduced for 128,584 samples the 800 wavelength features derived from the four regions to nineteen features (accounting for 95% data variance). In this context, each PC represents a combination of features visible in the hull normalised spectra of the four wavelength regions. Figure 9.4 displays PC1 is accountable for 25% of the data variance, and that a positive PC1 is mostly related to the 1405–1448 nm and the 1881–1962 nm features, both corresponding with water features. A positive PC2 indicates the 2323–2490 nm and 2215–2256 nm region affinity, probably picking up small mineralogical variations due to the Al-OH, Fe-OH and Mg-OH bonds in silicate minerals. Whereas in the negative PC4 component, this 2150–2297 nm region (slightly larger) is more related to the 1851–1872 nm and 1303–1354 nm region. This may show that vibrations picked up in these regions may be related to each other, and these relationships may not have been observed if only certain, closely constrained, wavelength and depth features were extracted. In addition, these (rather obvious) examples demonstrate that the proposed TerraSpec clustering approach produces

viable results. Furthermore, almost every region has dominance in a PC at either the positive or negative eigenvalue extremes. This suggests that all wavelength regions influence separation of the TS samples. See Supplementary Material Table A.1 from van Duijvenbode et al. (2022b) for an overview of the eigenvalues and loadings of all PCs.

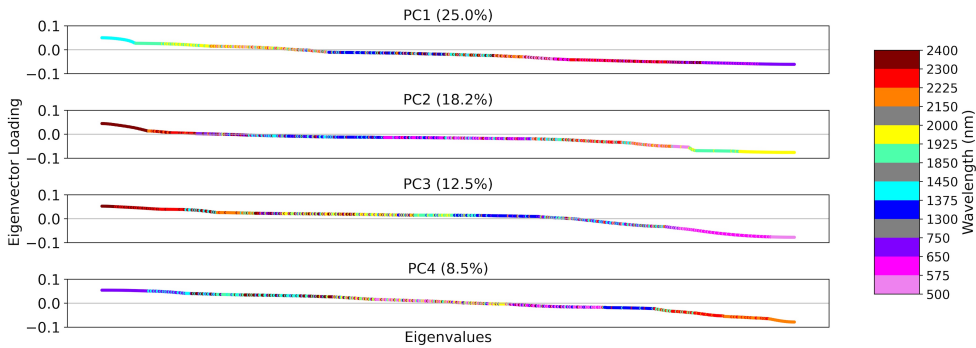


FIGURE 9.4: Scaled and ordered eigenvalues of PC1–PC4 for the TS clustering input wavelengths ($n = 800$).

The nineteen PCs were determined to represent the mineralogical signatures adequately and, thus, were subsequently clustered using agglomerative hierarchical clustering (Wierzchoń and Kłopotek, 2018). It was found that the VNIR-SWIR features can best be partitioned in six, seven or eight clusters (or classes) indicated by the peak and trough in the mean silhouette score, Calinski-Harabasz index and Davies-Bouldin index (Aggarwal and Reddy, 2014) and clustering dendrogram (shown in Supplementary Material Figures A.1 and A.2 of van Duijvenbode et al. (2022b)). It was chosen to select seven classes because a spatial contextual inspection showed that the additional separation (into TS classes 1 and 2) related to the weathered rock types that had been represented by only one class thus far. Eight classes would split TS class 3 which already had a fairly similar mineralogical composition to other classes. Further analysis of the classes is done using 1) histograms of the deepest absorption feature (Hecker et al., 2019) in each region, 2) results of analysing a subset of 31,489 samples using the TSG software and 3) spatial observations. Figure 9.5 shows histograms of the wavelength at the maximum depth for several features per TS class and region and helps identify the main features separating and characterising the classes. Note that these classes resemble distinct mineralogical mixture patterns related to the gold-bearing material and accompanying dilution. Supplementary Material Figure A.3 of van Duijvenbode et al. (2022b) contains numerical overviews of other extracted VNIR-SWIR spectral features from the TSG sample subset.

Classes 1 and 2 comprise mostly of weathered material with clay-rich mineral phases and minor siderite (Table 9.2). Three main characteristics define these classes. Firstly, the histogram peak (Figure 9.5) between 510–530 nm indicates that the ferric iron absorption bands (Fe-oxide intensity) typically observed in weathered material are more dominant than the other deepest absorption features around 600 or 700 nm (Zhou and Wang, 2017). Secondly, the weathered- and fresh-material indicator is low, indicating weathered material (Table 9.1). TS classes 1 and 2 have an average

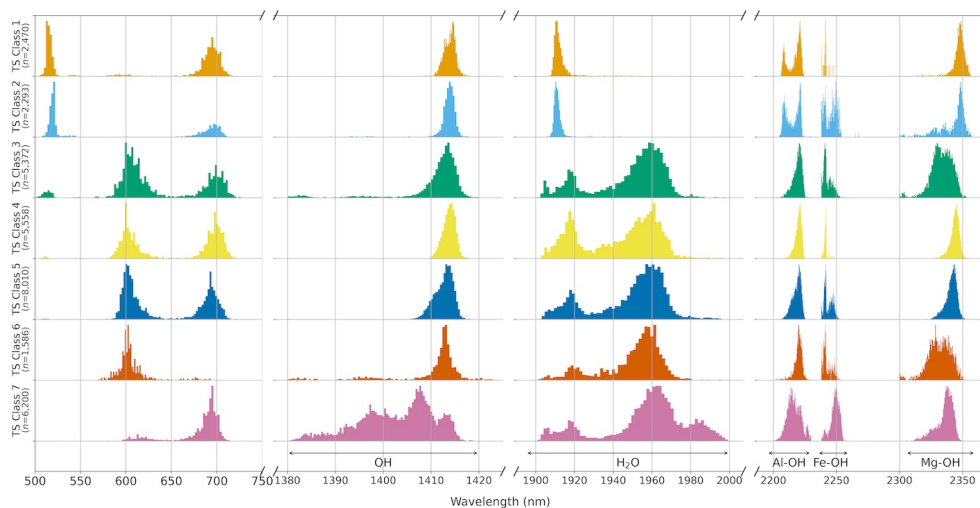


FIGURE 9.5: Histograms of the wavelength at the maximum depth of the region 1, 1400 nm OH, 1955 nm H₂O, Al-OH, Fe-OH and Mg-OH absorption features for the TSG sample subset.

ratio between 1.3–1.4, whereas the other classes have a ratio between 2.5–5.0 (see Supplementary Material Figure A.3 from van Duijvenbode et al. (2022b)). Finally, these samples are found at shallow depths (<50 m) near the surface. Differences between the classes can be found in the mineral composition, where TS class 1 has a phengite-illite-siderite composition and TS class 2 a phengitic-illite-montmorillonite composition. These classes may meaningfully influence processing behaviour as it will generally define softer but more clay-rich material.

Classes 3, 4 and 5 have white mica (phengite) as the dominant SWIR active mineral

TABLE 9.2: Contingency table of the joint probability distribution (%) from the proportion of primary and secondary minerals in each TS class. Notation: <mineral1%> / <mineral2%>.

Mineral	TS class 1 <i>n</i> = 2,470	TS class 2 <i>n</i> = 2,293	TS class 3 <i>n</i> = 5,372	TS class 4 <i>n</i> = 5,558	TS class 5 <i>n</i> = 8,010	TS class 6 <i>n</i> = 1,586	TS class 7 <i>n</i> = 6,200
Phengite	36.4/8.4	12.5/5.4	47.5/28.4	96.8/2.8	87.8/9.4	48.8/22.4	24.7/32.4
Phengitic illite	42.8/9.2	28.6/8.5	0.3/0.1	0.8/-	0.4/-	-/-	0.1/0.1
Siderite	6.3/33.9	25.1/21.8	29.0/33.3	1.9/50.6	6.0/40.0	19.4/28.8	11.1/10.9
Montmorillonite	0.7/4.8	14.4/29.1	0.6/12.6	-/0.1	0.1/0.4	0.2/9.9	0.2/7.0
Chlorite-Mg	0.2/18.4	6.5/13.0	5.3/22.0	0.2/42.7	3.0/44.5	7.8/32.4	40.8/18.5
Chlorite-FeMg	0.1/-	0.9/0.4	0.6/0.5	-/0.4	0.9/1.9	0.2/0.7	17.5/6.1
Kaolinite-PX	9.5/20.5	7.4/15.5	-/-	-/0.1	-/-	-/0.1	-/0.2
Muscovite	0.6/0.5	0.5/0.1	0.7/2.1	0.3/0.1	1.6/1.2	0.9/4.3	1.2/13.9
Ankerite	-/0.7	-/0.7	-/0.1	-/2.9	-/1.9	-/0.2	-/1.6
Aspectral ¹	-/-	0.5/-	15.8/-	-/-	0.1/-	22.7/-	3.4/-
Other	3.4/3.6	3.6/5.5	0.2/0.9	-/0.3	0.1/0.7	-/1.2	1.0/9.3

¹ An spectral response is a spectrum that does not match any of the library spectra. This could be due to a dark/noisy spectrum, mineral not in the library, a silicate mineral without any absorption in the SWIR (such as pyroxenes or feldspars).

(Table 9.2), reflecting the mineralogy found in the K-feldspar and mica-dominated domains. Hence, the sericite crystallinity (definition in Table 9.1) can be used to differentiate their composition. The class compositions transition from a low SWIR crystalline white mica in TS class 3 (ratio=2.15), followed by TS class 4 (ratio=3.87) to a high SWIR crystalline white mica in TS class 5 (ratio=4.81). This higher crystallinity would indicate that all feldspars are (almost) completely converted to white mica/sericite. This would imply less brittle material and being softer with regards to crushing. Yet resistive to milling given their capacity to absorb milling or grinding energy. With lower crystallinity, significant remnants of the feldspars are still present (Dalm et al., 2014). Spatially, these classes occur as larger domains alternating with each other (Figure 9.6).

TS class 6 has a distinct shorter wavelength (600 nm) histogram and occurs as small lodes with a similar mineralogical composition to TS class 3 (phengitic-siderite-chloriteMg). These lodes are characterised by elevated sulphur concentrations (double compared to TS classes 4 and 5). Finally, TS class 7 discriminates waste rock (intrusion-related dilution within and surrounding the mineralised zone) as it is characterised by a low ratio of the dAlOH/dMgOH indices, where values <0.8 indicate mafic rocks (see Supplementary Material Figure A.3 of van Duijvenbode et al. (2022b)). In addition, this class has a distinct Fe-OH absorption shoulder of chlorite around 2250 nm (Figure 9.5), indicating the more mafic nature or rocks affected by chlorite alteration compared to the felsic rock-related mineralisation. Table 9.2 defines the primary mineralogy as chlorite-Mg (40.8%) and chlorite-FeMg (17.5%) with associated phengite (24.7%).

Mineralogical features clustering summary: Most of the TS classes have at least one distinctive and characteristic feature which can be attributed to the mineralogy found within the mineralised zone. The composition and co-occurrence of the TS classes will be further explained where necessary in the subsequent sections. The benefit of this TS clustering using regions rather than a more common feature extraction

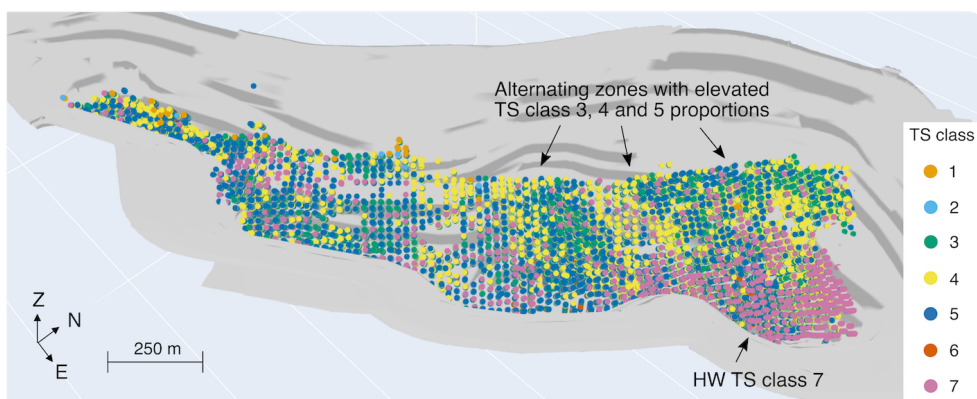


FIGURE 9.6: Oblique view of the Tropicana pit displaying the pit outline in light grey with samples ($n = 46,485$) coloured by TS class. Alternating zones occur in SW to NE direction and by depth. HW: hanging wall.

will be demonstrated in Section 9.3.5. Additionally, feature extraction is not always possible because some spectra do not have any of the extracted features. This results in an incomplete data matrix, and missing value imputation must be done prior to clustering. The demonstrated approach is not affected since it only needs a normalised hull-quotient spectrum, which can always be generated from a spectrum. The TS classes were combined with the pXRF dataset into block features and clustered into material types as described in the next section.

9.3.2 Block feature PCA and clustering

After preparation of the block model and its features (Figure 9.1), only blocks with more than three TS and pXRF samples were selected. This selection means that at least three 1 m composites describe the $12 \times 12 \times 3$ m block composition. On average, there were between 3 and 4 TS samples and between 4 and 5 pXRF samples per block, and there were 19,201 blocks in total. Prior to clustering, the seven TS class block proportions and fifteen pXRF elemental concentrations (clr transformed) were transformed into fifteen PCs explaining 95% of the data variance.

Figure 9.7a shows the covariance biplot of the first two PCs, accounting for 34.5% of the data variance. This shows the relation between the PCs and block features (represented as vectors) and links the features with the clustering classes (from now onwards, also called material types or MT). Each $12 \times 12 \times 3$ m block is represented by a scatter point and is coloured by the material type (class). A few generalised features are evident from the biplot defined by similar vector orientation and magnitudes of the block features: 1) the positive PC1 loadings group of TS classes 1 and 2, Al and Si indicate weathered material; 2) a positive PC1 and PC2 contains the grouping of major elements, e.g., Fe, Cr, Mn, Zn, Ca, and TS class 7 which generally indicates more intermediate to mafic material. Within the mineralised zone, this would generally characterise (mafic) intrusion-related dilution; 3) the negative loading of PC2 with related K and Rb, and Zr and Nb indicate potassic alteration and a grouping of two relatively immobile elements, respectively. Together with 4) a negative PC1 and S, Pb, and TS class 3 loadings, this would indicate the most potassic rock types associated with higher-grade mineralisation.

The 19,201 block samples represented by fifteen PCs were clustered using agglomerative hierarchical clustering, resulting in nine material types (the classes). This number was determined to be optimal based on the mean silhouette score, Caliński-Harabasz index and Davies-Bouldin index, which are shown in Supplementary Material Figure A.1 from van Duijvenbode et al. (2022b). These metrics are commonly used in determining the optimal number of classes as they will measure the similarity of samples and resulting classes (Aggarwal and Reddy, 2014). In addition, a pre-screening of the resulting classes, including analysis of the clustering dendrogram (see Supplementary Material Figure A.4 of van Duijvenbode et al. (2022b)), was done to confirm they would make geological sense. Figure 9.7b shows the block samples coloured by the resulting clustering classes and will be further analysed in the next section. The PCs, elemental concentrations, TS classes and extracted features, logged lithology, logged alteration, and spatial context (Section 9.3.3) were considered jointly to study the material properties of the identified material types.

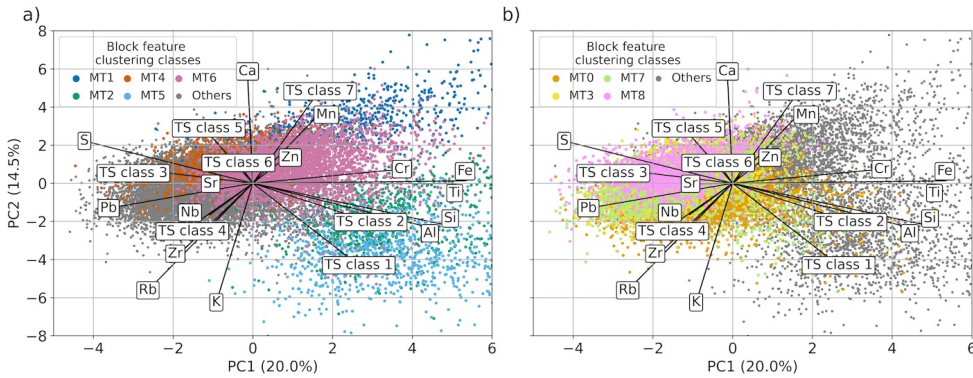


FIGURE 9.7: Principal component covariance biplot of PC1-PC2 with the 22 block feature loadings. Blocks samples ($n = 19,201$) are coloured by the clustering classes (split for better visualisation).

Material types: A first impression of the material types is obtained by finding their relationship with the degree of mineralisation. Note that the Au concentration was not one of the clustering variables but that the Au content is used to define lower and higher-grade material types. The Au (ppm) boxplot in Figure 9.8a shows that MT2 and MT5 have the lowest gold grade, followed by MT1 and MT6. Material types 0, 3, 7 and 8 resemble higher grade material.

Further insights into the mineralogical and geochemical composition of the material types are given using Figure 9.8. The molar K/Al ratio (Figure 9.8a) will be used to indicate the framework silicate modal mineralogy. Within the feldspathic gneiss units, lower values (<0.4) typically resemble a more plagioclase-rich feldspathic gneiss, whereas higher values (>0.4) indicate a higher perthite K-feldspar content (Hardwick, 2021). K-feldspar rich feldspathic gneiss samples (high K/Al) are more closely related to higher Au grade shoots (Blenkinsop and Doyle, 2014). The boxplots suggest that the material types can be divided into three categories: weathered types 2 and 5 (lowest Au grade), slightly higher Au grade, plagioclase-rich and non-feldspathic gneiss material types 1, 4 and 6 and high Au grade perthitic K-feldspar rich types 0, 3, 7 and 8. The following section will briefly discuss the main characteristics of each material type. More details are given while discussing the spatial contextual relationships (Section 9.3.3) and material hardness (Section 9.3.4).

Material type 2 and 5 are two material types having significant weathering characteristics:

- Material type 2 (MT2, $n = 891$ blocks) and 5 are the only types with elevated TS classes 1 and 2 proportion, see Figure 9.8c. This type is characterised by 87% TS class 2 and 10% TS class 1 and characterises a siderite-montmorillonite clay-rich upper saprolite unit. This material is slightly more weathered than material type 5, indicated by the weathered/Fresh indicator (Table 9.1).
- Material type 5 (MT5, $n = 978$) has TS class proportions reversed to that of type 2: 12% TS class 2 and 84% TS class 5. This indicates a phengitic-illite-siderite



FIGURE 9.8: Box and whisker plots of attributes of the block feature clustering blocks ($n = 19,201$); a) Interpreted material features; b) pXRF elemental concentrations; c) TerraSpec (TS) classes. *The n blocks for part a) are less as not all parameters are acquired for all blocks.

with more kaolinite. Both material types have a low Ca and S concentration compared to the more elevated concentrations found in Fresh rock, see Figure 9.8b.

Material types 1, 4 and 6 were classified as being more related to plagioclase rich end-members of the feldspathic gneiss using the molar ratio of K/Al. A lower K/Al molar ratio may also imply lithologies different from feldspathic gneiss.

- Material type 1 (MT1, $n = 844$) is diagnostic with a high Ca, Fe, Mn and Ti, and has a distinct low K concentration, see Figure 9.8b. This type is mainly characterised by TS classes 7 and 5 and display shifts to longer >2248 nm Fe-OH absorption wavelengths. These elemental concentrations and TS class signatures signify a more intermediate or mafic \pm amphibolitic \pm garnet gneiss with Mg-rich chlorite \pm sericite-biotite alteration.
- Material type 4 (MT4, $n = 757$) is the only material type that is characterised using TS class 6, which characterises phengitic-siderite-chloriteMg mineralogy. This material has a high S and Si concentration but also has a distinct shorter 600 nm absorption peak (TS class 6). This diagnostic signature is not frequently found as it has the fewest blocks. The shift to longer wAlOH wavelengths and low K/Al (molar) suggest a more plagioclase rich feldspathic gneiss, but with a significant conversion of feldspars to phengite.
- Material type 6 (MT6, $n = 3,724$) is mainly composed of 49% TS class 5 and 34% TS class 4, indicating a phengite dominated material type. The lower K/Al ratio suggests that limited alteration took place, that this type slightly mafic is similar to material type 1, and lithological logging indicates that the feldspathic gneiss is amphibolite bearing and quartz-rich with a sericite-biotite \pm chlorite alteration.

Material types 0, 3, 7 and 8 are closely related to higher-grade mineralisation (Figure 9.8a) and indicates that Au grade-based domaining will not account for material variability. These types also have elevated K/Al molar ratios above 0.4 (Figure 9.8a). These are more perthite-rich feldspathic gneiss material types having minor variations in mineralogical composition; however, the white mica is mostly phengitic in composition. Overall, these material types contain elevated concentration in K, Nb, Rb, S, Sr and Zr:

- Material type 0 (MT0, $n = 4,964$) is the largest material type and is characterised primarily by TS class 4 (76%) and TS class 5 (16%). It has longer 1400 nm OH features and a Mg-OH absorption shoulder around 2343 nm. It is assumed that this stronger Mg-OH feature is due to a higher proportion of biotite and minor chlorite.
- Material type 3 (MT3, $n = 3,039$) has a phengitic mineralogy identified by TS class 5 (63%), but due to an elevated TS class 7 proportion, it also shows that some blocks relate with internal more mafic dilution within the mineralised zone. It has a more distinct H₂O feature around 1950 nm, whereas the other three types show variable wavelength positions. This type has the highest relative biotite content (<1.3 ratio of the Al-OH and Mg-OH absorption feature depths), relating to an Au-rich biotite-sericite altered rock type.
- Material type 7 (MT7, $n = 2,556$) is identified by a high proportion of TS class 3 (68%), not seen in other material types. Some of the blocks have elevated smectite proportions indicating that this material type may be spatially closer to a lower saprolite unit. Overall, there is a relatively low SWIR crystalline white mica (Dalm et al., 2014), indicating that more remnants of the feldspar are still present.

- Material type 8 (MT8, $n = 1,448$) has a mineralogical composition characterised by a mixture of TS classes 3, 4 and 5, which means that it also has a mixed composition from material types 0, 3 and 7. This type is elevated in Pb and Zn, and has relatively shorter wAlOH (2218 nm) compared to the other three perthitic K-feldspar material types (2220 nm).

Chapter 8.4.2 demonstrated how the proportionality of the material classes within the different orebody domains might explain the material hardness observed across the entire mine. Following that, the current chapter and material types aims to further explain the between and within material type differences. The smaller spatial context of each block particularly better represents the local material type conditions, which may allow for a more selective loading and hauling strategy.

9.3.3 Spatial context

To further understand potential hardness relationships within and between the different material types, it is important to consider spatial contextual relationships. Results from Chapter 8.4.2 showed various orebody domains constrained by shear zones and the ≥ 0.3 ppm Au grade resource domains from the mine. Each domain was geochemically characterised using four acid digestion data, whereas this chapter uses pXRF and VNIR-SWIR data. The current study primarily focuses on the four domains defined within the Tropicana orebody region (their names are TP_1, TP_2, TP_3, and TP_4) also shown in Figure 9.9.

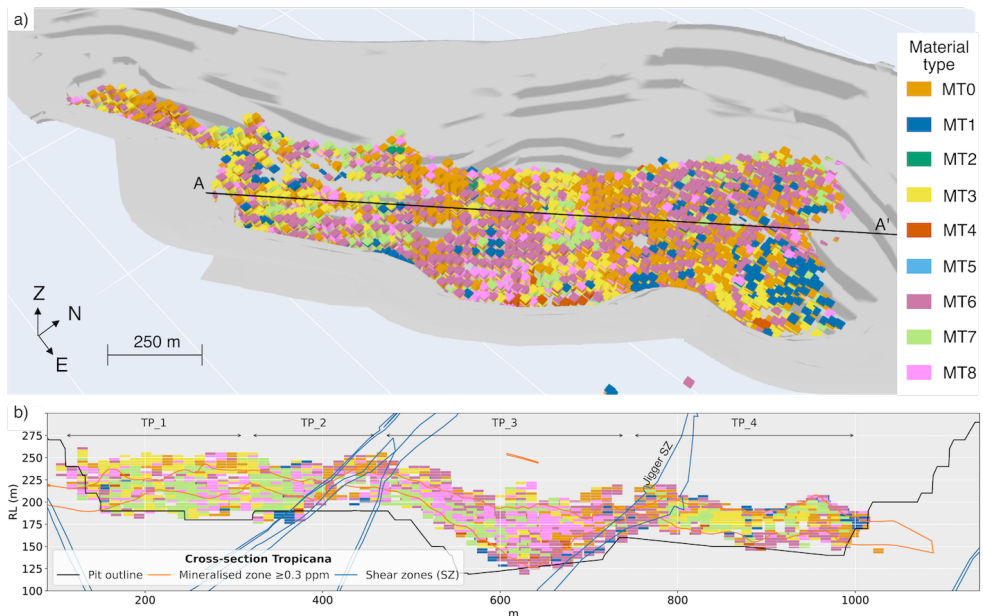


FIGURE 9.9: Block model ($12 \times 12 \times 3$ m blocks) blocks coloured by material type class label; a) oblique view of the Tropicana pit displaying the pit outline in light grey; b) SW-NE 50 m thick cross-section along line A-A'.

Figure 9.9a shows a three-dimensional representation of the Tropicana pit and the spatial configuration of the material types represented as blocks; Figure 9.9b shows a 50 m thick section view and indicates the four different estimation domains defined based upon shears crosscutting the mineralised zone. These domains are similar to those used in van Duijvenbode et al. (2022a) and refer to Supplementary Material Table A.2 of van Duijvenbode et al. (2022b) for an overview of all average elemental concentrations and proportional TS class values per domain, including those not shown. The summary statistics of the domains show that blocks within the mineralised zone outline of TP_1 have proportions of 25% MT0, 29.3% MT3, 19.2% MT7 and 12.9% MT8. Transitioning to TP_2, the proportion of MT3 decreases by 10.6% and MT6 and MT7 increase by 3.5%, where the change in composition relates with a lower abundance of biotite (picked up by TS classes 3, 4 and 5) due to the shear zone. The material types indicate a more sericite-chlorite dominated zone rather than a biotite-pyrite dominated zone.

The mineralised zones at TP_3 and TP_4 are slightly deeper than TP_1 and TP_2 (Figure 9.9b). The TP_3 domain has relatively similar characteristics to TP_1 and TP_2, but it has elevated Ca and K concentrations and decreased Fe, Ti indicating the transition to a more felsic (perthitic) K-feldspar and lower plagioclase proportions. TP_4 is located NE of the Jigger shear zone. This domain has an elevated MT0 (44.2%) proportion and a reduced MT8 (4.6%) proportion. This difference is picked up by TS class 4 (49%) and a lower TS class 5 proportion (28%) together with an elevated S concentration. TS class 4 picks up longer Al-OH absorption wavelengths indicating a more perthitic K-feldspar rich and phengitic rock type.

The proportional co-occurrence of material type blocks across the other domains show similar differences between domains. For example, at Havana (Figure 9.10a), MT0 and MT3 predominantly occur in the FW domain (named as HA_3), whereas at Boston Shaker, MT0 occurs in the HW domain (BS_2) and MT3 more in the FW (BS_1), although limited. Various material types are also found at different depths. For example, MT7 is found at Havana (Figure 9.10a) near the bottom of the pit and characterises a phengitic K-feldspar rich domain (also with elevated sulphur, Figure 9.2). Conversely, at Havana South (Figure 9.10b) this domain is found closer to the surface, resembling a more smectite rich material type. MT2 and MT5 are also found closer to the surface, and MT1 and MT6 are more associated with the boundaries of the HW and FW. MT4 occurs as small lodes indicating a domain with elevated S, Pb and Zn.

9.3.4 Hardness proxy relationships

The spatial representation of material types is associated with different alteration assemblages, mineralogical compositions, elemental enrichments or depletions and textures. These properties define each material type, determine the physical properties and can therefore be used to identify hardness characteristics. The available legacy hardness proxies (penetration rate, Equotip, BWi and Axb) allow (Figure 9.11) some preliminary hardness estimates to be made for each material type. For example, most of the weathered material (MT2 and MT5) has been mined out already, which means that the penetration rate (m/hr) provides a spatially wide-spread indication of the hardness. The weathered material is significantly easier (>100 m/hr) to penetrate

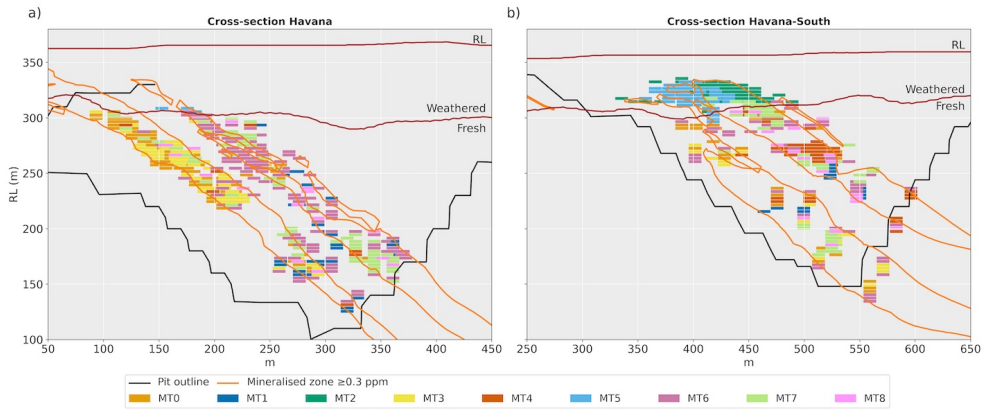


FIGURE 9.10: Cross-section view 50 m thick; a) Havana, section similar to Figure 9.2; b) Havana South section.

(softer) than Fresh rock (harder, <60 m/hr). Only subtle variations in the penetration rate occurs across the remaining material types. The softer rock character is also observed in the Equotip measurements, where MT2 has a Leeb hardness value of 642 ± 119 (mean \pm 1 SD, only known in three blocks), while MT5 is not tested at all mainly due to friability of the drill core (weathered/oxidised core falls apart if tested). MT0, MT1, MT3 and MT6 have an Equotip hardness of 768 ± 64 Leeb, whereas MT4 and MT7 are slightly harder (799 ± 53 Leeb).

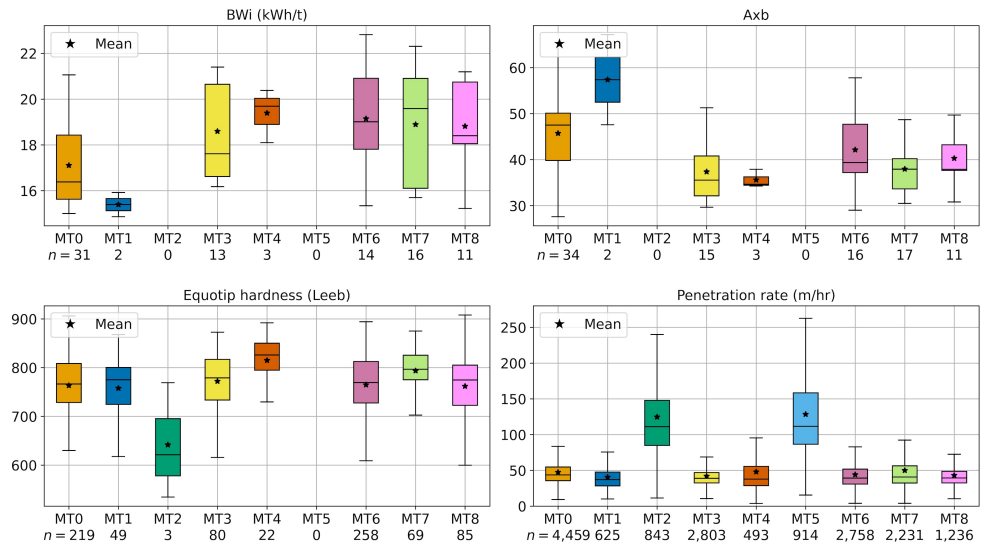


FIGURE 9.11: Hardness characteristics per material type.

The BWi is a direct measure of the work index used to model the ball mill performance. This can be used to indicate the material hardness in terms of energy consumption required to grind the material from a given feed size to a specified

product size (Lynch, 2015). Harder rocks require more energy to grind to the same target grind size than softer rocks. In contrast, the *Axb* is a rock breakage parameter, where a higher value indicates that it is harder to break the rocks. Figure 9.11 shows that especially MT3, MT4, MT6, MT7 and MT8 are harder than MT1 and MT0. At TGM, higher *BWi*, lower *Axb* are found in K-feldspar rich ore, whereas lower *BWi* and higher *Axb* are found in biotite-sericite ore, such as in MT0 (Roache, 2018). Section 9.4.1 will go into more detail about these hardness differences.

Despite the variability in hardness proxies, it is still a commonly accepted methodology to project relatively sparse metallurgical test data over a whole block or domain (e.g., King and Macdonald, 2016; Montoya et al., 2011). However, such an approach is prone to estimation errors and is only valid for some mining blocks. A preferred approach would obtain an additional material hardness estimate by determining a relationship between the Leeb hardness (Equotip) and *BWi* per material type. The more frequently (rapid and low cost) collected Equotip rebound hardness measurements, constrained to specific material types, can then be used to estimate the *BWi* and construct a hardness model. This hypothesis was tested earlier by van Duijvenbode et al. (2021) but showed no correlation between the *BWi* and Equotip at TGM, possibly due to sub-optimal data collection/processing procedures, ineffective compositing and low sample representivity. However, extrapolating the material hardness has been demonstrated to be effective in other case studies. For example, a correlation between *BWi* and Equotip was determined in deposit types where a significant difference in material hardness is present, such as a *BWi* range from 5–18 kWh/t and associated Leeb values from 300 to 900 (van Duijvenbode et al., 2021). Typically such a correlation can only be found if due care has been taken to effectively constrain material composites used for higher-order hardness tests by distinct material types. The mineralised zones at TGM exhibit a relatively narrow hardness range between 15–20 kWh/t and 700–850 Leeb as this zone is only composed of a feldspathic gneiss rock composition which complicates the finding of Equotip–*BWi* correlations.

Furthermore, the summary statistics (Figure 9.11) suggest within material type hardness variability. Ideally, classes could be further subdivided (e.g., for MT0, a Leeb value between 728–808 may relate with a *BWi* between 15.6 and 18.4 kWh/t) to potentially split into a softer and harder subclass (as shown in Section 9.4.1). This observation may seem strange because every material type already captures similar and distinct geochemical and mineralogical properties. However, clear explanations may be found in, for example, the texture, fabric and proportionalities of the material types. For example, various studies have shown the significant influence of the mineralised textures on the breakage behaviour of ores (e.g., Bonnici, 2012; Díaz et al., 2019). These affecting properties may lead to potential variations in hardness results depending on whether a destructive (*BWi*) vs non-destructive (Equotip) test is carried out. Exploring these within material type variabilities may be done using the VNIR-SWIR data and can further refine the hardness domains, as will be shown in the next section for an example at the Tropicana orebody region. Applying these domains to effectively constrain and target different material types may yield more conclusive comminution results.

9.3.5 Within material type variability

Specific VNIR-SWIR absorption features or regions can provide more information about the relative abundance and nature of mineral intergrowths related to mineral proportions, crystallinity and texture related hardness indications. For example, the relative proportion of white mica (wAlOH) could indicate sericitic vs feldspar dominated zones and thus provide macroscale-related mineralogical parameters (crystallinity, mineral composition) about the samples and the relation between Leeb hardness and BWi (hardness and brittleness).

The Tropicana orebody is a good location to investigate differences in mineralogical parameters, texture and their relationship with mineralogical composition. Figure 9.12a shows an oblique three-dimensional representation of the Tropicana pit with some of the major shear zones crosscutting the deposit in E to SE direction (Blenkinsop and Doyle, 2014). The blocks are $12 \times 12 \times 3$ m and are coloured by the BWi (kWh/t) corresponding to metallurgical composites found within the blocks. The northern end of the pit (domain TP_4) is bisected by the large Jigger shear zone obliquely intersecting the line of mineralisation. There is softer material (~ 15 – 18 kWh/t) in the NE end compared to harder material (>20 kWh/t) in the SW (domain TP_3). Another set of relatively softer blocks is found near the faults in the middle of Figure 9.12a. It is possible to use the phengite distribution to model these shear structures and demonstrate a relationship between geology and the material domains.

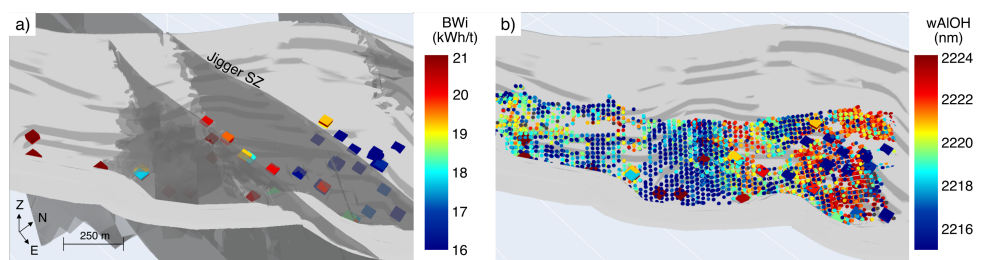


FIGURE 9.12: Oblique view of the Tropicana pit displaying the pit outline in light grey; a) major shear zones striking E to SE (dark grey) and blocks ($12 \times 12 \times 3$ m) coloured by BWi (kWh/t) corresponding to a metallurgical composite found within; b) GC samples coloured by wAlOH.

Figure 9.12b shows GC samples (within the ≥ 0.3 ppm Au zone) located within the blocks from Figure 9.9. This shows that the shear feature and NE zone can be mapped by a larger relative proportion of phengite (wAlOH features >2216 nm) in the SWIR data. The longer wavelength Al-OH suggests that there is not a discrete fault but rather a ductile zone (damage zone) comprised of multiple shears, as will be further discussed in the discussion section. Texturally this rock has more schistosity and indicates a mica schist-dominated ore type (Roache, 2018). Thus, the phengite-rich rocks to the north of the shear zone, at TP_4 correspond to finer-grained, schistose material (less competent) whereas the relatively-low phengite concentrations in the SW imply harder K-feldspar-bearing material. In this context, the schist would be softer (milling) since there are more platy micas and structurally strained/sheared textures. The only problem is that the overall ore signature is also relatively phengitic

(across all material types and deposits). Therefore, a mica-schist character would plot close to the mineralised zone spectra for white mica. Additionally, there are no major geochemical differences in a competent sample vs a sample having progressive foliation.

The white mica abundance shows a product of the alteration taking place in this domain and, in addition, at some locations, the white mica also indicates schistosity and thus a potential change in material hardness at TGM. The definitive relationship between white mica and texture is quite restricted in this context and is not yet extractable as a feature of the material types. Therefore, there is the necessity to understand geological structures to implement, for example, a white mica-schist texture proxy. For example, no elevated phengite proportion is found near the other faults displayed in Figure 9.12. Reassessing the geochemical and mineralogical differences between the main material types in TP_3 and TP_4 (see Supplementary Material Table A.2 of van Duijvenbode et al. (2022b)) showed a remarkable match between the normalised hull-quotient spectra in the 600–700 nm region and hardness domains primarily caused by the change in MT0 and MT8 proportion. There is a change in the wavelength of the deepest absorption feature in the 600–700 nm region in especially TS classes 3, 4, 5 and 6 (refer to Figure 9.5 for the maximum depth locations). Therefore, this match may be useful to domain orebody hardness and predict the work index. There are also small variations in the average Nb, Zn, S and Mn concentration, however, these are not the explanation for the hardness variations.

Figure 9.13 shows the average hull-quotient corrected spectra from the Tropicana domains. The average reflectance spectrum of TP_4 has its minimum absorption close to 605 nm, whereas the reflectance of the other domains has a more distinct minimum absorption around 690 nm. Commonly, this VNIR region is indicative of iron-bearing minerals (ferric iron (Fe^{3+}) absorption of haematite and goethite) or hydroxylated silicates with Fe, such as chlorite, biotite or epidote (Pontual et al., 2008). Figure 9.13 shows that this feature matches quite well with the hull normalised spectra of epidote in this region (Kokaly et al., 2017). The minimum absorption wavelength of epidote is around 618–620 nm, but within TP_4, this feature may have shifted slightly due to spectral mixing. This new w605 nm feature in combination with wAlOH indicates an epidote-phengite dominant ore type, which significantly correlates with softer material (low BWi) due to the shearing foliation.

The w605 feature of GC samples within the ≥ 0.3 ppm Au zone at Tropicana is visualised in Figure 9.14 and coloured by the minimum absorption wavelength between 580 and 630 nm. This range is chosen because it captures the minimum absorption wavelength for the TP_4 ore around $605 \text{ nm} \pm 25 \text{ nm}$ (w605 feature). A low w605 value indicates that there is a minimum within this zone and thus that the remaining hull-quotient spectrum increases, whereas a higher value ($>625 \text{ nm}$) indicates that the minimum absorption will be at a higher wavelength (typically around 690 nm). Within the Tropicana orebody, a high w605 value and phengitic white mica composition correspond with significantly harder ore and vice versa.

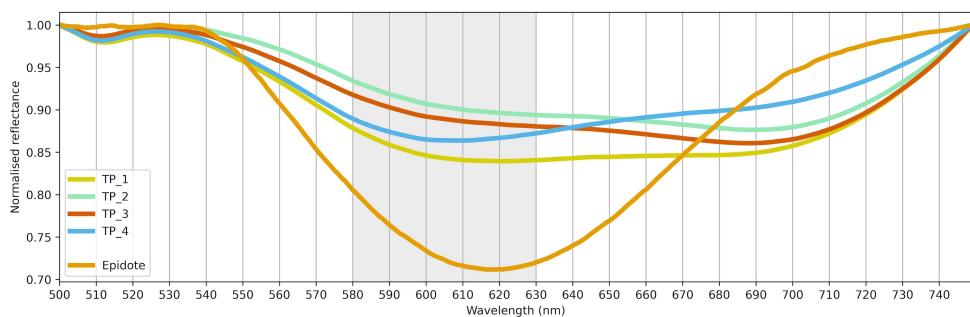


FIGURE 9.13: Average hull normalised spectra from Tropicana domains. The spectrum of epidote (Kokaly et al., 2017) is provided as a reference for the identified 605 ± 25 nm feature within TP_4.

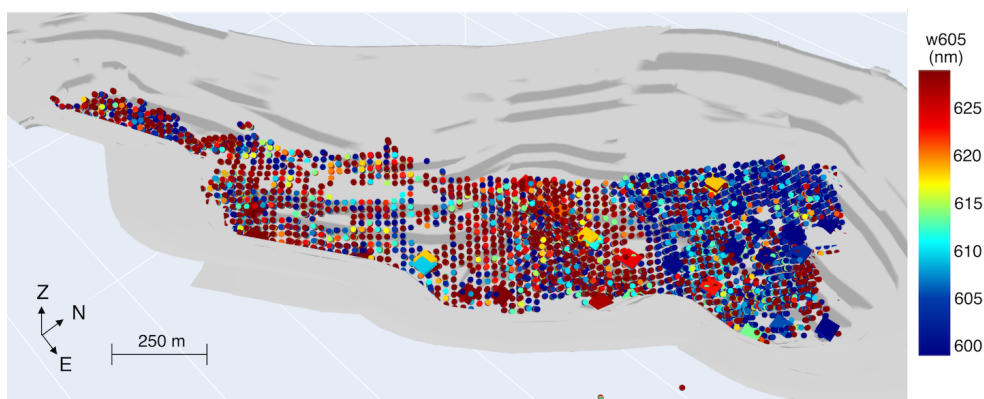


FIGURE 9.14: Oblique view of the Tropicana pit displaying the pit outline in light grey and GC samples coloured by w605. Blocks are coloured by BWi (kWh/t), as in Figure 9.12

9.4 Discussion

A relationship between the material types and hardness has been explored using a substantial data analysis. For instance, there were distinct mineralogical and geochemical differences in the predominantly weathered and Fresh material types. However, as shown in Figure 9.11, there was still variability in hardness within the specific material types. This variability may have been easier to separate in simpler deposit styles with more distinct rock types. At TGM, this was more complicated because the Fresh mineralised rock is a felsic gneiss with various degrees of alteration and a significant mesoscale deformation history (Blenkinsop and Doyle, 2014). Therefore, the relationship between material type and hardness is more evident after including a spatial context which captures the rock deformations. This reveals the shared material type attributes (e.g., high wAlOH, low w605) within the larger domain. The revealed differences or commonalities within material types gave rise to the measured variations in hardness. These could then be used to subdivide the material types further.

However, before that can be achieved, a deeper understanding of the material type composition is required, as was obtained by the block feature clustering approach.

It may be possible to better understand the hardness variability through geostatistical clustering (Fouedjio et al., 2017) or by including additional datasets such as penetration rate, Equotip or a proxy for texture. For instance, hyperspectral imaging of drill chips (from GC drilling) may add textural-structural, physical or other mechanical rock properties to the material types, as demonstrated by various other studies (e.g., Harraden et al., 2019; Koch et al., 2019; Schaefer et al., 2021). These additions may also give insight into geotechnical issues (mine design, slope stability) or drill and blast considerations (fly rock prediction, blast designs). The main limitation is that adding new variables may also reduce the number of block samples if enough measurements are not available. This may only be solved by improved correlations, more samples, or modelling of the geochemical, mineralogical and other proxies while considering the modelling limitations. In contrast, it would be preferable for daily operations to only use the geochemical and mineralogical data as this is already rapidly and routinely acquired (as done for TGM, see Section 9.2.1). These data may then be directly incorporated into a classification model that will determine the material type.

9.4.1 Material hardness and the w605 feature

A significant benefit of the material types with the w605 feature is that the types can be split into hard and soft components. For example, the 31 blocks of MT0 with BWi measurements of 17.1 ± 1.8 kWh/t (Figure 9.11) can be split based upon an arbitrarily chosen w605 cut-off at 615 nm into a softer and harder part. The shorter w605 blocks ($n = 19$) have an average BWi of 16.6 ± 1.6 kWh/t, whereas the longer w605 blocks ($n = 12$) have a BWi of 17.9 ± 2 kWh/t. This separation is also true for the other material types, and the softer blocks normally have a higher wAlOH. Within the Tropicana pit, this feature splits the material into a softer (~ 15 – 18 kWh/t) and harder (>20 kWh/t) domain.

Epidote was indicated as one of the minerals associated with the softer sheared rock type found at TP_4. Typically, epidotes result from hydrothermal and metamorphic processes (Abweny et al., 2016) and form after various minerals, including feldspar, amphiboles, pyroxenes and micas, all present within the feldspathic gneiss at TGM. More evidence of this epidote feature was collected by analysing the diagnostic absorptions at 1550, 1830 and 2250 nm. There were relationships found between phengite+epidote at shorter 605 nm wavelengths and hornblende+epidote at longer 605 nm wavelengths. This would indicate that the newly found 605 nm feature is indeed one of the diagnostic features of epidote, but not exclusively limited to epidote. The wavelength position would change accordingly with the assemblage epidote sits in, which relates to the texture and resulting material hardness. This also explains why the deepest absorption features in Figure 9.13 are not exactly at the same wavelength as that from epidote. Further research could focus on choosing an additional intermediate spectral range (1500–1850 nm) during the spectral clustering (Section 9.2.2) as this may help with mapping epidote and possibly discriminating it from other Fe hydrated silicates (biotite/chlorite).

The difference in BWi found at TP_3 and TP_4 has also been confirmed to be controlled by the mica content. The mineralised zone at TP_3 has a shorter wAlOH at 2217 nm, whereas TP_4 is at 2221 nm. Therefore, elevated epidote and phengite abundance correlate with short w605 and schistosity in paragenetic terms. On the other hand, relatively low abundance epidote+chlorite/biotite/amphibole are broadly associated with long w605 and static alteration of gneiss (T. Roache, personal communication). This also applies to other domains. For example, the HW domain at Havana South (Figure 9.10) has a phengitic white mica composition (wAlOH at 2219 nm) and short w605. However, this domain is more plagioclase-rich with epidote feldspar, thus having slightly harder material characteristics than the more perthitic K-feldspar at TP_4. The BWi (one composite only) is 18.4 kWh/t, and the average Equotip reads 795 Leeb.

9.4.2 Shear zone behaviour and structural geological control

Figure 9.12a shows how the Jigger shear zone is modelled as a discrete fault plane intersecting the Tropicana orebody. However, the phengite-rich northern part of the pit suggests a wide, ductile sheared structure characterising an entire shear zone and not a discrete fault. In fact, the discrete planes do exist as a late brittle overprint but are filled with chlorite and smectite rather than phengite-biotite. The change in material composition and contribution to the change in hardness may be the result of feldspar-to-mica reactions occurring in these fault zones. During these processes, the released silica may have precipitated in the dilatant sites, increased the rock strength by cement hardening, and reduced permeability (the SW side). Whereas on the NE side, the transition of feldspars into phengitic (schist-like) micas may have been the dominant strength-controlling (softening) mechanism (Wibberley, 1999).

The resulting material hardness is a product of the feldspar-to-mica reactions described above, but also due to brittle-ductile transition periods after the peak high-grade metamorphic conditions (D3 and D4, Blenkinsop and Doyle, 2014). At the SW part of Tropicana, plagioclase broke down to micas which localises strain within anastomosing and only simple ductile shears. Whereas in the NE part, the K-feldspar has a more brittle response from the breakdown within an apparent low-strain and pure shear-dominated domain resulting in brittle deformation textures (Olierook et al., 2020). The current study demonstrates for the first time how the effects of shear zone processes are captured within the physical behaviour of material types. The kinematic effects on each type's material texture and hardness can be further split accordingly using the w605 (and wAlOH) features.

The formation and folding of the gneissic fabric at TGM was subordinate to the deformation history (Blenkinsop and Doyle, 2014) and resulted in the final material hardness of the rock before being mined. Blast hole drilling is the first activity affected by the material hardness and may therefore provide routine early proxies for hardness on a spatially dense scale. The between material type penetration rate average, excluding MT2 and MT5, was 44.8 ± 20.9 m/hr indicating that the mineralised zone has a fairly consistent hardness. Figure 9.15 displays the penetration rate variability for the Tropicana cross-section shown earlier. The very hard region (<25 m/hr) above the TP_4 mineralised zone is a garnet-bearing quartzofeldspathic gneiss unit. The softer regions closer to the surface are affected by weathering. Note that penetration

data for the first ~50 meters in the pit was not available. The average penetration rate within the mineralised zone for TP_1, TP_2, TP_3 and TP_4 are 43.2, 45.1, 42.4 and 45.5 m/hr, respectively. The small but existing penetration rate difference suggests that the penetration rate can be used as an early hardness indication of the material to be processed. Especially, the spatial abundance and ease of obtaining this dataset benefit the fingerprinting of material types.

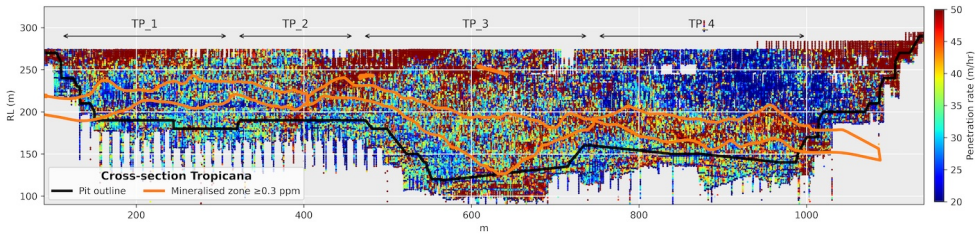


FIGURE 9.15: Cross-section view through Tropicana (50 m thick, similar to Figure 9.9) showing the penetration rate (m/hr) composited at 1 m intervals.

9.5 Conclusions

Material fingerprinting at Tropicana Gold Mine has been used to demonstrate a link between rapidly acquired geochemical, mineralogical and hardness data (BWi, Axb, Equotip and penetration rate) of various material types. These linkages define fingerprints, which are proxies for the constitutive material hardness properties and provide a more comprehensive understanding of comminution behaviour. Each fingerprint was constructed by clustering pXRF data and spectral class proportion of samples found within a small block. Clustering of these block features resulted in nine classes representing different material types. These types showed between and within material type variability attributed to the elevation/depletion of geochemical concentrations, absence/presence of minerals, spectral features, hardness proxies and spatial contextual relationships.

The material fingerprinting revealed, amongst others, the following four attributes: 1) representative variations of plagioclase-rich or perthitic K-feldspar rich domains using the proportionalities of material types; 2) modifications of material types by overprinting alteration and deformations. This was discerned by the abundance/presence of chlorite, sericite or epidote within each material type; 3) spatial contextual relationships, which showed how the material types relate to the progressive breakdown of feldspar into phengitic white micas in zones of intense foliation; 4) how shear zone processes are captured within material types. Using the above, elevated epidote and phengite abundance were found to correlate with short w605 nm and schistosity. Conversely, relatively low abundance of epidote+chlorite/biotite are broadly associated with long w605 nm and static alteration of gneiss.

Considering the within material type variability, it was evident that the material hardness (BWi) matched with the newly recognised w605 nm region. The wavelength position changes accordingly with the assemblage epidote sits in, which relates to the

texture and resulting material hardness. Additionally, this indicates the usefulness of the visible wavelength region. This feature could be utilised to separate material types into a softer ($\sim 15\text{--}18$ kWh/t) and harder (>20 kWh/t) material component. These results may be used for further domaining orebody hardness and processing response. The simple representation of material types with unique within material type variability gives a qualitative indication of the hardness abundance. The numerical data features (e.g., material type proportion, w605, wAlOH) would further enable interpolation of the data and allow easy visualisation and a quantitative hardness indication. This outcome has a significant implication for preparing material blends for processing, as well as optimised metallurgical sampling and compositing for each material type. Finally, it is expected that one would readily detect these material types downstream and infer material characteristics (i.e., for ore/waste separation and material tracking).

10

Material tracking simulation



This chapter presents the application of material attribute (fingerprints) tracking using a material tracking simulation model. The model replicates ore movements from the pit to the stockpiles and crusher. This will facilitate the finding of relationships between the crusher input feed and the mill and leach circuit processing responses shown in the next chapter.

10.1 Introduction

After the geology team characterises the material to be mined, there is generally a handover of the material information to the mine planning and scheduling team. They will ensure that the material is mined efficiently and allocated to the correct destination, i.e., unmineralised material is allocated to the waste dump and higher-grade material to the stockpile or the crusher. A common practice in the mining industry is to characterise stockpiles using a single arithmetic weighted average of grade and tonnage values (Morley and Arvidson, 2017), resulting in a lack of knowledge about the material variability and spatial variability within the stockpiles themselves.

Typically, 50 to 60% of the operating costs for an open-pit mine are related to haulage and material handling (Afrapoli and Askari-Nasab, 2017). This large-scale movement of material also results in the loss of much of the compositional understanding (upfront characterisation) of the material (van Duijvenbode et al., 2022a). This can be attributed to the fragmentation, dissemination and blending of material, but also results from the available information being averaged or insufficiently tracked and utilised (apart from some Au-focused reconciliation work). Proper material destination allocation, tracking and handling increase the likelihood of having quantified stockpile compositions that can be intelligently blended to add significant value during processing as opposed to natural mixing which may not be aligned to specific blending objectives. For example, accurate grade and geometallurgical attribute indices, such as throughput and reagent consumption per stockpile, can be assigned. This all helps to maximise the resources efficiently and minimise environmental impact.

The challenge of better allocation and handling of the material is commonly not related to drivers hauling material to wrong locations, but rather with the loss of information during the process itself. For example, mining blocks from the Resource block model are geochemically and mineralogically well characterised, and the actual processing characteristics should correspond well with metallurgical test results from comparable material. Therefore the simple goal is to adequately trace these blocks from the moment they are mined to the mill and optimally process this material according to its specific requirements in order to gain the maximum profit. A block containing deleterious, hard material or lower Au grade (Figure 10.1) can be blended such that the penalties incurred would spread across a larger volume of material and lesser impact if it is considered as a whole. However, the material is often processed using suboptimal conditions because optimal settings are not known, achieved or are unrelated to material attributes. The available fleet management systems are equipped with optimisation suites that consider blending objectives in which the plant head-grade requirement is simply constrained by an upper and lower limit (Afrapoli and Askari-Nasab, 2017). These systems do not account for preferred material blending types as most geological information is not currently linked to the data processes.

The problem of creating optimised blends is not simply solved because the mine is restricted in material availability at a given time. There is often a limitation in the allocation and placement of material at different run-of-mine (ROM) fingers because the processing plant still needs to fulfil its throughput demands to maintain constant

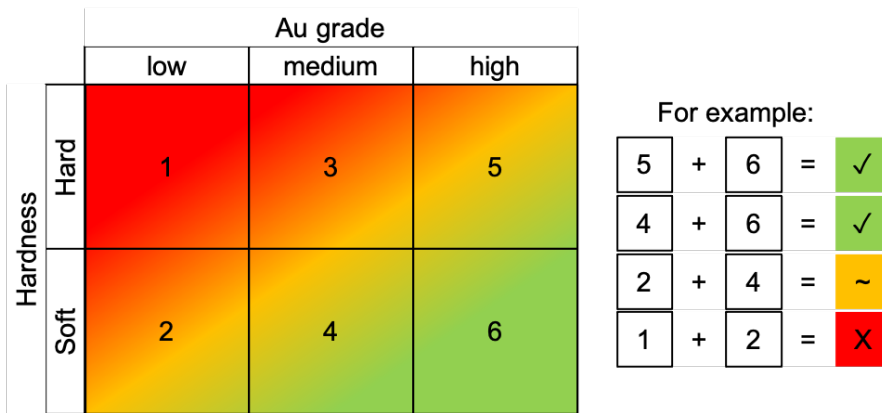


FIGURE 10.1: Simplistic schematic overview showing preferred or non-preferred blending options.

production. Therefore, it is of utmost importance that one actively monitors what material is processed at any given time to enable optimisation of the processing characteristics of the incoming feed. Note that the notation of stockpile and ROM fingers is used interchangeably to comply with the notation of the Tropicana Gold Mine.

This chapter presents the new material tracking simulation designed for TGMs material handling and has two objectives. Firstly, to assign grade and geometallurgical attributes to material in trucks, stockpiles and crusher feed. Secondly, to facilitate the spatial and temporal comparison of geometallurgical attributes with actual plant performance. This is possible after running the simulation because the model output provides the material attributes entering the plant as crusher feed and can be directly linked to the plant performance. In addition, results from the model can be used for reconciliation purposes and back-tracking of processing responses to block models. There are three parts to this chapter: 1) the tracking model will be explained in detail; 2) the spatial modelling of stockpiles will be explained; and finally, 3) the results will focus on the mine-to-crusher movements, insights from the crusher feed attributes, a case study showing blending and model validation. The chapter will not focus on finding and discussing the relationships between geology and metallurgical plant performance, as this will be part of the next chapter.

10.2 Methods

10.2.1 Forward simulator

The main aim of the material tracking forward simulator is to track material fingerprints from the moment of mining until it becomes crusher feed. Within this simulation time or tracking period, the material can be directly transported from the pit → crusher or from the pit → stockpile → crusher. On rare occasions, material may be reallocated from stockpile A → stockpile B → crusher. When the material

is dumped on a stockpile, there are instances where a dozer is used to flatten the stockpiles, displacing material or to tidy up the ROM pad area. In the model (10.2.2) these stockpiles will be modelled as hexagons to resemble the stockpiles as realistic as possible. The stockpiles or ROM fingers function as a temporary storage location of material and can be used to blend material coming from different mining locations. These movements were not tracked but are assumed to be within constrained spatial proximity of the truck dump and to account for this, small dump coordinate adjustments were calculated. However, each material movement adds greater uncertainty to where the material is located within the stockpile. A simulator that carefully considers and tracks these material movements should give detailed insights into the material attributes at any given moment and location. The implementation of such a data-driven simulation model will be discussed next. Note that no attributes are simulated. The simulation here addresses the recreation of the data flow, not a stochastic simulation of grades or other variables. Material attributes were retrieved from a block model and truck movements from the fleet management system, see Section 10.2.3.

Figure 10.2 shows a schematic implementation of the material tracking forward simulator. All hauling movements originating from the fleet management system were stored in a central database. Each record consists of a load-dump cycle and contains various attributes, including truck ID, source and dump location, departure and arrival time and payload. From this database, one can (Step 1) select a tracking period. All truck movements from this period will be split (Step 2) into a dump and reclaim instance and sorted based on execution time. This will be the departure time for a reclaim instance, whereas, for a build instance, this is the dumping time. Moreover, while trucks are in transit (waiting to be executed), nothing is done with data. Material hauled from the pit to a waste dump is not further discussed or shown. Then, three databases are initialised (Step 3): a database that stores all incoming *crusher* feed attributes, one *stockpile model* database and a so-called *trucks in transit* database. Initiating the stockpile model can be done from an empty run-of-mine (ROM) pad area with no previous attributes stored or start with predefined tonnes and attributes. A reclaim instance may query the stockpile model when no tonnes are available from the stockpile model, then tonnes can be queried, but no attributes will be assigned to this payload. These situations may occur at the inception of the simulation or on rare occasions during the simulation. In practice, this should not be possible, but, for example, some dozer and loader payload movements were not tracked and may result in inaccuracies in the simulation. The workings of the stockpile model are explained in Section 10.2.2.

The next part of the simulator simulates all truck movements (Step 4). Then, depending on the instance to be executed (reclaim or build), a specific path will be initiated:

Reclaiming: A Type 1 or Type 2 path starts when a reclaim instance initiates. Type 1 initiates when the truck is at the ROM pad area (Figure 10.3). The truck source coordinates are matched with the closest non-empty ROM pad hexagon (see Section 10.2.2, for further details), and the instance will request the truck payload from the stockpile model. It will then link the payload, and associated material attributes to the truck ID and store it in the *trucks in transit* database. Similarly, a Type 2 path initiates when the

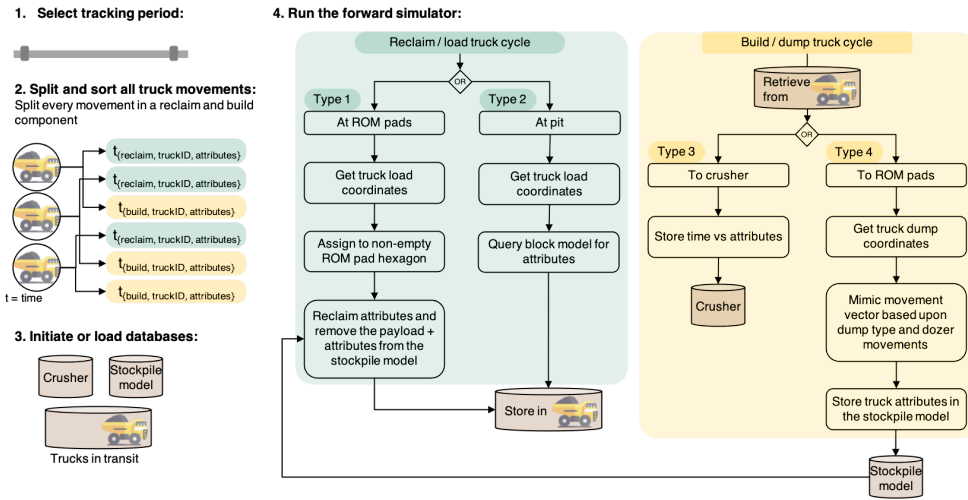


FIGURE 10.2: Schematic representation of the material tracking forward simulator. Only showing ore handling processes.

truck instance is located within the pit. After initiation, the truck source coordinates link to a specific block from the truck block model and all trackable attributes (material fingerprint) will be linked to the truck ID. The Type 2 path ends by storing the truck ID and its payload, including attributes in the *trucks in transit* database.

Building: A Type 3 or Type 4 path starts when a dumping instance initiates. Type 3 represents the actions when the truck destination is the crusher (Figure 10.4). The simulator will retrieve the truck ID and attributes from the *trucks in transit* database and store this in the *crusher* database. A Type 4 path starts when the truck destination is the ROM pad area. Then, based on the original dumping coordinates, a small adjustment vector is added to mimic material movements caused by dumping or dozer pushes (see Section 10.2.2, for further details). This defines the final coordinates and available hexagons to which the truckload attributes can be stored.

The forward simulator stops after iterating through the entire truck movement list. A time series of the crusher feed can subsequently be analysed to link the incoming material attributes with the actual plant response. There is no module that describes the material flow in the comminution circuit as was done by Wambeke et al. (2018). Instead, a fixed time delay is assumed to relate the crusher feed attributes and the corresponding plant actuals, this will be discussed in Section 11.2.

10.2.2 Stockpile model

The workings of the stockpile model are constructed to represent reality as closely as possible. For example, a mining truck body is about 7 to 8 m wide, and creates a cone-shaped stockpile with a diameter of about 10 m after dumping the bucket load. Therefore, the stockpile model uses hexagonal prisms to mimic this stockpiling

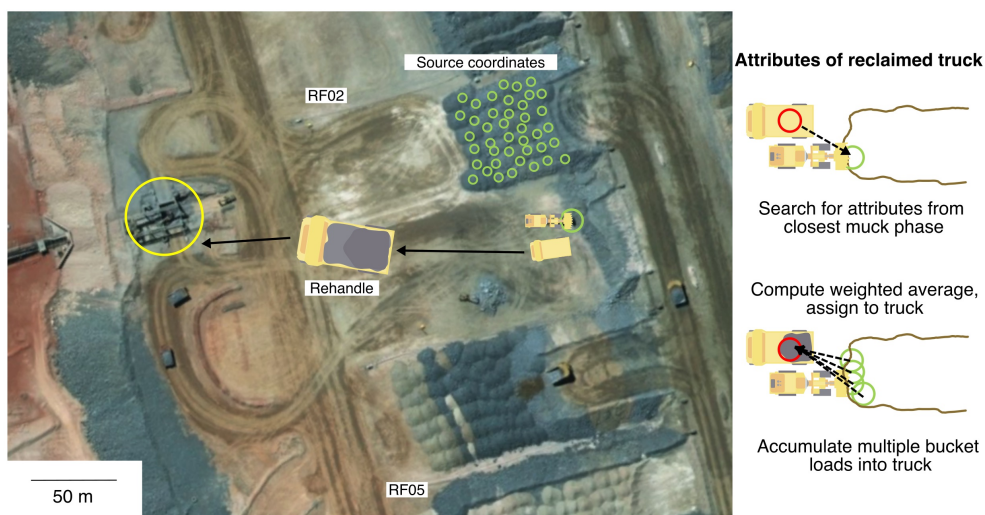


FIGURE 10.3: Tracking concept – Reclaiming. Aerial photo of the ROM stockpile layout. Date: 12 September 2018, (ESRI, 2009).

behaviour. The ROM pad area is modelled using a hexagonal grid, and the maximum height of each hexagonal prism represents the maximum stockpile height (8 to 10 m). This entails that each hexagonal prism can typically represent about 1,500 t of ore (six to eight truck dumps).

At TGM, ROM finger stockpiles are created using a heaped fill stockpiling scenario (Young and Rogers, 2021) which contains two dumping phases. See Figure 10.5 for an oblique view of one ROM finger and the implementation (simulation) of the dumping and reclamation cycle superimposed on the actual ROM pad area surface. The height difference between the ROM floor area and the skyway dumping level is about 8 to 10 m. Firstly, a series of paddock (paddy) dumps are placed to form the base layer of the stockpile (refer to the blueish hexagons in Figure 10.5). The main purpose of the paddy dumping series is to form a base of material such that when phase two dumping starts, no material will roll/move to unwanted locations and block off entry (for people and vehicles) to this active working area. For instance, it may happen that one ROM finger is being constructed, while the neighbouring finger is simultaneously reclaimed. Secondly, the stockpile construction involves building an upper layer above an area of paddy dumps using skyway dumps (Young and Rogers, 2021). Dumping occurs until the stockpile bench is full or until the geology department closes the ROM finger.

Each ROM finger is modelled using an individual stockpile model. Figure 10.5 shows the build and reclamation cycle of one ROM finger progressively. This will be used to explain the dumping (Type 4) and reclamation (Type 1) simulation paths in Figure 10.2. Based upon the truck z-coordinates, one can determine whether the truck was located at the ROM pad floor level or at the skyway level and define the dump type as either a paddy or skyway dump. Usually, at $t = 0$, these are paddy dumps and based upon the x and y coordinates, the corresponding hexagon prism is identified. The x and y coordinates correspond to the middle of the truck's rear axle,

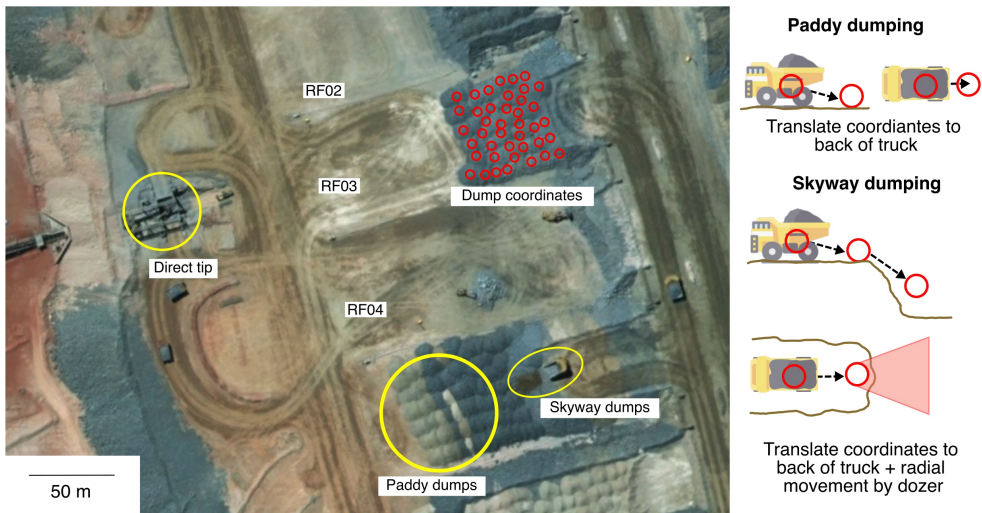


FIGURE 10.4: Tracking concept – Building. Aerial photo of the ROM stockpile layout. Date: 12 September 2018, (ESRI, 2009)

so a displacement vector towards the back of the truck is applied for the final dump coordinates. The final coordinates were defined for skyway dumps by applying a dozer and dumping movement vector (Figure 10.4), as this will mimic the dozer movement to flatten the ROM pad surface. The coordinates are translated to the back of the truck and moved in a radial direction based upon the distance towards the ROM finger centreline.

After dumping, the truckload attributes are stored within the hexagon, which itself is modelled using a first-in-first-out (FIFO) query because a reclaiming dozer will likely pick up material from the bottom and not from the top of the stockpile. The hexagon is full when it reaches its maximum payload, and the remaining payload will then be allocated to the nearest non-full hexagon. Figure 10.5 shows that until $t = 12$ days, more paddy dumps are placed, and simultaneously skyway dumps are dumped to construct the upper layer of the stockpile. Construction of this ROM finger is finished after twelve days after which it is used as crusher feed. Within four days, the entire ROM finger is reclaimed. Each truck reclaiming (Type 1) requests the nearest non-empty hexagon from the model and removes the attributes. Multiple hexagons may accumulate in the truck, and the final truckload attributes are defined using a weighted average. This will typically happen until the ROM finger is zeroed, and afterwards, the cycle starts again. Reclaiming a stockpile is typically much faster than constructing it.

10.2.3 Simulation

The material tracking simulated 886,552 trucks and material movements spanning 6 years from 27-10-2015 until 21-10-2021. The movements took place across all open pit areas, but in the early years, more trucks were coming from Tropicana and Havana, whereas in the later years, mining predominantly took place in Havana South and

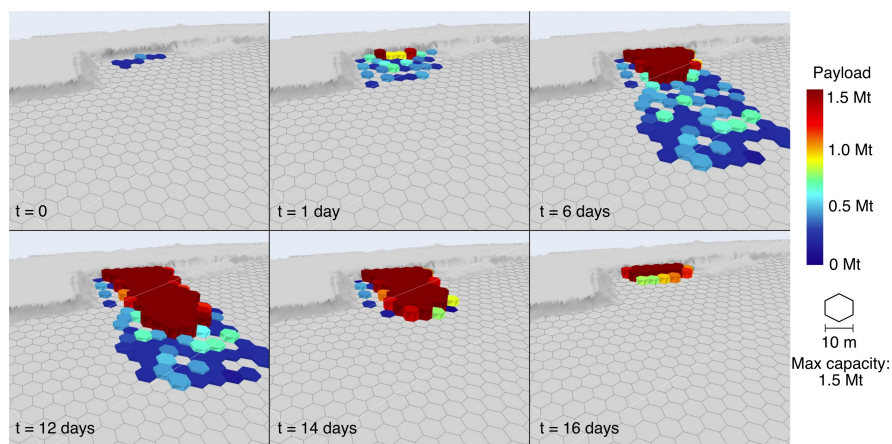


FIGURE 10.5: Oblique view on the 3D stockpile model progressively showing the build-up and reclamation of a stockpile simulated with the actual truck movements.

Boston Shaker. Material from the pits was either hauled to the stockpiles at the ROM pads or directly fed to the crusher; waste was not tracked. Figure 10.6 shows an aerial view of the ROM pad and stockpile configuration in September 2018. In total, the forward simulator tracked ten individual stockpile models (RF01-RF09 and SF02, RF = ROM finger, SF = stockpile finger) and the crusher. All ROM pads were zeroed at the start of the simulation, and tracking of a ROM finger could only start with a build cycle. SF01 is not tracked as it had limited build and no reclaim activity within the considered tracking simulation time frame. SF02 is a lower-grade stockpile which was already partially built in 2015. Therefore, the initial shape and state of the corresponding stockpile were reconstructed based upon an existing digital terrain model surface. No geometallurgical properties were assigned as it was unclear where the material originated from. Other stockpiles seen in the aerial photo have limited activity or are used for long term storage and are therefore not considered.

All tracked attributes are sourced from a reclaim query of a truck in the pit (Type 2). The fleet management system assigns coordinates to a truck when an excavator fills it. This coordinate is used to query the ($12 \times 12 \times 3$ m) Resource block model for material attributes. The block model is populated with a number of geometallurgical parameters: elemental concentrations from pXRF measurements, mineralogical attributes from VNIR-SWIR analysis, penetration rate and metallurgical test results (BW_i, A_xb, recovery). Only the Au, S and specific gravity (density) values were simulated during the construction of the block model. All other parameters were simply assigned to blocks based upon the survey coordinates of the samples/measurements. These values are averaged per block and parameters, and thus not all blocks contain all parameters. The model can work with any variable modelled or populated in a block model. Note that the block models also have indices related to the material fingerprint classes discussed in Chapter 8 and Chapter 9.



FIGURE 10.6: Aerial photo of the ROM stockpile layout. Note that the layout and location of ROM fingers changes over time. Date: 12 September 2018, (ESRI, 2009).

10.3 Results

After executing the material tracking simulation for six years of data (November 2015 – November 2021), it was possible to analyse the mine-to-mill material movements, effects of blending and/or the crusher feed attributes from the different databases created. See Table 10.1 for summary statistics of the material tracking simulation. All further analysis was done by capturing the state of the stockpiles in intervals of 12 hours. Every sequential step of 12 hour shows the progress of building or reclaiming the stockpiles. The material moved towards the crusher in that time interval represents the incoming crusher feed attributes and can be related to, for instance, the ball mill performance or recovery and leach kinetics. Relating the crusher feed to plant performance is done in Chapter 11. This chapter analyses the material until the moment it enters the crusher. The chapter concludes by comparing the actual and tracked monthly tonnes and includes a validation using the stockpile model state vs the surveyed mine plan at various points in time.

10.3.1 Mine-to-crusher movements

Figure 10.7 shows an example of the state of the stockpile maps with the main physical (payload, density, penetration rate), mineralogical (wAlOH) and geochemical (Au, S, Si, K/Al) variables. The shape of the stockpiles can be identified by looking at the dump coordinates of the mining trucks and its payload. Some hexagons contain only payload because the material represented was sourced from Resource model blocks where these attributes were not known. Such a detailed stockpile map can be used to understand grade and geometallurgical variability inside the ROM fingers. For example, one can observe that RF09 is located on top of stockpile SF02 (Figure 10.6) by looking at the density and penetration rate outlining the stockpile shape. RF01,

TABLE 10.1: Summary statistics of the material tracking simulation.

General	
Period	27-10-2015 - 21-10-2021
Movements	886,552
Stockpiles	10 (9 × ROM fingers, 1 × long-term stockpile)
Tracking steps (12 h)	4,374
Crusher feed	
Tonnage from known movements	48,537 Mt
Tonnage tracked	41,372 Mt
Percentage payload tracked	85.25%
Direct tips	9.60%
Rehandled at stockpiles	90.40%

RF02 and RF09 contain easier to penetrate, thus softer material with a lower density. Investigation of the source location from this material shows that it mainly comes from Transitional ore located in Havana South and Havana. It has a slightly lower Au grade than the other ROM fingers, and is more muscovitic in composition (shorter wAlOH). RF03, RF05 and RF06 (RF04 was not used between November 2017 and December 2020) contain Fresh hard, higher density ore with a more phengitic composition, and higher Au and S content. This material primarily comes from the deeper parts of the Tropicana pit (domain TP_3) as will be discussed in Section 10.3.3. The material located at RF08 has a higher K/Al molar ratio than the other stockpiles indicating that it has slightly more potassic feldspar-rich material with a lower Si percentage than the RF01-RF06 material. This material predominantly comes from a different part of the Tropicana pit (domain TP_4).

Figure 10.8 shows the Au, S, and penetration rate variability during RF02 build and reclaim cycles. The weighted averages (weighted using truck payload) of the stockpile cycles are indicated by the scatter points and the weighted standard deviation by the error bars. Each build/reclaim cycle is standalone, and there is no relationship between consecutive cycles. A large spread around the mean indicates a significant amount of truck dumps containing material with either higher or lower attribute values. These results show that there is roughly 1.4 ppm of Au variability, 0.6 ppm S variability and 14 m/hr penetration rate variability within the material dumped at the stockpile in one cycle. This variability is relatively large and should ideally be lowered by, for instance, splitting the material over stockpiles dedicated for the higher and lower halves. The variability indicates that the commonly accepted weighted average is not a preferred metric to use. Thus, a more detailed insight into the material variability at the stockpiles itself is preferred, as can be achieved using the material tracking simulation.

Looking at the source location of material dumped within a cycle gives insights into some of the blending or scheduling objectives. For instance, RF02 was used during cycles 7, 21 and 26 for Oxide and Transitional ore from Havana South (Figure 10.8). The material was typically softer (higher penetration rate) and had lower S values. This material has a larger variability in penetration rate than the Fresh ore due to the variable weathering characteristics of the material. Cycle 26 matches the situation

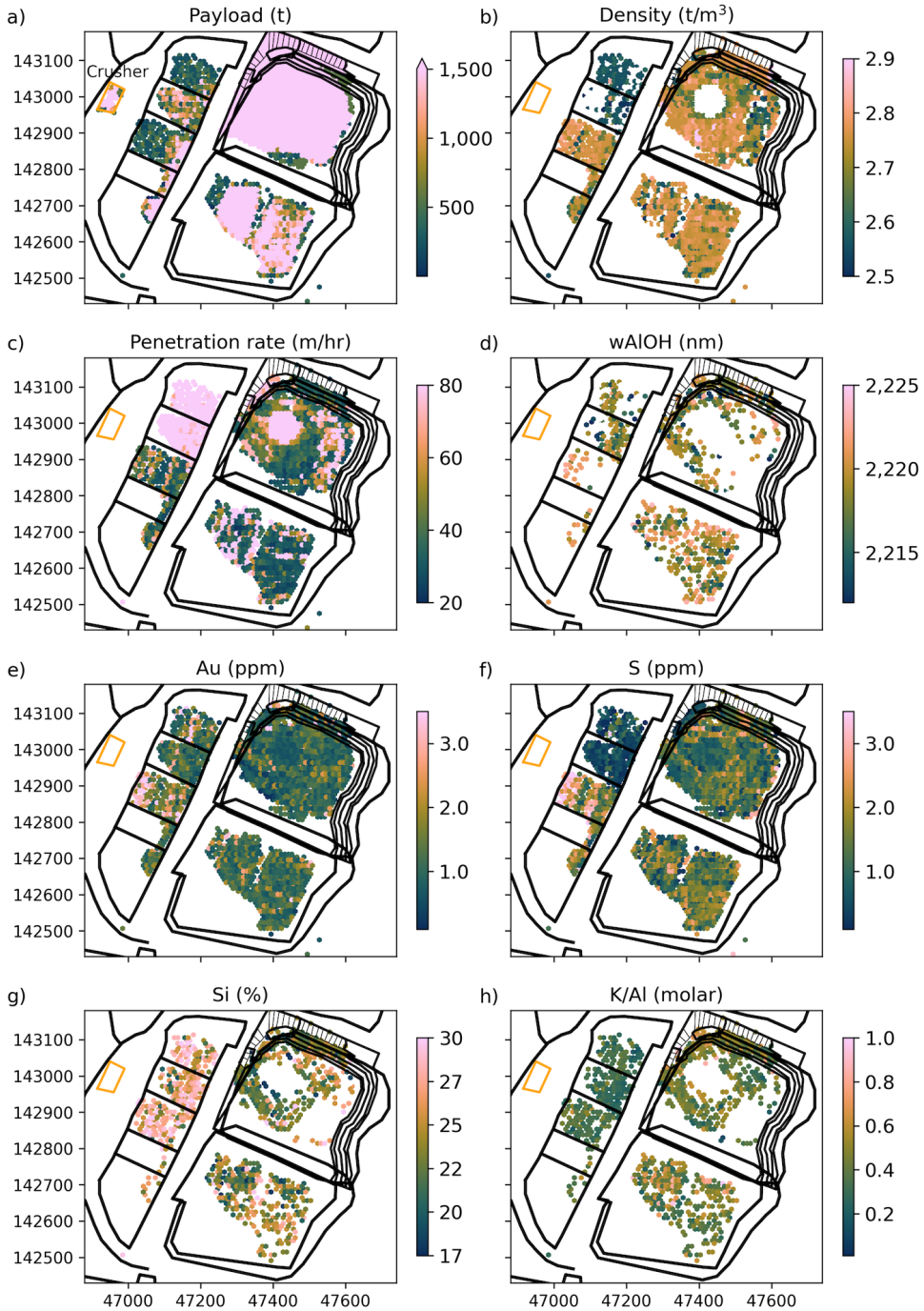


FIGURE 10.7: ROM pad overview showing selected physical (payload, density, penetration rate), mineralogical (wAlOH) and geochemical (Au, S, Si, molar K/Al) variables; stockpiles state at 07-03-2019 (local mine grid coordinates).

shown in Figure 10.7. One could argue that the highly variable material should be split across multiple stockpiles, but there is no space available close to the crusher due to material placed at the other stockpiles (Figure 10.7). Reclamation during this stockpile cycle is spread over three months as the material is blended with the harder Fresh ore from the other stockpiles to lower the average sulphur value. Material feed with a high sulphur grade typically indicates more sulphides in the material, which need to be combated by an increased oxygen addition in the leach tanks, however, this may also result in a higher lime requirement in order to maintain the desired pH.

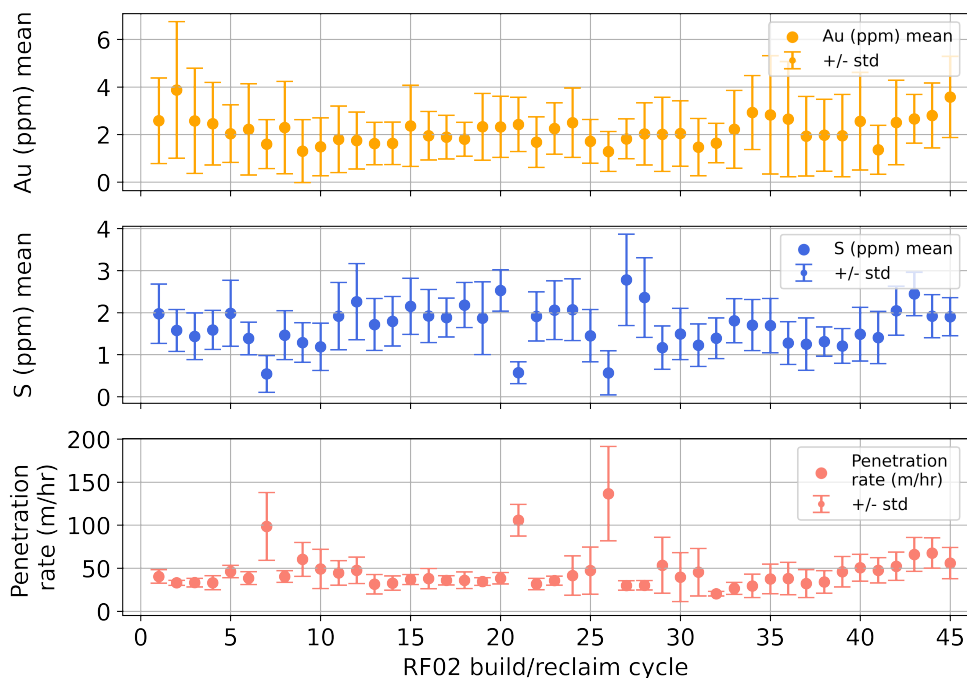


FIGURE 10.8: Weighted average and weighted standard deviation of the stockpile Au (ppm) grade, S (ppm) grade and penetration rate (m/hr) for stockpile build and reclaim cycles of RF02 showing significant variability within individual stockpiles.

If the crusher material handling is considered as a first in – first out unit, then the sequence of trucks dumping at the crusher indicates the crusher feed attribute variation across time. Insights from this part of the material tracking simulation are easily generated using the tracking model. The trucks arriving at the crusher come from one of the ROM pads or directly from the pit. The top part of Figure 10.9 shows the total payload per 12-hour interval going towards building the tracked ROM pads. The lower part shows the reclaiming payload component for the ROM area and indicates from which ROM pad material is reclaimed as crusher feed. The crusher feed also consists of material directly hauled from the pit area and other stockpiles or locations not modelled. The build/reclaim cycles of the individual stockpiles are distinctively visible. For instance, RF05 is constructed between 11 February 2019 and 15 February 2019 and then fully reclaimed by 25 February 2019. Similar build and

reclaim patterns are observed for the other ROM fingers. Low-grade stockpile SF02 is steadily constructed during the entire period shown and only reclaimed by June 2020. The blending strategy discussed in the previous paragraph using the softer Oxide/Transitional material located at RF02 and the relatively harder material at the other stockpiles is visible in Figure 10.9. There is a steady blend ratio of $\sim 10\%$ RF02 material with $\sim 90\%$ RF03, RF05 or RF06 material in the shown period. Between the end of January and the beginning of February 2019, there is a period in which no crusher feed is provided. Most likely, the processing plant was not operated during this period due to maintenance.

The crusher installed at TGM is designed to treat 2,500 t/h, which means that theoretically, 30,000 t (30 kt) can be crushed every 12 hours. In contrast, the average crusher throughput is above 2,000 t/h, but there is, on average, only between 5 kt and 20 kt of material processed per 12 hours. This means that the crusher is not run for 24 hours per day. In practice, this is also unnecessary because the limiting factor for throughput in the metallurgical plant is the ball mills operating at 1,050 t/h for 24 hours per day with as little downtime as possible. After the primary crusher is a large coarse ore stockpile where material can reside for up to 8 hours before being conveyed towards the cone crushers. This stockpile is typically maintained at 80% capacity, meaning that the crusher does not need to operate for 24 hours per day and that trucks don't need to constantly deliver material to the crusher.

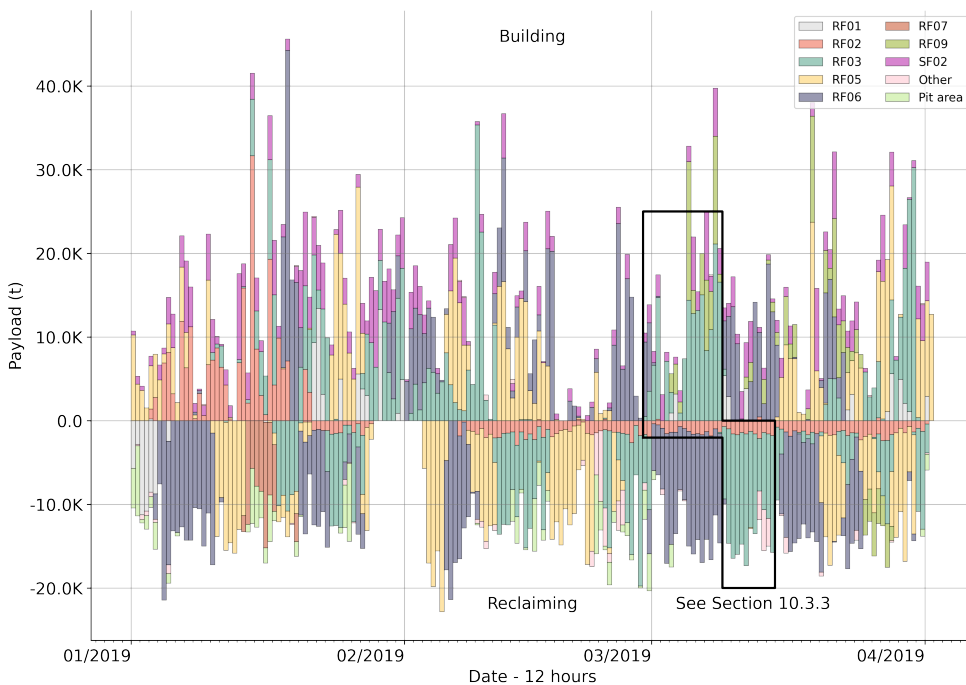


FIGURE 10.9: Selected time frame showing the total payload moved towards (building) or from (reclaiming) the tracked ROM pads per 12-hour interval. The reclaiming payload also indicates the direct crusher feed component from the pit area.

During the entire modelling time horizon (6 years), 9.6% of the total crusher payload was dumped by direct tips, whereas 90.4% of the payload was rehandled and temporarily stored in stockpiles before being fed to the crusher. This high percentage of material rehandling shows the importance of a detailed stockpile model capable of accurately modelling and reconciling the dumped material and its attributes. Visualisations of the stockpile build and reclaim cycles in 12-hour steps gave sufficient resolution while the spatial-temporal modelling and visualisations exhibit realistic geological variability and spatial cohesion while enabling temporal reconciliation of the data. Having the ability to track any geological parameter attributed in a block model is of great value. This was the first validation showing that the tracking model can capture the truck movements with sufficient detail and track the material attributes across time. Furthermore, it allows for the reconciliation of the processing response by looking at the material attributes fed and processed during a target period. A more numerical and visual validation of the material tracking model follows in Section 10.3.3.

10.3.2 Crusher feed attributes

Using the material tracking simulation, it was possible to identify and characterise all crusher dumps (stored in the crusher database). There were almost 295,000 crusher dumps in the 6 years considered. The crusher feed attributes are equal to the set of parameters tracked from the block models as described in Section 10.2.3. Firstly, all dumps were grouped with a frequency of 12 hours and the observed payload and its attributes were adequately composited. A frequency of 12 hours was selected as this matched the resolution of the processing actuals. The total payload was the sum of all individual dumps; the density, geochemical attributes (Au, Al, Ca, Cr, Fe, K, Mn, Nb, Pb, S, Si, Sr, Ti, Zn and Zr) and mineralogical attributes (wAlOH, biotite abundance, wFeOH, w605) were expressed using a weighted average with the payload as weight; for the generic material attributes, including the penetration rate, Equotip hardness, BWi, Axb, recovery, lime consumption and NaCN consumption was the median value taken. Most of these attribute indices are non-additive in nature, and therefore, the median was found more appropriate than the mean. Any further analysis using these parameters should be undertaken with caution, and the non-additive character should be considered.

Secondly, the information contained in the 12-hour intervals was used to calculate a moving average to reduce noise in the time series dataset. This helps to identify periodical trends of higher and lower attribute values that are more likely linked to rock properties of the material processed. Each attribute is a moving average using fourteen consecutive 12-hour observations (7 days) calculated with a minimum of six observations (3 days). Figure 10.10 shows the seven-day moving average of the crusher feed attributes; for visualisation purposes, the values are rescaled with zero mean and standard deviation of one. This shows, for instance, how the penetration rate and density are typically negatively correlated with each other. There is a higher penetration rate in periods with a low density, probably related to the softer Oxide material, and in periods with a low penetration rate, the density is higher (Fresh material). Generally, the geochemical material variability is lower between 2017 and 2020 because the source material comes from domains with similar geochemical

characteristics. Not all attributes were observed during the entire time horizon. For instance, biotite abundance was not populated in all blocks from the block model and is therefore only tracked from mid-2019.

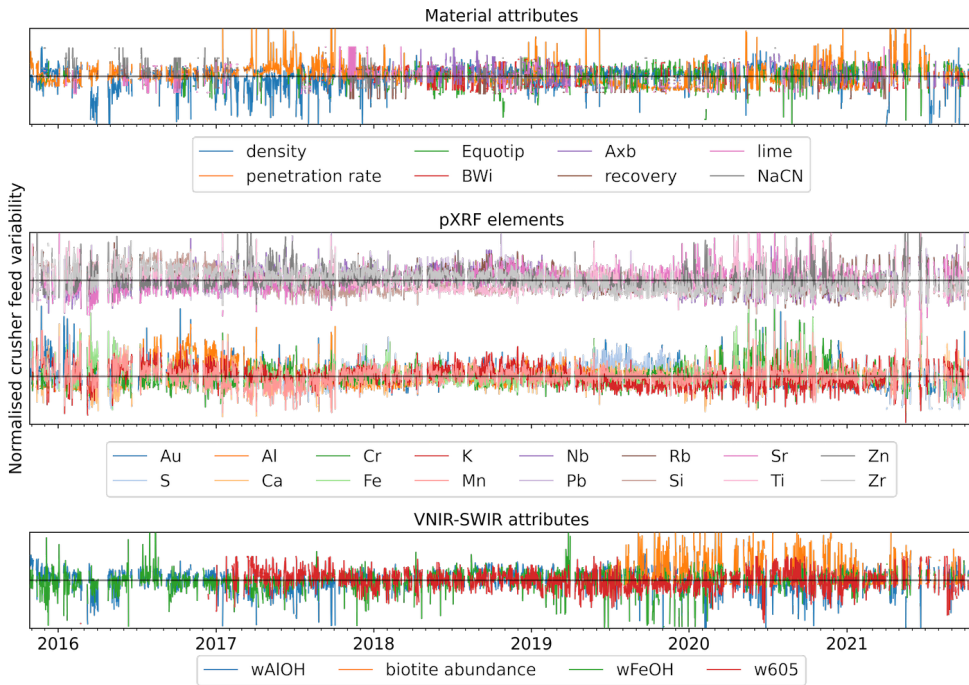


FIGURE 10.10: Time series data visualisation of the seven-day moving averages for each tracked crusher feed attribute.

The BWi, Axb and recovery related attributes were infrequently observed. These parameters were not spatially modelled in a block model and were simply attributed to individual blocks (and thus trucks) based upon the survey location from the tested metallurgical composite. If the material from these blocks were not blended or spread over multiple time horizons, then these metallurgical test results should match the corresponding and observed production actuals. However, there are two issues with testing this correlation. Firstly, the tested metallurgical composites are frequently composited from multiple drill holes. Therefore, this material may or may not have a similar mineralogical and geochemical composition. Ideally, samples should not be blended such that the true material response can be characterised. However, results from Section 10.3.1 revealed that a significant amount of material blending occurs with material coming from different locations with different compositions. Therefore, sometimes it is better to test a material blend that is aligned with the expected feed blend such that the additive material characteristic can be defined. Secondly, the current block model blocks have a size of $12 \times 12 \times 3$ m and contain roughly 1,200 t (Fresh – density = 2.78 t/m^3) of material. It would take between five to seven trucks to haul this material from the pit to the ROM area and take approximately 1 hour to mill an entire Resource block if a throughput of 1,050 t/h is maintained.

The observability of this single block is thus fairly easily distorted, and it remains a question whether this 1-hour mill signature is also reflected in the 12-hour processing response resolution.

As alternative to the crusher feed attributes it was also possible to directly look at the material types defined in Chapter 9. For this, the proportion of each material type within the geometallurgical domains (Figure 8.12) was defined and applied to each truck payload leaving a specific domain. Then, the proportion of each material types payload defines the new input fingerprint and should reflect mining of different domains, different blends and thus resulting in different crusher feed compositions. These compositions inherently reflect the geochemical and mineralogical variation from Figure 10.10.

Figure 10.11 shows the material type proportions as a function of the crusher feed over time. The material types are similarly coloured as in Chapter 9. Since not all crusher feed could be adequately tracked due to unmodelled stockpiles, there is also a new category called “other”. This other material can be of any composition and, therefore, it’s proportion should preferably be as low as possible which indirectly also indicates that most material is well tracked. The results show, for instance, that almost no MT2 and MT5 was mined which indicated Oxides or weathered material. This makes sense, because most material mined in this period is from the deeper parts in the Tropicana pit, and thus indicate that limited Oxide-related material characteristics are expected in the processing plant. Most time domains have their crusher feed composition characterised by MT0, MT3, MT6, MT7 and MT8. Furthermore, these material type proportions will be used as input dataset in Chapter 11 to link with the actual processing response.

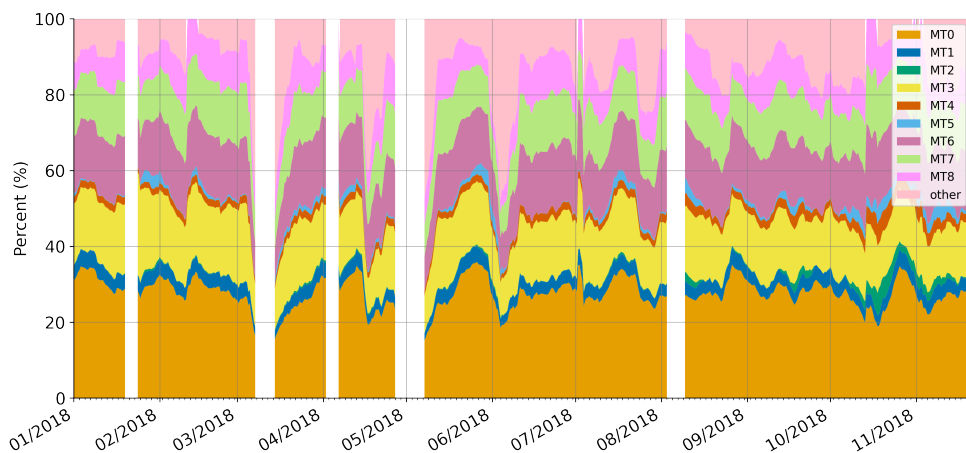


FIGURE 10.11: Material type proportions as a function of the crusher feed over time.

Overall, various distinct periods and patterns of higher or lower attribute values or material types can be identified. This implies that the selected geological attributes should be able to sufficiently characterise the incoming crusher feed material in terms of geochemical and mineralogical composition. Together with the spatially abundant penetration rate and Equotip data there is a large set of pertinent features available

that will likely be informative for the actual plant performance. Hence, the next step is to align these crusher feed attributes with the actual plant performance to identify any correlations between the geological features and processing response.

10.3.3 Validation

Tropicana material blending: This section presents a focused case study concerning the material mined at TGM and shows the material flow and its blending from mining until processing. This pit region is selected because Figure 9.14 showed that metallurgical test results from this region indicate a relatively large difference in material hardness. Domain TP_3 has relatively harder material than domain TP_4, and it is interesting to observe and evaluate what happens with these two different material types during mining and processing. The study period comprises about two weeks, from 01-03-2019 until 15-03-2019 and involves the building (9 days) and reclaiming (7 days) of the RF03 stockpile, see the cycle highlighted in Figure 10.9.

The case study considers the simultaneous mining of four benches, of which two are near the bottom of the Tropicana pit, and the material hauled to RF03. Building of the ROM finger starts with TP_3 material, followed by material from Havana, Havana South and TP_4. In total the RF03 blend is composed of 37.6% TP_3, 20.92% Havana, 18.25% Havana South and 22.2% TP_4 material. This example highlights the considerable amount of blending at one stockpile and indicates the importance of defining the material composition accurately. Figure 10.12 shows an enlarged view of RF03 with the stockpile composition on 07-03-2019 (same as in Figure 10.7), which is shortly before the building is completed. It can be observed that the ROM finger consists of a blend due to the variability in the various material attributes. For example, the penetration rate indicates a relatively hard material (greenish) with a few dumps of soft (pink/yellowish) material blended. Furthermore, the stockpile has higher Au and S grade material on the left side (deposited as paddy dumps coming from TP_3) than on the right side. Unfortunately, there is not enough wAlOH information available to characterise the entire stockpile because this parameter was not populated in the Resource block model at the source location of this material. The material characterised has a longer wavelength wAlOH, indicating a phengitic composition corresponding to the TP_3 material.

This example shows that there is a low likelihood of finding the unique processing character associated with the softer TP_3 or harder TP_4 in the processing plant due to extensive blending of this material at the stockpile, as well as while being fed to the crusher. This means that when processing actuals are traced back to a Resource block model, one would observe the geological processing response of blended material. As long as the material types being blended are well characterised, then understanding the response characteristics can still be useful. These results suggest that it will be interesting to trace back processing responses where almost a pure material blends (a fingerprint) were fed for a longer period.

Tracked tonnes: The current material tracking model tracked the ten largest stockpiles used in the considered period and, therefore, could track 85% of all the payload that entered the crusher (Table 10.1). The remaining 15% of the material comes from other stockpile fingers (longer-term), overflow stockpiles (surge), or stockpiles used for

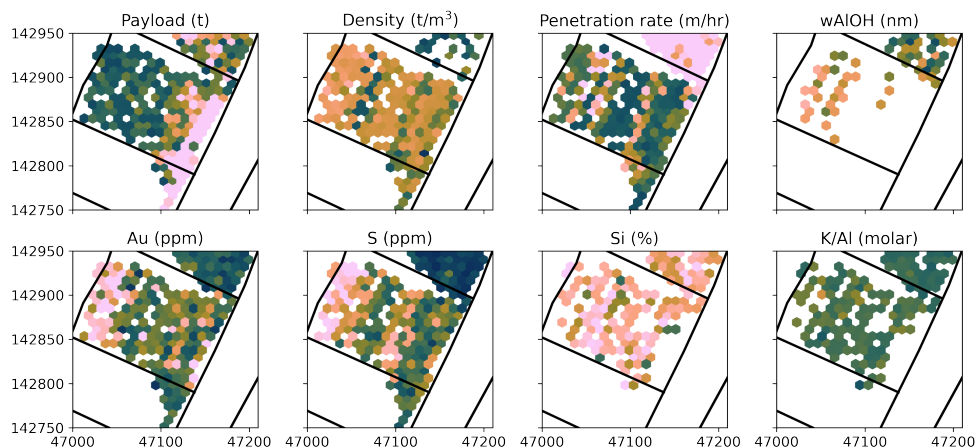


FIGURE 10.12: Detailed information about RF03 of Figure 10.7 (zoom images, similar colour bar scales).

sorting to ensure no ground engaging tools (drill rods, drill bits, etc.) make their way into the primary crusher. To further evaluate the validity of the model, statistical indicators such as the determination of coefficient (R^2) and root mean square error (RMSE) were calculated for tonnes tracked per month.

Figure 10.13 shows a scatterplot of the monthly tracked tonnes versus the actual primary crusher tonnes processed. The relatively high value of R^2 and low tonnes of RMSE show that the simulation model is capable of capturing and segregating the material movements across the stockpiles with a high degree of accuracy. This is as expected and adequately represents the 85% of material tracked. Some months have higher tracked tonnes than the actuals, which seems odd, but this discrepancy may be caused by the different metrics used to calculate the total tonnages. The actual crusher tonnes are measured by the conveyor belt moving crushed rocks to the coarse ore stockpile, whereas the truck tonnes are derived from the pressure sensors mounted on the rear suspension of the trucks. These pressure sensors may not be perfectly calibrated or may give inaccurate readings if the payload is not equally distributed in the truck body. When the tonnes tracked correspond well with the actual tonnes observed in the plant, then there is a high likelihood that the other parameters tracked show a similar degree of representativity and thus can be used to inform the material characteristics of the processed material.

Apart from the numerical validation, it is also important to validate the visual correspondence of the actual ROM pad configuration with the simulated models at specific times. Figure 10.14 shows a side-by-side comparison of the surveyed mine plan and the tracked payload across the ROM pad area at various moments in time. The model hexagons (right side) are coloured by the payload within each hexagon. The colour bar scale is chosen such as to discriminate between an empty and full ROM finger (1,500 t is the maximum payload in a ROM hexagon). The hexagons at SF02 are completely pink because this stockpile is almost 30 m high and has a higher maximum payload.

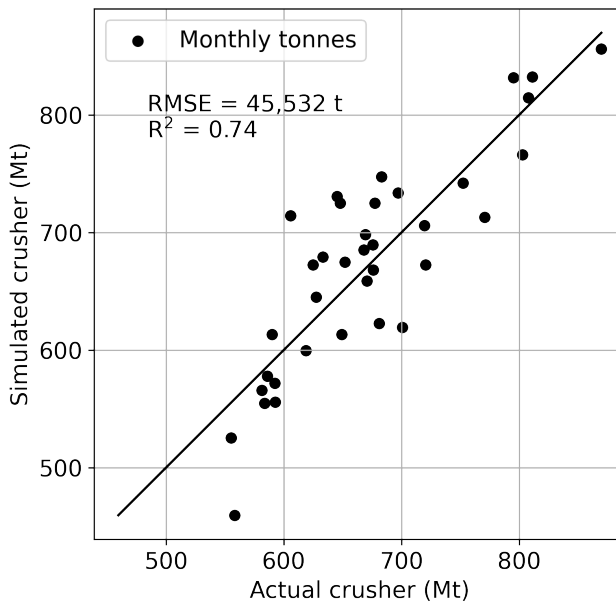


FIGURE 10.13: Monthly values of the simulated (tracked) crusher tonnes versus the actual crusher tonnes reported by the production actuals.

Especially in the early years, there is a high level of agreement between reality and simulation. One design feature from the model is that there are no hard resets of the payload or attributes tracked in the hexagons when a stockpile is supposed to be empty. This causes material to remain available in the modelled stockpile, which slightly affects the accuracy of the model and its correlation to reality (for example, see RF05 at the end of 2017). The plots from the end of 2020 and July 2021 show that the ROM pads are almost empty. The main reason is that at this moment, material from the underground mining operation starts being fed in combination with already stockpiled material from SF02. The plot from July 2021 also shows payloads located at RF02, which was not observed in the surveyed mine plan.

Construction of the SF02 model (and its outline) was constrained by the shape of the stockpile at the end of the year seen by the black lines in Figure 10.14. This helped the model assign the payload to the correct hexagons and guarantee that the actual configuration is simulated as closely as possible. As a result, there is a good spatial resemblance during the construction phase of SF02, which stretches to June 2020, and the 7 Mt of tracked tonnes match up with the actual stockpile outline. The stockpile is then fully reclaimed within a year, and the final stockpile outline and empty hexagons show the empty pad area. It is of great value for the mine that such a large stockpile can be characterised before being used as crusher feed.

In summary, the spatial-temporal modelling and visualisations show realistic geological variability and spatial cohesion and enable the temporal reconciliation of the data. Furthermore, it is observed that there is a minor difference in the tracked payload and visual configuration of the actual and modelled stockpiles. The model captured truck movements with great detail, indicated by the variability observed

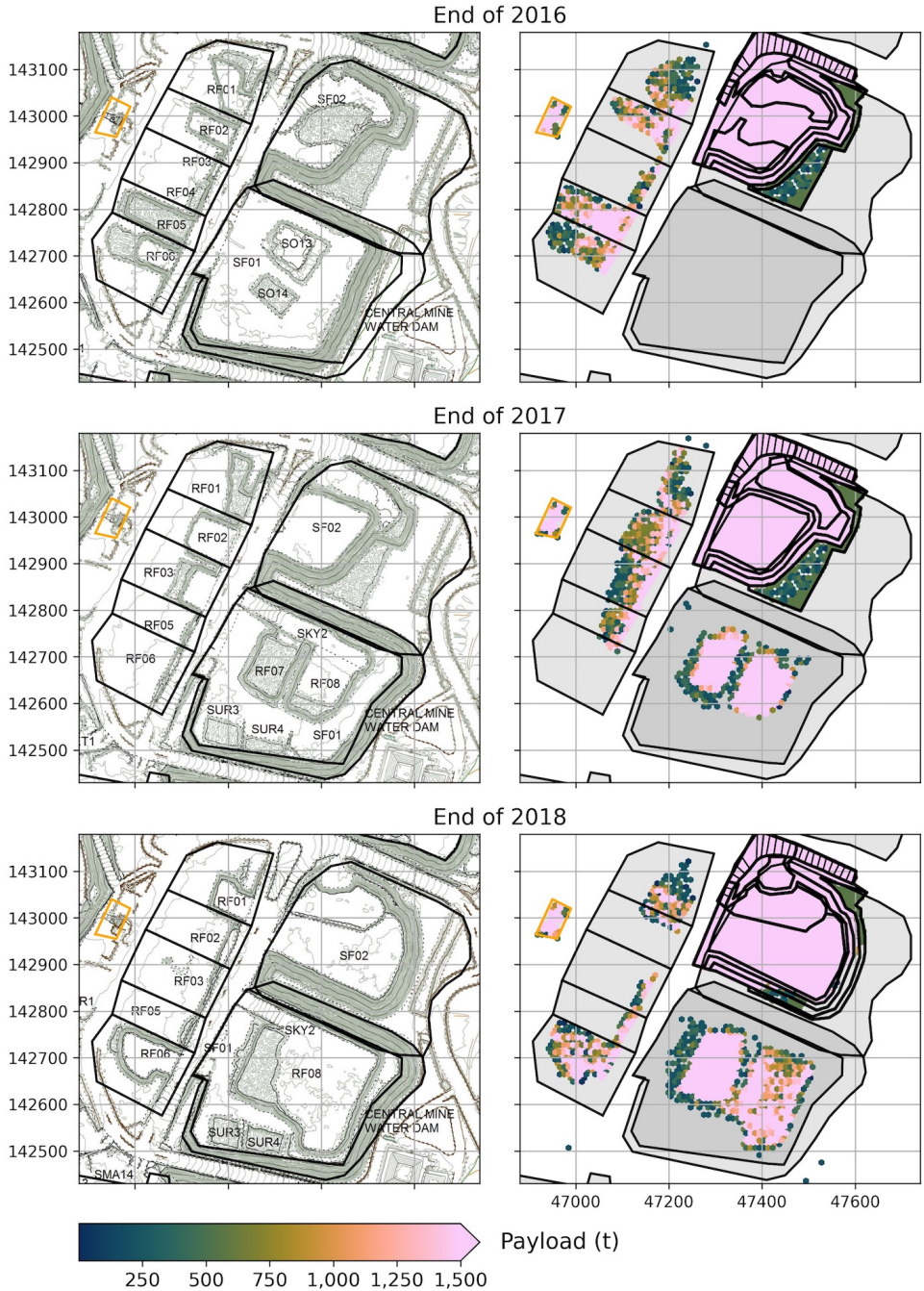


FIGURE 10.14: Comparison of the surveyed mine plan (left) and the material tracking simulation model (right) across time. The right side shows the model hexagons coloured according to the payload at the indicated time.

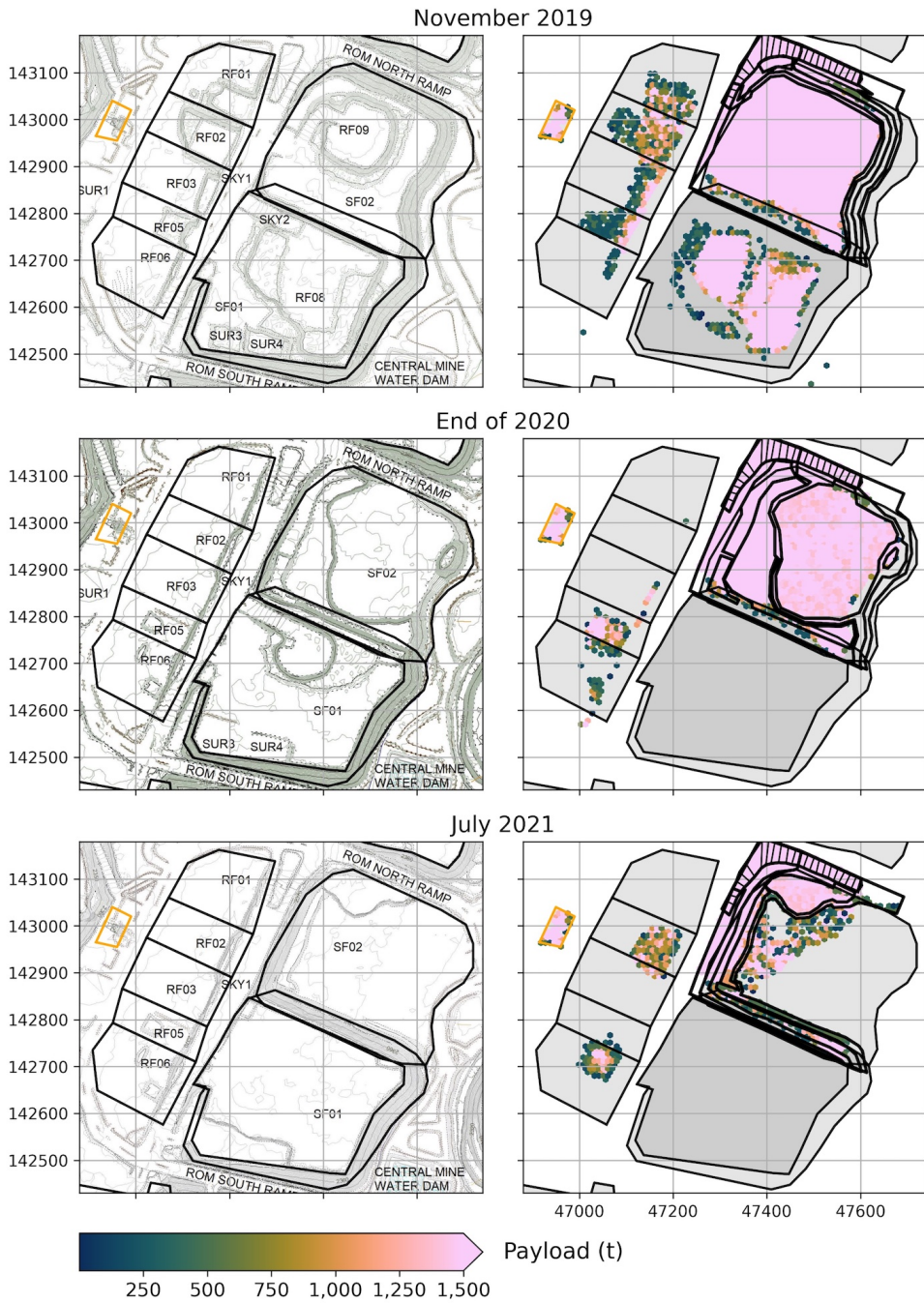


FIGURE 10.14: Continued.

in the material attributes distribution. If desired, the observed material attribute variability can reliably be traced back to the source location. Accordingly, the material tracking simulation model is deemed to be of good quality and would certainly add value in understanding the relationship between geology and processing actuals.

10.4 Discussion

While this study has yielded promising results with good simulation performance, the obtained models have some limitations and can be further refined, which would lead to an even more robust material tracking simulation:

- The model does not account for material displacements caused by blast movements. A post-blast survey should ideally provide a three-dimensional displacement vector of the material, indicating movements caused by the blasting. These vectors can be applied to redistribute the in-situ block model attributes before being assigned to trucks.
- Currently, the truck GPS coordinates define the pick-up location of material attributes in the pit and at the stockpiles. Ideally, these GPS coordinates should be defined by the excavator or loader picking up the material and filling the truck. These coordinates were not available for this study and could therefore not be used.
- From an operational perspective, it is of utmost importance to know what material is handled and therefore, an accurate fleet management system at the mine is necessary. Unfortunately, during data cleaning and preparation, it was frequently observed that truck movements could not be used because either the GPS or destination information was unreliable.
- A future study can look into model enhancement and validation using RFID tags, similar to what was done in Jansen et al. (2009). This would validate the tracking component and more accurately define the material processing and recirculation in the processing plant. It would also be able to give insights on the compaction, compression and settling and at stockpiles over time. Degradation of material quality over time would also need to be investigated.
- The GPS and RFID tags may also cause challenges in underground mining operations due to connectivity issues. RFID tags are not always reclaimed in multi-mining layouts using open stope designs. Furthermore, ore is usually drawn from various ore passes in order to account for variability per domain. If this is not well documented and tracked this may distort the fingerprint signals.
- The ten most used stockpiles were selected and modelled in this study. Modelling the smaller and irregularly used stockpiles and other longer-term stockpiles could fine-tune the model. However, this would require a relatively time-consuming pre-characterisation of the stockpile, and this may not be beneficial in terms of the tonnes (resolution) gained. Future work may focus on modelling SF01 as this longer-term stockpile is currently reclaimed and used as mill feed.

The results already demonstrated that this model could assist the mine planning team prepare the material blends for more accurate processing. Better-optimised decisions can be made on truck destinations because trucks can be allocated based on the truck attributes as well as those from the different stockpiles. However, they can also better optimise the reclaims from stockpiles and ensure that a mill feed blend with specific characteristics is obtained. This tracking is also of interest for the process operators because they can get advanced knowledge of what the material attributes of the feed will be. At a shorter-term planning resolution, this model enables the operators to decide what to change in the comminution or leach circuit to minimise the impact of varying material as shown by any of the tracked attributes. At a longer-term resolution, this material tracking model is of significant value as it can characterise the lower-grade stockpiles (Young and Rogers, 2021) created in the early days of the mine life. Due to insufficient knowledge of the material characteristics from such stockpiles, it is often a guess as to how this material will respond in the plant. These stockpiles are often more heterogeneous and could contain a mix of Oxide, Transitional and Fresh material. Providing insights to the characteristics of such a stockpile could significantly improve the metallurgical processing performance.

There are often one to three stockpiles constructed and reclaimed simultaneously to create a relatively constant mill blend over time, which will further optimise the processing plant performance. Insights from modelled ROM and stockpile fingers may change this perspective as the plant can be run differently and optimised explicitly for different material types. The mine planning team can still feed the plant with a constant blend, but the blend composition will be more frequently changed over time. Instead of running a constant and average quality blend, they may opt for running lower or higher quality end blends. Processing of the lower quality blend may then be accounted for by the benefits gained from processing the higher quality blend. This trade-off may yield better outcomes than processing the average blend in terms of increased Au extracted, reduced reagent consumption, lower energy consumption, etc. Contrastingly, operating the processing plant with a certain quality and consistent performance is already difficult enough; hence the suggested challenge may be unpractical or impossible. However, it may be feasible due to the insights gained from the material tracking simulation.

The simulation model demonstrated here is referred to as a forward simulator as it exhibited its capability to forward track material attributes. However, since the model creates a direct link between the material source location and the moment of processing, it is also possible to use the model as a reverse simulator. This facilitates the tracking of processing responses back in time and spatially seats these geometallurgical performances back into a block model. Studying the spatial-contextual relationship of the local geology and response will enhance any further geometallurgical material characterisation. One application of such an exercise will be shown in Section 11.5.

10.5 Conclusions

In this chapter, a forward simulator model tracks ore material from the pit through stockpiles to the crusher. This model was developed to track material from the

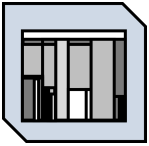
moment of mining to its destination and determines how, when and where this material was blended. The tracked trucks included those going directly from the pit to the crusher, but more than 90% of the truck movements were related to material rehandling (pit → stockpile → crusher). Therefore, these movements had to be spatially and temporally modelled to account for stockpiling and blending effects.

Results of the spatial-temporal modelling show realistic geological variability and spatial cohesion, which enables temporal reconciliation of the data. The produced stockpile maps show that relatively large differences in material compositions may occur and thus indicate that care should be taken in producing a blending strategy. Furthermore, they can be used to understand grade and geometallurgical variability inside the ROM fingers and crusher feed. The physical, geochemical and mineralogical data variability across time is significant and suggests that these differences may result in a change in processing response.

The next step would be to align these crusher feed attributes to the actual plant performance to identify any correlations between the geological features and processing response (see Chapter 11). However, as seen in the focused Tropicana case study, this may be challenging due to the material blending. If the model is deployed in production, it can provide real-time, 3D ore control models of stockpiles which can be used to optimise mine planning and mineral processing decision making and outcomes. This could help to further maximise resource efficiency and gold recovery.

11

Processing performance



This chapter presents the application of a continuous wavelet tessellation and data mosaic method to assess relationships between the crusher input feed and the comminution and leach circuit processing responses. The chapter is a sequel to the previous chapter and uses the tracked material fingerprints as input for further analysis.

11.1 Introduction

Machine performance optimisation in comminution circuits is important for mining companies because crushing and grinding units are among the most energy-demanding machines whose high operation expenses account for up to 4% of global electrical energy consumption (de Bakker, 2013; Bortnowski et al., 2021; Jeswiet and Szekeres, 2016). Besides that, a non-optimal leach process will lower the extraction potential of gold and thus have a direct impact on the mine's revenue. Thus, processing plants require high yields and low operating costs to ensure profitability. Therefore, a key question is how should a blend be processed optimally. In order to answer this, it is important to first understand how geology impacts metallurgical plant performance. Logically, if variable geological behaviour becomes better understood, then machine performance can also be understood, controlled and optimised.

There are many factors that can influence a plant's metallurgical performance. For instance, Both and Dimitrakopoulos (2021) showed evidence that for Tropicana, processing typically harder material corresponds to a lower throughput while feeding softer material allows higher throughputs to be achieved. Other factors that may affect ore processing characteristics include volumes that are silicified, clay rich, sheared, and/or have internal dilution (Hoal and Frenzel, 2022). There are also many possible reasons for poor gold extraction by leaching, for instance, poor gold grain exposure due to insufficient grinding efficiency, variability in gold speciation, complex gangue mineralogy including cyanide and oxygen consumers (arsenic, sulphides) or other deleterious minerals (clay) or coarse gold which requires longer retention times (Coetzee et al., 2011).

Most of these factors are easily detectable pre-mining and early characterisation of material types that possess these, or similar attributes is definitely possible, as shown in Chapter 8 and Chapter 9. After defining these material types, the final step is to link them with the processing actuals by means of material tracking (Chapter 10), as will be done in this chapter, and to assess and interpret any observed relationships.

The main aim of this chapter is to understand which and how specific material attributes affect the metallurgical plant performance in terms of comminution and leach behaviour. This chapter is a sequel to the previous chapter and uses the outputs shown in Figure 10.11 as input for further analysis. Some attributes (fingerprints) may either negatively impact the comminution performance or be deleterious to the reagent consumption or leach performance but alternatively could boost any of these processes. Analysing this will be done by a multiscale and multivariate analysis that transforms time series signals into continuous temporal domains consisting of samples of similar material composition. These domains show material variability at different scales and are used to analyse the corresponding metallurgical plant performance. The results will be analysed in terms of comminution and leach performance. Finally three case studies go into more detail to diagnose the actual root cause of specific performance signatures.

11.2 Methods

11.2.1 Time series data preparation

Time series data related to actual plant performances were only available for three out of the six years of corresponding trucking data described in Chapter 10. These data, observed with a resolution of 12 hours, were further processed using the following two steps: firstly, it was decided to calculate a moving average of the 12-hour intervals data to reduce the noise of shutdowns and plant operating conditions. This helps to identify periodic trends of higher and lower attribute values that are more likely linked to rock properties of the material processed rather than machine variation. Similar to the preparation of the feed attributes described in Section 10.3.2, each attribute is smoothed by a moving average using fourteen consecutive 12-hour observations (seven days) calculated with a minimum of six observations (three days). Secondly, some of the responses were shifted backwards to align the responses of the grinding and leach circuit with the crusher feed input. This is necessary because the material needs time to travel through the equipment, bins/screens or conveyor belts, see, for example, Varannai et al. (2022) and Wambeke et al. (2018); otherwise, the time-averaged responses do not match. For instance, processing responses measured directly after the ball mill and before the leach circuit (head grade, lime, cyanide and oxygen) were shifted by 12 hours (one time frame), and the down-stream leach responses (recovery and P_{80} tails) were moved by 36 hours (three time frames) to account for the stockpiling and tank residence time.

11.2.2 Wavelet tessellation and data mosaics

The need for automated methods to rapidly incorporate and analyse geochemical logging data resulted in the development of a multivariate and multiscale method (e.g., Hill et al., 2020) that upscales the data using a wavelet tessellation. This method is a combination of two techniques. Firstly, the continuous wavelet transform (CWT), which is the process of performing multiscale edge detection (Mallat, 1991, 2009) on a signal to provide spatially continuous domains consisting of samples of similar compositions. Secondly, the tessellation visualisation, which is a mapping of regularised geometries onto the wavelet transform to better visualise the signal. The wavelet transform is based upon the idea that a particular wavelet shape will capture the signal variation by applying a wavelet scaling and shifting approach. The scaling will stretch or shrink the signal in time by the scaling factor, where the stretched wavelets capture slow changes and shrunken wavelets capture abrupt changes in the signal. Then, the shifting translates the differently-scaled wavelets from the beginning to the end of the signal (Cooper and Cowan, 2009; Hill et al., 2021; Torrence and Compo, 1998; Witkin, 1983).

The tessellation implementation of Hill et al. (2020) was designed for down-hole univariate and multivariate data. However, after testing, it was noticed that time series data from the processing performance (or any other) share the same data attributes as the down-hole data and, therefore, could form a suitable input for the powerful tessellation approach. The benefit of using the CWT is that it provides

multiscale results by effectively smoothing the signal to simulate larger time frames as the wavelet scale increases (Hill et al., 2021).

A summary (Figure 11.1) of the method is as follows: the absolute values of the CWT coefficients derived from the input signal are used to measure boundary strengths. This boundary strength is used as a measure of scale in the multiscale domains and the location of the zero contour on the CWT at the smallest scale is used to estimate the depth of the boundary. The strength and depth are combined

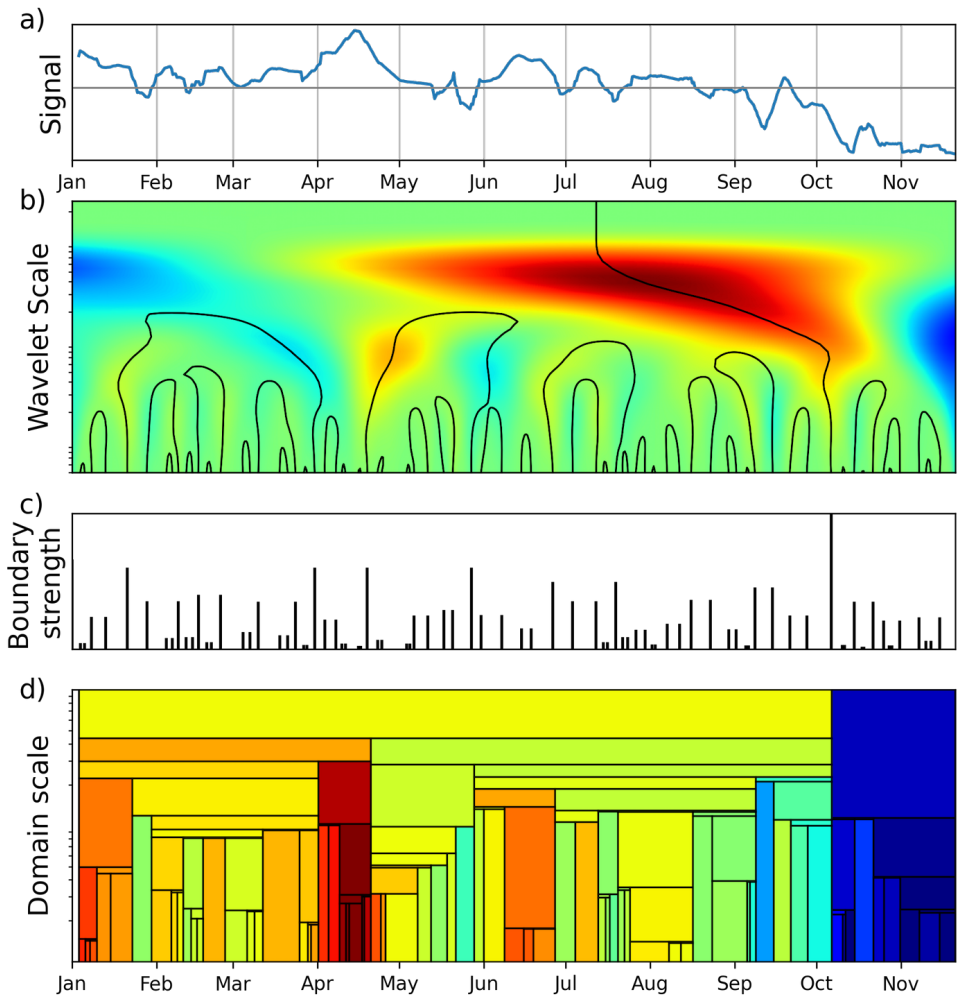


FIGURE 11.1: Workflow for tessellation and data mosaic for a time series signal: a) input signal; b) continuous wavelet transform, colours are first derivative wavelet coefficients (blue, low; red, high), black lines are zero contours of the second derivative; c) time-corrected boundaries from CWT; and d) tessellation the boundary location and strengths. The colours are the mean values of the samples in the domain (blue, low; red, high).

to form domains which can be coloured by the signal median or mean value from the samples within the domain (Hill et al., 2021). An in-depth description of the wavelet tessellation method and its steps to construct a mosaic plot is beyond the scope of this chapter and dissertation. A detailed description can be found in Hill et al. (2015a,b); Hill and Uvarova (2018); Hill et al. (2020, 2021) and is further visually summarised in Appendix A.1. The tessellation approach shown in this chapter was self-programmed following the description in (Hill et al., 2020). Readers may want to refer to <https://research.csiro.au/data-mosaic/> to test the application using the mosaic application provided by CSIRO Australia.

The final analysis of these results includes the generation of the mosaic plots and pseudo-logs (horizontal slices) for comparative purposes and domain clustering using agglomerative hierarchical clustering. This clustering groups domains with similar input signal characteristics and allows for comparison of the metallurgical plant response to corresponding fingerprints. The data visualisation provided by the classified mosaic plots also offers an intuitive display of multiscale analysis and variability that can be evaluated at different scales aligned to various strategic and tactical geometallurgical objectives. Pseudo-logs taken at different domain scales will determine whether the observed variability is deterministic for strategic or tactical decision making and inform on targeted variability/optimisation opportunities. These different scales might even be considered in establishing aspirational targets for either strategic or tactical optimisation initiatives.

11.3 Processing response data

11.3.1 Measurement descriptions

At Tropicana, the target throughput of the ball mills has changed over the years from ~ 930 t/h to $\sim 1,050$ t/h and up to $\sim 1,150$ t/h (currently). One of the key mechanisms to realise a constant throughput is keeping the (mill) bins above the wet screens just before the ball mills (see Figure 11.2) at a certain threshold level. This ensures that sufficient feed is available to run the mills at any time. Achieving this involves an interplay between the amount of material circulating in the crushing circuit and additional stacking at or reclaiming from buffer/emergency stockpiles. The plant operators have a number of options to consider in order to maintain a constant throughput as outlined below:

- **Capacity building (preferred):** The amount of material handled in the primary and secondary crushing circuit exceeds the throughput of the ball mill and allows for buffering a part of the HPGR fines product as buffer material at a stockpile outside the plant. This could exceed 100 t/h and is the ideal situation as it ensures that enough mill feed is available when the crushing circuit has downtime, when harder material is expected or when the mill bins are at a low threshold.
- **Maintaining:** If harder material is processed in the crushing circuit, there is a higher recirculation load, reducing the HPGR product amount. Both secondary crushers have to run in order to maintain throughput which comes at the cost

of increased machine wear. The mill bins can still remain at their threshold at the expense of no or limited additional fines stacking.

- **Critical:** If the recirculation load is too high for too long, it means that no buffer stockpiles can be built, and thus, the mills need to run with lower throughput, or when the throughput remains constant, then the grind (P_{80}) will increase. This happens because less material is screened, giving coarser particles in the mill which, resulting in a lower recovery. A critical situation occurs when the mill bin levels are too low and must be continually replenished from the emergency stockpiles.

This shows that the recirculating load percentage (ratio) in the crushing circuit is a direct proxy for the material hardness, amount of fines (related to P_{80}) and the state of operation of the circuit. The ratio expressed as a percentage is derived from the tonnages conveyed in each 12-hour interval from the secondary screen oversize and undersize fraction, as shown in Equation 11.1:

$$\text{recirculation load (\%)} = \frac{\text{oversize tonnage}}{\text{undersize tonnage} + \text{oversize tonnage}} \quad (11.1)$$

The oversize fraction is returned to the secondary crushers, while the undersize is directed towards the HPGR circuit. The recirculation load percentage decreases for softer materials and increases for harder material. Especially the combination of a high recirculation percentage and low tonnage for buffering indicates hard problematic material. Identifying this type of material gives optimisation opportunities as the mine can better forecast and predict how much stacking occurs while processing specific material or needs to be done prior to running a certain material type or blend. This ensures that the plant can achieve the same throughput and avoid compromising the grind, resulting in higher recoveries.

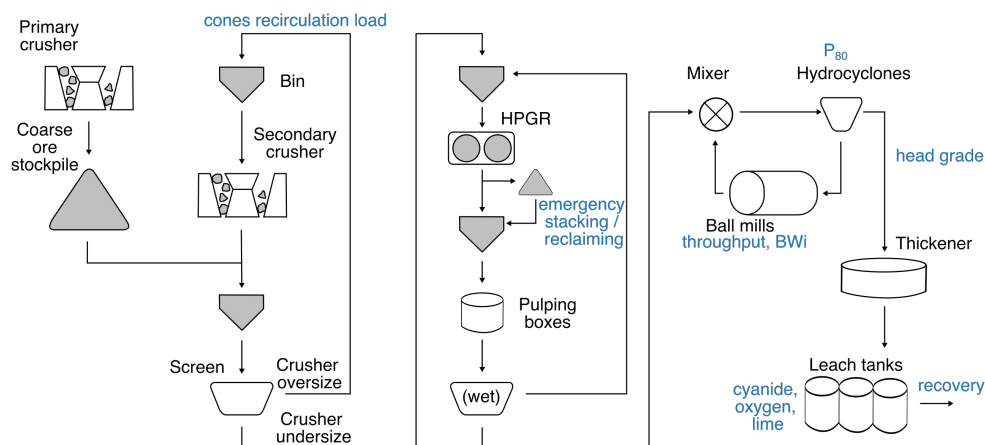


FIGURE 11.2: Schematic overview of the processing circuit, adapted from Wambeke et al. (2018) with the main processing proxies indicated in blue.

After milling, the ball mill product (slurry) is classified through a cluster of cyclones to separate coarse and fine particles. The fine (small) particles discharge from the system as overflow and get further processed through a conventional carbon in leach (CIL) process plant to extract the gold. A cyclone overflow sampler unit measures the shift composite particle size (P_{80}), and after the leach feed thickener, there is a leach feed sampler that takes periodical samples which are sent to the lab for Au grade analysis to determine the final recovery. A common procedure at the mine is to further analyse leach variability on a monthly composite of these samples to increase confidence in recovery results. This composite sample is tested using a diagnostic leach test which is comprised of a series of selective leach steps becoming sequentially more aggressive. Each step indicates the amount of gold extractable by targeting using a different deportment (occurrence) mechanism and are as follows (Coetzee et al., 2011):

- Cyanide leach (CN soluble): targets the free gold, which is free cyanide soluble. This test should resemble the leaching conditions of the plant.
- Strong cyanide leach – cyanide-soluble gold: is the gold that is extractable under a higher NaCN concentration.
- HCl digest (carbonates locked): targets the carbonates and reactive sulphides, including calcite, dolomite, galena, and pyrrhotite.
- SnC_2 + HCl digest: targets the part of the gold-related with iron oxides.
- HNO_3 digest (arsenopyrite locked): determines the part of the gold interlocked within arsenopyrite and other reactive sulphides.
- Aqua regia digestion (pyrite locked): gold-related with the remaining pyritic sulphide minerals and acid-soluble minerals.
- Total fire assay smelt (silicates locked): this should capture all remaining gold that is mechanically interlocked/encapsulated within the remaining silicate (gangue) mineralogy or graphitic carbon gold.

The recovery from the plant should ideally match the first cyanide leach percentage as then most of the potential extractable gold is indeed extracted. The distribution over the other categories indicates where the remaining gold is locked, and changing proportions over time may indicate different material types. For example, a higher percentage in the strong cyanide leach category may indicate the presence of reagent-consuming minerals or slow leaching gold because the particles (nuggets) are bigger or the Au species is more difficult to dissolve. A high proportion of silicate-locked gold means that only a product with a finer grind size, thus higher degree of liberation/exposure to cyanide, would potentially unlock these gold particles. Optimising the grind size in response to this material would improve the gold recovery.

11.3.2 Actual plant performance

Figure 11.3 shows the seven-day moving average for a selection of the plant actuals data; for visualisation purposes, the values have been rescaled with zero mean and a

standard deviation of one. The variables are grouped in three parts; corresponding to 1) the crushing circuit, 2) the grinding circuit, and 3) the leach circuit. There is a considerable amount of variability observed in the processing actuals, including outliers, which mostly correspond to plant shutdowns. The variability indicates periods with higher or lower processing responses corresponding to the strategic changes in plant operating conditions. The throughput of the ball mill is taken as a guideline to separate the data into different periods because it represents the ultimate processing target.

Three distinct periods were identified; period 1 spanned from January 2018 to November 2018 and was characterised by a low ball mill throughput (~ 930 t/h) with low BWi and high P_{80} s. In contrast to the other periods, only one ball mill was operating in the plant at this time. Period 2, spanned from December 2018 to June 2021, a period with a throughput of $\sim 1,050$ t/h, and finally, a period with a throughput of $\sim 1,150$ t/h.



FIGURE 11.3: Time series data visualisation of the seven-day moving averages for selected processing performance indicators.

Further analysis of the plant operating conditions and corresponding actuals (ignoring the impact of material differences) focuses on the ball mill BWi and leach circuit recovery. The combined BWi response (also see Figure 11.4a) of the mills exhibited the following behaviour:

- A common pattern is that the BWi increases shortly before the maintenance or shut down period of the mill and remains slightly higher for some time (~ 12 hours to 1 day) after the start-up. This pattern is a combination of emptying

the ball mill circuit, running the ball mill with a limited payload or increased emergency payload (Figure 11.4a) because earlier units were already shut down or running with a lower capacity. This results in a slightly different feed composition in terms of throughput and P_{80} , thus giving a higher BWi.

- The BWi can also increase if a significant proportion of emergency feed is used (reclaiming in Figure 11.4a), for instance, during days 32–38 when the crushing circuit was briefly shut down. During normal operations, this feed is stored (stacking in Figure 11.4a) after the HPGR for periods when the primary or secondary crusher or HPGR are not in operation and thus cannot provide enough tonnes to the mills. In this case, the emergency stockpiles are reclaimed and directly fed to the bins before the wet sieves and ball mill. When the HPGR is not running, it is impossible to return the wet sieves oversize proportion back to the HPGR and thus ends up in the mills where it increases the fraction of the coarse particles and thus increases the recirculation load, energy consumption, BWi and lowering the effective throughput.

The leach circuit showed the following processing-related correlations (Figure 11.4b):

- The recovery goes up when the head grade increases and the P_{80} decreases. This common relationship exists because the gold-bearing particles are ground finer, thus there is more surface area (gold grain exposure) for the cyanide to react with gold, especially when the head grade is higher.
- Generally, the recovery will be lower if the reagent concentrations are not at the right level. For example, if there is less cyanide or oxygen in the leach tanks. This could result from cyanide consuming minerals or poor pH control as CN (NaCN solution) undergoes hydrolysis and is lost as HCN(g) at low pH. A change in pH could result due to the presence of material with a higher lime demand or oxygen consumption. Oxygen can increase the leach rates and decrease cyanide consumption.

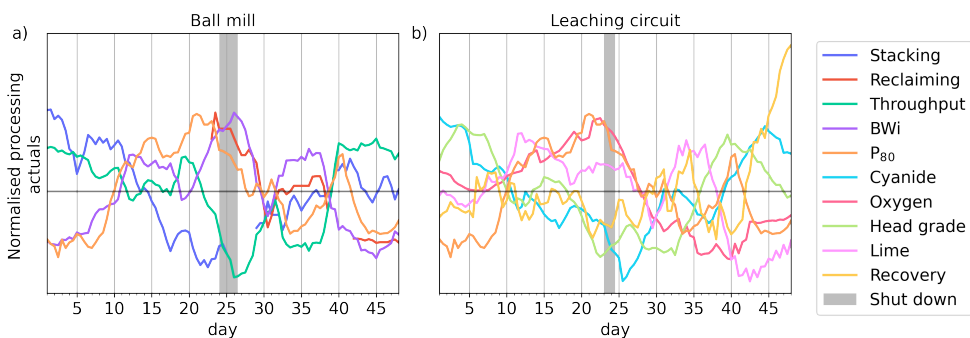


FIGURE 11.4: Zoom in on the ball mill and leach circuit response.

All of the above considerations should be taken into account when the impacts of geology on the metallurgical plant performance is further investigated. It is acknowledged that the significance and frequency of these occurrences will make it difficult to find the root cause for specific operating conditions.

11.4 Results

11.4.1 Mosaic plots from crusher fingerprints

The first results focus on a tessellation of the period 1 crusher feed composition to link geology to metallurgical plant performance. These incoming material types (fingerprints) were initially defined in Chapter 9 and displayed as a function of time for the crusher feed in Figure 10.11. The material type proportions were input (Figure 11.5a) for the multiscale wavelet tessellation method for boundary detection. Material type proportions were interpolated at periods without data, and the resulting domains can be ignored because, in reality, this gap corresponded to a shutdown period. The resultant mosaic plot, produced using wavelet tessellation, is shown in Figure 11.5b, where each domain corresponds to a specific material composition. At high domain scales from ~ 10 to 100, a pseudo-log (a horizontal slice) shows the longer-term variability that may correspond to different mining domains. Whereas at the lower domain scale, pseudo-logs indicate the shorter-term variability that typically corresponds to material variability from different stockpiles or within a mining bench.

Visual comparison between the mosaic plot (Figure 11.5b) and the input signals (Figure 11.5a) indicates how closely the boundary locations are related to the material fingerprints of the tessellation. Boundaries of the periods were controlled by the strength of the signal change corresponding to a change in material composition. For example, the most abrupt changes in the signals gave a stronger boundary and thus extended/persisted to a higher domain scale (>30). Material fingerprints from these periods are thus different from those of the previous period and thus should correspond with an observable change in the processing performance. Some of these strong boundaries also correspond to periods in which no crusher feed was fed to the crusher; see, for instance, the domains in March and May; note that short periods with no crusher feed should not significantly influence the results.

The 472 domains represented by the average material fingerprint proportions within each domain were normalised by removing the mean and scaling to unit variance. These normalised domain values were then clustered using agglomerative hierarchical clustering, resulting in ten classes. Similar to the clustering exercises in Chapter 8 and Chapter 9, this number was determined to be optimal based on the mean silhouette score, Caliński-Harabasz index and Davies-Bouldin index. The resultant mosaic plot in Figure 11.5c shows the domains coloured by the clustering class and indicates three larger periods at a domain scale of ~ 30 with variable material compositions.

Analysis of the hierarchical clustering structure showed that the ten classes originated from five distinct larger branches with the following attributes: 1) Tessellation Classes (TC) 2, 6 and 9 have elevated MT2 and MT4 – MT8 and themselves differ mostly in MT6, MT7 and MT8 (see Figure 11.5a); 2) TC3 has the largest proportion of unknown material and corresponds to missing data (shutdown of the crusher, no feed) which was interpolated during data pre-processing; 3) TC1 and TC10 are not particularly distinct in any class, but rather show average material type proportions; they differ themselves mostly in MT5; 4) TC4 and TC8 have a relatively low MT2 and MT5 with higher unknown material proportion, and their main difference is in

MT0; finally 5) TC5 and TC7 are distinct predominantly due to their high proportion of MT0, MT1 and MT3 and they distinguish from each other in MT3. These class differences related to different material types and will be further linked to processing actuals in the next sections.

Further analysis showed that the change from TC1 (grey) to TC5 (pink) in mid-May resulted from a change in rock composition with an abrupt change where MT0 increased by 8.6% and MT8 and the unknown material decreased by 4%. By comparison, the boundary at the start of April (TC5 and TC10) had a much weaker strength as the change in material composition was only in three of the ten material variables; i.e., MT0, MT3 and MT8, but only by -5%, +2% and +2%, respectively. TC3 showed the strongest boundaries and corresponded to the missing data (shutdown of the crusher, no feed), which was interpolated during data pre-processing.

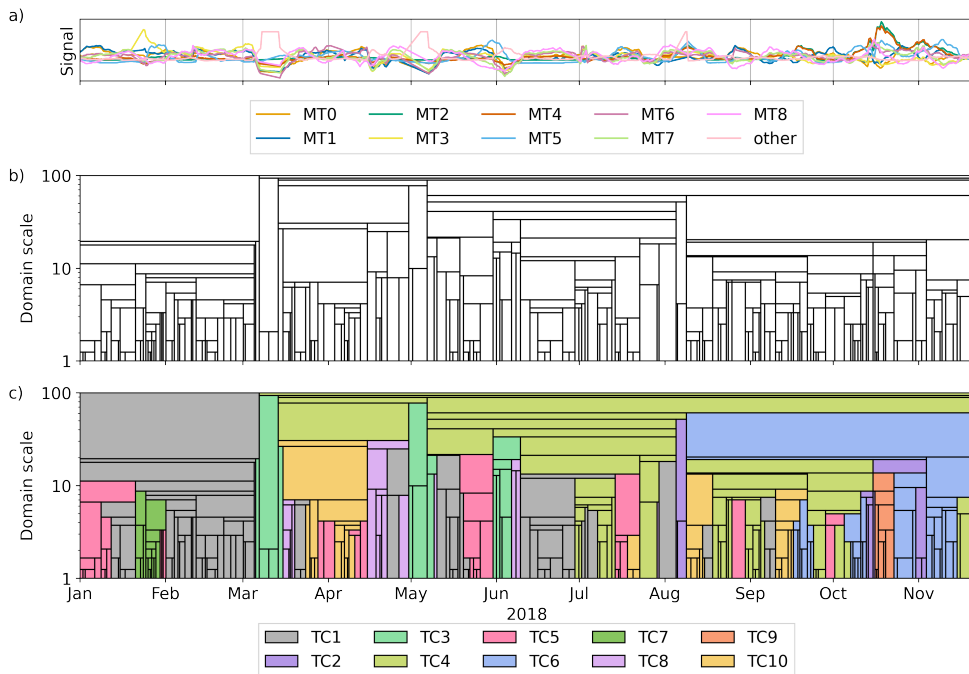


FIGURE 11.5: Tessellation results from the material fingerprint crusher feed proportion for period 1; a) input signals from the material type proportions; b) multiscale mosaic plot; c) classified mosaic plot by tessellation clustering class (TC).

11.4.1.1 Comminution actuals

The subsequent analysis step was to link the classes and domains to the corresponding average processing performance, as this would make a direct link to the processed material fingerprints. For this, the period from each domain is linked to the corresponding seven-day rolling mean signals of the processing actuals (Figure 11.3). Table 11.1 shows the summary statistics per clustering class for selected comminution-related production actuals. The classes show distinct comminution performances

and thus confirm further relationships with the incoming material fingerprint. In addition, the statistics indicate similar comminution production actual values for those classes that are most alike.

For instance, TC5 and TC7 are the two classes with the lowest BWi and P_{80} and highest penetration rate, which is indicative of soft material and thus requires less energy to grind. TC7 only occurs in one period in late January (Figure 11.5), whereas TC5 is a fingerprint that occurred more frequently (although irregularly). In contrast, TCs 2, 6 and 9 have the highest BWi and P_{80} but show differences in terms of their respective ball mill throughputs. TC2 and TC9 did not occur often and suggests a unique situation where the crusher payload is also blended with the emergency feed (higher reclaiming tonnes). Such a signature usually corresponds to a partial or total shutdown of the crushing and/or grinding circuits (thus lower throughput), as discussed in Section 11.3.1. TC6 likely represents a hard blend (also indicated by the corresponding low penetration rate), resulting in a high BWi and thus increasing the P_{80} (throughput maintained). Furthermore, TC1 and TC10, and TC4 and TC8 exhibit the typical operating conditions (throughput ~ 930 t/h, BWi: 16.2 kWh/t and a P_{80} of 84 μm . TC1 and TC8 show a slightly higher crusher recirculation ratio.

TABLE 11.1: Average comminution production actuals for each mosaic classification class.

	n domains	Specific gravity	Penetration rate (m/hr)	Crushing recircula- tion ratio	Stacking (t)	Reclaiming (t)	Ball mill through- put (t/h)	Ball mill bwi (kwh/t)	P80 (μm)
TC1	133	2.75	37.1	0.43	913	2,831	929	16.1	83.6
TC2	15	2.74	34.1	0.42	667	3,702	890	17.2	90.5
TC3	18	2.75	37.6	0.42	922	4,603	928	16.0	82.0
TC4	85	2.76	35.1	0.41	944	4,809	939	16.1	85.7
TC5	66	2.74	38.5	0.41	1,125	2,610	935	15.6	80.3
TC6	51	2.75	34.3	0.42	804	1,880	944	16.1	89.5
TC7	19	2.73	48.4	0.44	670	2,517	935	15.8	81.5
TC8	25	2.75	36.2	0.43	951	2,514	936	16.0	84.2
TC9	10	2.73	35.9	0.40	876	6,970	840	17.5	87.8
TC10	50	2.75	35.2	0.41	1,029	3,471	917	16.4	85.2

The cross-class comminution variability (Table 11.1) was combined with the temporal variability from the material types by colouring the mosaic plot, produced using wavelet tessellation by the average processing response in each domain, see Figure 11.6. This shows, for example, that the variation in feed composition (TCs 1, 5 and 7, Figure 11.5c) in January, February and March resulted in a change in the ball mill throughput and amount of energy required to grind the rocks, with minor variation in the P_{80} . The softer rocks from TC7 (also higher penetration rate) resulted in higher throughput, whereas the blend from TC1 typically resulted in a slightly lower throughput due to harder material. The change in P_{80} towards the end of 2018 related to TC6, which indicates more MT4 and MT5, which thus result in a higher P_{80} .

The material source location in early January was from TP_4, TP_3 and TP_1, whereas later in January, there was also HA_3 material blended. A similar situation occurred in July, where the blend changed from TC4 to TC5 (TC10) and again back to TC4, caused by a change in material blend. During the period from TC5, a portion of the HA_3 material changed by softer material from TP_4, which was thus

observable in the material feed composition (Figure 11.5a). During late August and early September, there was an almost pure blend coming from TP_4, represented by TC5 and TC4, followed by a period with a pure blend from TP_3 (TC1 and TC10). In Chapter 9 it was identified that TP_3 relates to a more phengitic plagioclase-rich domain, which is supposed to be harder compared to the softer TP_4 domain which is more phengitic-epidote K-feldspar rich. A comparison of the material blend composition and the results in Figure 11.6 validate these hardness-related observations made earlier (in Chapter 9).

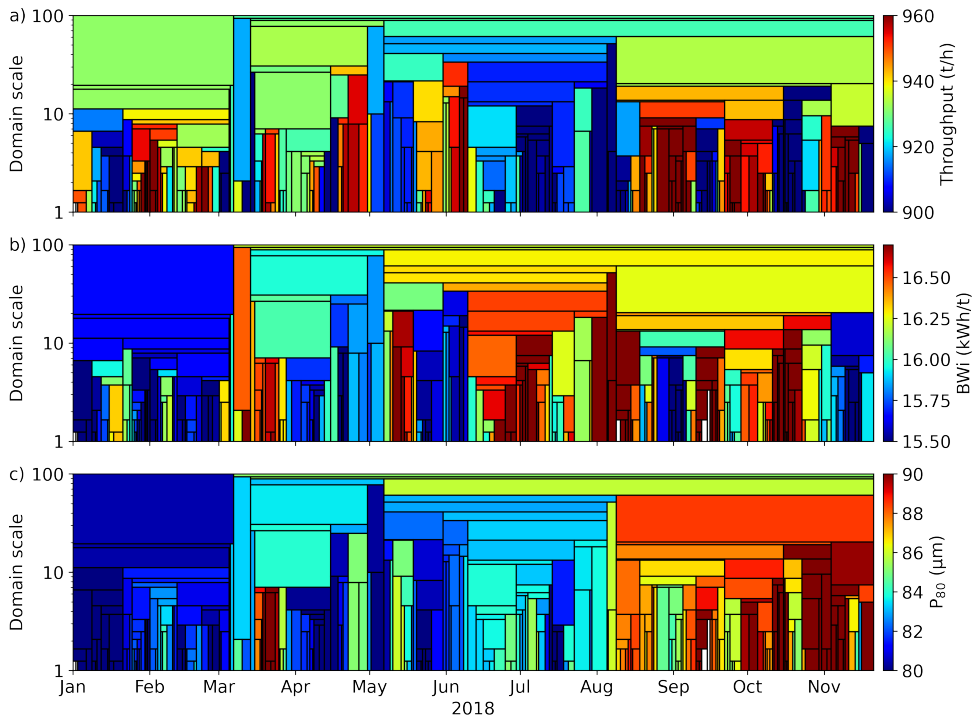


FIGURE 11.6: Data mosaic from period 1 coloured by comminution actuals: a) ball mill throughput (t/h); b) ball mill BWi (kWh/t), and c) P_{80} μm .

11.4.1.2 Leaching actuals

A similar analysis was carried out for the recovery-related proxies and leaching consumables using the tessellation and visualised in Figure 11.7 and Figure 11.8. Visual comparison of the head grade (measured after the thickener) and leach recovery in Figure 11.7 shows that the gold grade increased slightly over time from <2 ppm to >2.2 ppm, whereas the recovery remained constant at 88.5%. A pseudo-log at a scale of 40 shows that the large mid-March to May domain has a relatively lower gold grade but higher recovery than the May to August domain, with a slightly higher gold grade but lower recovery. On this scale (40), both domains were classified as TC4 (Figure 11.5c). However, at a lower scale (shorter period), these domains were

characterised by TC10 and TC8, and predominantly TCs 1, 5 and 4, respectively. This indicates that at a monthly or yearly resolution, the plant will likely achieve its gold recovery target of $\sim 88.5\%$. However, there were distinct periods (and related to different material types) which had worse and better recovery performances. The gold grade and associated recovery of material are thus truly a function of the different material compositions processed and can be identified using the material types.

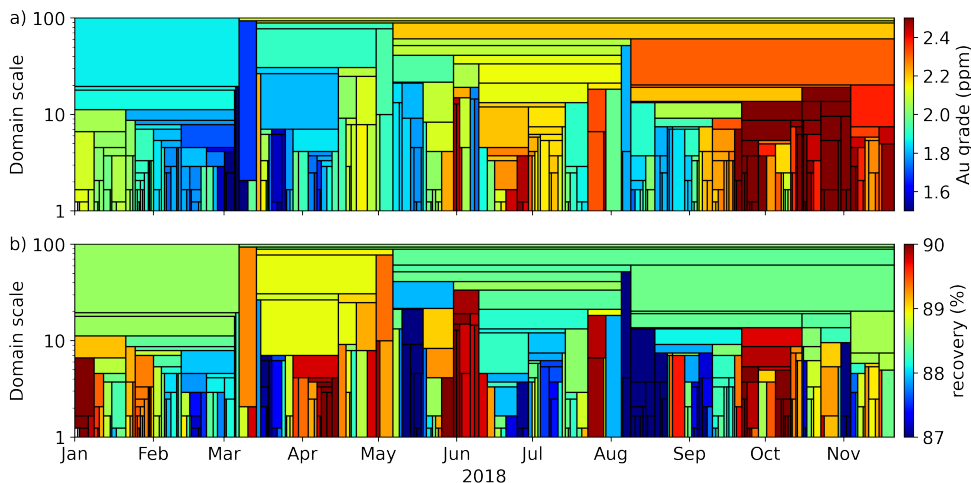


FIGURE 11.7: Data mosaic from period 1 coloured by recovery-related actuals: a) head grade (ppm); and b) recovery (%).

Figure 11.8 shows the data mosaic coloured by the lime, cyanide and oxygen consumption in the leach circuit. Comparing the domain classes again shows that the identified classes exhibit a fairly distinct reagent consumption. For instance, the large TC10 domain at a scale of 20 in April indicates high lime, cyanide and oxygen requirements. This could potentially be related to material with an elevated base metal concentration, such as Cu, Zn, Fe rich material related to the increased proportion of MT6.

Towards the end of the year, the lime consumption remained relatively constant, however, the cyanide and oxygen requirements decreased. The drop in oxygen consumption may indicate a decrease in oxygen-consuming ore types corresponding to the decreasing proportion of Tropicana and increasing proportion of Havana South material. The constant consumption of lime may indicate that there was not a major change in the proportion of sulphide minerals which needed to be depressed and neutralised with lime. Section 11.4.2.2 will further analyse a case study for causes of low and high recovery.

11.4.1.3 Summary

The combination of the time series material blend tessellation and processing actuals allowed for linking geology with metallurgical plant performance because 1) the mosaic domains were constrained by the temporal geological variability expressed in the proportion of material types and subsequently grouped in classes by the clustering;

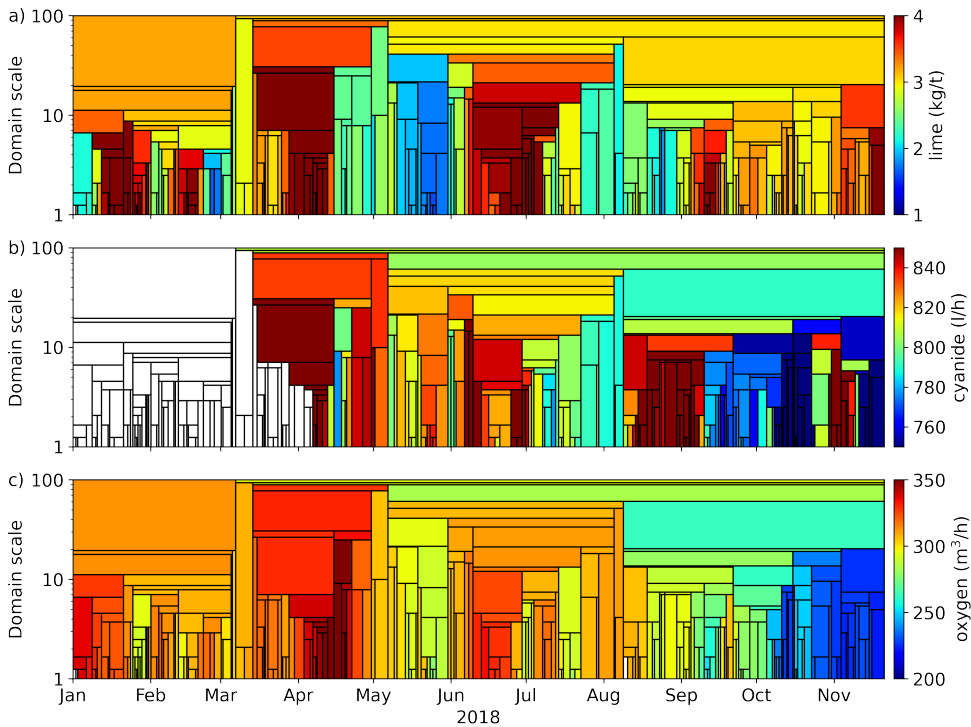


FIGURE 11.8: Data mosaic from period 1 coloured by consumable actuals: a) lime (kg/t); b) cyanide (l/h); and c) oxygen (m³/h). White domains had no processing data available.

and 2) superimposing the processing performance to the domains and considering the temporal changes further exposed the root cause of the metallurgical performance caused by temporal geological variability. This opens the door to identifying these drivers more proactively and thus can inform and prioritise future modelling initiatives, resulting in fit for purpose models with a higher likelihood of being relevant and being accepted or implemented.

As described in Chapter 10, there occurs a high degree of blending which was expected to obscure the plant responses. However, despite the high degree of blending it is remarkable that the tessellation can still observe the variability in material blends at multiple scales. Some classes defined a high or low processing actual value, whereas others defined those related to periods of equipment shutdown. Similar results were observed for a tessellation of the material type proportions in period 2 (predominantly Havana and Havana South material) and period 3 (increasing proportion of long-term stockpiled material). The following sections will show some of these results related to specific case studies.

11.4.2 Case Studies

Each of the following three sections briefly discuss a case study in which a particular geological blend is linked to the corresponding processing response or vice versa, where a particular processing response is linked back to the geological characteristics of the input feed. The variability observed is at a tactical resolution, and the ability to observe and act upon these changes would optimise the processing performance.

11.4.2.1 Case Study – Crushing circuit recirculation

Figure 11.9 displays a zoomed in view of the tessellation and data mosaic results from period 2 as defined in Section 11.3.2. The classes shown are from a new clustering of the material type proportion time series data and are thus different to those from Section 11.4.1. Figure 11.9a exhibits a change in material composition indicated by the change from predominantly TC9 to TC1 at the end of December 2019. This change also corresponds to a decrease in crushing recirculation. As a result, a higher recirculation ratio (>43%) was achieved between July and mid-December (called period 2a), followed by a period (called 2b) with <40% recirculation.

The geological root cause separating these subperiods was further investigated. It was found that the material composition from period 2a originated predominantly

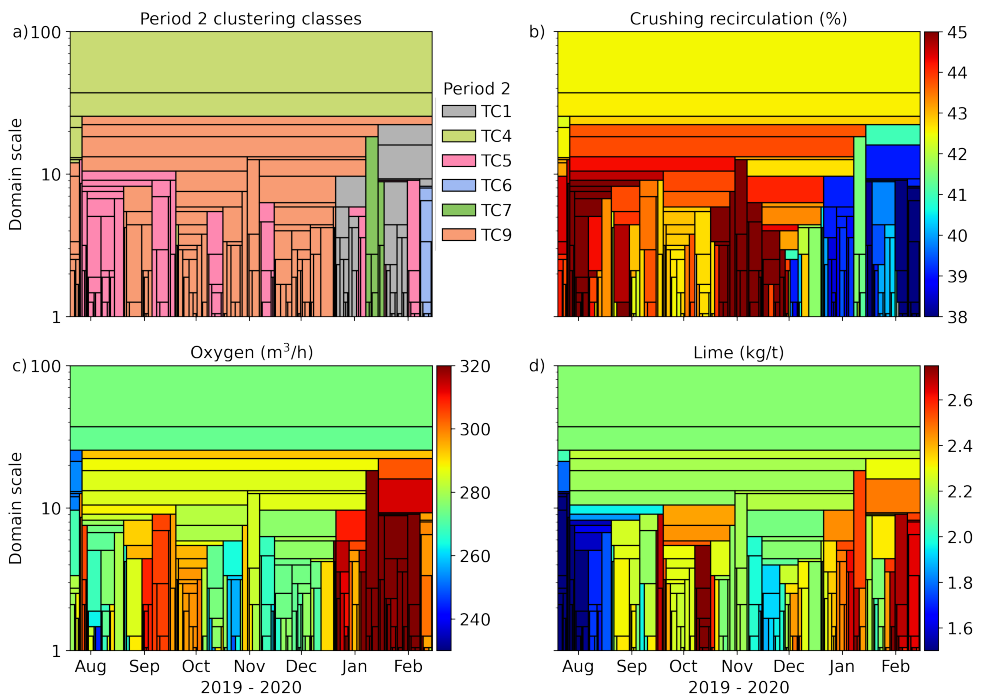


FIGURE 11.9: Data mosaic results from period 2 (zoomed) coloured by a) clustering classes; b) crushing recirculation load; c) oxygen consumption; and d) lime consumption. Note: classes from a) are different than those defined in Figure 11.5.

from Havana and Havana South, whereas in period 2b, a large proportion of Havana material was displaced by Boston Shaker payload. This was the first time since July 2018 that Boston Shaker material was mined and processed as it came from a new Boston Shaker domain. The main geological difference compared to Havana is that this is a predominantly muscovite-bearing Transitional material layer with less phengite and montmorillonite. This results in a more clay-rich, lower density, and softer material blend that is generally easier to process and thus results in a lower recirculation ratio in period 2b (Figure 11.9b). A direct side-effect was the opportunity for a simultaneous increment of emergence feed stacking (Section 11.3.1) and increased ball mill throughput.

Furthermore, in period 2b also saw an increase in oxygen and lime demand (Figure 11.9c/d), confirming that the clay is usually deleterious to the leaching, as it acts as a physico-chemical adsorption buffer against lime-induced pH increase and defines the high lime use (du Plessis et al., 2021) to avoid the hydrolysis and corresponding volatilisation of CN as HCN(gas). The increase in oxygen was probably required to increase the surface area of the clay particles since they tend to be “stickier”. The use of additional oxygen also increases the contact of cyanide with gold particles and enhances the leaching efficiency.

11.4.2.2 Case Study – Recovery

This case study shows the analysis of several benches mined in Havana South and Havana, where the mineralogical and geochemical differences, with respect to recovery, are further explored. These results are part of a similar material type tessellation and clustering as was presented in Section 11.4.2.1, and spans period 2. This period occurred between May and August 2019 and was further subdivided into four sub-periods based upon the material types and corresponding recovery, see Figure 11.10. A pseudo-log at a domain scale of ten shows that during the first period, and mid-May, there was a high recovery (90.4%), followed by an average recovery of 90% up to end-June. The early-July period exhibits the highest recovery (90.7%), followed by a low-recovery period with 88.7% that spans till August. Apart from the recovery, these domains are also distinct in terms of their cyanide and oxygen consumption and, to a lesser extent, with regards to lime consumption.

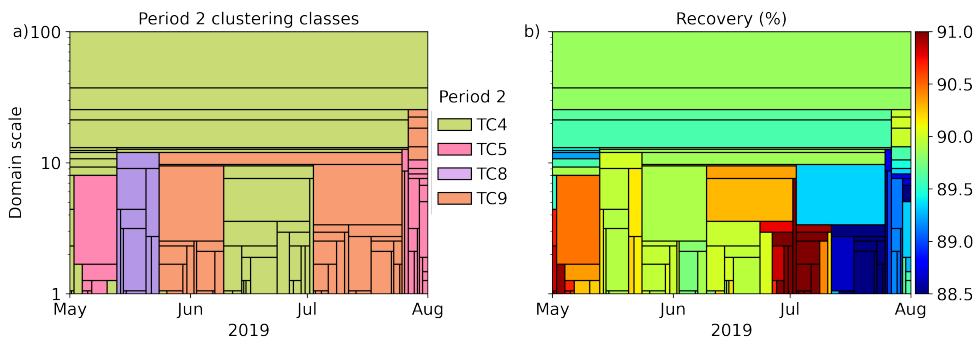


FIGURE 11.10: Data mosaic results from period 2 (zoomed) coloured by a) clustering classes; and b) recovery (%).

The material classes (Figure 11.10a) were not distinct enough to form a direct relationship to the recovery behaviour, and, therefore, further analysis of the material origin and within-class variability was conducted. The main variability in primary mineralogy occurs as zones that zone from hanging wall to footwall and depth down-dip (Roache, 2016). Mineralogical analysis was conducted as part of the material type analysis described in Chapter 9 and un-published reports. The following observations were made:

- Early-May period: this material comprised a distinct larger MT2 and MT5 proportion (the late July had mostly MT2), indicating a larger proportion of weathered material. This proportion is characterised as a more phengite \pm chlorite \pm montmorillonite domain. These partly weathered lower saprolite layers generally contain fewer sulphides than the Fresh rock and thus coincide with higher recoveries. The average sulphur concentration in this period was 1.72% compared to 2.1 – 2.5% in the others.
- Mid-May to end-June period: The bulk of the material mined during this period was characterised as Fresh. Initially, the TC2 material represented a pure blend of the Havana FW, which is phengite \pm chlorite dominant, over muscovite in the mined region. During the latter part of this period, there was more TC9 and TC4 material, comprised of a blend of the Havana HW and FW as well as Havana South; refer to Figure 9.10. This introduced more phengite with biotite + quartz (from the HW) into the blend. This complex blend, containing two material types (phengite + biotite and muscovite + chlorite) thus resulted in an achieved recovery of \sim 90%. Interestingly, this blend does not require as much cyanide as the other domains, possible due to localised, increasing concentration of calcite veins in the mineralised rock (Kirkland et al., 2015), possibly also with less sulphides. This calcite may be a natural pH buffer which depresses cyanide destruction.
- Early-July period: this represents a period in which the Havana FW proportion decreased, while the Havana South FW contribution increased, resulting in a slightly softer blend (Figure 8.14) with more K-feldspar and Al-rich muscovite \pm chlorite \pm epidote. This appears to be an easier-to-handle blend giving a high recovery.
- End-July: The TC9 part of this period was predominantly Havana HW material that was more MT6 rich, exhibiting the phengite, biotite and quartz composition. Towards the end of July, there was again a blend of predominantly Havana HW and FW was processed, however, from a different region than what was processed during the second subperiod. In general, this was a slightly lower Au grade, harder and denser (higher specific gravity) material. The larger proportion of biotite (+magnetite) correlates with higher sulphide concentrations (high S: 2.5%) and inclusion free pyrite, typically with distinct euhedral character (Roache, 2019), which thus ultimately lowers the recovery. This texture occurs in the early stages of the (S3) alteration assemblage typically within weakly to moderately deformed structural domains of the feldspathic gneiss (Hardwick, 2021).

11.4.2.3 Case Study – Long-term stockpile

This case study examines the situation that gave rise to highly favourable processing conditions experienced when processing low-grade, very fine material during period 3. Figure 11.11 shows an oblique three-dimensional representation of the ROM pad area (similar to Figure 10.6). Each dot represents a truck reclaim locations indicating the material fed to the crusher between 17 February 2021 and 3 April 2021. The reclaim locations indicated that the plant feed was a combination of the ROM fingers, SF01 and SF02 material with limited direct crusher dumps. However, the main focus is on the SF02 material, which comprised 81% of the total payload fed to the crusher in this period and is thus expected to determine the processing characteristics predominantly.

The main comminution characteristics observed in this case study's period were a low recirculation ratio (41.7%), good stacking rates (>100 t/h), high throughput (1,055 t/h), low BWi (16.2 kWh/t), and an incredibly low P_{80} of 67 μm . In terms of recovery proxies, the material feed has a very low Au concentration (1.27 ppm), but, surprisingly, a superb recovery of 91.3% with very low consumable rates; oxygen (200 m³/h), lime (1.9 kg/t) and cyanide (676 l/h). The material feed is thus low grade and very soft, but the gold particles are easily liberated and recovered. Usually, these favourable conditions do not all coincide since softer material normally contains a higher amount of clay. Thus there is something particular about the material stored at SF02 that drives these results. Section 10.3.3 already addressed the construction of SF02 and showed that the stockpile was created over a period of more than three years, with material from various locations. This would make any relationship between material composition or mineralogy and these processing actuals implausible since it is expected to be comprised of a wide range of material of varying qualities. The most plausible explanation for the observed response is that due to having to bear

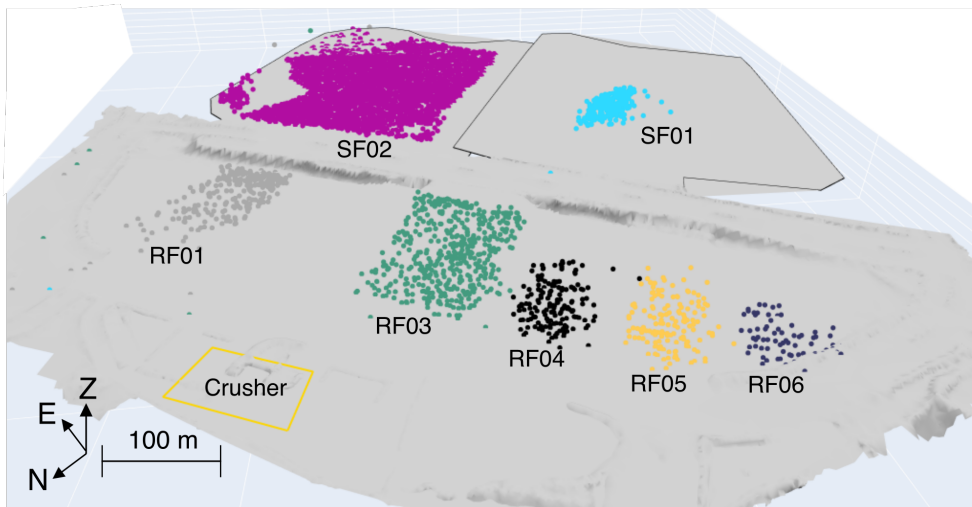


FIGURE 11.11: Oblique view of the ROM pad area showing the truck reclaim locations indicating the material fed to the crusher between 17 February 2021 and 3 April 2021.

the weight (pressure) of the overlaying rocks stacked on top of this bottom layer, the lower SF02 rocks were crushed and as a result, became finer in size over time. Originally, there were 25 to 30 m of rocks stockpiled on top of this layer, and the prolonged exposure to this weight probably caused fractures to appear in the rocks, effectively pre-conditioning the material and thus resulting in favourable processing conditions.

This study implies that favourable processing conditions may be expected when other bottom layers of long-term stockpiles are processed. In future, the mine should aim to blend such material with rocks exhibiting unfavourable processing characteristics (e.g., hard, high sulphur, low Au grade, deleterious minerals) as the crushed rocks would be expected to partly compensate for these characteristics. The next opportunity of this nature occurs after reclamation of SF01.

11.5 Discussion

Case Studies I and II demonstrated that the reagent consumption and leach performance depend on each other. In some cases, the offset in reagent demands caused by the material composition implies that the target pH may not be consistently achieved or that enough free cyanide may not be available in the leach tanks. For instance, it was concluded in Case Study I that clay content was a major contributor to higher reagent consumption. However, in Case Study II, there was a higher recovery due to the weathered material (more clay) and fewer sulphides. Here the lower sulphide content is likely to be the dominant effect and thus suggest that the clay/sulphide ratio may in fact be the determining factor. Recovery is likely to be most negatively impacted by a combination of high sulphide- and high clay content, as in the case with a Transitional/Fresh blends whereas higher clay content in the absence of sulphides (i.e., normal Oxide feed) seems to have less impact.

Continuous wavelet tessellation was demonstrated to be an effective method for domain temporal crusher feed material compositions (as time series data) at different scales and showed the same potential here as when the method was applied to litho-geochemical classification by Hill et al. (2020). Geologists frequently face difficulty in determining the appropriate resolution at which to model geological variability for the resulting model to provide meaningful information to the processing team. The described tessellation approach may thus help identify the appropriate resolution at which geological variability should be modelled for strategic use cases such as mine planning and processing plant design. This resolution can then be refined as GC data becomes available, allowing for enhanced and optimised tactical decision-making. In an aspirational sense, this boundary between strategic and tactical resolution and the responsiveness to each can progressively be moved to a finer resolution to drive optimised processing performances.

Identifying the geological root causes that affect the metallurgical plant performance is not as straightforward as initially believed. Five main impediments, related to complex material blends, were found to complicate this exercise and make it more challenging. 1) The geological variability within one truckload may be limited, however, due to the severe blending of multiple truckloads on a single stockpile, variability increases. 2) There are typically multiple active mining faces at different

benches or pits (currently also underground) causing the final crusher blend to be a mix of distinct geometallurgical domains. 3) The weighted averaging of fingerprints impedes a more granular distinction of analysis of the true geochemical and mineralogical variability previously assigned to geometallurgical domains. 4) Shut-downs of machines earlier in the process affect the downstream machine performance because the material is not subjected to the same processing efficiency as it would otherwise have been. Therefore, the observed processing response only partly reflects the response related to its unique geological signature. 5) Emergency stockpile feed might be blended or processed to reach the mill target throughput in case of crushing circuit related shutdowns. This material could be completely different to the original processed blend. In summary, finding the root cause is thus a truly complex geometallurgical task as it requires a thorough understanding of the geology, material tracking, processing and their complex interactions.

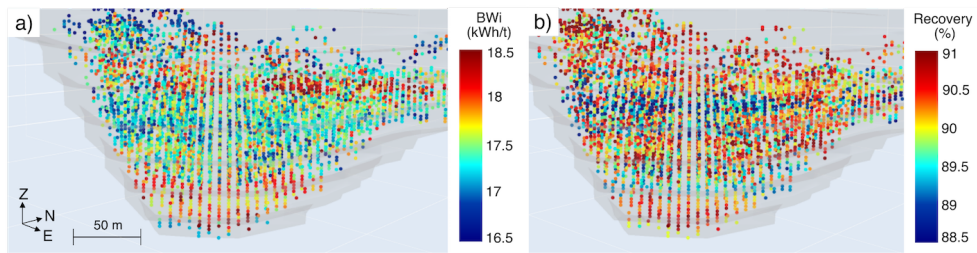


FIGURE 11.12: Backtracked actual processing responses into the geometallurgical Resource model from Havana.

The causes mentioned above also partially hinder the desire to back-track actual process performances to a geometallurgical pit model and perform real-time reconciliation. In specific, constrained scenarios, this would indeed work as was tested by Wambeke et al. (2018), however, the findings of this study highlighted a range of significant complications. For instance, Figure 11.12 shows the back-tracked processing response from the ball mill (BW_i) and leach recovery for the Havana geometallurgical Resource model. This shows that the spatial patterns of processing results returned in a block model are a temporal-related combination of 1) the down-dip bench mining pattern, 2) the blending of the bench material with material from different locations as this was stockpiled and/or fed, 3) how the plant was operating at a given time, and 4) the actual response that can be attributed to inherent material characteristics. Unfortunately, this conflicts with the assumption (and perhaps reality) that the entire region should give a somewhat similar response, apart from some fluctuations due to local geological variability. The time delay between mining, at different benches, will thus always be observable in the corresponding discrete processing responses.

11.6 Conclusions

This chapter presented results from an investigation of the root cause of process performance variations. This complex geometallurgical task was achieved using an integration of geology, expressed as material fingerprints, material tracking and the

actual processing responses. For this, the time series data of material fingerprint compositions acted as a proxy for the constitutive material properties perceived in the processing plant. Analysing this elucidated the expected mineralogy and geochemistry and revealed the root causes for the observed plant performance.

The analysis was done using a multivariate and multiscale wavelet tessellation method (called data mosaic). The multiscale domains represented the material type variability and were subsequently used as input for clustering to identify domains (either large or small) in which a similar material composition was processed. The classified multiscale mosaic plot provided a visual tool to domain periods with similar fingerprint compositions and allowed for linking geology with metallurgical plant performance.

A pseudo-log at a high domain scale characterised long-term geological variability (or consistency) and identified the processing conditions that need to be accounted for at strategic decision levels. The geological variability observed at strategic levels matched with the distinct modes of processing, whereas at a tactical resolution (pseudo-log at low domain scale), this related to the smaller scale variability in the processed blend compositions resulting in either suboptimal or optimised processing conditions. Some domains defined a high or low processing actual value, whereas others defined those periods related equipment shutdown.

No single root cause for processing variability was identified, but rather a fluctuation across the mine life and also dependent on the material feed blend. For instance, blends with higher proportions of weathered or Transitional material were truly easier to process in terms of throughput and lower energy consumption, lower sulphur-bearing blends indeed had better recovery values, and blends with more clays required more reagents to reach target processing conditions. These results from the three Case Studies presented matched the expectations and made geological sense, thus bolstering confidence in the method and interpretation applied in this study.

12

Discussion

This chapter provides a general discussion of the key findings in the thesis and links the research objectives with the results achieved. Afterwards, several perspectives and limitations are given for a further practical implementation of the material fingerprinting approach.

12.1 Synthesis of research objectives

The present dissertation was mainly focused on demonstrating the use of a material fingerprinting framework that enabled the mapping of geometallurgical classes, which were representative of comminution and recovery behaviour. Accordingly, in relation to that, the objectives formulated in Section 1.2 were addressed as follows:

Objective 1: The dissertation showed the construction of a material fingerprinting framework based primarily upon geochemical and mineralogical data clustering. Agglomerative hierarchical clustering was selected as the tool to identify classes of samples with similar geological attributes. The geochemical and mineralogical class signatures could explain typical hard/soft material or low/high recovery properties, which could be useful for processing optimisation choices.

Objective 2: Geochemical and mineralogical clustering resulted in material classes with distinct processing characteristics. The combined geological characteristics relating to anomalous or outlier classes were typically explanatory for the observed behaviour. Additionally, considering the (geo)spatial contextual relationships shed light on the distinct behaviours. For example, some classes were more favourable to the milling processes than to the recovery processes, and others exhibited the opposite. Since the characteristics of these classes are generally well understood, it would be possible to make a classifier model predict its corresponding response for a newly identified fingerprint.

Objective 3: The decisions to optimise the plant feed as a function of the incoming material blend and its operational control were examined. A detailed analysis of the decisions and subsequent results and conclusions was presented in Chapter 11. Generally, performance reduction or losses were due to a combination of the blend feed composition and operating conditions. The proposed optimisation opportunities relate to trade-offs for processing materials with different qualities separately rather than as a blend. From an operational perspective, this may not be desired as this requires a more flexible operating plant, which may come at the cost of its consistency and reliability.

Objective 4: The strategic (longer-term) performance of the processing plant relates largely to the characteristics of the predefined geometallurgical ore body domains. Material from domains showing undesired characteristics is frequently blended, causing this characteristic to be faint, resulting in a limited impact, and showing the average processing response of the domains. For instance, the long-term planning objectives may be forecasted using the proportion of orebody domains mined across time or using the gradually changing material composition relating to the mining depth. Contrastingly, a larger influence is seen from the processing conditions themselves at a tactical (short-term) performance resolution. For example, the performance can be significantly influenced by shutdowns of processing units, recirculation of material or adding emergency feed. Therefore, significant cleaning or filtering of the processing data is required to identify the actual relationships between the material fingerprints and the response.

The following section presents general interpretations and implications of the main results. The final section gives several perspectives and limitations for practically implementing the material fingerprinting approach.

12.2 Interpretation and implications of the main results

12.2.1 Geology and metallurgical plant performance

A large part of this dissertation focused on material hardness being one of the main geological factors influencing the metallurgical plant performance. This raises the question of how the results from this dissertation help understanding the metallurgical plant performance since the primary data input is not hardness. Simply answered, the importance of this dissertation relies on the interpretation of the obtained results from the fingerprinting methodology and their implications for the hardness understanding. The fingerprinting technique makes an important contribution to the synthesis and description of geological attributes by providing a new data layer that groups samples which have similar geological features in an objective manner.

The main rationale behind this approach is that each geological feature of the ore may have significance to some aspect of the operation. For instance, studying the individual hardness characteristics from within classes (available for some of the samples) has proven to be indicative of the hardness of the entire class. The research showed that combining the material classes with spatial contextual relationships could largely explain any further physical transformations the material underwent, resulting in hardness changes. For example, the material located in a heavily sheared domain (Tropicana NE) tends to be softer due to more brittle behaviour exhibited during deformation. This brittle behaviour resulted in more fractures acting as fluid pathways giving locally more veining or gneissic banding. Other classes related to the oxides tend to be closer to the surface, being weathered and thus also showing softer characteristics. Finding the classes or class combinations that are more present in such regions, suggests an initial relationship which can be transferred and tested on regions with little knowledge about the deformation history.

Addressing and characterising domains based upon the fingerprint compositions and proportions was successful in constraining geometallurgical variability. The benefits of such fingerprint-based domaining are that it identifies domains which have a tendency for higher throughput rates than others and that consist of minerals with a higher or lower recovery rate or produce a certain quality product. The results further showed, for instance, how domains with a higher K/Al (molar) ratio, indicative of the feldspar composition, had various relationships with the processing characteristics. For example, a higher K/Al ratio relates to the higher grade mineralised samples, which tend to be more sulphur rich, and, therefore, have more impact on the processing due to their increased oxygen and lime demands.

Finally, the geology of the rocks is not further changed due to material handling, however, the geological composition of the plant feed can be changed significantly. Blends are the combined geological product processed in the metallurgical plant, and thus, it is of utmost importance that the blend composition is understood. Knowing which blend is processed at which moment in time enables a direct comparison of

the production actuals with the blend, which subsequently can be related to the compositional geology and the dig location of the material. However, the results showed that a significant amount of blending took place. This was not only blending caused by from hauling material from different sources to the stockpiles but also by constructing a crusher feed by reclaiming from different stockpiles simultaneously. Only a reliable and accurate material tracking model can help with this last part of the linkage and understanding of how the geology impacts metallurgical plant performance.

12.2.2 Hybrid characteristics of material fingerprints

One of the aims of this research was to create material fingerprints, which was achieved using various datasets mainly representing the geological characteristics of the mineralised feldspathic gneiss at the Tropicana Gold Mine. In this work, there was not a major focus on finding commonalities or differences between the different fingerprints because they were stand-alone examples. However, such differences were present (and, in fact, already shown) as can be explained by three hybrid characteristics of the fingerprints:

1. The ability to reclassify or update fingerprints with additional data availability.
2. Representation at various sample support scales.
3. Fingerprint identification throughout processes.

Hybrid characteristic 1: Fingerprint reclassification is possible by adding additional data and results in an enhanced granularity to which geological details of the fingerprints can be explained. For example, in Chapter 8, the fingerprints were composed of ME data and in Chapter 9 of pXRF and VNIR-SWIR spectral data. Results from both studies reflected the collection of constitutive material attributes relative to the considered input parameters. The studies did not use the same samples as an input, but the sample measurements did reflect the same material and resulted in similar results. For example, both studies picked up the mostly weathered/Oxide material, the mafic intrusive rocks and different variations of the feldspathic gneiss.

This implies that if two almost identical fingerprints are combined, then the new fingerprint is expected to show similar constitutive attributes but potentially with more details. This can be achieved by re-clustering the set of attributes. The resulting fingerprints then show significant overlapping characteristics with the signatures of the original fingerprints. This hybrid or data-driven character of the fingerprints makes them more suitable for large-scale and automated processes. If the same task had to be done by an expert, this would be subjective, time-consuming, repetitive and prone to errors.

Hybrid characteristic 2: The second aspect of a hybrid fingerprint character relates to the sample support scale and its natural ability to inform about metallurgical plant performance. For example, geological and spatial contextual relationships were obtained using widely spaced exploration hole samples. Despite this coarse resolution, the fingerprinting class characteristics and spatial distribution showed

geochemical variability at the deposit scale. These results may be broadly useful for mine planning and strategic geometallurgy. Similarly, fingerprints from the GC data (pXRF and VNIR-SWIR) were closely spaced and more spatially abundant, giving a higher-resolution impression of the internal geochemical, mineralogical and metallurgical variability. These datasets and results are more useful for identifying local-scale ore variability, which plays an important role in tactical-related geometallurgical decisions (i.e., short-term scheduling, dig-limit optimisation, blending).

Another aspect regarding the support scale of fingerprints is its relation to the dataset size reflected by the type of measurement conducted. Even when a dataset (e.g., penetration rate, metallurgical test work indices) is too small to be considered as an input for the clustering, it can still be used afterwards to inform about a typical response of the classes. The measurements conducted on a subset are, due to their geological similarity within classes, also representative of the other samples. Similarly, petrographical studies, logged lithology or alteration indices from individual samples or metallurgical test results from composites are transferable to the fingerprints at the considered support scale. Therefore, the constitutive response and characteristics of the fingerprints are defined using data from different scales of support.

Hybrid characteristic 3: Fingerprints were still indicative of the processing response at a later stage in the process, as shown by the tracking and not only after initial identification and delineation in the Resource model. Generally, ROM fingers are constructed using material from different mining locations, which results in a new material blend. These blends still showed the previously identified fingerprint characteristics and could be observed in the processing plants.

12.2.3 Clustering considerations

The main methodology applied throughout this dissertation was agglomerative hierarchical clustering. An often-described fundamental challenge in applying this technique is finding the optimal number of classes. However, exploring differences between the different number of classes also yields insights into the underlying relationships determining the partitioning. Hierarchical-based methods exactly indicate which new class is obtained if further subdivision takes place and also indicate the parental relationships if one decides to go with fewer classes as it is known which two classes are merged next. From this, the main take away is the knowledge of the hierarchical dependency itself. As soon as this is understood, one can further subdivide to get sufficient details required for the task to be solved. Therefore, it can be questioned whether understanding the partition cause might be more important than selecting the number of classes and should be focused upon first.

Example 12.1: Imagine an igneous rock dataset describing the mineral composition of ultramafic, mafic, intermediate and felsic rocks. Since there is a geologically-driven dependency in the proportion of olivine, pyroxene, plagioclase feldspar, quartz, amphibole, biotite, muscovite and K-feldspar in these rocks, it means that most likely, samples with a similar composition will group together. Thus, one of the first partitions is likely splitting the olivine and pyroxene-related class from the K-feldspar and quartz-bearing class. Later partitions may be less trivial as they may only focus on subdividing, for instance, two felsic rock types.

Knowing that the class incremental and related partition takes place within the mafic or felsic rock-related classes, within waste-bearing classes or Au-mineralised classes, is the most important and may decide whether more classes are desired or not. For example, if one partition separates a mineralised class into a waste and higher-grade class, it may be easy to decide that one additional clustering class is preferred. Similar considerations were frequently analysed in this dissertation and resulted in an optimal number of classes for this dissertation. Variables from the input dataset are representative of the geological evolution of the rock surrounding the sample and, therefore, having that degree of within-class variation simply represents the natural variability of the rock and is thus desired to capture within the clustering classes.

Most clustering techniques are based upon a distance metric measuring the dissimilarity, similarity or proximity between the samples. Since this metric depends on the input data representation (e.g., raw data, normalised, transformed, nominal, categorical), one will often get roughly similar class signatures regardless of the algorithm chosen. The main difference in the outcomes is a higher between-class similarity as there is still significant overlap with other classes. However, a class representing a more felsic rock composition will generally still be distinct from a mafic one. Also, geochemical signatures indicating the weathered or upper saprolite rock units were distinct from the rest.

12.3 Perspectives and limitations

The following selected considerations put the results from this dissertation into different perspectives and show avenues in which fingerprints can be used:

- The fingerprinting approach enhanced the understanding of material characterisation beyond the typical information these input datasets provide. For example, the clustering results discriminated unmineralised and mineralised classes and, in a later stage, also different degrees of mineralisation, all without considering the Au grade itself.
- The feature described in the previous point can be used for mineral exploration purposes and ore-waste sorting/separation. Mineral exploration relies heavily on finding and measuring either the target element or minerals of interest. In

gold exploration, a target may be missed due to the nuggety effect of gold. However, if the fingerprint of your target fits the expectation, then it may still be worthwhile to further explore within the same area. In this case, the fingerprint is a good proxy for being close to the target mineralisation as it can detect the associated alteration halo. This dissertation also showed how fingerprinting could discriminate intermediate grade material around the cut-off grade. This is typically considered much more challenging compared to ore-waste separation.

- The research methodology applied and types of data used in this dissertation are in line with applications and trends seen in the current literature (Hoal and Frenzel, 2022; Jooshaki et al., 2021). For example, one trend is to engineer data to extract more information from existing datasets by finding relationships between the input and output. Several other researchers had success in fingerprinting or characterising material classes using supervised learning with random forests (Bhuiyan et al., 2019; Hood et al., 2018; Tusa et al., 2020), support vector machine (Tessier et al., 2007) or neural networks (Both and Dimitrakopoulos, 2021). This dissertation applied unsupervised learning algorithms to engineer data. Future research may also use block chain technology to tie the material characterisation, tracking, processing and dispatching further together.
- Clustering of VNIR-SWIR regions rather than extracted features showed that a fingerprinting approach could provide the same mineralogical discrimination as one would get by looking at the features only. In fact, one of the regions is commonly overlooked or only linked to specific Fe-absorption features, whereas this research showed its correspondence with epidote mineralogy. Further experimenting with data-driven learning approaches will make it likely that similar results and new relationships will be found in the future.
- The tessellation approach may help identifying the appropriate resolution at which geological variability should be modelled for strategic use cases such as mine planning and processing plant design. This resolution can then be refined as GC data becomes available, allowing for enhanced and optimised tactical decision-making. In an aspirational sense, this boundary between strategic and tactical resolution and the responsiveness to each can progressively be moved to a finer resolution to drive optimised processing performances.

The following considerations discuss several limitations from this research and provide a foundation for future research to build upon:

- During the research work of this dissertation, there was the desire, accompanied by a trade-off, for including hardness-related proxies as variables in the clustering. On the one side, these data were available and could have allowed a direct hardness proxy in the material classes. On the other side, these proxies were only available for a subset of the geochemical or mineralogical dataset. This reduction in sample size is a serious threat to the representativity of the results. Especially since the metallurgical test samples were not specifically selected for the identified classes or material types in this study. Therefore, it was, for now, more important first to capture the range of material variability by excluding the proxies.

- The previous trade-off highlights one of the major shortcomings in using already existing data for a fingerprinting approach. The biggest challenge in this project was that the drill hole intervals with the geochemical and mineralogical fingerprints did not overlap with the metallurgical testing and validation datasets. The composites analysed for Equotip, BWi, Axb or recovery are typically gold grade and geologically-constrained metallurgical samples and thus incompletely reflect in-situ geochemical and mineralogical variability. Some composites were so large that they spanned multiple material types or were composed of rocks from different spatial domains and thus could not be used in this study. In an ideal scenario, one should carefully select and test samples for each combination of geological composition and spatial (sub)domain to improve understanding of the hardness and recovery characteristics. It is recommended to ensure that spatially constrained samples are used that cover the geological and mineralogical variability of the deposit.
- The material tracking simulation uses Resource block models as input to query the material fingerprints for each of the truck movements. This block model can be attributed with as many attributes as desired and is necessary to fingerprint the material. The block model used in this dissertation only had Au and S as block simulation values. Other variables were only available in blocks closest to the original sample location. This resulted in a not completely filled block model, thus limiting the geochemical and mineralogical resolution that was potentially achievable when all these other variables were modelled. Most samples originate from GC drilling giving by default a close spatial resolution and thus not limiting the spatial resolution of the geochemical and mineralogical data.
- The ability to discriminate the root cause of metallurgical plant performance may be limited by the ability to find classes, maximise across-class variability, minimise within-class variability, and connect classes with the root causes. This may only be solved by improved correlations, more samples, or modelling of the geochemical, mineralogical and other proxies while considering the modelling limitations.
- A lot of data cleaning had to be performed in order to use the truck GPS coordinates adequately in the forward simulation model. This reduced the overall accuracy of determining the pick-up locations of the material in the pit or stockpiles and the exact dumping location. Therefore, improving the data-quality control checks is recommended before storing the truck data in a fleet management system database. This will ease the data cleaning steps and improve fingerprint composition descriptions.
- Depending on the planned maintenance, there was a variety in the length of shutdowns for each unit in the processing plants. For example, mill shut downs occurred every 17 weeks and took either 24 or 48 hours according to the schedule. However, in reality, these shutdowns may take longer or shorter and can also start or finish in the middle of a shift. Since the processing actuals were aggregated in a resolution of 12 hours, it was thus evident that some of

the production actuals were influenced by the reduced run hours. This required initial data cleaning before the data could be tessellated and may have slightly affected the results (as in the rolling mean). If the production actuals were to be aggregated at a finer resolution (e.g., per 4 hours), then these effects will faint and thus, the shutdowns will have less impact on any derived results. However, this would also require that the crusher feed compositions match the 4 hours resolution of the plant actuals. This can easily be achieved because every truck was individually tracked, and thus could be aggregated at a 4-hours resolution.

13

Conclusions and recommendations

The last chapter of the dissertation presents a brief overview of conclusions describing the impact of geology on metallurgical plant performance. It also provides recommendations for a further practical implementation of the material fingerprinting approach.

13.1 Conclusions

This dissertation introduced fingerprints derived from machine learning and applied them as a tool for linking material attributes and blend compositions with the expected and obtained processing behaviour. The fingerprints were defined as a machine-learning-based classification of measured material attributes compared to the range of attributes found within an exploration area or defined using available mineral resources or reserves. These fingerprints were typically derived from high-confidence-based data and could measure and then track the material attributes throughout the unit operations of a mine. This ability gave confidence in the use and ability of fingerprints. Results from this dissertation showed that material fingerprinting proved being a successful tool and a way of thinking about data characterising the material attributes. The fingerprints allow an operation to identify material through the process, regardless of resembling a block model's block, truckload, stockpile, or mill feed.

The first fingerprints were created using an agglomerative hierarchical clustering approach with high-quality multi-element geochemical data from the Tropicana Gold Mine, Western Australia. These fingerprints were very effective in classifying the logged lithology, alteration or mineralisation and could, for example, discriminate unmineralised, marginal-grade and high-grade gold classes. The work involved exploring classes for their unique geochemical signature, relating classes with their typical comminution and recovery parameters, and explaining the observed processing attributes and their cause.

The clustering was primarily driven by the dominant mafic, felsic, garnet-bearing, garnet-absent, chert or quartz containing geochemical signatures of the gneissic rock found in each class. This demonstrated that the classes picked up different original host rocks and alteration assemblages seen across domains. The two gold-bearing classes were easily separated from the others (without using Au as input). A re-clustering of the gold-bearing classes showed that a greater emphasis was placed on grouping assemblages with relatively increased or decreased elemental concentrations rather than separating the major rock units. The main lesson learned from this fingerprinting exercise was that the geochemical fingerprints were plausible in a geological and spatial context and thus could be used to explain the differences in observed breakage properties (Leeb, BWi, Axb) and recoveries.

These first relationships between fingerprints and metallurgical plant performance indices were encouraging and hinted that including mineralogical data would enhance the found relationships. Additionally, it was tested whether fingerprints created from a poorer-quality but more abundant and rapidly acquired dataset (pXRF and VNIR-SWIR) could at least reveal similar, but hopefully new relationships.

The new fingerprints were constructed by clustering pXRF data and mineralogical class proportions of samples found within a small block. Clustering these block features resulted in nine classes representing different material types. Amongst others, these types revealed the following four attributes: 1) representative variations of plagioclase-rich or perthitic K-feldspar rich domains using the proportionalities of material types; 2) modifications of material types by overprinting alteration and deformations. This was discerned by the abundance/presence of chlorite, sericite or epidote within each material type; 3) spatial contextual relationships, which showed

how the material types relate to the progressive breakdown of feldspar into phengitic white micas in zones of intense foliation; 4) how shear zone processes are captured within material types.

This analysis provided a newly recognised w605 nm region feature, where the wavelength position of the deepest feature changes according to the assemblage epidote sits in, which relates to the texture and resulting material hardness. This feature could be utilised to separate material types into a softer (~15–18 kWh/t) and harder (>20 kWh/t) material component. These results may be used for further domaining orebody hardness and processing response.

After defining the fingerprints, the next step included linking them with the actual plant performance. For this, it is essential to match the moment a particular fingerprint is mined with the time it entered the plant (as crusher feed). This required the replication (simulation) of dispatch movements from the pit to the stockpiles and the crusher, as was realised using the forward simulation model. The model spatially and temporally modelled stockpiles and accounted for blending effects. Assessment of the spatial-temporal modelling showed realistic geological variability similar to that seen in the pit and spatial cohesion, which enabled temporal reconciliation of the crusher input feed composition.

Finally, these input fingerprints were linked to the actual plant performance using the same time stamp and thereby creating a time series. The multivariate time series signals were further transformed in continuous temporal domains using a continuous wavelet tessellation and data mosaic method. These domains represented short or long periods in which a similar material fingerprint composition was processed. Afterwards, these domains were classified by the actual processing performance observed to analyse and determine any causal relationships between the geology and metallurgical plant performance. Three case studies showed various results related to the root cause of the observed processing performance. For example, blends with higher proportions of weathered or Transitional material were truly easier to process in terms of throughput and lower energy consumption, lower sulphur-bearing blends indeed had better recovery values, and blends with more clays required more reagents to reach target processing conditions.

In conclusion, the results from this dissertation matched the expectations that a constitutive representation of the material attributes makes geological sense and thus can represent material types. Furthermore, they are indicative of the root cause of changing plant performance and thus bolster confidence in the methods and interpretations applied in this dissertation. Implementing the material fingerprinting approach throughout the mining process could significantly contribute to sustainable mineral industry development and eventually lower operational costs.

13.2 Recommendations

This dissertation presented the results of a material fingerprinting framework, with one of the strengths of this framework being that the fingerprints were constructed in a data-driven approach. This eliminated most of the subjectivity while analysing or manually grouping the data and finding the relationships between input and output. The results of this dissertation were auspicious and hopefully inspired others to

consider unsupervised learning methods to explore their data. Hence, the following recommendations may foster the implementation of the fingerprint framework in geometallurgical practises and further research.

Suggestions for practical application:

- A fingerprinting approach could be implemented during the exploration stage to aid generating a simple domaining of the deposit and preliminary describe how the deposit geology will affect metallurgical behaviour. Since at this stage, there is still much uncertainty about the exact mineralogy, formation or textural relationships, it would be beneficial to describe the material as classes with similar constituents. Then further investigation will determine the exact composition and effect on metallurgical behaviour.
- Several geological drivers of geometallurgy, such as the textural, structural, and compositional features that record both the original formation of the deposit as well as any subsequent deformation, alteration, or modification, were not sufficiently captured as a dataset in this research. Such datasets are expected to be a great asset to improve the results and give further insights into the impact of geology on metallurgical plant performance.
- One benefit of the fingerprinting approach is that it allows to proactively domain the deposit of interest and align subsequent metallurgical sampling to the resulting domains. This ensures more effective coverage and adherence to the true geological variability that may impact metallurgical performance. These aspects are especially important when dealing with the allocation of sparse higher-order (expensive) tests. Furthermore, it can help troubleshoot potential mine challenges at an early stage. For example, ore characterisation in a spatial context and linking it to the scheduled timeline of the mine life can help to predict or forecast those moments in time this material is expected to be processed.
- Modelling the geometallurgical and mineralogical parameters and any other geochemical variable other than Au has been considered one of the main shortcomings in this work. It is identified to be necessary for future implementation of the fingerprinting approach. Although the results in this dissertation were built upon a vast quantity of data, it is acknowledged that there is unused geological data already collected and ready to be used but either not in the right format or directly accessible. A block model with block dimensions of $12 \times 12 \times 3$ m was found to be sufficient as a high-resolution model and is recommended in any follow-up geometallurgical study, but may be deposit specific.
- Unsupervised clustering results of the ME, pXRF and VNIR-SWIR data showed to be deterministic in separating unmineralised from mineralised material. This feature could be used for a bulk Au grade sorting application. However, it could also be applied in prospectivity mapping during exploration work as it can identify samples with similar mineralogical or geochemical assemblages as the typically mineralised material.

- Fleet management systems should give more reliable and accurate GPS readings for truck and excavator activities. It is desirable to fingerprint each truck and make truck-by-truck decisions. However, one should carefully record which material is loaded by excavators and where the material is hauled.
- Integration of the fingerprinting approach would benefit from having sensor data collection for geochemical and mineralogical attributes at multiple locations (e.g., belt conveyors). This should be linked with the dispatch system and adequate and consistent stockpile management to get a fully integrated fingerprint tracking system.

Suggestions for further research:

- The introduction of this dissertation highlighted the absence of geometallurgical factors in the revenue-based valuation of mines. Therefore, it would be recommended, after gaining insights from a study such as this one, to execute a techno-economic assessment to semi-quantify or quantify the true financial benefits. On the one hand, this may help in discussions around the drive for constant optimisation and trade-offs between reduction in costs or getting higher recoveries. On the other hand, it also gives insights into managing environmental limitations by optimising reagents consumption and identifying where the real geometallurgical-driven revenue potential is.
- Another suggestion is to develop further mathematical relationships between the different levels of the tiered geometallurgical principles. This would help to create a direct link between the proxy and metallurgical test work data. Defining such relationships was attempted during the research, however, the main limitation was that many samples were not colocated and thus reduced the number of samples. This has to be overcome to further reveal relationships.
- Further research using fingerprinting could focus more on the recovery characteristics of the material types. Gold recovery in the leaching circuit is usually considered as one of the important processing indicators and directly related to the mine's revenue. Therefore, it would be interesting to study the reconciliation of gold from each material type and perhaps do additional gold liberation tests where necessary.
- The fingerprinting approach could be further tested on, for instance, satellite imagery data or geophysical data for mineral exploration, ore sorting, environmental monitoring or mine face and stockpile mapping. For example, radiometrics, conductivity or magnetic susceptibility attributes of rocks would be useful in defining rock competency indicators. These applications are deposit and location-specific, but it would be interesting to see the further adoption of material fingerprints in the mining industry.

References

- Abweny, M. S., F. J. A. van Ruitenbeek, B. de Smeth, T. Woldai, F. D. van der Meer, T. Cudahy, T. Zegers, J.-K. Blom, and B. Thuss (2016). Short-wavelength infrared (SWIR) spectroscopy of low-grade metamorphic volcanic rocks of the Pilbara Craton. *Journal of African Earth Sciences* 117, 124–134.
- Administrators, C. S. (2011). National Instrument 43-101 Standards of Disclosure for Mineral Projects. Report, British Columbia Security Commission. Online available at <https://mrmr.cim.org/media/1017/national-instrument-43-101.pdf>, last accessed on October 16, 2022.
- Afrapoli, A. M. and H. Askari-Nasab (2017). Mining fleet management systems: A review of models and algorithms. *International Journal of Mining, Reclamation and Environment* 33(1), 42–60.
- Aggarwal, C. C. (2015). *Data mining: The textbook*, pp. 746. Cham, Switzerland: Springer.
- Aggarwal, C. C. and C. K. Reddy (2014). *Data Clustering. Algorithms and Applications*, pp. 648. Chapman & Hall / CRC Data mining and Knowledge Discovery Series. New York, USA: Taylor & Francis Group.
- Aitchison, J. (1986). *The Statistical Analysis of Compositional Data*, pp. 416. Monographs on Statistics and Applied Probability. Dordrecht, the Netherlands: Chapman & Hall.
- Aitchison, J. (1999). Logratios and natural laws in compositional data analysis. *Mathematical Geology* 31(5), 563–580.
- Aitchison, J. and J. Egozcue (2005). Compositional data analysis: Where are we and where should we be heading? *Mathematical Geology* 37(7), 829–850.
- Alruiz, O. M., S. Morrell, C. J. Suazo, and A. Naranjo (2009). A novel approach to the geometallurgical modelling of the Collahuasi grinding circuit. *Minerals Engineering* 22(12), 1060–1067.
- AngloGold Ashanti (2016). AngloGold Ashanti lifts Tropicana ore reserve and production outlook. Online available at <http://www.tropicanajv.com.au/irm/PDF/63836f80-2bcc-4518-b609-2859087c38a1/AngloGoldAshantiLiftsTropicanaOreReserveandProductionOutlook>, last accessed on October 16, 2022.

- AngloGold Ashanti and Independence Group NL (2010). Tropicana Gold Project overview. Unpublished report by AngloGold Ashanti Australia, Tropicana Operation.
- Arne, D., E. House, S. Pontual, and J. Huntington (2016). Hyperspectral interpretation of selected drill cores from orogenic gold deposits in central Victoria, Australia. *Australian Journal of Earth Sciences* 63(8), 1003–1025.
- Assimi, H., B. Koch, C. Garcia, M. Wagner, and F. Neumann (2021). Modelling and optimization of run-of-mine stockpile recovery. In *Proceedings of the 36th Annual ACM Symposium on Applied Computing*, Online, pp. 450–458.
- Austin, K., K. Choros, A. Job, and R. McAree (2019). Real-time mining face grade determination using hyperspectral imaging techniques - MRIWA Project M0518. Report, School of Mechanical and Mining Engineering, The University of Queensland.
- Baker, S. (2020). Tropicana Gold Mine Havana 4 5 6 PFS. Unpublished report by AngloGold Ashanti Australia, Tropicana Operation.
- Bhuiyan, M., K. Esmaeili, and J. C. Ordóñez-Calderón (2019). Application of data analytics techniques to establish geometallurgical relationships to Bond Work Index at the Paracutu Mine, Minas Gerais, Brazil. *Minerals* 9(5), 302.
- Bhuiyan, M., K. Esmaeili, and J. C. Ordóñez-Calderón (2022). Evaluation of rock characterization tests as geometallurgical predictors of bond work index at the Tasiast Mine, Mauritania. *Minerals Engineering* 175, 107293.
- Blenkinsop, T. G. and M. G. Doyle (2014). Structural controls on gold mineralization on the margin of the Yilgarn craton, Albany-Fraser orogen: The Tropicana deposit, Western Australia. *Journal of Structural Geology* 67, 189–204.
- Bond, F. C. (1952). Third theory of comminution. *Mining engineering* 4, 484–494.
- Bond, F. C. (1961). Crushing and grinding calculations, Part II. *British Chemical Engineering* 6, 543–548.
- Bonnici, N. K. (2012). *The mineralogical and textural characteristics of copper-gold deposits related to mineral processing attributes*. Ph.D. Thesis, University of Tasmania, Australia.
- Booyesen, R., S. Lorenz, S. T. Thiele, W. C. Fuchsloch, T. Marais, P. A. M. Nex, and R. Gloaguen (2022). Accurate hyperspectral imaging of mineralised outcrops: An example from lithium-bearing pegmatites at Uis, Namibia. *Remote Sensing of Environment* 269, 112790.
- Bortnowski, P., L. Gładysiewicz, R. Król, and M. Ozdoba (2021). Energy efficiency analysis of copper ore ball mill drive systems. *Energies* 14(6), 1786.
- Both, C. and R. Dimitrakopoulos (2021). Applied machine learning for geometallurgical throughput prediction - A case study using production data at the Tropicana Gold Mining Complex. *Minerals* 11(11), 1257.

- Boubanga-Tombet, S., A. Huot, I. Vitins, S. Heuberger, C. Veuve, A. Eisele, R. Hewson, E. Guyot, F. Marcotte, and M. Chamberland (2018). Thermal infrared hyperspectral imaging for mineralogy mapping of a mine face. *Remote Sensing* 10(10), 1518.
- Brauhart, C. W. (2019). The role of geochemistry in understanding mineral systems. *ASEG Extended Abstracts 2019*(1), 1–5.
- Bruce, L. M., C. H. Koger, and L. Jiang (2002). Dimensionality reduction of hyperspectral data using discrete wavelet transform feature extraction. *IEEE Transactions on Geoscience and Remote Sensing* 40(10), 2331–2338.
- Bulled, D., T. Leriche, M. Blake, J. Thompson, and T. Wilkie (2009). Improved production forecasting through geometallurgical modeling at iron ore company of Canada. In *Proceedings of the 41st Annual Meeting of Canadian Mineral Processors*, Ottawa, Canada, pp. 20–22.
- Caciagli, N. (2016). Multielement geochemical modelling for mine planning: Case study from an epithermal gold deposit. In *Proceedings of the International workshop on compositional data analysis - CoDaWork 2015*, Volume 187 of *Compositional Data Analysis*, L'Escala, Spain, pp. 45–61.
- Caliński, T. and J. Harabasz (1974). A dendrite method for cluster analysis. *Communications in Statistics - Theory and Methods* 3(1), 1–27.
- Carranza, E. J. M. (2011). Analysis and mapping of geochemical anomalies using logratio-transformed stream sediment data with censored values. *Journal of Geochemical Exploration* 110(2), 167–185.
- Caterpillar (2020). Cat Minestar - Today's technologies open up new opportunities. Online Article, available at <http://s7d2.scene7.com/is/content/Caterpillar/CM20170227-38180-01087>, last accessed on February 3, 2020.
- Clark, R. N. and A. N. Rencz (1999). Spectroscopy of rocks and minerals, and principles of spectroscopy. *Manual of Remote Sensing* 3(11), 3–58.
- Coetzee, L. L., S. J. Theron, G. J. Martin, J. van der Merwe, and T. A. Stanek (2011). Modern gold department and its application to industry. *Minerals Engineering* 24(6), 565–575.
- Cooper, G. R. J. and D. R. Cowan (2009). Blocking geophysical borehole log data using the continuous wavelet transform. *Exploration Geophysics* 40(2), 233–236.
- Corescan (2021). Hyperspectral core imaging applications - porphyry deposits. Report, Corescan. Presentation available at https://corescan.com.au/wp-content/uploads/2021/09/Corescan_DepositSummary_Porphyry_202109_ENG_UK_PDF-2.pdf, last accessed on October 16, 2022.
- Crawford, A. J. and M. G. Doyle (2016). Granulite-hosted gold: Tectonic setting and litho-geochemistry of the Tropicana deposit, Western Australia. *Economic Geology* 111(2), 395–420.

- CSA Global (2018). Integrated assessment of regional stream-sediment geochemistry for metallic deposits in Northwestern British Columbia (Parts of NTS 093, 094, 103, 104), Canada. Report CSA Global Report No 110.2018, CSA Global Canada Geoscience Ltd.
- Dalm, M. (2018). *Sensor-based sorting opportunities for hydrothermal ore deposits: Raw material beneficiation in mining*. Ph.D. Thesis, Delft University of Technology, the Netherlands.
- Dalm, M., M. W. N. Buxton, and F. J. A. van Ruitenbeek (2017). Discriminating ore and waste in a porphyry copper deposit using short-wavelength infrared (SWIR) hyperspectral imagery. *Minerals Engineering* 105, 10–18.
- Dalm, M., M. W. N. Buxton, and F. J. A. van Ruitenbeek (2018). Ore-waste discrimination in epithermal deposits using near-infrared to short-wavelength infrared (NIR-SWIR) hyperspectral imagery. *Mathematical Geosciences* 51(7), 849–875.
- Dalm, M., M. W. N. Buxton, F. J. A. van Ruitenbeek, and J. H. L. Voncken (2014). Application of near-infrared spectroscopy to sensor based sorting of a porphyry copper ore. *Minerals Engineering* 58, 7–16.
- Davies, D. L. and D. W. Bouldin (1979). A cluster separation measure. *IEEE transactions on pattern analysis and machine intelligence PAMI-1*(2), 224–227.
- Davies, J. F. and R. E. Whitehead (2006). Alkali-alumina and MgO-alumina molar ratios of altered and unaltered rhyolites. *Exploration and Mining Geology* 15(1-2), 75–88.
- de Azevedo Barbosa, P., M. G. Bergerman, E. da Fonseca, and R. Kwitko-Ribeiro (2021). Determination of abrasiveness in copper-gold sulfide ores: A contribution to the geometallurgical model of the Sossego deposit. *Minerals* 11(12), 1427.
- de Bakker, J. (2013). Energy use of fine grinding in mineral processing. *Metallurgical and Materials Transactions E* 1(1), 8–19.
- Díaz, E., G. Pamparana, L. Voisin, W. Kracht, and P. Martínez (2019). Exploring the effect of the geological texture at meso and micro scale on grinding performance. *Minerals Engineering* 144, 106032.
- Dominy, S., L. O'Connor, A. Parbhakar-Fox, H. Glass, and S. Purevgerel (2018). Geometallurgy - A route to more resilient mine operations. *Minerals* 8(12), 560.
- Donskoi, E., A. Poliakov, R. Holmes, S. Suthers, N. Ware, J. Manuel, and J. Clout (2015). Iron ore textural information is the key for prediction of downstream process performance. *Minerals Engineering* 86, 10–23.
- Doyle, M. G., T. G. Blenkinsop, A. J. Crawford, I. R. Fletcher, J. Foster, L. Fox-Wallace, R. R. Large, R. Mathur, N. J. McNaughton, S. Meffre, J. R. Muhling, S. Occhipinti, B. Rasmussen, and J. Savage (2014). Tropicana deposit, Western Australia: An integrated approach to understanding granulite-hosted gold and the Tropicana gneiss. Report, Geological Survey of Western Australia, Record 2014/6.

- Doyle, M. G., I. R. Fletcher, J. Foster, R. R. Large, R. Mathur, N. J. McNaughton, S. Meffre, J. R. Muhling, D. Phillips, and B. Rasmussen (2015). Geochronological constraints on the Tropicana gold deposit and Albany-Fraser Orogen, Western Australia. *Economic Geology* 110(2), 355–386.
- Doyle, M. G., D. Gibbs, J. Savage, and T. G. Blenkinsop (2009). Geology of the Tropicana Gold project, Western Australia. In *Smart Science for Exploration and Mining, 10th Biennial SGA Meeting*, Townsville, Australia, pp. 50–52.
- Doyle, M. G., B. Kendall, and D. Gibbs (2007). Discovery and characteristics of the Tropicana gold district. In *Proceedings of Geoconferences (WA) Inc. Kalgoorlie '07 Conference*, Kalgoorlie, Australia, pp. 186–190.
- Doyle, M. G., J. Savage, T. G. Blenkinsop, A. J. Crawford, and N. J. McNaughton (2013). Tropicana: Unravelling the complexity of a +6Moz gold deposit hosted in granulite facies metamorphic rocks. In *AusIMM World Gold 2013 Conference*, Brisbane, Australia, pp. 87–93.
- du Plessis, C. A., H. Lambert, R. S. Gärtner, K. Ingram, W. Slabbert, and J. J. Eksteen (2021). Lime use in gold processing - A review. *Minerals Engineering* 174(2021), 107231.
- Escolme, A., R. F. Berry, J. Hunt, S. Halley, and W. Potma (2019). Predictive models of mineralogy from whole-rock assay data: Case study from the Productora Cu-Au-Mo deposit, Chile. *Economic Geology* 114(8), 1513–1542.
- ESRI (2009). World Imagery - World Topographic Map. Online Article, available at <https://www.arcgis.com/home/item.html?id=7dc6cea0b1764a1f9af2e679f642f0f5>, last accessed on May 21, 2022.
- Everitt, B. S., S. Landau, M. Leese, and D. Stahl (2011). *Cluster Analysis* (5th ed.), pp. 330. Wiley Series in Probability and Statistics. Chichester, UK: John Wiley & Sons Ltd.
- Faraj, F. and J. M. Ortiz (2021). A simple unsupervised classification workflow for defining geological domains using multivariate data. *Mining, Metallurgy & Exploration* 38(3), 1609–1623.
- Fouedjio, F., E. J. Hill, and C. Laukamp (2017). Geostatistical clustering as an aid for ore body domaining: Case study at the Rocklea Dome channel iron ore deposit, Western Australia. *Applied Earth Science* 127(1), 15–29.
- Frank, S., C. Frehner, and A. Akhlaghi (2019). Portable hardness testing: Leeb, portable rockwell and UCI. Report, Equotip Application Booklet, Proceq SA. Online available at https://media.screeningeagle.com/asset/Downloads/Equotip_Application_Booklet_Portable_Hardness_Testing_Using_Leeb_Portable_Rockwell_UCI.pdf, last accessed on October 16, 2022.

- Gaillard, N., A. E. Williams-Jones, J. R. Clark, P. Lypaczewski, S. Salvi, S. Perrouy, N. Piette-Lauzière, C. Guilmette, and R. L. Linnen (2018). Mica composition as a vector to gold mineralization: Deciphering hydrothermal and metamorphic effects in the Malartic district, Quebec. *Ore Geology Reviews* 95, 789–820.
- Gardula, A., D. Das, M. DiTrento, and S. Joubert (2015). First year of operation of HPGR at Tropicana Gold Mine - Case study. In *SAG Conference*, Vancouver, Canada, pp. 1–22.
- Gazley, M. F., K. S. Collins, J. Roberston, B. R. Hines, L. A. Fisher, and A. McFarlane (2015). Application of principal component analysis and cluster analysis to mineral exploration and mine geology. In *AusIMM New Zealand Branch Annual Conference*, Dunedin, New Zealand, pp. 131–139.
- Gazley, M. F. and L. A. Fisher (2014). A review of the reliability and validity of portable X-ray fluorescence spectrometry (pXRF) data. In *Mineral Resource and Ore Reserve Estimation - The AusIMM Guide to Good Practice*, Book section 2, pp. 69–81. Melbourne, Australia: The Australasian Institute of Mining and Metallurgy.
- Grunsky, E. C. (2010). The interpretation of geochemical survey data. *Geochemistry: Exploration, Environment, Analysis* 10(1), 27–74.
- Grunsky, E. C. and P. de Caritat (2019). State-of-the-art analysis of geochemical data for mineral exploration. *Geochemistry: Exploration, Environment, Analysis* 20(2), 217–232.
- Grunsky, E. C., U. A. Mueller, and D. Corrigan (2014). A study of the lake sediment geochemistry of the Melville Peninsula using multivariate methods: Applications for predictive geological mapping. *Journal of Geochemical Exploration* 141, 15–41.
- Grunsky, E. C. and B. W. Smee (1999). The differentiation of soil types and mineralization from multi-element geochemistry using multivariate methods and digital topography. *Journal of Geochemical Exploration* 67(1-3), 287–299.
- Guntoro, P. I. (2019). *X-ray microcomputed tomography (μ CT) as a potential tool in Geometallurgy*. Licentiate Thesis, Luleå University of Technology, Sweden.
- Gupta, R. P. (2017). *Remote Sensing Geology* (3rd ed.), pp. 438. Berlin, Germany: Springer.
- Halley, S. (2020). Mapping magmatic and hydrothermal processes from routine exploration geochemical analyses. *Economic Geology* 115(3), 489–503.
- Hardwick, B. (2021). *Mineralised textures at the Tropicana gold mine: implications for the genetic model and deportment of gold*. MSc Thesis, University of Tasmania, Australia.
- Harraden, C. L., M. J. Cracknell, J. Lett, R. F. Berry, R. Carey, and A. C. Harris (2019). Automated core logging technology for geotechnical assessment: A study on core from the Cadia East porphyry deposit. *Economic Geology* 114(8), 1495–1511.

- Hecker, C., F. J. A. van Ruitenbeek, H. M. A. van der Werff, W. H. Bakker, R. D. Hewson, and F. D. van der Meer (2019). Spectral absorption feature analysis for finding ore: A tutorial on using the method in geological remote sensing. *IEEE Geoscience and Remote Sensing Magazine* 7(2), 51–71.
- Hill, E. J., A. Fabris, Y. Uvarova, and C. Tiddy (2021). Improving geological logging of drill holes using geochemical data and data analytics for mineral exploration in the Gawler Ranges, South Australia. *Australian Journal of Earth Sciences* 53(1), 1–27.
- Hill, E. J., M. A. Pearce, and J. M. Stromberg (2020). Improving automated geological logging of drill holes by incorporating multiscale spatial methods. *Mathematical Geosciences* 53(1), 21–53.
- Hill, E. J., J. Robertson, and Y. Uvarova (2015a). Detecting gradational change in data from exploration drill holes. In *IAMG 2015 International Association of Mathematical Geosciences*, Freiberg, Germany, pp. 1186–1190.
- Hill, E. J., J. Robertson, and Y. Uvarova (2015b). Multiscale hierarchical domaining and compression of drill hole data. *Computers & Geosciences* 79, 47–57.
- Hill, E. J. and Y. Uvarova (2018). Identifying the nature of litho-geochemical boundaries in drill holes. *Journal of Geochemical Exploration* 184, 167–178.
- Hoal, K. E. O. and M. Frenzel (2022). Ores drive operations - Economic geology is the foundation of geometallurgy. *SEG Discovery* (129), 30–43.
- Hodkiewicz, P. F., D. I. Groves, G. J. Davidson, R. F. Weinberg, and S. G. Hagemann (2008). Influence of structural setting on sulphur isotopes in Archean orogenic gold deposits, Eastern Goldfields Province, Yilgarn, Western Australia. *Mineralium Deposita* 44(2), 129–150.
- Hood, S. B., M. J. Cracknell, and M. F. Gazley (2018). Linking protolith rocks to altered equivalents by combining unsupervised and supervised machine learning. *Journal of Geochemical Exploration* 186, 270–280.
- Hood, S. B., M. J. Cracknell, M. F. Gazley, and A. M. Reading (2019). Element mobility and spatial zonation associated with the Archean Hamlet orogenic Au deposit, Western Australia: Implications for fluid pathways in shear zones. *Chemical Geology* 514, 10–26.
- Horwitz, W. and R. Albert (2006). The Horwitz ratio (HorRat): A useful index of method performance with respect to precision. *Journal of AOAC International* 89(4), 1095–1109.
- Hu, Z. and L. Qi (2014). Sample digestion methods. In *Treatise on Geochemistry* (2nd ed.), Book section 15.5, pp. 87–109. Oxford, UK: Elsevier.
- Hunt, G. R. (1977). Spectral signatures of particulate minerals in the visible and near infrared. *Geophysics* 42(3), 501–513.
- Hunt, J. A. and R. F. Berry (2017). Geological contributions to geometallurgy: A review. *Geoscience Canada* 44(3), 103–118.

- Intertek Genalysis (2019). Minerals services - Schedule of services & charges. Report, Intertek. Online available at <https://www.intertek.com>, last accessed on October 16, 2022.
- IPMI (2015). Fire assay analysis of precious metals. Report, International Precious Metals Institute. Online available at https://www.kitco.com/pr/3127/article_06282015232139.pdf, last accessed on October 16, 2022.
- Jansen, W. M., R. D. Morrison, M. Wortley, and T. Rivett (2009). Tracer-based mine-mill ore tracking via process hold ups at Northparkes mine. In *AusIMM 10th Mill Operators' Conference*, Adelaide, Australia, pp. 345–356.
- Jeswiet, J. and A. Szekeres (2016). Energy consumption in mining comminution. In *23rd CIRP Conference on Life Cycle Engineering*, Volume 48, Berlin, Germany, pp. 140–145.
- JKTech Laboratory Services (2015). Jk drop weight test. Online available at <https://www.yumpu.com/en/document/read/35142825/jk-drop-weight-test-in-detail-jktech>, last accessed on February 14, 2022.
- Johnson, C. L., D. A. Browning, and N. E. Pendock (2019). Hyperspectral imaging applications to geometallurgy: Utilizing blast hole mineralogy to predict Au-Cu recovery and throughput at the Phoenix Mine, Nevada. *Economic Geology* 114(8), 1481–1494.
- Jolliffe, I. T. (2002). *Principal Component Analysis* (2nd ed.), pp. 488. Springer Series in Statistics. New York, USA: Springer.
- Jooshaki, M., A. Nad, and S. Michaux (2021). A systematic review on the application of machine learning in exploiting mineralogical data in mining and mineral industry. *Minerals* 11(8), 816.
- JORC Code (2012). The 2012 Australasian Code for Reporting Exploration Results, Mineral Resources, and Ore Reserves. Report, Australasian Joint Ore Reserves Committee. Online available at https://www.jorc.org/docs/JORC_code_2012.pdf, last accessed on October 16, 2022.
- Jupp, K., T. J. Howard, and J. E. Everett (2013). Role of pre-crusher stockpiling for grade control in iron ore mining. *Applied Earth Science* 122(4), 242–255.
- Kazimoto, E. O. (2020). Short wavelength infrared spectral characterization of the mineralogy of Gokona and Nyabigena andesite-hosted gold deposits in North Mara, Tanzania. *Tanzania Journal of Science* 46(2), 354–370.
- Keeney, L. (2010). *The Development of a Novel Method for Integrating Geometallurgical Mapping and Orebody Mapping*. Ph.D. Thesis, University of Queensland, Australia.
- Keeney, L., S. G. Walters, and T. Kojovic (2011). Geometallurgical mapping and modelling of comminution performance at the Cadia East Porphyry Deposit. In *1st AusIMM International Geometallurgy Conference*, Brisbane, Australia, pp. 73–83.

- Kent, M., B. C. Catto, M. G. Doyle, D. Gibbs, M. Matheson, R. Singer, B. M. Kendall, and J. Vann (2014). Tropicana Gold Mine, Western Australia - A case study of non-linear mineral resource estimation. In *Mineral Resource and Ore Reserve Estimation - The AusIMM Guide to Good Practice*, Book section 4, pp. 301–310. Melbourne, Australia: The Australasian Institute of Mining and Metallurgy.
- King, G. S. and J. L. Macdonald (2016). The business case for early-stage implementation of geometallurgy - An example from the Productora Cu-Mo-Au Deposit, Chile. In *3rd AusIMM International Geometallurgy Conference*, Perth, Australia, pp. 125–133.
- Kirkland, C. L., C. V. Spaggiari, R. H. Smithies, M. T. D. Wingate, E. A. Belousova, Y. Gréau, M. T. Sweetapple, R. Watkins, S. Tesselina, and R. Creaser (2015). The affinity of Archean crust on the Yilgarn - Albany-Fraser Orogen boundary: Implications for gold mineralisation in the Tropicana Zone. *Precambrian Research* 266, 260–281.
- Koch, P.-H., C. Lund, and J. Rosenkranz (2019). Automated drill core mineralogical characterization method for texture classification and modal mineralogy estimation for geometallurgy. *Minerals Engineering* 136, 99–109.
- Kock, F., L. Siddall, I. Lovatt, M. Giddy, and M. DiTrento (2015). Rapid ramp-up of the Tropicana HPGR circuit. In *SAG Conference*, Vancouver, Canada, pp. 1–22.
- Koerting, F. (2021). *Hybrid imaging spectroscopy approaches for open pit mining - Applications for virtual mine face geology*. Ph.D. Thesis, University of Potsdam, Germany.
- Kokaly, R. F., R. N. Clark, G. A. Swayze, K. E. Livo, T. M. Hoefen, N. C. Pearson, R. A. Wise, W. M. Benzel, H. A. Lowers, R. L. Driscoll, and A. J. Klein (2017). USGS Spectral Library Version 7. Report 2327-638X, USGS.
- Kurz, T. H. (2011). *Integration of ground-based hyperspectral and lidar scanning in virtual outcrop geology*. Ph.D. Thesis, University of Bergen, Norway.
- Lamberg, P. (2011). Particles - The bridge between geology and metallurgy. In *Conference in Minerals Engineering*, Luleå, Sweden, pp. 1–16.
- Laukamp, C., A. Rodger, M. LeGras, H. Lampinen, I. C. Lau, B. Pejčić, J. Stromberg, N. Francis, and E. Ramanaidou (2021). Mineral physicochemistry underlying feature-based extraction of mineral abundance and composition from shortwave, mid and thermal infrared reflectance spectra. *Minerals* 11(4), 347.
- Little, L., A. N. Mainza, M. Becker, and J. Wiese (2017). Fine grinding: How mill type affects particle shape characteristics and mineral liberation. *Minerals Engineering* 111, 148–157.
- Lopera, P. A. M. (2014). *Geometallurgical mapping and mine modelling - comminution studies: La Colosa Case Study, AMIRA P843A*. MSc Thesis, University of Tasmania, Australia.

- Lund, C., P. Lamberg, and T. Lindberg (2015). Development of a geometallurgical framework to quantify mineral textures for process prediction. *Minerals Engineering* 82, 61–77.
- Lynch, A. (2015). *Comminution Handbook*, pp. 324. AusIMM Spectrum Series 21. Melbourne, Australia: The Australasian Institute of Mining and Metallurgy.
- Madenova, Y. and N. Madani (2021). Application of gaussian mixture model and geostatistical co-simulation for resource modeling of geometallurgical variables. *Natural Resources Research* 30, 1199–1228.
- Mallat, S. (1991). Zero-crossings of a wavelet transform. *IEEE Transactions on Information Theory* 37(4), 1019–1033.
- Mallat, S. (2009). *A Wavelet Tour of Signal Processing* (3rd ed.), pp. 805. Burlington, USA: Elsevier.
- Martín-Fernández, J. A. (2003). Dealing with zeros and missing values in compositional data sets using nonparametric imputation. *Mathematical Geology* 35(3), 253–278.
- Martín-Fernández, J. A., K. Hron, M. Templ, P. Filzmoser, and J. Palarea-Albaladejo (2012). Model-based replacement of rounded zeros in compositional data: Classical and robust approaches. *Computational Statistics & Data Analysis* 56(9), 2688–2704.
- Meech, J. A. and G. R. Baiden (1987). Simulating the mine-mill interface. *International Journal of Surface Mining, Reclamation and Environment* 1(3), 191–198.
- Michaux, S. and L. O'Connor (2020). How to set up and develop a geometallurgical program. Report, Geological Survey of Finland - Economic Minerals Unit. Online available at <https://smi.uq.edu.au/files/54219/How%20to%20set%20up%20a%20geometallurgical%20program.pdf>, last accessed on October 16, 2022.
- Miller, J. D., R. Y. Wan, and X. Díaz (2016). Preg-robbing gold ores. In *Gold Ore Processing* (2nd ed.), Book section 49, pp. 885–907. Amsterdam, the Netherlands: Elsevier.
- Mining Modular (2017). DISPATCH[®] Fleet Management system (FMS) helps mine optimize its haulage cycle and dramatically reduce truck idle times. Online Article, available at <https://www.modularmining.com/case-studies/dispatch-fms-helps-mine-optimize-haulage-cycle/>, last accessed on February 3, 2020.
- Mining Technology (2022). Fuel and power costs rising most for miners, with 45% looking for other suppliers. Online Article, available at <https://www.mining-technology.com/comment/fuel-power-rising-miners/>, last accessed on October 16, 2022.
- Molnár, F., H. O'Brien, Y. Lahaye, M. Kurhila, A. Middleton, and B. Johanson (2017). Multi-stage hydrothermal processes and diverse metal associations in orogenic gold deposits of the Central Lapland Greenstone Belt, Finland. In *Mineral Resources to Discover, 14th SGA Biennial Meeting*, Quebec City, Canada, pp. 63–66.

- Montoya, P., L. Keeney, R. Jahoda, J. Hunt, R. Berry, U. Drews, V. Chamberlain, and S. Leichter (2011). Geometallurgical modelling techniques applicable to pre-feasibility projects - La Colosa case study. In *1st AusIMM International Geometallurgy Conference*, Brisbane, Australia, pp. 103–111.
- Morley, C. and H. Arvidson (2017). Mine value chain reconciliation - Demonstrating value through best practice. In *Proceedings of the 10th International Mining Geology Conference*, Hobart, Tasmania, pp. 279–292.
- Motoki, A., S. E. Sichel, T. Vargas, D. P. Melo, and K. F. Motoki (2015). Geochemical behaviour of trace elements during fractional crystallization and crustal assimilation of the felsic alkaline magmas of the state of Rio de Janeiro, Brazil. *Anais da Academia Brasileira de Ciências* 87(4), 1959–1979.
- MPC (2018). LeachWELL 60X. Report, Mineral Process Control (MPC) Pty Ltd. Online available at http://mineralprocesscontrol.com.au/wp-content/uploads/2021/11/Leach_WELL-60X-info-sheet.pdf, last accessed on October 16, 2022.
- Mustapha, A., R. K. Asamoah, G. Ofori-Sarpong, R. K. Amankwah, A. Mustapha, R. K. Asamoah, and G. Ofori-Sarpong (2014). Preg-robbing characteristics of gold ores in Ghana. In *3rd UMaT Biennial International Mining and Mineral Conference*, Tarkwa, Ghana, pp. 192–196.
- Mwanga, A., J. Rosenkranz, and P. Lamberg (2015). Testing of ore comminution behavior in the geometallurgical context - a review. *Minerals* 5(2), 276–297.
- Napier-Munn, T. J., S. Morrell, R. D. Morrison, and T. Kojovic (1996). *Mineral comminution circuits: Their operation and optimisation* (2nd ed.), pp. 413. Monograph Series in Mining and Mineral Processing. Brisbane, Australia: Julius Kruttschnitt Mineral Research Centre, University of Queensland.
- Occhipinti, S., I. Tyler, C. V. Spaggiari, K. Martin, and M. G. Doyle (2017). Unravelling Tropicana - Where, what, how and why? In *Proceedings of Exploration 17: 6th Decennial International Conference on Mineral Exploration*, Toronto, Canada, pp. 413–417.
- Occhipinti, S. A., I. M. Tyler, C. V. Spaggiari, R. J. Korsch, C. L. Kirkland, R. H. Smithies, K. Martin, and M. T. D. Wingate (2018). Tropicana translated: A foreland thrust system imbricate fan setting for c. 2520 Ma orogenic gold mineralization at the northern margin of the Albany-Fraser Orogen, Western Australia. *Geological Society, London, Special Publications* 453(1), 225–245.
- Ogunsola, N., B. Olaleye, and M. Saliu (2017). Effects of weathering on some physical and mechanical properties of Ewekoro Limestone, South-Western Nigeria. *International Journal of Engineering and Applied Sciences* 4(11), 72–81.
- Olierook, H. K. H., K. Rankenburg, S. Ulrich, C. L. Kirkland, N. J. Evans, S. Brown, B. I. A. McInnes, A. Prent, J. Gillespie, B. McDonald, and M. Darragh (2020). Resolving multiple geological events using in situ Rb-Sr geochronology: Implications for metallogenesis at Tropicana, Western Australia. *Geochronology* 2(2), 283–303.

- Ordóñez-Calderón, J. C., S. Gelcich, and F. Fiaz (2017). Lithogeochemistry and chemostratigraphy of the Rosemont Cu-Mo-Ag skarn deposit, SE Tucson Arizona: A simplicial geometry approach. *Journal of Geochemical Exploration* 180, 35–51.
- Palarea-Albaladejo, J., J. A. Martín-Fernández, and A. Buccianti (2014). Compositional methods for estimating elemental concentrations below the limit of detection in practice using R. *Journal of Geochemical Exploration* 141, 71–77.
- Parker, B. (2009). *Simulation and analysis of particle flow through an aggregate stockpile*. MSc Thesis, Virginia Polytechnic Institute and State University, USA.
- Parsons, C., E. Margui Grabulosa, E. Pili, G. H. Floor, G. Roman-Ross, and L. Charlet (2013). Quantification of trace arsenic in soils by field-portable X-ray fluorescence spectrometry: Considerations for sample preparation and measurement conditions. *Journal of Hazardous Materials* 262, 1213–1222.
- Pawlowsky-Glahn, V., J. J. Egozcue, and R. Tolosana Delgado (2011). Lecture notes on compositional data analysis. Report, University of Girona, Spain. Online available at <http://www.sediment.uni-goettingen.de/staff/tolosana/extra/CoDa.pdf>, last accessed on October 16, 2022.
- Pereira, B., A. Vandeuren, B. B. Govaerts, and P. Sonnet (2016). Assessing dataset equivalence and leveling data in geochemical mapping. *Journal of Geochemical Exploration* 168, 36–48.
- Pontual, S., N. Merry, and P. Gamson (2008). *G-MEX Spectral Interpretation Field Manual* (3rd ed.). Sydney, Australia: AusSpec International Ltd.
- Rai, P., H. Schunesson, P. A. Lindqvist, and U. Kumar (2015). An overview on measurement-while-drilling technique and its scope in excavation industry. *Journal of The Institution of Engineers (India): Series D* 96(1), 57–66.
- Ramanaidou, E. R. and M. A. Wells (2011). Hyperspectral imaging of iron ores. In *10th International Congress for Applied Mineralogy (ICAM)*, Trondheim, Norway, pp. 575–580.
- Regis Resources Limited (2022). Mineral resource and ore reserve update at Tropicana. Report, ASC Announcement. Online available at <https://wcsecure.weblink.com.au/pdf/RRL/02489965.pdf>, last accessed on October 16, 2022.
- Rivera, C., R. Rodríguez, and S. Pimentel (2011). Horwitz Equation as Quality Benchmark in ISO/IEC 17025 Testing Laboratory. In *IIE Annual Conference*, Reno, USA, pp. 1–7.
- Roache, T. J. (2016). Phase 1 Geometallurgical Products. Unpublished report by AngloGold Ashanti Australia, Tropicana Operation.
- Roache, T. J. (2018). Boston Shaker underground pre-feasibility: Geometallurgical domaining. Unedited contribution to the Boston Shaker underground pre-feasibility study report. Unpublished report by AngloGold Ashanti Australia, Tropicana Operation.

- Roache, T. J. (2019). aiSIRIS mineral interpretation assessment. Unpublished report by AngloGold Ashanti Australia, Tropicana Operation.
- Roache, T. J. (2020). Dolerite proxy classification from GC drilling. Unpublished report by AngloGold Ashanti Australia, Tropicana Operation.
- Rodger, A., A. Fabris, and C. Laukamp (2021). Feature extraction and clustering of hyperspectral drill core measurements to assess potential lithological and alteration boundaries. *Minerals* 11(2), 136.
- Romary, T., F. Ors, J. Rivoirard, and J. Deraisme (2015). Unsupervised classification of multivariate geostatistical data: Two algorithms. *Computers & Geosciences* 85, 96–103.
- Rossi, M. E. and C. V. Deutsch (2014). *Mineral Resource Estimation*, pp. 332. Dordrecht, the Netherlands: Springer.
- Rousseeuw, P. J. (1986). Silhouettes: A graphical aid to the interpretation and validation of cluster analysis. *Journal of Computational and Applied Mathematics* 20, 53–65.
- Saunders, J. (2006). *Pressure-temperature-composition-time constraints of the Tropicana gold deposit, Western Australia*. BSc Thesis, University of Western Australia, Australia.
- Schaefer, L. N., G. Kereszturi, M. Villeneuve, and B. Kennedy (2021). Determining physical and mechanical volcanic rock properties via reflectance spectroscopy. *Journal of Volcanology and Geothermal Research* 420, 107393.
- Servin, M., F. Vesterlund, and E. Wallin (2021). Digital twins with distributed particle simulation for mine-to-mill material tracking. *Minerals* 11(5), 524.
- SGS (2020). Geochemistry Guide - The foundation of project success. Report, Societe Generale de Surveillance SA. Online available at <https://www.sgs.com/en/-/media/sgscorp/documents/corporate/brochures/sgs-analytical-guide.cdn.en.pdf>, last accessed on October 16, 2022.
- Spaggiari, C. V., C. L. Kirkland, M. J. Pawley, R. H. Smithies, M. T. D. Wingate, M. G. Doyle, T. G. Blenkinsop, C. Clark, C. W. Oorschot, L. J. Fox, and J. Savage (2011). *The geology of the East Albany-Fraser Orogen - A field guide*, pp. 98. Record 2011/23. Perth, Australia: Geological Survey of Western Australia.
- Spaggiari, C. V. and I. Tyler (2014). *Albany-Fraser Orogen seismic and magnetotelluric (MT) Workshop 2014: extended abstracts*, pp. 182. Record 2016/6. Perth, Australia: Geological Survey of Western Australia.
- Suriadi, S., S. J. J. Leemans, C. Carrasco, L. Keeney, P. Walters, K. Burrage, A. H. M. ter Hofstede, and M. T. Wynn (2018). Isolating the impact of rock properties and operational settings on minerals processing performance: A data-driven approach. *Minerals Engineering* 122, 53–66.

- Terracore (2022). How geospectral imaging works. Online Article, available at <http://terracoregeo.com/how-geospectral-imaging-works/>, last accessed on July 7, 2022.
- Tessier, J., C. Duchesne, and G. Bartolacci (2007). A machine vision approach to on-line estimation of run-of-mine ore composition on conveyor belts. *Minerals Engineering* 20(12), 1129–1144.
- Tiu, G. (2017). *Classification of drill core textures for process simulation in geometallurgy: Aitik mine, Sweden*. MSc Thesis, Luleå University of Technology, Sweden.
- Tiu, G., Y. Ghorbani, N. Jansson, and C. Wanhainen (2021). Tracking silver in the Lappberget Zn-Pb-Ag-(Cu-Au) deposit, Garpenberg mine, Sweden: Towards a geometallurgical approach. *Minerals Engineering* 167, 106889.
- Tøgersen, M. K., R. A. Kleiv, S. Ellefmo, and K. Aasly (2018). Mineralogy and texture of the Storforshei iron formation, and their effect on grindability. *Minerals Engineering* 125, 176–189.
- Torrence, C. and G. P. Compo (1998). A practical guide to wavelet analysis. *Bulletin of the American Meteorological Society* 79(1), 61–78.
- Tusa, L., M. Khodadadzadeh, C. Contreras, K. Rafiezadeh Shahi, M. Fuchs, R. Gloaguen, and J. Gutzmer (2020). Drill-core mineral abundance estimation using hyperspectral and high-resolution mineralogical data. *Remote Sensing* 12(7), 1218.
- van den Boogaart, K. G. and R. Tolosana-Delgado (2018). Predictive geometallurgy: An interdisciplinary key challenge for mathematical geosciences. In *Handbook of Mathematical Geosciences*, Book section 33, pp. 673–686. Cham, Switzerland: Springer.
- van Duijvenbode, J. R. and M. W. N. Buxton (2019). Use of time series event classification to control ball mill performance in the comminution circuit - A conceptual framework. In *Real Time Mining - 2nd International Raw Material Extraction Innovation Conference*, Freiberg, Germany, pp. 114–123.
- van Duijvenbode, J. R., M. W. N. Buxton, and M. Soleymani Shishvan (2020). Performance improvements during mineral processing using material fingerprints derived from machine learning - A conceptual framework. *Minerals* 10(4), 366.
- van Duijvenbode, J. R., L. M. Cloete, M. Soleymani Shishvan, and M. W. N. Buxton (2021). Material fingerprinting as a potential tool to domain orebody hardness and enhancing the prediction of work index. In *Application of Computers and Operations Research in the Mineral Industry (APCOM 2021)*, Online, pp. 181–192.
- van Duijvenbode, J. R., L. M. Cloete, M. Soleymani Shishvan, and M. W. N. Buxton (2022a). Interpreting run-of-mine comminution and recovery parameters using multi-element geochemical data clustering. *Minerals Engineering* 184, 107612.

- van Duijvenbode, J. R., L. M. Cloete, M. Soleymani Shishvan, and M. W. N. Buxton (2022b). Material fingerprinting as a tool to investigate between and within material type variability with a focus on material hardness. *Minerals Engineering* 189, 107885.
- Varannai, B., D. Johansson, and H. Schunnesson (2022). Crusher to mill transportation time calculation - The Aitik case. *Minerals* 12(2), 147.
- von Stosch, M., R. Oliveira, J. Peres, and S. a. Feyeo de Azevedo (2014). Hybrid semi-parametric modeling in process systems engineering: Past, present and future. *Computers & Chemical Engineering* 60, 86–101.
- Wambeke, T., D. Elder, A. Miller, J. Benndorf, and R. Peattie (2018). Real-time reconciliation of a geometallurgical model based on ball mill performance measurements - A pilot study at the Tropicana gold mine. *Mining Technology* 127(3), 115–130.
- Ward, J. H. (1963). Hierarchical grouping to optimize an objective function. *Journal of the American Statistical Association* 58(301), 236–244.
- Wibberley, C. (1999). Are feldspar-to-mica reactions necessarily reaction-softening processes in fault zones? *Journal of Structural Geology* 21(8-9), 1219–1227.
- Wierzchoń, S. T. and M. A. Kłopotek (2018). *Modern Algorithms of Cluster Analysis*, pp. 433. Studies in Big Data. Cham, Switzerland: Springer.
- Wikedzi, A., M. A. Arinanda, T. Leißner, U. A. Peuker, and T. Mütze (2018). Breakage and liberation characteristics of low grade sulphide gold ore blends. *Minerals Engineering* 115, 33–40.
- Witkin, A. P. (1983). Scale-space filtering. In *8th International Joint Conferences on Artificial Intelligence*, Karlsruhe, Germany, pp. 1019–1022.
- Yamasaki, S.-i., A. Takeda, K. Kimura, and N. Tsuchiya (2016). Underestimation of chromium and zirconium in soils by hydrofluoric acid digestion and inductively coupled plasma-mass spectrometry. *Soil Science and Plant Nutrition* 62(2), 121–126.
- Young, A. and W. P. Rogers (2021). Modelling Large Heaped Fill Stockpiles Using FMS Data. *Minerals* 11(6), 636.
- Zhao, S., T.-F. Lu, B. Koch, and A. Hurdsmann (2015). Automatic quality estimation in blending using a 3d stockpile management model. *Advanced Engineering Informatics* 29(3), 680–695.
- Zheng, A. and A. Casari (2018). *Feature Engineering for Machine Learning*, pp. 200. Sebastopol, USA: O'Reilly Media, Inc.
- Zhou, K.-F. and S.-S. Wang (2017). Spectral properties of weathered and fresh rock surfaces in the Xiemisitai metallogenic belt, NW Xinjiang, China. *Open Geosciences* 9(1), 322–339.
- Zhou, S., K. Zhou, J. Wang, G. Yang, and S. Wang (2017). Application of cluster analysis to geochemical compositional data for identifying ore-related geochemical anomalies. *Frontiers of Earth Science* 12(3), 491–505.

- Zhou, X., D. Liu, H. L. Bu, L. L. Deng, H. M. Liu, P. Yuan, P. X. Du, and H. Z. Song (2018). XRD-based quantitative analysis of clay minerals using reference intensity ratios, mineral intensity factors, Rietveld, and full pattern summation methods: A critical review. *Solid Earth Sciences* 3(1), 16–29.

Appendix

A.1 Wavelet tessellation presented in Chapter 11.2.2

The following steps show an overview of transforming a (time-series) signal into a tessellation image. These steps are similar to those described in Hill et al. (2020) and only differences compared to their methodology are highlighted.

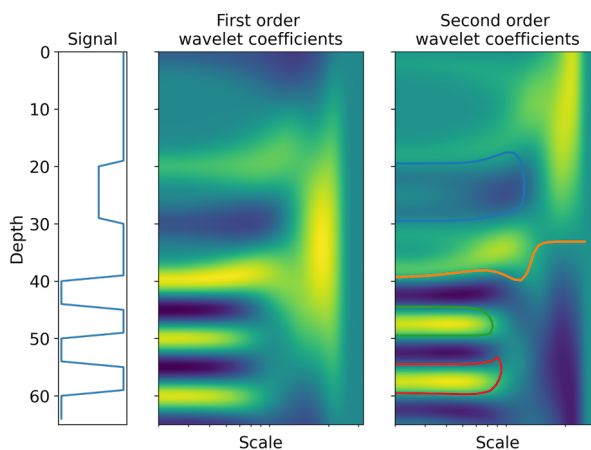
The overview of signal tessellation is as follows:

1. Extraction of zero contours of the second order wavelet coefficients:
 - (a) Calculate the first and second order wavelet coefficients at scales
 - (b) Find the zero contours in the second order wavelet coefficients
2. Select the first order coefficient values which correspond to the path of the second order zero contour
3. Split zero contours which are not truncated by the edge of the plot
4. Define boundaries from each zero path:
 - (a) Obtain the boundaries from the zero paths
 - (b) Normalise boundaries
5. Calculate domains and tessellate

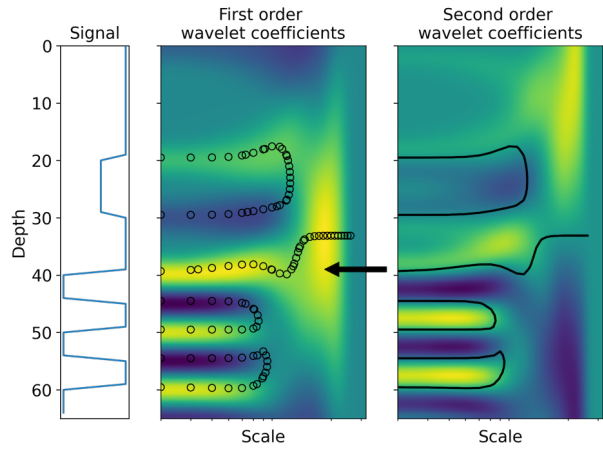
Step

1. Extraction of zero contours of the second order wavelet coefficients: a) Calculate the first and second order wavelet coefficients at different scales; b) Find the zero contours in the second order wavelet coefficients

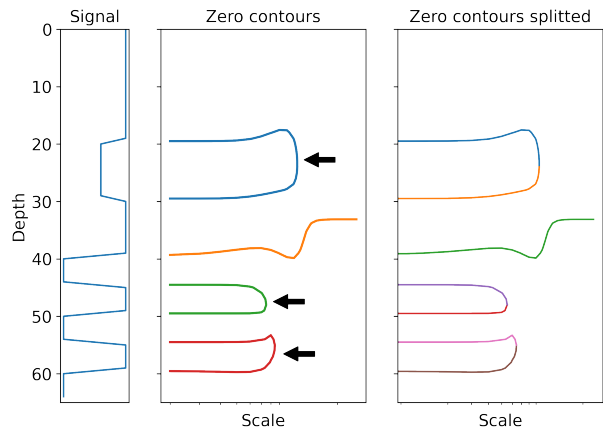
Analysis steps visualised



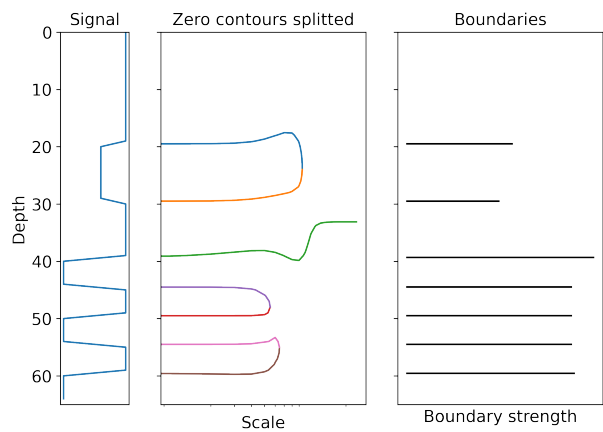
2. Link contours with coefficients: Obtain the value of the first order wavelet coefficient that corresponds to each scale on the path of the second order zero contour.



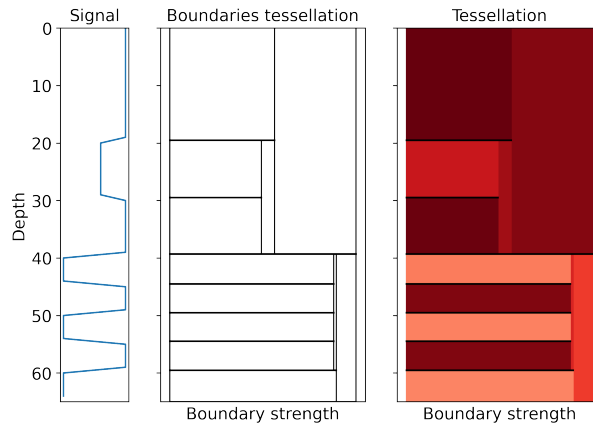
3. Split zero contours. Each zero contour that is not truncated by the edge of the plot is split into two parts at the maximum scale, to form a pair of zero paths.



4. Define boundaries from zero paths: a) Get the boundaries from the zero paths. The depth is the minimum wavelength scale and the strength is the maximum absolute first order wavelength coefficient on the path. b) Normalise boundaries.



5. Tessellate domains; create the mosaic plot. Create domains from the boundaries and colour them according to the mean or median value of the signal.



Curriculum Vitae

Jeroen Robert van Duijvenbode was born on the 6th of May 1994, in Hellevoetsluis, the Netherlands. He has a **BSc** degree in Molecular Science & Technology obtained at Delft University of Technology (TU Delft) in the Netherlands in 2015. After a minor program in Resource Engineering, he decided to join for his **MSc** degree the European Mining Course (EMC cohort 2015-2017). His master studies was a joint program between Aalto University in Helsinki, Finland, RWTH Aachen University in Germany, and TU Delft in the Netherlands. After obtaining his MSc degree, Jeroen started his **doctoral research** at the department of Geoscience and Engineering at TU Delft, within the Resource Engineering section. As part of his first year's PhD learning experience he spent four months in Reno (NV), USA. During the second year he also visited the Tropicana Gold Mine in Western Australia. His interests include technical programming, data science and machine learning aspects of the research. More recently, he started to apply the data science skills for mineral exploration purposes. The promoters of his doctorate were Dr. M.W.N. Buxton and Prof. dr. ir. J.D. Jansen. Dr. M. Soleymani Shishvan was his copromotor.

✉ jrvanduijvenbode@hotmail.com

in [linkedin.com/in/jeroen-van-duijvenbode](https://www.linkedin.com/in/jeroen-van-duijvenbode)



Publications

Journal papers

- 4 **van Duijvenbode, J.R.**, and M. Soleymani Shishvan (2022). Stochastic analysis of dig limit optimization using simulated annealing. *Journal of the Southern African Institute of Mining and Metallurgy* 122(12), pp. 715-724.
- 3 **van Duijvenbode, J. R.**, L. M. Cloete, M. Soleymani Shishvan, and M. W. N. Buxton (2022). Material fingerprinting as a tool to investigate between and within material type variability with a focus on material hardness. *Minerals Engineering* 189, 107885.
- 2 **van Duijvenbode, J. R.**, L. M. Cloete, M. Soleymani Shishvan, and M. W. N. Buxton (2022). Interpreting run-of-mine comminution and recovery parameters using multi-element geochemical data clustering. *Minerals Engineering* 184, 107612.
- 1 **van Duijvenbode, J. R.**, M. W. N. Buxton, and M. Soleymani Shishvan (2020). Performance improvements during mineral processing using material fingerprints derived from machine learning - A conceptual framework. *Minerals* 10(4), 366.

Conference proceedings

- 2 **van Duijvenbode, J. R.**, L. M. Cloete, M. Soleymani Shishvan, and M. W. N. Buxton (2021). Material fingerprinting as a potential tool to domain orebody hardness and enhancing the prediction of work index. In *Application of Computers and Operations Research in the Mineral Industry (APCOM 2021)*, Online, pp. 181–192.
- 1 **van Duijvenbode, J. R.** and M. W. N. Buxton (2019). Use of time series event classification to control ball mill performance in the comminution circuit - A conceptual framework. In *Real Time Mining - 2nd International Raw Material Extraction Innovation Conference*, Freiberg, Germany, pp. 114-123.